Antarctic Meteorites XXIII

Papers presented to the Twentythird Symposium on Antarctic Meteorites

June 10-12, 1998

NATIONAL INSTITUTE OF POLAR RESEARCH, TOKYO

国立極地研究所

Wednesday, June 10, 1998

0900 - 1200	Registration	Auditorium (6th Floor)
0925 - 0930	Opening Address	**Takeo Hirasawa** Director-General National Institute of Polar Research

*Speaker

Chairmen: Kimura M. and Nagahara H. **Page**

Thursday, June 11, 1998

Chairmen: Mikouchi T. and Misawa K.

Friday, June 12, 1998

Chairmen: Funaki M. and Sugiura N.

Poster Session **Page**

Abstract only

ABSTRACTS

A PRESOLAR SiC GRAIN WITH AN UNUSUAL Si-ISOTOPIC COMPOSITION. Sachiko Amari[1,2], Ernst Zinner[1], and Roy S. Lewis[2], [1]McDonnell Center for the Space Sciences and the Physics Department, Washington University, One Brookings Dr., St. Louis, MO 63130-4899, [2]Enrico Fermi Institute, University of Chicago, 5630 Ellis Ave., Chicago IL 60637-1433.

Presolar SiC grains can be classified into different populations. The majority of grains (about 94%) are mainstream grains, other minor populations such as grains A, B, X, Y, and Z, comprise the rest [1]. Figure 1 shows the C- and N-isotopic ratios of different grain types. Here we describe a SiC grain with highly unusual isotopic compositions, which does not fit into any of the above populations.

This grain was found during a survey of SiC grains for future CHARISMA studies. Silicon carbide grains of the KJG fraction (with an average size of 3μm) extracted from the Murchison meteorite [2] were dispersed onto and pressed into a gold foil. Approximately 1400 SiC grains were mapped by low-mass-resolution ion imaging in the ion microprobe to locate grains with highly anomalous $^{30}Si/^{28}Si$ ratios. Such grains were subsequently analyzed for their C-, N-, and Si-isotopic ratios at high mass resolution.

Among the grains located for further measurement, grain KJGP1-146-1 on mount CHRL 108 has an unusual Si-isotopic composition. Its $\delta^{29}Si$ and $\delta^{30}Si$ values are 2678±21‰ and 3287±43‰, respectively, the highest excesses in the neutron-rich Si isotopes ever measured in a presolar grain (Fig. 2). The grain has isotopically light C ($^{12}C/^{13}C$= 844±34) and slightly heavy N ($^{14}N/^{15}N$= 213±21) (Fig. 1). It should be noted that several thousand presolar SiC grains have been mapped in $^{30}Si/^{28}Si$ in the search for X grains [3, 4], yet this is the first identification of a grain with such an extreme ^{30}Si excess, indicating that grains of this type are extremely rare.

What stellar source can produce a grain with these isotopic characteristics? We consider the merits of 4 candidates; an AGB star, a nova, a Type II supernova, a Wolf-Rayet star. Spectroscopic evidence indicates that C-rich AGB (Asymptotic Giant Branch) stars produce SiC (see references in Hoppe et al. [1]). In fact, carbon stars have been identified as stellar sources of mainstream SiC grains [1], since the isotopic characteristics of these grains (isotopically heavy C, light N and modest excesses in ^{29}Si and ^{30}Si) can, in general, be successfully explained within the framework of AGB-star models. Amari et al. [5] proposed that Y grains originated from higly evolved AGB stars. Hoppe et al. [6] suggested that Z grains formed in low-mass low-metallicity AGB stars. Both types of grains have ^{30}Si excesses relative to the mainstream grains (Fig. 2). In AGB stars, neutron-capture in the He-shell produces large enrichments in ^{29}Si and ^{30}Si. However, when He-shell material is dredged up into the massive H-rich envelope during the thermally pulsing stage, the anomalous Si is diluted by the isotopically almost normal Si in the envelope so that predicted $^{29,30}Si$ excesses are generally only a few percent. Thus, it is highly unlikely that the large ^{29}Si and ^{30}Si excesses observed in grain KJGP1-146-1 can be achieved in the envelope, where SiC grains condense.

Most novae produce dust (e.g., references in Starrfield et al. [7]). In a few CO novae, it has been observed that a single outburst produces several kinds of grains such as silicate and carbonaceous grains (e. g., [8] and references therein). Dust formation is also observed in ONeMg novae. Gehrz et al. [9] proposed SiC formation in nova Aquilae 1982 in order to explain the 10μm emission feature in its IR spectrum. In CO novae, Si-isotopic ratios remain close to solar, since the temperature remains too low for nuclear reactions that might affect them. On the other hand, the nova ejecta from a ONeMg White Dwarf of $1.25M_{\odot}$ are expected to be highly enriched in ^{30}Si (×6 solar $^{30}Si/^{28}Si$), whereas $^{29}Si/^{28}Si$ ratios are close to solar [7]. A common feature of nova ejecta are very low $^{12}C/^{13}C$ ratios (0.5-2.5), in contrast to the ratio measured in the grain, eliminating a nova origin for grain KJGP1-146-1.

Type II supernovae have been proposed as stellar sources of SiC X grains (1% of the total meteoritic SiC) and low-density graphite grains [3, 4, 10-12]. All X grains and many graphite grains show ^{28}Si excesses. Since the condition C/O >1, required for grain formation, is only realized in the outer zones and ^{28}Si is produced in the innermost zone, the ^{28}Si excesses in the grains indicate that supernova ejecta experience extensive mixing [12]. A different mix might have

produced the grain of this study. Neutron-capture occurs in the C-rich He/C and C/O zones (following the terminology coined by Meyer et al. [13]) and the O-rich zones. In the He/C zone excesses in the neutron-rich Si isotopes are too small (200-300‰ in the $15M_{\odot}$ model of [14]) to account for the excesses in our grain. In the C/O zone, excesses in ^{29}Si and ^{30}Si are much larger ($\delta^{29}Si$=4,800 and $\delta^{30}Si$=10,000‰ in the $15M_{\odot}$ model). Since both the He/C and C/O zones are highly enriched in ^{12}C, and ^{15}N is produced at the bottom of the He/C zone by explosive nucleosynthesis, high $^{12}C/^{13}C$ and low $^{14}N/^{15}N$ ratios can be qualitatively reproduced by the mixing of these 2 zones with the He/N zone. However, the $\delta^{29}Si/\delta^{30}Si$ ratio of the mix is much lower than the ratio measured in the grain. This problem of underproduction of ^{29}Si in supernova models has previously been pointed out [12] and seems to be a deficiency of the models. Recently, Clayton et al. [15] suggested that in an explosive environment the condition C/O>1 is not required for the condensation of carbonaceous grains. He argued that during supernova explosions energetic electron created by the deay of radiogenic nuclei such as ^{56}Ni, ^{56}Co, and the ubiquitous He^{+} in certain layers dissociate CO, thus freeing up C to condense as grains even if C/O<1. This would extend the source regions for SiC formation but it remains to been whether grains can condense and grow in such a hostile environment.

A Wolf-Rayet (WR) star origin is another possibility. These massive stars (>$25M_{\odot}$) with high mass-loss rates lose the envelope at the onset of core He-burning. The He-burning products are thus exposed at the surface and removed in stellar winds, with extremely high $^{12}C/^{13}C$ ratios (C is essentially ^{12}C) and low N content and low $^{14}N/^{15}N$ ratios (1 to 100 in a $85M_{\odot}$ model with solar metallicity [16]). Excesses in the neutron-rich Si isotopes by neutron capture at the end of core He-burning are expected to be very large; calculated values are $\delta^{29}Si$=6,200‰ and $\delta^{30}Si$=15,000‰ [17]. Similar to the case of Type II SN models, ^{29}Si is deficient relative to ^{30}Si compared to Si in the grain (and in the solar system). Besides the problem of relative under-production of ^{29}Si in WR stars, predicted anomalies are too high to explain the ratios of the grain, suggesting that some kind of dilution has to occur before grain formation, if the grain formed in the outflow from such a star.

Finally, a binary system seems a promising candidate. It has been known that a significant number of Wolf-Rayet stars are binaries. Collisions of winds in WR and O star binary systems have been observed. Williams et al. [18] studied HD1933793 (WR140), a binary system of a WC7 and a O4-5 star, in the radio, infrared, and X-ray regions. They modeled the composition of the WR wind to explain the observed X-ray spectra and concluded that the wind's CNO content is intermediate between the solar system value and that predicted by models of evolved massive stars. These authors interpreted the infrared observations in terms of the formation of amorphous carbon in the wind of the WC star and subsequent cooling of the dust. Thus, it is not unreasonable to assume that SiC grains form in such an environment.

We conclude that a Wolf-Rayet and O star binary, or possibly a Type II supernova are the most probable candidates for the source of this grain.

REFERENCES:

[1] Hoppe P. *et al.* (1994) *Astrophys. J.*, **430**, 870. [2] Amari S. *et al.* (1994) *Geochim. Cosmochim. Acta,* **58**, 459. [3] Hoppe P. *et al.* (1995) *Lunar Planet. Sci.* **XXVI**, 621. [4] Nittler L. R. *et al.* (1995) *Astrophys. J.*, **453**, L25. [5] Amari S. *et al.* (1997) *Lunar Planet. Sci. XXVIII,* 33. [6] Hoppe P. *et al.* (1997) *Astrophys. J.*, **487**, L101. [7] Starrfield S. *et al.* (1997) In *Astrophysical Implications of the Laboratory Study of Presolar Materials,* (T. Bernatowicz and E. Zinner) 203. AIP, New York. [8] Mason C. G. *et al.* (1998) *Astrophys. J.*, **494**, 783. [9] Gehrz R. D. *et al.* (1984) *Astrophys. J.*, **281**, 303. [10] Amari S. *et al.* (1992) *Astrophys. J.*, **394**, L43. [11] Nittler L. R. *et al.* (1996) *Astrophys. J.*, **462**, L31. [12] Travaglio C. *et al.* (1998) *Astrophys. J.*, submitted. [13] Meyer B. S. *et al.* (1995) *Meteoritics,* **30**, 325. [14] Woosley S. E. and Weaver T. A. (1995) *Astrophys. J. Suppl.*, **101**, 181. [15] Clayton D. D. (1998) *Lunar Planet. Sci.* **XXIX**, abstract #1016, Lunar Planetary Institute, Houston (CD-ROM). [16] Arnould M. *et al.* (1997) In *Astrophysical Implications of the Laboratory Study of Presolar Materials,* (T. Bernatowicz and E. Zinner) 179. AIP, New York. [17] Prantzos N. *et al.* (1987) *Astrophys. J.*, **315**, 209. [18] Williams P. M. *et al.* (1990) *Mon. Not. R. astro. Soc.*, **243**, 662.

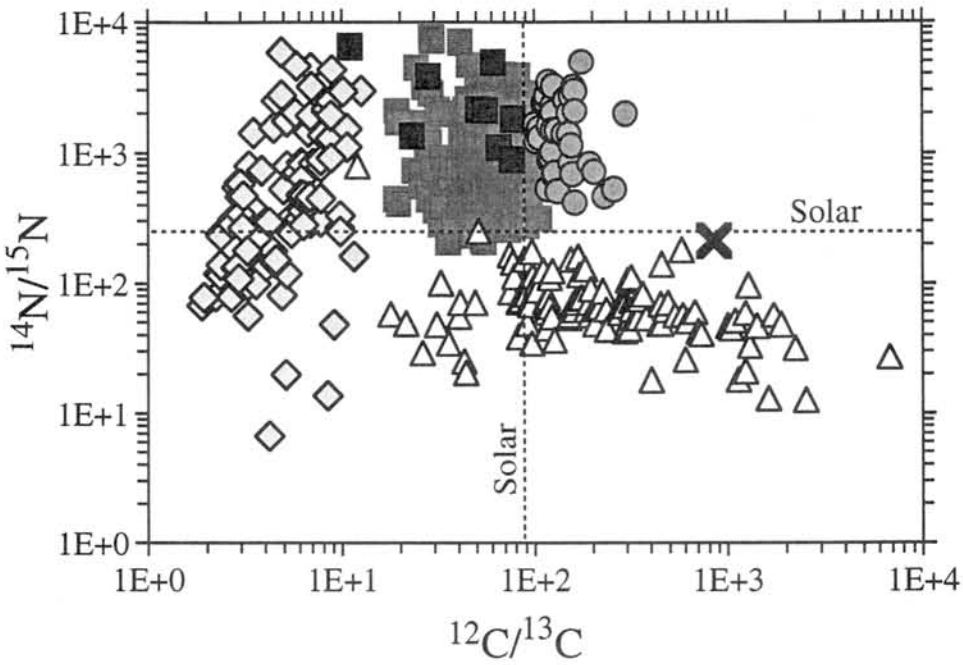

Fig. 1 Carbon and N-isotopic ratios of grain KJGP1-146-1 are plotted with those of other types of presolar SiC grains.

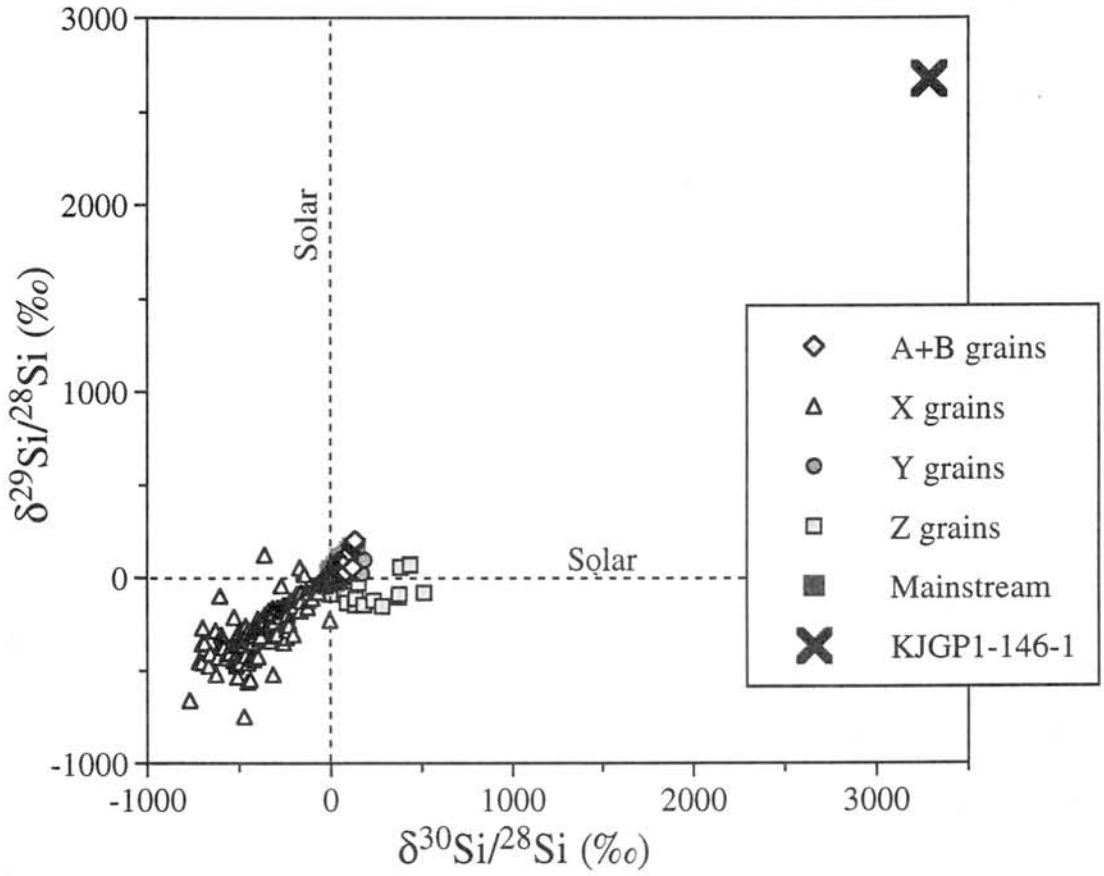

Fig. 2 Silicon isotopic ratios of grain KJGP1-146-1 are plotted with those of other types of presolar SiC grains.

POINT OF INFLEXION BETWEEN E and H CHONDRITES: SEARCH ON THE BASIS OF PATHS OF THERMAL EVOLUTIONARY TRANSITIONS IN THEIR BULK COMPOSITIONS FROM STATISTICAL ANALYSES OF THE NIPR ANTARCTIC METEORITE DATASET (III)

Sz. Bérczi[1,3], *B. Lukács*[2]

[1] Eötvös University, Cosmic Mat. Res. Gr. Dep. Petrology, Geochem., H-1088 Budapest, Múzeum krt 4/a
[2] Hungarian Academy of Sci. Central Res. Inst. Phys. RMKI, H-1525 Budapest 114. P.O.Box 49.
[3] Eötvös University, Dept. G. Technology, H-1088 Budapest, Rákóczi út 5. Hungary

ABSTRACT

On the basis of **1**. *datasets* on meteorite bulk compositions (i.e. Jarosewich, 1990, Yanai, Kojima, Haramura, 1995), **2**. large number of *examples for transitional meteorites* between chondrites and achondrites (Olsen, Jarosewich, 1970, Mittlefehldt, 1979, Takeda et al. 1984, Mittlefehldt et al. 1979, 1990, Yanai, Kojima, 1991, Ikeda et al. 1991, Kimura et al. 1991, Torigoye et al. 1993, Casanova et al. 1995, Mittlefehldt et al. 1995, Ikeda, Prinz, 1996, Lin, Kimura, 1997, Yugami et al. 1997), **3**. *melting experiments* on primitive achondritic compositions (i.e. McCoy et al, 1997) and on E-chondritic compositions (Dickinson et al. 1992, Fogel et al. 1996, McCoy et al. 1997a, 1997b) and **4**. *thermal evolution paths of chondritic meteorite parent bodies* (Bérczi, Holba, Lukács, 1995, Lukács, Bérczi, 1996) we tried to reconstruct **the inflexion point on the Urey-Craig Metallurgic field**, where meteorites with bulk composition **between E and H groups** can be found after their thermal upheated, before-differentiation stage. Over this inflexion E chondrites (the only group where reduction does not stop at petrologic type 4) run toward more reduced stages, H chondrites turn back to became more and more oxidized. These events of thermal evolution of E and H can be described by parameters of C/H2O ratio which shows the competition of compounds in chondrites for Fe. Fe may change its carrier mineral by reduction and oxidation. Reducing agent is C, oxidizing agent is H_2O, but their activities start at different temperatures. But after the initial period of upheating, these volatile components annihilate each other in those meteorites, which had the exact ratio of them, so being representative to the infelxion point composition. So the inflexion point is initial bulk composition dependent. We also extended the reductional compositonal path onto the Si-Ni-in-metal plot for E-chondrites, which have Si-bearing irons.

THE OBSERVATIONAL DATASET

There are multiple number of observations of textural evidences that thermal metamorphism form gradual transitional mineral assemblages and compositions between chondritic, achondritic and differentiated meteorites. After classification of chondritic metamorphism (van Schmus, Wood, 1967) examples for transitional textures from chondritic to achondritic ones became in focus of research in the last 20 years. (for example see, Olsen & Jarosewich, 1970; Mittlefehldt, 1979; Takeda & al. 1984; Kallemeyn & Wasson, 1985, Mittlefehldt & al. 1979, 1990; Yanai & Kojima, 1991; Kimura & al. 1991; Torigoye & al. 1993; Casanova & al. 1995; Mittlefehldt & al. 1995; Ikeda & Prinz, 1996; Lin & Kimura, 1997; Weisberg & al. 1997; Yugami & al. 1997). The textural and compositonal sequences form a thermal evolutionary model for the hypothetical chondritic parent body precursors.

Thermal evolution is a complex process. Like the evolutionary model reconstruction in the history of geology it needs at least **two different sequences of processes**, which advance parallel in the same parent body. The two parallel processes used in meteoritics were the *changes of oxidation state of iron* in its compounds and the *thermal metamorphism of chondritic textures*. We can summarize these two parallel processes by **their mutual projections on each other** and draw their changes in a basic compositonal field. The first such field was the Urey-Craig one of the ferrous compounds of chondrites (Urey & Craig, 1953). The second one in our paper is projection of reduction participant main components, (i.e Fe, Fe, C) averages for all petrologic types (PT) in each chondrite groups (E, H, L, LL, C). Components summed up as mixed colors on the van Schmus-Wood table will represent this second projection.

The first evolutionary path reconstruction was the work of Lux et al. (1981) for H-chondrites. Using the new Catalog of Antarctic Meteorites dataset of NIPR (Yanai, Kojima, Haramura, 1995) in their statistical analyses Bérczi & et al. (1995), Lukács & Bérczi, (1997) found that reduction is the first global change between 3 and 4 petrologic type at each of E, H, L, LL chondrite groups. But E-chondrites were the only group where reduction did not stop at petrologic type 4 but continued in the metallic phase, too. Therefore in our work we extended the reductional compositonal path of the bulk parent body for its metal

segregate onto the Si-Ni-in-metal plot (see i. e. Keil, 1968, Neal & Lipschutz, 1981; Weeks & Sears, 1985; Nagahara, 1991; Weisberg & al. 1997). This path of evolution (with heating up and separation) partly overlaps with that of shown on the Urey-Craig field earlier (Bérczi & Lukács, 1995; Bérczi, Holba & Lukács, 1995; Lukács & Bérczi, 1996, 1997). In these early papers the reduction was shown, but the subsequent separation of aubritic achondritic and high Si metallic phases yet were not mentioned. However, E-chondrite (Indarch, EH4) melting experiments of the Washington and New York groups during the last 5 years (Dickinson & al. 1992; Dickinson & Lofgren, 1992; Fogel & al. 1996; Weisberg & al 1997; McCoy & al. 1997a., 1997b) showed that - in a temperature interval of 1100-1425 C centigrade - melting produces even higher reduced metals than those of chondritic grains.

DOES C/H2O COMPETITION FOR IRON SELECT BETWEEN E AND H GROUP?

Confirming Wiik's pioneering result on a larger (NIPR Antarctic Meteorite Compositional) Data-Set in our earlier studies we have shown (Lukács, Bérczi, 1996, Bérczi, Lukács 1997) that for the bulk Fe content chondrites fall into 2 separate groups (Wiik, 1956): higher, ca. 27% (E, H, C) & lower, ca. 21% (LL, L). In these statistical calculations we have found that the distributions of E, H and C chondrites overlap. The more than 550 "points" of NIPR dataset made it possible to restudy the possibility of the common origin of these three chondrite types: Including all analysed NIPR E, H and C chondrites into our earlier discussion, we considered the Fe/Si ratio as having been selected for a parameter characterizing initial conditions, because other distinctive parameters of the E, H, and C types might have been the consequences of thermal transformations inside the parent body. First we plotted the "Chondritic Hertzsprung-Russell Diagram" (C-HRD) for the oxide Fe/non-oxide Fe content (Si normalized) of E, H, L, LL, and C types of chondrites from NIPR Dataset (Bérczi, Holba, Lukács, 1995) and from averages for all petrologic types of E, H, L, LL, C we have got a bulk path of chemical evolution.

Now let us focus our attention to the competition of C and H2O for Fe during the thermal evolution of only E and H group of chondrites. They both have a common trend between 3 and 4 type: reduction. After it in the case of H oxidation begins, turning the direction of the path of thermal evolution back, while in the case of E the dominating transformation remains reduction. For the case of H this path of thermal evolution showed that reduction could start at lower temperatures, while oxidation switched on later. The tendency of the increasing metallic iron content with type (between 3 & 4) was measured earlier (Lux & al. 1981.)

DISCUSSION

EVOLUTIONARY PATH OF E-CHONDRITES AND THEIR DERIVATES

Only the E-chondrite evolutionary path showed that reduction advanced and continued after the petrologic type 4. Because reduction of iron in E-chondrites attained very low FeO/FeO+MgO values in silicates the path of thermal evolution needs extension of the compositional field. In advanced E's there practically no oxidised Fe remains, so the reduction cannot be seen anymore on the Fe-FeO plot. But another a composition field is at hand. As early as in 1961 Ringwood found that the FeNi metal phase of the enstatite chondrites contains reduced Si. Studies of enstatite chondrites showed that Si content of the metal phase gradually changed with petrologic type (Keil, 1968; Neal & Lipschutz, 1979; Weeks & Sears, 1985; Nagahara, 1991; Weisberg & al. 1997). *This way another "metallurgic" field (over the Urey-Craig field) exists where reduction of iron compounds of the E-chondrites to achondrites may be represented parallel with the chondrule metamorphism.* This is the Si-Ni-in-metal field. But till E-chondrite melting experiments no measured genetic links were proven for the extreme derivates of anomalous high Si-bearing iron meteorites and stony irons to E-chondrites. (Dickinson & al. 1992, 1996, Fogel & al. 1996, McCoy & al. 1997a&b).

First melting experimens (in reduced conditions) of the EH4 chondrite Indarch (Dickinson & al. 1992) revealed that such fragments can be imagined as precursors of high Si-bearing meteorites, if they had melted between 1100-1425 C centrigrade. The measurements identified those phases which appear and coexist at higher temperatures. (Between 1100-1425 degrees first metallic, sulfide, -for an interval two sulfides- and silicate phases coexisted, but at 1400 C only two phases remained: silicate melt which took up all the sulphur, and metal phase which solved large amount of silicon. (Fogel & al. 1996; McCoy & al. 1997.) The fact that higher Si-bearing iron metal was produced during E-chondritic melting, showed that high Si-bearing irons might have been products of thermal evolution of E-chondritic parent body.

In the Si-Ni-in-metal plot we can see (Weisberg et al., 1997) that Si content of the metal phase increases with petrologic type even for EL chondrites. The evolutionary path for E-chondrites in the Urey-Craig field has shown that at 5 and 6 petrologic types total Fe content of E chondrites decreased, suggesting Fe outflow. The melting experiments have shown that FeNi metal is the first melt, next one is sulfide. These

all are in accord with the fact that first metal melts and flows out in E-s but with higher than chondritic Si content.

POINT OF INFLEXION BETWEEN E AND H

Obviously the final trends are very different for high petrologic types of E`s and H`s. There is even the well known gap between enstatite and bronzite chondrites, We admit that we do not yet understand the lack of intermediate chondrites. However, it is tempting to visualize such ones and we can think Acapulco, Lodran, Winona and IAB irons as far relatives. If such chondrites exist then for them the thermal evolution has approached a critical point in which perhaps no one terminated its evolution, being this bulk compositional „place" a repulsor for such evolutionary path points. Imaging such evolution: the first melt is the metal Fe-Ni-S eutectic, see i.e. McCoy et al. 1997, second melt is the basaltic one with plagioclase and pyroxene. For E-s the range of higher Si content in the first and later melts means that partial melting carries the majority of Si. (The highest Si content of Si-bearing iron meteorites is 2.6 wt %, in the case only if these irons were produced with melting most of the iron phase in the E-chondritic precursor.) (We mention that the complete analogon of the Urey-Craig field would be a SiO_2-Si plot. However in all cases Si is minor to SiO_2, so changes in the latter are not significant. However in this paper we concentrate on Si, not on Ni.)

FOR C AND H2O COMPETITION

As seen, Fe for E, H and C overlap, but does not Mg. (Lukács, Bérczi, 1996). It seems as if later C's had evolved from the high Mg tail of the ancestral distribution, and E's did of the low Mg tail. It is strange that the fate of a meteorite group may depend on the bulk Mg content, since Mg does not enter into the chemical transmutations. But in types 3 the H2O content correlates positively with Mg. Let us use the working hypothesis that silicates with high Mg content keep H2O better than ferrous ones; if mineralogical experiments confirm this, then one may expect that *oxidation balances the reduction better at higher Mg contents, therefore those run toward reduction if they have enough carbon.* Oxidized Fe correlates positively with Mg in type 3, while there total Fe correlates negatively with Mg (Lukács, Bérczi, 1996). Their figure of H2O vs. reduction at type 3; the correlation is indeed negative (the same is true for all types, not shown here); although the E line seems separate.

CONCLUSIONS

NIPR data do not contradict a kind of C vs. H2O competition for Fe in the case of H's & E's as:

- I: For higher than average H_2O/C and/or MgO/FeO the reduction starts, but FeO and H_2O uses up C at some stage, while H_2O is retained.
- II: For most initial conditions (average H_2O/C and MgO/FeO, or high H_2O/C but low MgO/FeO or low H_2O/C but high MgO/FeO) most C and H_2O are used up or diffuses away before the stage type 3. Therefore if the thermal impact is sufficient to reach later stages of higher PC's, the possibilities for reduction or oxidation are moderate and balanced. This resembles H3-6.
- III: For lower than average H_2O/C and/or MgO/FeO some C is used up, but at type 3 C still dominates H_2O, so reduction keeps going. This resembles E3-6.

The almost parallel melting of Fe-FeS and basaltic melts in Acapulco/Lodran achondrites is observable, because they had ballanced H_2O/C ratio to their Fe/FeO content not to run to the reduction of E-s and not to develop by gradual oxidation as H-s. Therefor we can say that Acapulco/Lodran achondrites represent an infelxion point in the chondritic meteoritic compositional field between E and H groups.

REFERENCES

Bérczi Sz., Holba Á., Lukács B. (1995): *Acta Min. Petr. Szeged,* **XXXVI**. 143, **Bérczi Sz., Holba Á., Lukács B.** (1995): *20th NIPR Symp. Antarct. Met.*, Tokyo, 26, **Bérczi Sz., Lukács B**. (1995): *20th NIPR Symp. Antarct. Met.*, Tokyo, 30, **Bérczi Sz., Holba Á. & Lukács B.** (1996): *21th NIPR Symp. Antarct. Met.*, Tokyo, 17, **Bérczi Sz., Holba Á., Lukács B.** (1996): *KFKI-1996-15.* pp. 38. Budapest, **Bérczi Sz., Lukács B., Földi T., Holba Á., Józsa S., Marosi G., Szabó Sóki L., Szakmány Gy.** (1997): *Antarct. Met., XXII.* Tokyo, 12, **Bild, R.W., Wasson, J.T.** (1977): *Science*, **197**. 58, **Buseck, P.R.** (1977): *GCA*. **41**. 711, **Casanova, I., Graf, T., Marti, K.** (1995): *Science*, **268**. 540. **Casanova, I., Keil, K. Newsom, H.E.** (1993): *GCA*, **57**. 675, **Casanova, I., McCoy, T.J., Keil, K.** (1993): *LPSC XXIV*. 259, **Dickinson, T.L., Lofgren, G.E.** (1992): *LPSC XXIII*. 307, **Dickinson, T.L., Lofgren, G.E., Casanova, I.** (1992): *LPSC XXIII*. 309, **Dickinson, T.L., McCoy, T.J.** (1996): *LPSC XXVII*. 309, **Fogel, R.A.** (1996): *LPSC XXVII*. 369, **Fogel, R.A., Weisberg, M.K., Prinz, M.** (1996): *LPSC XXVII*. 371, **Graham, A.L., Bewan, A.W., Hutchison, R**. (1985): Catalogue of Meteorites. BM(NH), London, **Hiroi T., Takeda H.** (1991): *Proc. NIPR Symp. Antarctic Meteorites* **4**. 163, **Ikeda Y.** (1989): *Proc. NIPR Symp. Antarctic Meteorites* **2**. 109, **Ikeda Y., Prinz, M**. (1996): *Proc. NIPR Symp. Antarctic Meteorites* **9**. 143, **Jarosewich, E.** (1990): *Meteoritics,* **25.** 323, **Keil, K.** (1968): *J. Geophys. Res.* **73**. 6945, **Keil, K., Ntaflos, Th., Taylor, G.J., Brearley, A.J., Newsom, H.E., Romig, Jr., A.D.** (1989): *GCA,* **53.** p. 3291, **Kimura K., Lin Y., Ikeda Y., El Goresy, A., Yanai K., Kojima**

H. (1993): *Proc. NIPR Symp. Antarct. Meteorites,* **6**, 186, **Kubovics I., Bérczi Sz., Ditrói-Puskás Z., Gál-Sólymos K., Nagy B., Szabó A.** (1997): *Acta Min. Petr. Szeged,* **XXXVIII.** 35, **Lin Y., Kimura K.** (1997): *LPSC XXVIII.* p. 817, **Lukács B., Bérczi Sz.** (1996): *21th Symp. Antarct. Met.*, Tokyo, 90, **Lukács B., Bérczi Sz.** (1997): *Antarctic Meteorites XXII.* 94, **Lukács B., Bérczi Sz.** (1997): *LPSC XXVIII.* 853, **McCoy, T.J., Dickinson, T.L., Lofgren, G.E.** (1997): *LPSC XXVIII.* 903, **McCoy T.J., Dickinson, T.L., Lofgren, G.E.** (1997): *Antarctic Meteorites XXII.* 103, **McCoy T.J., Keil, K., Muenow, D.W., Wilson, L.** (1997): *GCA,* **61.** 639, **Nagahara H.** (1991): *Proc. NIPR Symp. Antarctic Meteorites* **4**. 144, **Nagahara H.** (1992): *Proc. NIPR Symp. Antarctic Meteorites* **5**. 191, **Neal, C.W., Lipschutz, M.E.** (1981): *GCA,* **45**. 2091, **Newsom, H.E., Drake, M.J.** (1979): *GCA,* **43**. 689, **Olsen, E., Jarosewich, E.** (1971): *Science*, **174.** 583, **Otting, Zahringer,** (1966): *GCA,xxx* **Ringwood, A.E.** (1961): *GCA*, **25**. 1, **Scott, E.R.D., Wasson, J.T.** (1973): *Rev. Geophys. Space Phys.* **13.** No. 4. 527, **Sears, D.W., Kallemeyn, G.W., Wasson, J.T.** (1982): *GCA*, **46**. 597, **Takeda H., Huston, T.J., Lipschutz, M.E.** (1984): *Earth Planet. Sci. Letters,* **71.** 329, **Takeda H., Yugami K., Bogard, D., Miyamoto M.** (1997): *LPSC XXVIII.* 1409, **Wai C.M., Wasson, J.T.** (1969): *GCA*, **33**. 1465, **Wai C.M., Wasson, J.T.** (1970): *GCA*, **34**. 408, **Wasson, J.T., Wai C.M.** (1970): *GCA,* **34**. 169, **Wasson, J.T., Wang J.** (1986): *GCA*, **50**. 725, **Wasson, J.T.** (1990): *Science*, **249**, 900, **Weeks, K.S., Sears, D.W.G.** (1985): *GCA*, **49**. 1525, **Weisberg, M.K., Prinz, M., Nehru, C.E.** (1997): *LPSC XXVIII.* 1525, **Urey, H.C., Craig, H.** (1953): *GCA*, **4**. 36, **Yanai K., Kojima H.** (1991): *Proc. NIPR Symp. Antarctic Meteorites* **4**. 118, **Yanai K., Kojima H., Haramura H.** (1995): *Catalog of the Antarctic Meteorites.* NIPR, Tokyo, **Yugami K., Takeda H., Kojima H., Miyamoto M.** (1997): *Antarctic Meteorites XXII.*103, **Zellner, B., Leake, M., Morrison, D., Williams, J.G.** (1977):. *GCA*, **41**. 1759.

CONSTRUCTION OF A PLANETARY LANDER PROBE, HUNVEYOR, TO EMPHASIZE THE ROLE OF CONNECTIONS BETWEEN PLANETARY SCIENCE AND TECHNOLOGY (ROBOTICS) EDUCATION. THE USE OF HUNVEYOR IN ANTARCTIC RESEARCH

Sz. Bérczi[1,2], V. Cech[2], S. Hegyi[3], B. Drommer[2], T. Borbola[2], T. Diósy[2], Z. Köllõ[2], Sz. Tóth[2]

[1]Eötvös University, Dept. Petrology and Geochemistry, H-1088 Budapest, Múzeum krt 4/a. Hungary,
[2]Eötvös University, Dept. G. Technology, H-1088 Budapest, Rákóczi út 5.(bercziszani@ludens.elte.hu)
[3]Janus Pannonius University, Dept. Appl. Math. Informatics, H-7625 Pécs, Ifjúság u. 6. Hungary.

HISTORICAL

In the last 23 years Eötvös University, Budapest, we had courses on Planetary Science, Cosmopetrography and Technologies. In a new program we connected these three subjects. With the conclusion of the International Space Camp, Alabama, 1993, by one of us (Sz. B.), this connection emphasizes the harmony between scientific background and constructive activities [1]. Our program synthesizes planetary science, technology and robotics education which are connected by the construction of a Surveyor like planetary lander space-probe (we call it Hunveyor). In this course we develop instruments to specific planetary conditions. Especially Antarctic conditions and Martian surface conditions are in many aspects parallel. Studying lander construction problems developed our attention and sensitivity to planetary problems, too. Such a way new scientific goals may also be achieved.

PRINCIPLES

There were three main blocks of principles in the foundation of our new program. They served as a framework to the planetary lander construction, although on a theoretical and educational basis.. One was the scientific achievements in **planetary geology**, i.e. Wilhelms [2], the other was how to summarize our **knowledge about technologies**, i.e. Bérczi et al. 1992, 1995, [3], and the third was a kind of summary of **planetary probe construction and operation**, i.e. Nick [4], and also a summary of measurements and results: The Surveyor Investigator Teams [5]. In our paper we try to summarize all three main aspects of our program, goals and results.

1. PLANETARY GEOLOGY, MEASUREMENTS ON THE SURFACE

First stratigraphic works on lunar geology selected and emphasized those principles of terrestrial geology, which can be extended to Solar System scale [6]. Identification of surface rocks were first done by their optical properties and morphologies, but later, the lander space probes (Surveyor, Luna, Viking) showed details of the surface. Characteristics of surface can be done by physical (mechanical, optical, thermal and magnetic properties, first approximation) measurements of:

- mechanical properties: strength, rigidity, porosity, depth of regolith, depth of surface powder, roughness of the soil and the largest blocks scattered on the surface, i.e. Christensen et al. [7], Choate et al. [8], Scott et al. [9], Scott et al. [10];
- optical properties to be studied by a television camera are: relative albedo, roughness, crater density, smoothness, height of the highest elevation in the vicinity of the lander, average inclination of the landscape, i.e. Shoemaker et al. [11], [12];
- thermal properties are: surface rock temperatures, thermal conductivity, i.e. Lucas et al. [13], Vitkus et al. [14],
- magnetic properties by passive magnet contacts. We intended to supply our space probe with measuring instruments for all these properties. We had a rich literature about earlier works of the Surveyor and Viking missions [5], [15].

2. TECHNOLOGIES

The design of space technologies needs a complex representation of processes working together. For traditional technologies we can arrange the technology steps - the operations - into a sequential and/or parallel way. This sequence of operations may be enriched with the representation of the interactions and feedbacks which regulate and control the processes. But first of all we developed an irreducible representation of raw material processing technologies (Bérczi, Cech, Hegyi, 1991, [16]), where technologies are repre-

sented as a forced (constrained) path motion of the main raw material, contrary to the free transformations of them in natural processes. (The constrained motion in physics was the example.) Later we developed a cross-effect matrix (the „technology/environment chesstable" [17]), where main interactions between natural streams and technology pollutions can be projeceted simultaneously, showing their mutual dependence.

IRREDUCIBLE REPRESENTATION OF TECHNOLOGIES

In a production technology throughout the sequence of operations raw materials are transformed to products. The sequence of operations may be represented by the tools, instruments (or machines), which work on materials, and which form a path of constraints for these materials transformed. (The path of constraints, the machines form a „riverbed", form a network with sequencial and parallel sections of operations). In our design of *irreducible representation of technologies* these networks are given in the form of three parallel threads: operations, materials and machines. Moreover, the parallel energetic and informatic lines are also attached to these threads. The operations themselves give a periodicity to the design.

SPACE TECHNOLOGIES

In space technologies the main object of technologies is the *data from measurements*. So our design of technology description should be adapted to the network for data-handling in the computer system on board of space probe. One part of the space technology used on board of Hunveyor will be some material flow, material transport through an instrument (i.e. the dust of planetary surface). Measurements transform these transports into data. The other part of the technology on the space probe is this data-transformations. The essentials of the material transports:

ENVIRONMENTAL NATURAL STREAMS OR CURRENTS

This forced (constrained) path description can be both used for the transportation of natural streams, from which technologies pick up auxiliary materials (in terrestrial environments: water, air, soil, mineral resources, etc.), and the data handling electronics which finally send the data by telemtrics. The benefit of this form of interrelation of processes is that it gives a common denominator for comparison, when the two kind of streams - technologies and natural currents - are interacting. (Local transformations of water: in limestone dolinas, limestone caves, in stalactite-stalagmite formation, in transportation and deposition of sediments, till the place where technologies extract quantities: all are characterised by the same formulation as technologies were given.).

THE TECHNOLOGY/ENVIRONMENTAL CURRENTS CHESSTABLE

After designing the two different types of processes, technologies and natural streams, we can give a comparable formulation to interrelate them. We constructed a relation-table, a matrix, which contains technologies in the horizontal rows of the table, and natural currents in the vertical columns of the table. Similar type operations from technologies, cunsuming water, air, mineral resources, thermal stream etc. as local streams were arranged one above the other in the same column. One well studied aspect of this relation table is that technologies pour pollutions to natural currents of the environment. Well known events of water circulation (evaporation, precipitation, waterflows) are polluted in this way. To all matrix elements we may correspond a critical values for pollution or treshold values of pollution in outpouring streams. These values are given from environmental scientists or life scientists.

SPACE PROBE HUNVEYOR:IT IS A REPRESENTATION OF THIS MATRIX

Visible and comparable for technologies and planetary currents, this matrix forms a valuable overview and educational benefit when comparison is focused on technologies to be settled onto a space probe, a lander type. The synthesis of this theoretical background and constructive realisation is: a minimal, lander type space probe [18].

3. CONSTRUCTION OF THE HUNVEYOR

TWO LEVELS OF CONSTRUCTION

We are building Hunveyor according to a two level program. In the **first level** we made the lander's skeleton, energetics and on board computer with minimal space probe experimental furniture like as televison camera with mirror, telescopic arm to mechanic operations, thermal unit for environmental measurements and communication system for these units. In the **second level** we plan to specify our space probe to local conditions. One such condition may be Antarctic research, which later will be useful comparison for Martian lander construction..

Tetrahedral skeleton of the load holding framework was the first unit we built. For a minimal probe personal minimal environmental observing activities were copied: visuality, touch, temperature experience. Televison camera with mirror to "see around", telescopic arm to dig small graben, and a bimetallic temperature measuring instruments can be corresponded to them.

The electronic system uses parallel measurements but time-parted and priority selected signal transport by telemetrics. First we operated it from the regular electronic network, by cable connections, but we begin to build the solar panel system as energy source. Later we separate it from electrical network and also use radio electronic connection. This Surveyor-like minimal probe, the Hunveyor, gave us many knowledge during construction, learning and pleasure. The sceleton was made from copper tubes with 12 mm diameter. The first robotics was constructed from the ROBOT EVOLUTION System of a Hungarian Engineer Group in Eger. It made possible to make working 3 motors, which was enough to make move the mirror of the television camera, and also in an other channel for the motion of the telescopic arm. But these electronics were unable to work them parallel, therefore the first task was in electronics design to build a parallel system interfaces and gates (interfaces were developed on Dept. Technology by B. Drommer).

4. ANTARCTIC USE OF THE HUNVEYOR TYPE TRAINING LANDER PROBE

We began to construct special equipment of Hunveyor type lander robot in Antarctic measurements. Over the minimal probe (TV camera, robotic arm, thermal and magnetic detectors) we furnished the lander with conductivity measuring instrument. We measure conductivity of ice between two needles penetrated into the ice below the landers skeletal body. We plan how classical school experiments can be adapted to such a lander robot, like as evaporating materials by a lupe, measuring the refraction index of molten ice, and measuring how it depends on the contaminants, even measuring pH value of the molten ice. This part of robotics initiative may develop not only constructive imagination of students but their attitudes for synthetic viewing in planetary science.

SUMMARY

We connected in our educational program the planetary science with robotics construction of a lander space probe. First level we build a minimal space probe and parallel we study mostly lunar and Martian surface results, and in the second level we specify our lander to different local use, of which one is an Antarctic lander station which investigates the icy world in space probe style. Many aspects of this Antarctic practice can be later used in Martian conditions, too.

ACKNOWLEDGEMENTS

Supported by the MKM 694/96 (ELTE 3363/96) and OMFB 96-97-47-1265-MÜI-TP-055/96 (ELTE 33131/96) grants.

REFERENCES

[1] Blackwell T. L.: *Teaching is effective, if it is attached with constructive activities and more effective, if space science education is connected to it.* (1993): Teachers Program. MSFC, Huntsville; [2] Wilhelms D. E. (1970) U.S.G.S. Prof. Paper No. 599-F, Washington; [3] Bérczi Sz., Cech V., Hegyi S., Sz.-Fabriczy A., Schiller I. (1995): Technology I. (in Hungarian), Keraban, Budapest; [4] Nick O. W. (1967) Off. Technology Utiliz. No. NASA SP-163. Washington; [5] The Surveyor Investigator Teams (1967) JPL, CIT. Techn. Report 32-1177. Pasadena; and The Surveyor Investigator Teams (1968) JPL, CIT. Techn. Report 32-1264, Part II. Pasadena; [6] Wilhelms D. E. (1987) U.S.G.S. Prof. paper No. 1348. Washington; [7] Christensen E.M. et al. (1967) NASA-JPL Techn. Report 32-1177, p.111-153. [8] Choate R. et al. (1968) NASA-JPL Techn. Report 32-1264, p.77-134, [9] Scott R. F., Roberson F. I. (1967) NASA-JPL Techn. Report 32-1177, p.69-110. [10] Scott R. F., Roberson F. I. (1968) NASA-JPL Techn. Report 32-1264, p.135-187. [11] Shoemaker E. M. et al. (1967) NASA-JPL Techn. Report 32-1177, p.9-67. [12] Shoemaker E. M. et al. (1968) NASA-JPL Techn. Report 32-1264, Part II. p.9-76. [13] Lucas J. W. et al. (1967) NASA-JPL Techn. Report 32-1177, p.155-188; [14] Vitkus G. et al. (1968) NASA-JPL Techn. Report 32-1264, Part II. p.187-208; [15] Corliss W. R. (1974) NASA-SP-334 Washington; [16] Bérczi Sz., Cech V., Hegyi S. (1991): Irreducible representation of technologies. Proc. of JPTE Univ. and Osijek Univ. Joint Progr. Osijek-Pécs, [17] Bérczi Sz., Cech V., Hegyi S., Sz. Fabriczy A., Lukács B. (1998): LPSC XXIX, 1371, , [18] Bérczi Sz., Cech V., Hegyi S., Borbola T., Diósy T., Köllő Z., Tóth Sz. (1998): LPSC XXIX, 1267,

SPHERULES IN A SOLAR SYSTEM WIDE STRATIGRAPHY

Sz. Bérczi [1], Cs. Detre [2], Gy. Don [2], L. Dosztály [2], V. Cech [1], B. Drommer [1], A. Gucsik [3], S. Józsa [4], B. Lukács [5], G. Marosi [6], P. Solt [2], L. Szabó Sóki [6], Gy. Szakmány [4], I. Vécsey [1].

[1]Eötvös University, Dept. G.Technology, H-1088 Budapest, Rákóczi út 5. Hungary, [2]Geological Institute of Hungary, H-1143 Budapest, Stefánia út 14. Hungary. [3]Yamaguchi University, Dept. Chemistry and Earth Sci. Yoshida, Yamaguchi 753, Japan, [4]Eötvös University, Dept. Petrology and Geochemistry, H-1088 Budapest, Múzeum krt 4/a. Hungary, [5] Central Res. Inst. Physics KFKI-RMKI, H-1525 Budapest 114. P.O.Box 49. Hungary, [6]Eötvös University, Dept. of Media and Technology of Education, H-1088 Budapest, Rákóczi út 5. Hungary.

ABSTRACT: We made a sketch of a Solar System wide stratigraphy for determined and undetermined (but probable) units which contain characteristic groups of spherules as inclusions, candidates for correlation. First we overview stratigraphic principles, the main types of spherule inclusions, and then we arrange them to spherule horizons in the Solar System.

PRINCIPLES - HISTORICAL: Geologic correlation uses at least two independent evolutionary processes mutually projecting them onto each other. To Steno's principle of superposition of rock-bodies on the planetary surface Earth a parallel independent succession (by fossil inclusions in strata) was selected: the law of Faunal Succession by W. Smith. Mutual projection (by inclusion) of these two evolutionary sequences resulted in the biostratigraphy on geological side and Darwin-Wallace's phylogenetical evolution model on the biology side.

Since inclusions with characteristic shape and composition are useful tools when they occur in extending layers (dataplanes), principle of inclusions helped mutual correlation by involving other parallel evolutionary processes, i.e. thos of inclusions themselves. (Radionuclides were one such inclusions.) Such classical stratigraphy principle is important to refer again, when used for dating layers in the Solar System (even if as thin ones as rims on chondrules or inclusions - are to be arranged into a time sequence).

PLANETARY STRATIGRAPHY: Stratigraphy of the Moon was first where both review of principles and extension of classical correlation were developed (Shoemaker et al. [1], Wilhelms [2]). New kinds of „inclusions" were needed for interplanetary correlation of geologic time. Craters fulfilled many requirement for inclusions, (somehow taking the place of the conventional terrestrial fossils of fauna and flora): they occurred with great multiplity and with own formation and degradation history on lunar strata. Craters were promisful for extension the method to other planetary bodies. Spherules from large enough impacts may be representative inclusions of the ejecta layer such way forming spherule horizons.

MICRO-MATERIAL STRATIGRAPHY: In meteoritics a characteristic inclusion can extend stratigraphy and can connect it to macrascopic material systems: the chondrules. They have the role of individual inclusions: once molten droplets of silicates, contained in about 85 % of meteorites (chondrites). They can characterize even a small amount of extraterrestrial material: the meteorite, but also its parent body. The Van Schmus-Wood [3] classification used up the slow transformation (metamorphosis) of these interplanetary fossils (chondrules). Their obscuring in the texture (by diffusion) is a consequence of the thermal transformation suffered by the host material of the parent body. Therefore chondrules may be used mostly to the stratigraphy of minor planets of which meteorites are fragments by collisions.

SPHERULE HORIZONS ON EARTH: Although deep sea spherules were discovered in the last century spherules began to play the role of inclusions in stratigraphy by their lunar counterparts: lunar spherules [4]. On the Moon they were of two different origin: impact and volcanic.

The role of spherules in terrestrial stratigraphy formed during the last 3 decades. Although they were known both as deep sea and rain residual types and they were found in Antarctic ice the International Geological Correlation Project 384 formulated the goal to use them as new tool for correlation [5]. It is an important goal of spherule horizons on Earth that they can be used even in Archaicum [6-8].

THE 5 MAIN SPHERULE TYPES: Common shape of spherules come the fact that they were once molten. But their composition and environment also contributed to their final form and composition. In our spherule stratigraphy overview the following basic types will be used:

- *Refractory spherules* from carbonaceous chondritic meteorites (Murchison, Allende, Kaba),
- *Chondrules* from stony meteorites,
- *Spherules from the Moon*:
  a) with impact origin (lunar samples and lunar meteorites), and
  b) with volcanic origin (lunar samples),
- *Terrestrial spherules* with impact or cosmic fragmentary or dust raining processes,
- Terrestrial *industrial spherules*.

I. THE SPINEL-RICH SPHERULES: Although in the time sequence refractory spherules begin Solar System's spherule stratigraphy, they were the last spherule types, discovered (first in the form of white inclusions [9-12], especially in spherule form [13]). Detailed description of the spinel-rich spherules began with those of Murchison CM2, (as peculiar chondrules [13]). By their chemistry, they were related to the refractory inclusions in carbonaceous chondrites, [20] and their spherulitic shape and inner texture suggested molten origin. Many spinel-rich, spinel-perovskite, spinel-hibonite and spinel-melilite spherules were later described mostly from Murchison, but later from Allende, too [14-16]. Today refractory spinel-rich spherules are known from more than a dozen carbonaceous chondrite [17-19]. The new KABA thin section [18] with large surface made it possible for us to look for them, mainly according to their characteristic size and form. Our spinel-rich spherule is in the rim region of a larger (2 mm diameter) chondrule. The spherule has 150 micrometers diameter, its inner core region is lighter pleonaste, the darker outer belt is Mg-Al-rich spinel. Pleonaste contains 5 micrometer sized perovskite grains. Models conclude that spinel-rich spherules might have been destillated from presolar materials, origined by their melting and Wark-Lovering type rims later deposited onto these refractory spherules [19-21]. Enclosed into the C2 and C3 chondrites they represent a first spherule stratigraphic unit in the Solar System.

II. CHONDRULES: Chondrules are well known, their main classification came from the end of the last century: granular, porphyritic, barred olivine, radial pyroxene, glassy types. Their sizes vary between 0.1 and 10 millimeter. Their age shows they represent the early solar system events: probably a) early heating (flares) b) interactions (i.e.drag) during formation of the Sun, condensation of the solar nebula. Brecciation by collisions of planetesimals formed chondrule horizons in the Solar System [22]. Over known chondrites from Hungary (Mező-Madaras, Mócs, Kaba, Knyahinya) we used the NIPR Antarctic Meteorite and NASA Antarctic Thin Section Sets. Important to note that a spherule was found in 62295 lunar sample [23].

III. LUNAR SPHERULES: Both two types of Lunar Spherules: those with impact origin and and those with volcanic ones occur in the NASA Lunar Sample Thin Section Set [24-27] [50-52].. Volcanic spherules represent Lunar thermal history events, impact ones represent the outer, solar system events by their age. Volcanic spherules are regional occurrences (orange soil, [28]), Imbrian impact spherules [26], crystalline spherules [52] form a large dataplain on the Moon, could reach Earth in lunar meteorites, so they become representative members of a Solar System spherule horizon.

IV. TERRESTRIAL SPHERULES: Terrestrial spherules are important new tools in the archaicum, and are used as new horizon defining inclusions, related to tektites [29-32], and extended to the important stratigraphical boundaries like as C/T and recently to P/T boundaries, and related to Tertiary impact events like as that of Ries crater in Germany [37], and other impacts from the phanerosoic past [5-8], [29-45]. The following examples will be shown:

- Late Devonian (Frasnian-Famenian) hor. [42],
- Permian-Triassic boundary horizon [45],
- Late-Triassic spherule horizon [46],
- Late-Eocene spherule horizon, [49],
- Spherule horizons in the Carpathian Basin, [5].

V. TERRESTRIAL INDUSTRIAL SPHERULES: They are contaminants in recent reasearch, but in the future they may be objects of research on other planetary surfaces, too.

SUMMARY: We constructed a tentative spherule stratigraphy in the Solar System. We overviewed most candidates for such a stratigraphy, using spherules as inclusions for correlation. Although stratigraphic principles were developed for terrestrial strata, with fossils as main inclusions, transport of spherules in the interplanetary space makes it possible to extend all important principles and methods for rocky-icy planet wide horizons. We also considered the main types of spherule inclusions, and then we arranged them to spherule horizons in the Solar System. We summarized our thoughts in a videofilm, too.

ACKNOWLEDGEMENTS: Supported by the OMFB 96-97-47-1265-MÜI-TP-055/96 (ELTE 33131/6), the T 014958 and T 025461 and the HJSTC 31/96 grants.

REFERENCES: [1] Shoemaker E.M., Hackman R.J., Eggleton R.E. (1962) *Advances Astronaut. Sci.* **8**. 70, [2] Wilhelms D.E. (1987) U.S.G.S. Prof. Paper No. 1348. Washington, [3] Van Schmus W. R. & Wood J. A., (1967) *GCA* ***31***, 737; [4] Lindsay J.F. (1976) *Lunar Stratigraphy and Sedimentology*. Elsevier, [5] Detre Cs., Bérczi Sz., Lukács B. eds. (1996) *Spherules and Global Events*, KFKI-1996-05/C, [6] Simonson B.M., Beukes N.J., Hassler S. (1996) *LPSC XXVIII*. 1323, [7] Lowe D.R., Byerly G.R. (1986) *Geology* ***14***, 83; [8] Byerly G.R., Lowe D.R. (1994) *GCA* ***58***, 3469; [9] Török J. (1858) *Ann. Phys. Chem. Poggendorff*, Ser IV. **15,** 329; [10] Sztrókay K., Tolnay V., Földvári-Vogl M. (1961): *Acta Geol. Hung.* 7. 17, [11] C. Michel-Levy (1968) Bull. Soc. Fr. *Mineral. Cristallogr.* **91**. 212, [12] Frost M.J., Symes R.F. (1970) *Mineral. Mag.* **37,** 724, [13] Macdougall J.D. (1981) *Geophys. Res.Lett.* ***8***, 966, [14] MacPherson G. J., Bar-Matthews M., Tanaka T., Olsen E., Grossman L. (1983) *GCA* ***47***, 823; [15] MacPherson G. J. et al. (1984) *JGR* ***89***, *Suppl.* C299, [16] Hashimoto A. & Grossman L. (1987) *GCA* ***51***, 1685, [17] Cohen R. (1985) Met. Soc. Meet. Bordeaux, [18] Kubovics I., Gál-Sólymos K., Bérczi Sz., Ditrói-Puskás Z., Nagy B. (1998) *LPSC XXIX*. 1120.pdf, [19] Kornacki A. S., Fegley B. (1984) *JGR* ***89***, Suppl. B588; [20] Kornacki A.S. Wood J.A.(1984) *JGR* ***89***, Suppl. B573; [21] Fegley B., Post J. E. (1985) *EPSL* ***75***, 297; [22] Scott E.R.D., Lusby D., Keil K. (1985) *JGR* ***90***, *Suppl.* B5137; [23] Roedder E., Weiblen P.W. (1974) *LSC V*. 639; [24] Meyer C. (1987) NASA Cur. Br. Publ. No. 76. Houston, [25] Norris, J.A., Keller, L.P., McKay D.S., (1992): *Workshop Geol. Apollo 17 Landing Site*, LPI Techn. Rep. No. **92-09**, Part I. 44, [26] Symes S.J.K. (1997) *LPSC XXVIII*. 1405, [27] Taylor S.R. (1973) *Earth Sci. Rev.* **9.** 101, [28] Pieters C., McCord T.B. (1974) *LSC V*. 605, [29] Li C-L., Ouyang Z-Y., Liu D-S., An Z-S. (1989) *Science in China,* **36,** 9. [30] Glass B.P., Burns C.A., Crosbie J.R., DuBois D.L. (1985) *JGR,* ***90, Suppl.*** D175, [31] Iwahashi J., Yoshida M., Miono S., Santosh G., Santosh M. (1991) *Proc. NIPR Symp. Antarct. Meteorites,* **4,** 420; [32] Miono S., Ono H., Nakayama Y., Shoji M., Nakanishi A. (1991) *Proc. NIPR Symp. Antarct. Meteorites,* **4,** 436, [33] Kotaro Ishida, Masayuki Yamashita, Hiroaki Ishiga (1992) *Geol. Rept. Shimane Univ.* ***11***, 39; [34] Tóth I., Detre Cs., Solt P., Don Gy., Dosztály L., Siegl-Farkas A., Uzonyi I., Bérczi Sz., Lukács B. (1997): *LPSC XXVIII*. 179, [35] Murray J., Renard A.F. (1891): Rep. Sci. Res. of H.M.S. Challenger, 1873; [36] Koeberl C., Hagen E.H. (1989): *GCA*, **53,** p. 937. [37] Sears D.W.G., S. Huang, Akridge G., Benoit P. (1996) *LPSC XXVII*. 1165, [38] Delano J.W., Lindsley D.H. (1982) *GCA*, **46,** 2447; [39] Zbik M, Gostin V.A. (1994) *ANTARCTIC METEORITES XIX*. 169; [40] Raukas A. et al. (1996) in: *Spherules and Global Events*, KFKI-1996-05/C, 59, [41] Tazawa Y. et al. (1995) *Proc. NIPR Symp. Antarct. Meteorites,* **8.** 249; [42] Claeys P., Casier J-G., Margolis S.V. (1992) *Science*, **257,** 1102; [43] Girad C., Robin E, Rocchia R., Froget R., Feist R. (1997) *Palaeo*, **132**, 391; [44] Zolensky et al. (1997) NASA Up. Atm. Cat. JSC, Houston, [45] Miono S. et al. (1998) *LPSC XXIX*. 1029.pdf, [46] Miura Y., Fukuyama S., Kobayashi H., Gucsik A. (1998) *LPSC XXIX*. 1550.pdf, [47] Detre Cs., Tóth I., Gucsik A., Kiss A., Uzonyi I., Bérczi Sz., (1998) *LPSC XXIX*. 1030.pdf, [48] Hassler S. W., Simonson B. M. (1998) *LPSC XXIX*. 1086.pdf, [49] Glass B. P., Koeberl C. (1998) *LPSC XXIX*. 1679.pdf, [50] Ruzicka A., Snyder G. A., Patchen A. D., Taylor L. A. (1998) *LPSC XXIX*. 1434.pdf, [51] Ruzicka A., Snyder G. A., Patchen A. D., Taylor L. A. (1998) *LPSC XXIX*. 1436.pdf, [52] Lindstrom D. J., Symes S.J.K., Martinez R.R. (1998) *LPSC XXIX*. 1799.pdf, [53] Deutsch A., Pesonen L.J., Freshake A., Pihlaja P., Kettrup D. (1998) *LPSC XXIX*. 1377.pdf, [54] Genge M.J., Grady M. (1998) *LPSC XXIX*. 1808.pdf, [55] Engrand C., McKeegan K.D., Leshin L.A., Grownlee D.E. (1998) *LPSC XXIX*. 1473.pdf,

FOLIATED KABA, CV3 CHONDRITE

Sz. Bérczi[1,2], Gy. Don[3], K. Gál-Sólymos[1], I. Kubovics[1], B. Lukács[4], K. Martinás[5], B. Nagy[6], Z. Puskás[1], P. Solt[3],

[1]Eötvös University, Dept. Petrology, Geochem., H-1088 Budapest, Múzeum krt 4/a. Hungary,
[2]Eötvös University, Cosmic Mat. Res. Gr. Dept. G. Technology, H-1088 Budapest, Rákóczi út 5.
[3]Hungarian Geological Institute, Cosm. Mat.Res.Gr. H-1146 Budapes, Stefánia út 14. Hungary,
[4]Central Res. Inst. Physics RMKI, Hung. Acad. of Sci. H-1525 Budapes, P.O.Box 49.Hungary,
[5]Eötvös University, Department of Atomphysics., H-1088 Budapest, Puskin u. 5-7. Hungary
[4]Hungarian Academy of Sciences, Xth. Class Off., H-1055 Budapes, Nádor u. 7. Hungary

HISTORICAL

Kaba carbonaceous chondrite has been stored at the Reform Church College at Debrecen, Hajdú-Bihar County, Hungary since its fall on 15th April, 1857. A new thin section at the Eötvös University, Budapest, has been prepared and studied. This larger surface, (ca. 4 cm^2) showed distinguished textural characteristic over the great variability of the unequilibrated textural components. This was an overall foliation, a kind of layered or laminated textural map. About 20 lineated textural elements were found on this surface, of which we report here some interesting arrangement. Reambulation of the strewn field served new spherule-like fragments of Kaba, too.

INTRODUCTION

The role of Kaba

- After the first general studies of Sztrókay et al. in 1961 [1] on KABA the modern petrographic descriptions of KABA considered (1.) classification of carbonaceous chondrites, [2-6], (2) showed the presence of condensational sequence minerals in white inclusions, CAI-s and AOA-s in carbonaceous chondrites [7-12], and discovered the presence of aquaeous alteration products in the carbonaceous chondrites, [13-15]. of these chondrites were always attractive and emphasized.

Actuality

- Research to solve fayalite origin in CV3 carbonaceous chondrites goes back to the early 90 years by [14-15]. But the metamorphic processes related global laminated texture was not mentioned yet.

We and other groups studied KABA material in order to reveal global thermal evolutionary history of this extraordinary carbonaceous chondrite and to summarize fayalite origin and layered structure of Kaba, although **Krot** et al. [26-27], with various arguments, have shown the role of **aquaeous alteration and subsequent dehydration** in formation of fayalitesm, both in Kaba and in other CV3 carbonaceous chondrites.

TEXTURE

The 42 BSE photographs of the new thin section made aboput Kaba were used to fit a large image. This image exhibited the overall oriented texture, which is well expressed not only by inclusion like objects but by the fine structure of matrix. The larger elongated inclusions have longer dimensions more than 1 mm in the direction of the overall foliation, and smaller than 1 mm perpendicular to it. Their number of more than 20 shows that not a selected region but a randomly selected part of the inner structure exhibits the phenomenon. (Large surface helped only the observation and recognition of this characteristic.) The general textural appearance of the thin section shows that in other respects this Kaba section is regular. Other CV3 carbonaceous chondrites also exhibit layered texture in a hand specimen overview, like Leoville, Allende (L. Grossman, 1998, personal communication), but the **layered-foliated character on the level of thin section** (and moreover on BSE image resolution) **has not been reported earlier**. [28].

Chondrules

Chondrule sizes vary between 0.2 and 3.5 mm in diameter. Many types of chondrules: can be seen in the matrix like as porphyritic olivine, granular, radial pyroxene and barred olivine types. The layered chondrules are common phenomena while mixed layered chondrules, where silicates and opaques form layers, also occurs as well. Chondrule cores are frequently surrounded by a ring of opaque belt and this is a common characteristic with CR chondrites [18]. Higher resolution BSE images revealed the structure of the opaque grains of these opaque belts because large majority of different coexisting metal, magnetite and sulfide assemblages can be found in the chon-

drules themselves.

Matrix: Fayalite, Magnetite, Maghemite

The Kaba matrix is composed mainly from olivine, which has variable fayalite content and contains olivine crystals in groups (up to 100 micrometers). These single or grouped olivines has rims with considerable fayalite component. Matrix also contains magnetite [1], and maghemite (Márton, [19], Vértes A., pers. comm. 1997). Matrix also contains sulfides: pentlandite and traces of troilite.

Inclusions

There are different types of refractory inclusions in KABA, [23-25]. We have found one remarkable spinel-rich spherule with 150 micrometers diameter. The BSE image showed the core: inner lighter spinel with considerable FeO content (pleonaste), and darker outer microcrystalline region of Mg-Al spinel. Remarkable enough, but well known from earlier works (strongly resembling to BB-1 from Murchison of [21] in size and character [23]) is, that the pleonaste inner region contained small (ca. 5 micrometers in diameter) perovskite grains. They are almost uniformly scattered throughout the spinell region. The spinel-perovskite chondrule or spherule has a Wark-Lovering type rim.

REAMBULATIONS ON KABA STREWN FIELD

The parallel work of strewn field reambulation (Solt, 1996) has produced more then 500 spherulitic fragments. The distribution of the different spherula types sketch the shape of the strewn field on the local area NW of Kaba village. This fragmentation zone also shows the falling direction. Special type of fragments, that is for example spherules in a matrix detect the real strewn filed of the meteorite. We use PIXE and INAA analyses (mainly the REE content of fragments) to separate real meteoritic fragments from those ones transported to the collecting area by other events.

SUMMARY

Our studies on the new thin section of KABA showed that an overall foliated, oriented, laminated type texture can be discovered on it. This is a new result not mentioned in earlier KABA studies and it is in accord with the fact that Kaba might have been an outer shell fragments from the CV3 type parent body. This foliation, the layered chondrules, spinel-rich inclusions, opaque assemblages are also common characteristics with other CV3 chondrites (Allende, Mokoia, [22-25]).

ACKNOWLEDGEMENTS

This work has been supported by the OTKA T 026660, HJSTC 31/96 and OMFB 96-97-47-1265-MÜI-TP-055/96 (ELTE 33131/6) grants.

REFERENCES

[1] Sztrókay K., Tolnay V., Földváriné Vogl M. (1961): *Acta Geol. Hung.* **7**. 17.; [2] Wiik, H. B. (1956) *GCA 9*, 279-289; [3] Van Schmus W. R. & Wood J. A., (1967) *GCA **31***, 737-765; [4] Wood, J. A. (1967) *GCA **31***, 2095; [5] Van Schmus W. R. & Hayes J. M. (1974) *GCA **38***, 47-64; [6] McSween H. Y. (1977) *GCA **41***, 1777-1790; [7] Grossman L. (1975) *GCA **39***, 433-454; [8] MacPherson G. J. & Grossman L. (1984) *GCA **48***, 29-46; [9] Blander M. & Fuchs L. H. (1975) *GCA **39***, 1605-1619; [10] Kornacki A. S. & Wood J. A. (1984) *GCA **48***, 1663-1676; [11] Wark D. A. & Lovering J. F. (1982) *GCA **46***, 2595-2607; [12] Kornacki A. S. & Fegley B. (1984) *JGR **89***, Supplem. B588-B596; [13] Hashimoto A. & Grossman L. (1987) *GCA **51***, 1685-1704; [14] Keller L. P. & Buseck P. R. (1982) *GCA **54***, 2113-2120; [15] Tomeoka K. & Kojima T. (1995) *Antarctic Meteorites XX*. NIPR Symp. Abstr. 252-254; [16] Wilkening L. L. (1978) *Naturwissenschaften, **65***, 73-79. [17] McSween H. Y. *(1979) Rev. Geophys. Space Phys.* **17**. 1059; [18] Weisberg M. K., Prinz M., Clayton R. M., Mayeda T. K. (1993) *GCA **57***, 1567-1586; [19] Márton P. (1996) *Annales Univ. Sci. Bud. R. Eötvös N. Sect. Geophys.* & Meteor. ***XII***, 33-49; [20] Rubin A. E. (1984) *GCA **48***, 1729-1739; [21] MacPherson G. J., Bar-Matthews M., Tanaka T., Olsen E., Grossman L. (1983) *GCA **47***, 823-839; [22] Cohen R. E., Kornacki A.S., Wood J. A. (1983) *GCA **47***, 1739-1757; [23] Fegley B. & Post J. E. (1985) *EPSL **75***, 297-310; [24] Liu I.-G. & Schmitt R. A. (1988) *LPSC XIX*, 684-685; [25] Liu I.-G., Schmitt R. A., Holmen B. A., Wood J. A., Kring D. A. (1988) *LPSC XIX*, 686-687, [26] Krot A.N., Scott E.R.D., Zolensky M.E. (1996) *LPSC XXVII*, 711-712, [27] Krot A.N., Scott E.R.D., Zolensky M.E. (1997) *Meteoritics and Planetary Science*, **32,** 31-49, [28] Kubovics I., Gál-Sólymos K., Bérczi Sz., Nagy B., Puskás Z. (1998) *LPSC XXIX, 1120*,

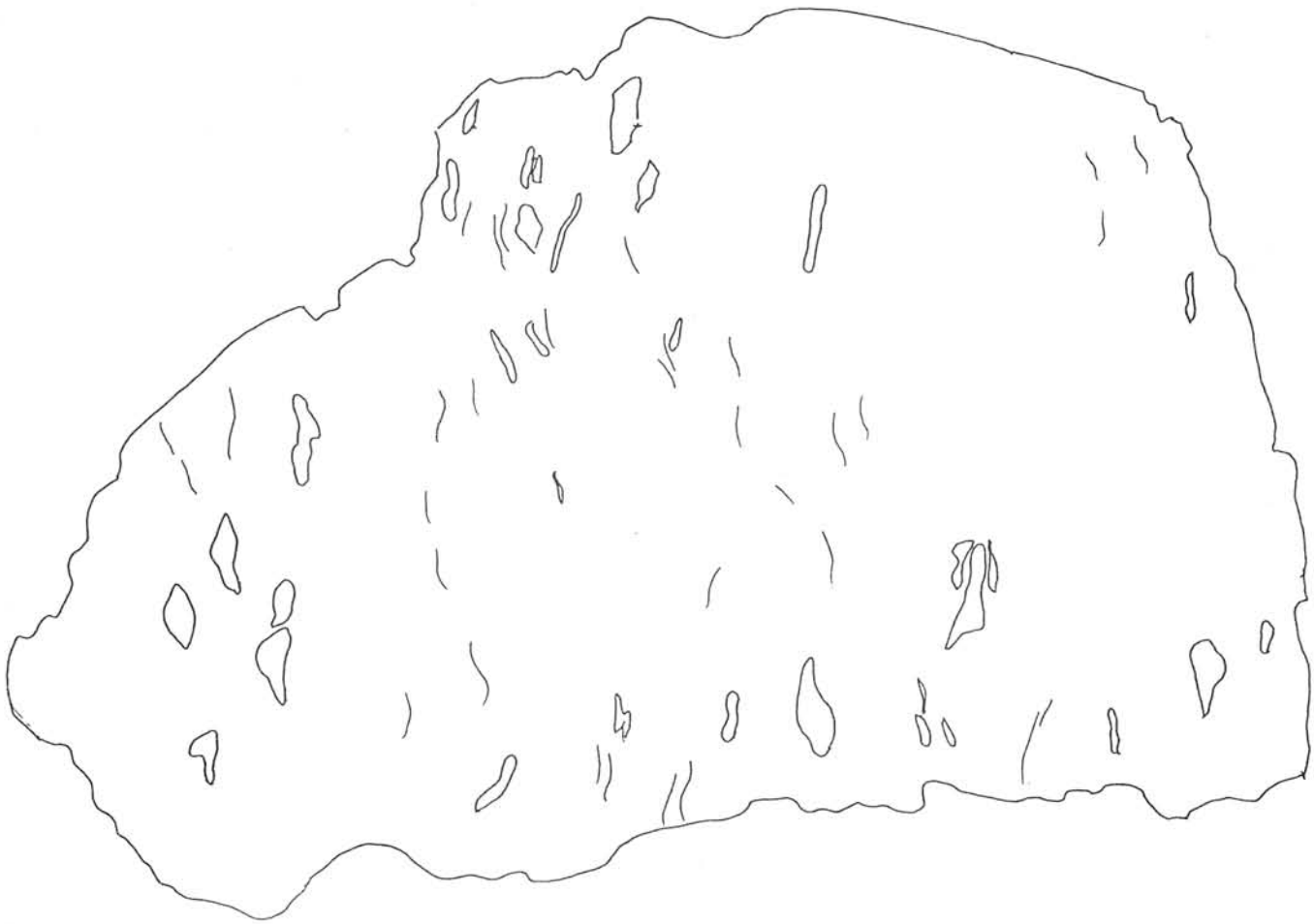

Fig. 1. Sketch of the overall foliated texture of Kaba CV3 chondrite. The sketch field is about 2 cm X 3 cm at edges.

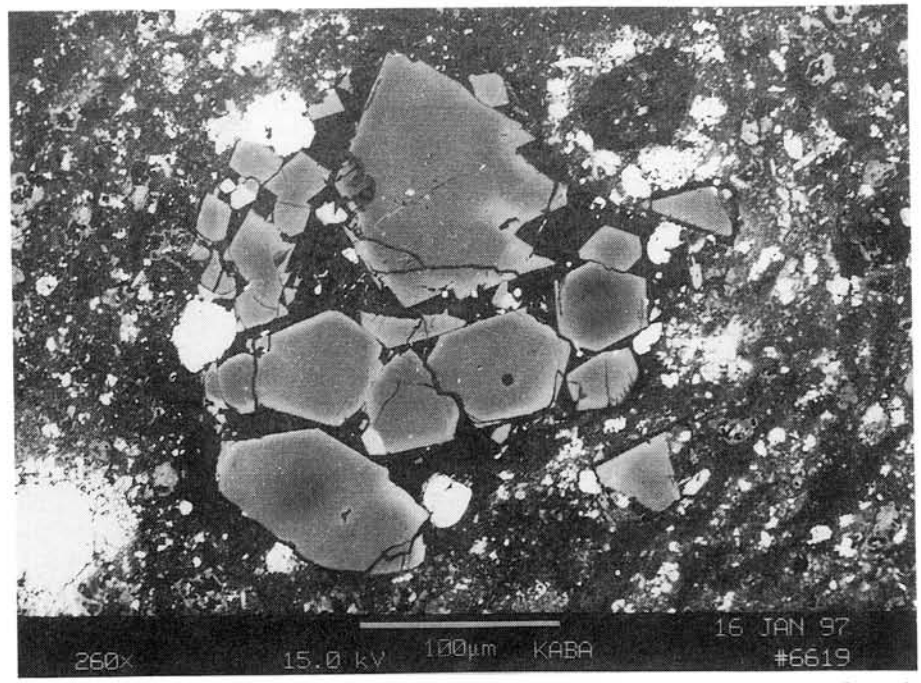

Fig. 2. Fayalite rims around large olivine crystals in the Kaba matrix.

Daubreelites in the EH3 chondrite MAC88180 and primitive EH chondrites: Assemblage and mineral chemistry

J. Chikami [1,2], A. El Goresy [2] and J. Janicke [2]

[1]Mineralogical Institute, Graduate School of Science, University of Tokyo, Bunkyo-ku, Hongo 7-3-1, Tokyo 113 Japan, chikami@min.s.u-tokyo.ac.jp

[2]Max-Planck-Institut für Kernphysik, Postfach 103980, 69029 Heidelberg, Germany

Introduction

Depletion of bulk Zn in chondrules compared to the concentration in matrices of various chondrites have been reported earlier (Grossman and Wasson, 1985; Wilkening et al., 1984; Rubin and Wasson, 1987; Kallemeyn and Wasson, 1981; Brearley et al., 1995). The following possible alternative mechanisms for Zn depletion in chondrules have been suggested by Palme (1988): evaporation, absence of precursor materials, or phase separation of Zn-bearing material. Recently, using X-ray microprobe techniques, Schnabel et al., (1998) demonstrated that chondrules in Semarkona (L), Muchison (CM) and ALH83100 (CM) display lower Zn contents than their matrices and that Zn in chondrules increases rimward. They suggested a diffusive mechanism to explain this phenomenon. Yet, the origin of Zn depletion in chondrules remains enigmatic and the mechanisms proposed are controversial.

Under the reducing condition prevailed during the formation of enstatite chondrites, Zn is chalcophile and is mainly cited in sphalerite (ZnS) and less in daubreelite (Cr_2FeS_4). MAC88180 is an EL3 chondrite (El Goresy et al., 1992) that contains large chondrules (1 cm in diameter) with daubreelite but no sphalerite. Daubreelite is also present in the matrix, however with sphalerite. This contrasting settings of Zn-bearing phases of chondrule and matrix in MAC88180 makes this meteorite suitable to investigate the relative abundances of Zn in both units and to address the Zn depletion issue in chondrules.

Zhang et al., (1995) suggested that EH and EL experienced a similar range of equilibrium temperatures, but texturally the EL chondrites appear to have experienced much higher levels of metamorphic equilibration than EH of similar equilibrium temperature. Our goal in this study is to compare the chemical abundances of minor elements in sulphides in MAC88180 (EL3) chondrite with those in ALH77295, Y74370 and Qingzhen (EH3) chondrites. In addition, we intended to explore the influence of the mineral assemblages on the distribution patterns of the minor elements in the sulphide species in EH and EL.

Samples and analytical methods

Daubreelite-bearing assemblages in polished sections from MAC88180,ALH77295, Y74370 and Qingzhen were studied in reflected light microscopy, scanning electron microscopy (SEM) and electron probe microanalyzer (EPMA). SEM observations were carried out with a Cambridge 180S scanning electron microscope and a Tacor Northern 5500 system. Quantitative analyses of the mineral phases were performed with an automated, computer controlled, SEMQ electron microprobe using wave-length dispersive procedures. Analyses were conducted at accelerating voltage of 15 kV and sample current is 24nA on brass. Pure synthetic stoichiometric Na-free daubreelite was used as an internal standard to monitor low Na concentrations in meteoritic daubreelite. The data were corrected for background, beamdrift, and matrix effects using conventional ZAF corrections.

Results

MAC88180 contains plenty of daubreelite grains (largest grain is 90 microns in diameter) in both chondrule and matrix. The daubreelite grains coexist with troilite, metal, silicate or alabandite. Daubreelite grains in MAC88180 show distinct chemical signatures as follows. (1) They are Na-free. (2) They contain significant amounts of Cu (0.4-0.6 wt%). (3) They have high Mn concentrations (0.7-1.6 wt%). (4) They are rich in Zn (~2.9 wt%). The Zn contents of daubreelite in matrix are higher than in chondrules. (5) They display significant

Ti concentrations (~0.18 wt%). Also the Ti content of daubreelite is different in matrix and chondrule. Table 1 summarized these results. (6) Daubreelite displays chemical zoning from to the adjacent troilite. The Cr and S contents degrease from the daubreelite core to rim, while the Fe-content is increasing along the same path. This reminiscent of Fe diffused from troilite to daubreelite and of Cr from daubreelite to troilite.

Discussion

Wilkening et al., (1984) reported that the interiors of the Chainpur carbonaceous chondrules are only slightly depleted in Zn relative to the whole rock. They noted that in terms of their compositions, matrix and chondrules are similar to one another. Our findings of different Zn contents of daubreelite in chondrule and matrix are inconsistent with Wilkening et al., (1984). They are in agreement with the Zn depletion in bulk chondrules reported by several groups (Grossman and Wasson, 1985; Wilkening et al., 1984; Rubin and Wasson, 1987; Kallemeyn and Wasson, 1981; Brearley et al., 1995). Since sphalerite is absent in chondrules, Zn is contained only in daubreelite. Zn depletion in daubreelite in chondrules thus signals bulk Zn depletion in chondrule.

Schnabel et al., (1998) reported that Zn is enriched in chondrule rim. They suggested that this is the result of inward diffusion of Zn from the surrounding material. We compared the Zn content of a daubreelite in the middle of a chondrule with that of another one at the boundary between chondrule and matrix. Our results are in accord with the findings of Schnabel et al. (1998). Zn is below detection limit in the core daubreelites (3 grains) while daubreelites at the boundary show high concentrations (0.1-0.5 wt%; 3 grains). Although our statistics are limited, the results indeed hint to the diffusion mechanism.

Greenland and Goles (1965) suggested that the Cu/Zn ratio is highly variable among carbonaceous, enstatite, ordinary chondrites indicating fractionation of Cu from Zn at some stage of their history. Our study indicates that the Zn content in matrix daubreelites is higher than in chondrule. In contrast the Cu content is similar in daubreelites of both chondrule and matrix. This may indicate Cu/Zn fractionation. The different behavior between Cu and Zn may be caused by the different volatility of these elements (condensation temperature of Cu is 1037°C, of Zn is 660°C; Palme, 1988). This suggests that either daubreelite in the MAC88180 chondrule was formed first after Zn is depleted at the stage of chondrule formation, or daubreelite in MAC88180 chondrule was produced from Zn-depleted material at 660-1037°C.

Ti content of daubreelite in chondrule and matrix are different. Chondrule contains lower modal abundance of sulfides mineral than matrix. We have also measured Ti content of troilite coexisting with daubreelite between in chondrule and matrix. There is no different Ti content of troilite between in chondrule and matrix.

We have compared the chemical compositions of daubreelites in MAC88180 with those in EH3 chondrites (ALH77295, Y74370 and Qingzhen) (Table 1). It is conceivable that the Zn content of daubreelite depends on the bulk modal abundance of Zn and on the partitioning coefficient of this element at the given temperature between daubreelite and sphalerite (ZnS). We have confirmed the presence of sphalerite with optical microscopy and SEM and compared MAC88180 with Y74370 and Qingzhen which have almost similar very low modal abundance of sphalerite. The Zn content of daubreelite in MAC88180 is lower than those in Y74370 and Qingzhen. This result is in agreement with the reported different bulk Zn contents in EH and EL chondrites (Palme, 1988). The Cu content (0.4-0.6 wt%) in MAC88180 daubreelites is slightly higher than that in EH3 chondrites (0.03-0.2 wt%). Also the Ti content is slightly higher than that in EH. This result is consistent with the different Ti contents in troilite in EH and EL (Zhang et al., 1995).

We have found that daubreelites in MAC88180 are chemically zoned. The microprobe profiles of daubreelite to the adjacent troilite show decrease in both Cr and S and increase in Fe. This is indicative of Fe diffusion from troilite into daubreelite and Cr and S diffusion from daubreelite into troilite. The chemical zoning from daubreelite to metal shows the same trend as those from daubreelite to troilite. These reverse zonings of daubreelites were also found in Qingzhen (EH3). The zoning in Qingzhen is in agreement with the reverse zoning

in ningerite to troilite reported before (Ehlers and El Goresy, 1988), reverse zoning in sphalerite and the young $^{39}Ar/^{40}Ar$ age (2.88 b.y.) (Müller and Jessberger, 1985). These findings are strong arguments for planetary endogenic process in both EL and EH. The reverse zoning of daubreelites may have resulted from thermal, probably planetary metamorphic episodes.

Conclusions

1) Zn content of daubreelite in MAC88180 chondrule is lower than that in matrix. This suggests that chondrule was produced from Zn depleted precursor.

2) Cu and Zn in daubreelite show different behavior in chondrule and matrix. This is the result of their different volatilities.

3) The different abundances of minor elements in EH and EL are consistent with the difference of their bulk composition.

4) The reverse chemical zoning of daubreelite in MAC88180 suggests a thermal metamorphic episode like in the Qingzhen EH3 chondrite.

Acknowledgments

This work was supported by JSPS Research Fellowship for Young Scientists (J. C.) and by the scholarship of Deutcher Akademischer Austauschdienst (DAAD).

References

Brearley A. J. et al., (1995) GCA, 59, 4307-4316.
Ehlers K. and El Goresy A. (1988) GCA, 52, 877-887.
El Goresy et al., (1992) LPSC, XXIII, 331-332.
Greenland L. and Goles G. G.(1965) GCA, 29, 1285-1292.
Grossman J. N. and Wasson J. T. (1985) GCA, 49, 925-939.
Kallemeyn G. W. and Wasson J. T. (1981) GCA, 45, 1217-1230
Müller N and Jessberger E. (1985) LPSC, XVI. 595-596..
Palme H.: Kerridge J. F. and Matheus M. S. (1988) Meteorites and the early solar system, 1269pp
Rubin A. E. and Wasson J. T. (1987) GCA, 45, 1217-1230.
Schnabel C. et al., (1998) LPSC
Wilkening L. L. et al., (1984) GCA, 48, 1071-1080.
Zhang Y. et al., (1995) JGR, 100, 9417-9438.

Table 1 chemical composition of minor elements in EH3 and EL3 daubreelites (wt%)

			Zn	Na	Cu	Ti	Mn
ALH77295	EH3	Coexiting with sphalerite	~7	0.4-0.5	0.04-0.08	-	0.3-0.5
		Others	4.0-5.0	~0.3	0.04-0.08	-	1.5-1.8
Y74370	EH3		2.3-3.5	0.15-0.22	0.07-0.17	0.02-0.07	0.35-0.53
Qingzhen	EH3		4.0-8.0	0-0.8	0.07-0.3	~0.04	~0.5
MAC88180	EL3	Matrix	0.8-2.85	-	0.4-0.6	0.05-0.14	0.7-1.6
		Chondrule	0-0.53	-	0.4-0.6	0.14-0.18	0.7-1.6

Mineralogical study of daubreelite in Qingzhen EH3 chondrite

J. Chikami[1)2)], A. El Goresy[2)] and J. Janicke[2)]
[1)] Mineralogical Institute, Graduate School of Science, University of Tokyo, Hongo 7-3-1, Bunkyo-ku, Tokyo 113, JAPAN [2)] Max-Planck-Institut für Kernphysik, Postfach 103980, 69029 Heidelberg, Germany
chikami@min. s. u-tokyo. ac. jp

Introduction:

In this study we will focus on daubreelite ($FeCr_2S_4$) which is one kind of thiospinel and has the spinel structure, in Qingzhen, enstatite chondrite. Daubreelite is found in only a few highly reduced and sulfur-rich meteorites. The enstatite chondrites are the most reduced group among chondritic meteorites. Because of this reduced condition, enstatite chondrites sometimes contain daubreelites. Based on differences in Fe/Si versus Mg/Si ratios, Sears et al., (1982) suggested two groups in the enstatite chondrites; (a) EH (high iron) and (b) EL (low iron). The unequilibrated members of the EH chondrites are enigmatic and the least understood among the enstatite chondrite clan. We have performed the mineralogical study for Qingzhen meteorite which is one of EH3 chondrites. The compositional differences of ningerite, kamacite and perryite reveal the presence of three subgroups in the EH group in order of increasing f_{S2} and decreasing f_{O2} (El Goresy et al., 1988). Qingzhen is considered to belong to the third subgroup same as Y74370, South Oman, Kota Kota, Kadium II and St. Marks (El Goresy et al., 1988) and to be the least equilibrated among the EH group (Okada et al., 1975: El Goresy et al., 1983; El Goresy et al., 1986; Ranbaldi et al., 1983). El Goresy et al., (1988) reported the troilite - daubreelite clasts in Qingzhen meteorite. It consists of major troilite with daubreelite and occasionally hydrated Na-Cr sulfide. They also reported (1) all daubreelites contain considerable amounts of Na. This is the first report of Na in a spinel-type mineral in meteorites. (2) Daubreelites in Qingzhen contain the highest Zn content ever found in EH chondrites. We have conducted mineralogical study about details of daubreelites in Qingzhen.

Sample and method:

Qingzhen was supplied from Institute of Geochemistry, Academia Sinica, China. Daubreelite-bearing assemblages in polished section from Qingzhen, was studied in reflected light, scanning electron microscopy (SEM) and electron probe microanalyzer (EPMA). SEM observations were carried out with a Cambridge 180S scanning electron microscope and a Tacor Northern 5500 system. Quantitative analyses of the mineral phases were performed with an automated, computer controlled, SEMQ electron microprobe. The analyses of daubreelite were corrected for background, beamdrift, and matrix effects using the conventional ZAF corrections. The accelerating voltage is 15 kV and beam current is 24nA. Pure synthetic Na-free daubreelite was used as an internal standard to monitor low Na concentrations in meteoritic daubreelite.

Results:

We have observed some daubreelite assemblages. 1) daubreelite - hydrated Cr sulfide - troilite - FeNi metal and 2) daubreelite - troilite - FeNi metal. The sizes of daubreelites which we have observed are 3 - 20 micro meters.

We performed the quantitative analysis for daubreelite grains. We have found that some daubreelite grains do not contain Na (under the detection limit), although it was reported that daubreelites in Qingzhen contain considerable amounts of Na (0.2-0.45 wt%) (El Goresy et al., 1988). We have analysed several daubreelite grains in three different portion. These grains do not contain significant Na (at most, 0.07 wt%). These daubreelites are located in portions where contain hydrated Cr-rich sulfide (Mineral A).

The range of Zn content in daubreelite grains which we have analysed are from 4.5 wt% to 8.7 wt%. This range is wider than the value which has been reported before (5.70-8.11 wt%) (El Goresy et al., 1988).

We have found the chemical zoning in daubreelite grains. This is the first report of the chemical zoning in the meteoritic daubreelite. The daubreelite grains in Qingzhen meteorites are not so large (at most 20 micro meters) for EPMA analysis. They contain many cracks. Because of these reasons, we could not get the line profile from daubreelite to next mineral. We compared the chemical composition of core to rim in daubreelites.

1) daubreelite next to hydrated Cr-sulfide

We have also compared the chemical composition between core and rim in daubreelite grains next to hydrated Cr-sulfide. The sizes of these daubreelites is 10-20 micro meters. We found that Cr, Fe, Zn contents in daubreelite are increasing from core to rim (Cr: 34.1-35.3, 33.5-34.1, 34.2-34.4; Fe: 12.2-12.7, 12.5-12.5, 12.4-12.5; Zn: 7.82-8.03, 8.14-8.50, 8.62-8.70 wt%), while S contents is decreasing towards rim (S: 43.6-43.5, 44.9-44.5, 45.5-45.4 wt%). But in another grain, Fe content is increasing towards rim (Fe: 12.57-12.94 wt%) and Cr and S content are decreasing (Cr: 35.91-35.30, S: 43.83-44.22). The chemical zoning from daubreelite to hydrated Cr-sulfide is controversial. The mineral next to the daubreelites which show the chemical zoning may be hydrated Cr-sulfide. High magnification BSE imaging with the SEM indicates that this mineral surrounds the daubreelite grains and they show much darker colour than daubreelites. We have performed the quantitative analysis for this mineral. Analysis totals usually sum to values 88%. The mineral contains Na (0.27-1.68 wt%). It also contains variable Fe content (0.87-2.97 wt%). The Cr and S contents are Cr; 35.7-36.5 wt% and S; 48.8-50.4 wt%. We guess that the low totals are due to the presence of H_2O or OH. The chemical composition of this mineral shows a similarity with mineral A which in Qingzhen by El Goresy et al., (1988).

2) daubreelite next to troilite

We have found some daubreelite grains (10-15 micro meters) whose next minerals are troilites. They show the chemical zoning from core to rim. Fe content is increasing towards rim (Fe: 14.31-17.16, 12.72-15.40 wt%), while Cr and S content are decreasing towards rim (Cr: 35.14-32.98, 34.84-32.81, S43.57-42.28, 44.37-42.54 wt%). As regards as Zn, it is controversial. We have analysed also the troilite grains next to these daubreelites. Troilite grains also show the chemical zoning. In troilite, Cr and S are increasing towards rim, while Fe is decreasing.

3) daubreelite next to Cr-Fe-Zn rich sulfide.

We have found Cr-Fe-Zn-rich chemical composition at the boundary between daubreelite and troilite. The size of this grain is about 3 micro meters. The BSE image shows heterogeneous composition. There is two possibilities. One is new phase of sulfide and another is a mixture of spharelite and daubreelite. The daubreelites show chemical zoning towards this composition. Zn content is increasing towards rim, while Cr and S content are decreasing.

4) daubreelites next to metal

We have found some daubreelites next to FeNi-metal. The size of these daubreelites is 10 micro meters. We compared the chemical composition of these daubreelites between core and rim. Fe content is increasing towards rim (Fe: 12.66-14.70, 12.34-18.71 wt%), while Cr and S contents are decreasing (Cr: 35.24-34.70, 35.39-32.08, S: 43.46-43.14, 42.14-38.53 wt%). The behaviour of Zn is different in each grain.

Discussion:

The daubreelites which we have analysed do not contain Na, although other daubreelites contain significant Na content (El Goresy et al., 1988). The next minerals to these daubreelites are Mineral A. It may be a possible explanation that daubreelites next to Mineral A do not contain significant Na content because Na prefer to retain in Mineral A. Na content of Mineral A next to the daubreelites is our study;

0.27-1.68 wt%, the former report; 1.13-1.14 wt% (El Goresy et al., 1988). The chemical composition of Mineral A shows heterogeneous, too. Mineral A usually occurs as thin lamellae in daubreelite. We do not think that no Na content of these daubreelites is due to the presence of the next Mineral A, that is, Na diffusion from daubreelite to Mineral A. It is not consistent with the facts that Mineral A is usually occurred as lamellae in daubreelite (maybe daubreelites in the former reports coexist with Mineral A. We suggest that Na is heterogeneous distributed in Qingzhen.

Zn content of core daubreelite shows various content from one to another grain (El Goresy et al., 1988.) We have also found various Zn content in one grain. Daubreelite grains in Qingzhen is not homogeneous for Zn. We could not find systematic Zn behaviour among daubreelite grains in Qingzhen. Qingzhen is unequilibrated enstatite chondrite. The variation of Zn content may be reflected inhomogeneous accretion in the solar nebular.

We could not find the consistent chemical zoning trend from daubreelite to hydrated Na-Cr- sulfide. Hydrated Na-Cr- sulfide in Qingzhen were never observed to occur with caswellsilverite ($NaCrS_2$) (El Goresy et al., 1988). They always occur with daubreelites as oriented intergrowth and with troilite (El Goresy et al., 1988). They also suggested the hydrated Na-Cr- sulfide in Qingzhen as products of preterrestrial events. The fact that the daubreelite next to Mineral A do not show the consistent chemical zoning, may suggest that it is not enough time to diffuse elements between daubreelite and Mineral A. Mineral A may be produced on young age. We need further study about it.

We have found the chemical zoning of daubreelites in Qingzhen. The chemical zoning from daubreelite to troilite shows Cr and S decreasing and Fe increasing. This is indicative of Fe diffusion from troilite into daubreelite and Cr and S diffusion from daubreelite into troilite. The chemical zoning from daubreelite to metal shows the same trend as those from daubreelite to troilite. Fe is increasing towards rim and Cr and S are decreasing. These reverse zoning of daubreelites in Qingzhen is in agreement with the reverse zoning from ningerite to troilite (Ehlers and El Goresy, 1988), zoning of spharelite and young $^{39}Ar/^{40}Ar$ age (2.88 b.y.) (Müller and Jessberger, 1985). These facts are strong evidence for planetary endogmatic process. The reverse zoning of daubreelites may have resulted from thermal, probably planetary metamorphic episodes. But Zn behaviour in daubreelites is not consistent in each grain. The diffusion coefficient of Zn may be large and Zn may diffuse very slowly. Zn behaviour in daubreelites may keep primary signature.

Conclusions:

1) We have found Na-free daubreelite and wide range of Zn content in daubreelites of Qingzhen. The variety of Na and Zn content of daubreelite suggest inhomogeneous accretion in the solar nebula.
2) The reverse zoning from daubreelites to troilite and metal suggest the thermal and planetary metamorphic episode.

Acknowledgements:

We are grateful to Quyang Ziyuan, Institute of Geochemistry, Academia Sinica, China for the loan of the Qingzhen meteorite. This work was supported by JSPS Research Fellowship for Young Scientists (J. C.) and by the scholarship of Deutcher Akademischer Austauschdienst (J. C).

References:

Ehlers K. and El Goresy A. (1988) GCA, 52, 877-887.
El Goresy A. et al., (1983) Meteoritics, 18, 293-294.
El Goresy A. et al., (1986) LPSC, XVII, 202-203.
El Goresy A. et al., (1988) Proc. NIPR Symp. Antarct. Meteorites, 1, 65-101.
Müllers N. and Jessberger E. (1985) LPSC, XVI, 995-996.
Okada A. et al., (1975) Mem. Natl. Inst. Polar. Res., Spec. Issue, 5, 67-82.
Rambaldi E. R. et al., (1983) LPSC, XIV, 626-627.
Sears D. W. et al., (1982) GCA, 46, 567-608.

A NEARBY SUPERNOVA EXPLOSION AT THE PERMO-TRIASSIC BOUNDARY

Cs. H. Detre *, I. Toth**, Gy. Don*, P. Solt*, A. Gucsik***, A. Z. Kiss****, I. Uzonyi****, Sz. Berczi*****

* Geological Institute of Hungary, Stefania ut 14, H 1143 Budapest, Hungary,
** Konkoly Observatory, Budapest P.O. Box 67-II 1525, Hungary,
*** Dept. of Earth Sciences, Yamaguchi University, 1677-1, Yoshida, Yamaguchi 753, Japan,
**** Institute of Nuclear Research, ATOMKI, Debrecen P.O. Box 51, H-4001 Hungary,
***** Dept. of Petrology and Geochemistry, L. Eotvos University, Rakoczi ut 5, H-1088 Budapest, Hungary.

The nearby supernova (10 - 500 pc from the Sun) explosions were frequent events during the history of Earth. Following the estimations which have been summarized by SHKLOWSKY (1966), TRIMBLE (1982, 1983) on the average rate of Type II supernova outburst occurs every 100 years whereas the rate of Type I supernova has two or three times less than the Type II one, i.e. Type I supernova event is every 200 or 300 years in our Galaxy.

It may expect that a "nearby" supernova event occurs in every few thousands years. In average at a distance 100 parsecs from the Sun the rate of supernova events is one per every one million years statistically.

Sun-supernova distances

Distance from the Sun	SN Type I (1 event: 300 years)	Type II (1 event 100 years)
10 pc	2.53×10^{9}	8.43×10^{8}
20 pc	3.16×10^{8}	1.05×10^{8}
100 pc	2.53×10^{6}	8.43×10^{5}
200 pc	3.16×10^{5}	1.05×10^{5}
500 pc	2.02×10^{4}	6.75×10^{3}

For a few months a supernova explosion can reach luminosity in excess $10^{9\text{-}11}$ solar luminosity. It is obvious that the more frequent Type II supernovae cold explode in every hundred million years within 20 parsecs from the Sun which are very close events at a "dangerous" distance in the point of view of enormous effects on the planetary environments in the Solar System. One of these statistically possible supernova events could have been in the P/Tr geological boundary.

The P/Tr episode is related to explosion of a nearby supernova and its consequences in the Solar System. The "creeping death" as a "stealth" can more in the form of enhanced radiation level and from radiation induced changes in the chemistry of the atmosphere (anoxia),climatic changes (e.g. dry climate) and changes in the life-spaces which had not been later available for taxa.

Could be unknown but possible consequences of this kind of catastrophic event due to the radiation induced mutations when the mutants cannot resistant for the changes the environment.

Other possible interstellar effects namely when the Solar System passes through a dense interstellar cloud should be excluded because there is no traces of any global ice age in the P/Tr as a possible consequence of this encounter.

The knowledge on the duration of the P/Tr transition is very uncertain. (see ERWIN 1993, SCHOENLAUB 1996). The range of uncertainty in the estimated age of the P/Tr boundary is about 20 Myr, it depends from the different facies. There are no generally accepted criteria. Stratigraphically the P/Tr is an extremely difficult problem.

More very sharp spherule layers are nailing through the different facies, which came from the different expanding envelopes of the supernova.

What is the origin of these spherule layers?

The temporal evolution of the supernova explosion as follow briefly:

1. Neutrino and gravitational radiation just immediately.

2. Order of day later tremendous release of energy due to the collapse blow-off of the outer layer of the star observed visible and ultraviolet light. A possible consequence for the terrestrial atmosphere. the temporal increasing of the ozone layer.

3. Several months after collapse: gamma and roentgen rays arrived. Gamma radiation is more effective to destroy the ozone than the UV rays increased that. There are unusual chemical reactions in the atmosphere (e.g. nitrogene-oxids are created and make further destruction of ozone layer. (See BRAKENRIDGE 1981)

The upper atmosphere can warmed up the lower atmospheric layers as the troposphere can become colder

This is not necessarily a global effect in terms of glaciation (ice ages) and really, there are no ice age during the Uppermost Permian..

4. Years later: corpuscular rays arrived. Further decay of atmosphere ozone shield depleted.

5. Few thousands of years later, the expanding gas and dust shell of the very nearby (10-20 pc) supernova remnant can reach the heliosphere and pushes the solar wind approximately.

The expanding supernova remnant can encounter with already interstellar material and can trigger that by its enormous mechanical and electromagnetic energy. The interstellar dust can be moved away by the supernova shock wave front and the grains both can be created and destroyed by the supernova shell. These moving or newly created dust grains can be the sources of that interstellar dust which collided with the atmosphere of the Earth and sedimented into the geologic layers and finally recorded as interstellar micro-spherules in the P/Tr boundary geochronological interval. (From the Uppermost Permian to the "traditional P/Tr biostratigraphical boundary", see DETRE et al. 1998).

Arguments of P/Tr SN event:

The SN is supposed flared up in the beginning of Upper Permian. Dramatic extinction of the taxa during the Upper Permian until the "traditional P/Tr boundary". A great part of the biomass was killed. The organic matter was mixed with different sediments producing world-wide sedimentary rocks and high of high organic content. Consequently anoxia and enrichment of CO_2. The increased electromagnetic radiation produced selective extermination in the living world: first of all among terrestrial plants, then among the plankton (e.g. Radiolaria) and "sessilis benthos" (e.g. Brachiopoda, Bryozoa, etc.) Uppermost Permian and "traditional P/Tr boundary" interstellar (probably of SN origin) spherules. The "traditional P/Tr boundary" was the end of the crisis and the beginning of a renaissance of the living world.

Selected literature:

SHKLOWSKY (1966):Supernovae.- New York, John Wiley and sons, BRAKENRIDGE (1981): Icarus, 46, TRIMBLE, V. 1982, Rev. Method. Phys. 54, TRIMBLE, V. 1983, Ibidem, 55., ERWIN 1993: The Great Paleozoic Crisis -Columbia Univ. Press, New York, SCHOENLAUB 1996: Abhandl. Geol. Bundesanst. Bd.53, Wien. MIONO 1996: Internat. IGCP 384 Meet. Spherules and Global Events, KFKI Rep. 1995-05/C, TOTH I. 1997: Terrestr. Impacts and Spherule Sympos. (TISS), Tokyo, DETRE et al. 1998: 29th LPSC Abstracts, No 1030.

Acknowledgements:

Hungarian-Japanese Sci. Techn. Cooperation (HJSTC) 31-96,
Hungarian Space Office,
Hung. Nat. Sci. Found. (OTKA), Grants nos T 014958, T T025461, T026660

MAGNETIC ANISOTROPIES OF GIBEON AND TOLUCA OCTAHEDRITE

Tetsuya FUKUHARA[1], Minoru FUNAKI[2] and Hiroyuki NAGAI[3]

[1]Department of Polar Science, The Graduate University for Advanced Studies, National Institute of Poler Research, 1- 9-10 Kaga Itabashi Tokyo 173-8515

[2]National Institute of Poler Research, 1-9-10 Kaga Itabashi Tokyo 173-8515

[3]Department of physics, Faculty of Science, Shinshu University, 3-1-1 Asahi Matsumoto Nagano 390-0802

Magnetic properties of iron meteorites provide basic information about the physical properties of meteorites and may also give us paleomagnetic information that is relevant to understanding the thermo-physical history of the parent body. Understanding the natural remanent magnetization (NRM) is the important first step in evaluating the magnetic properties of iron meteorites. Kukkonen and Pesonen (1983) reported variable NRM intensity ranging from 10^{-4} to 10^{-1} Am^2/kg in 9 iron meteorites. Pesonen et al. (1993) reported an average NRM intensity of 2.06×10^{-2} Am^2/kg for 131 iron samples. Although understanding the cause of NRM is also the important, unfortunately, it has not been cleared yet. Studying magnetic anisotropy would give a basic and useful information for understanding the cause of NRM. Brecher and Albright (1977) reported the magnetic anisotropy of 7 iron meteorites. It is reported that some octahedrites have the easy (111) plane of magnetization in the Widmanstätten structure.

We have examined the magnetic anisotropy of Toluca and Gibeon octahedrite. The purpose of this study is to clear the relationship between crystallization and magnetic anisotropies. Samples which were measured for their NRM values were less than 50 g in weight, because it is impossible to measure more than 50 g in weight due to exceed the sensitivity range of the spinner magnetometer.

To measure the magnetic anisotropy of the octahedrite, the samples were cut into cubes because the magnetic anisotropy depends on the shape of the sample. Each coordinate axis was determinated along the Widmanstätten structure (Fig.1). The cubic sub-samples were demagnetized by alternating field demagnetization up to 0.1 T and then they were accquired to the saturation isothermal remanent magnetization (SIRM) up to 0.8 T from the four different directions by an electromagnet, as shown in Fig. 2. The SIRM was acquired when the field was the perpendicular to [001] direction for the Gibeon and the parallel to [001] one for the Toluca.

Magnetic hysteresis loops were obtained at every 15° during stepwise rotation in a plane by using a vibrating sample magnetometer. From the hysterisis loop, the maximum value of spontaneous magnetization at 0.5 T appeared at 135° and 315° for Toluca and 90° and 270° for Gibeon. The results indicate that both samples have the uniaxial magnetic anisotropy which may relate to an axis or a phase of the Widmanstätten structure.

The magnetic anisotropy of Toluca was stronger than that of Gibeon. Funaki et al. (1986) reported tetrataenite lamellae at taenite lamellae formed along the Widmanstätten structure in Toluca. We also confirmed tetrataenite phases in Toluca by Bitter pattern method, but any evidences of tetrataenite could not be observed in Gibeon. We have estimated that the difference of magnetic anisotropy between both irons may be explained by the existence of tetrataenite.

References

Brecher, A. and Albright, L. (1977): The thermoremanence hypothesis and the origin of magnetization in iron meteorites. J. Geomag. Geoelectr., **29**, 379-400.

Kukkonen, I. T. and Pesonen, L. J. (1983): Classification of meteorites by petrophysical methods. Geol. Soc. Finland, **55**, 2, 157-177.

Pesonen, L. J., Terho, M. and Kukkonen, I. T. (1993): Physical properties of 368 meteorites: implications for meteorite magnetism and planetary geophysics. Proc. NIPR Symp. Antarct. Meteorites, **6**, 401-416.

Funaki, M., Nagata, T. and Danon, J. A. (1985): Magnetic properties of lamellar tetrataenite in Toluca iron meteorite. Mem. Natl Inst. Polar Res., Spec. Issue, **41**, 382-393.

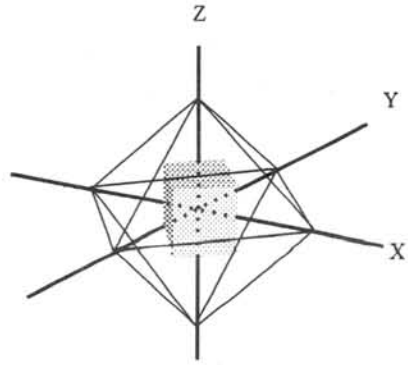

Fig.1 The relation between the Widmanstätten structure and a subsample cut into cube. Coordinate axes were determined along the Widmanstätten structure.

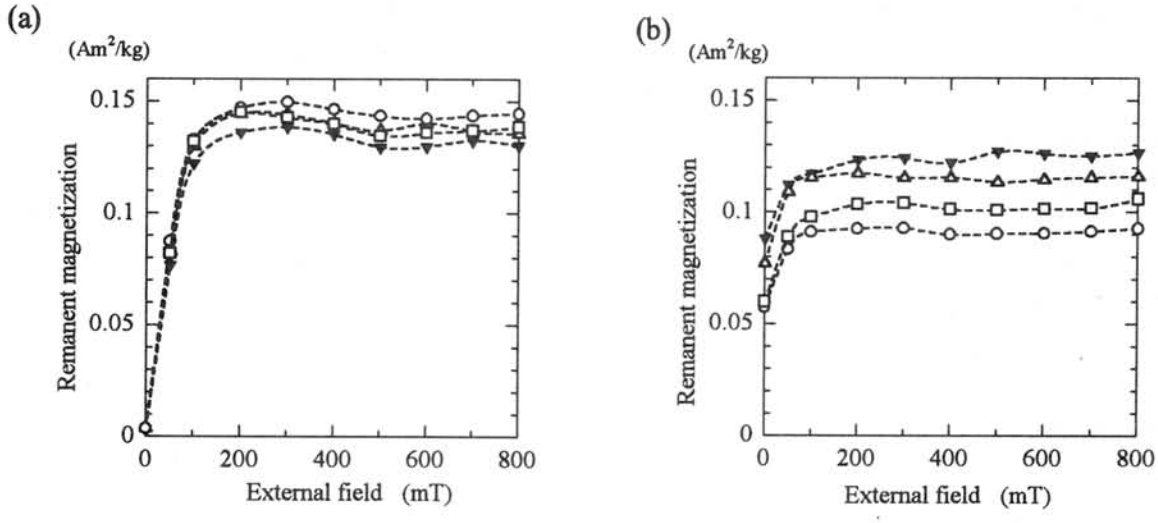

Fig.2 The SIRM acquisition curves for Gibeon (a) and Toluca (b). Four different directions of curves are measured up to 0.8 T external magnetic field.

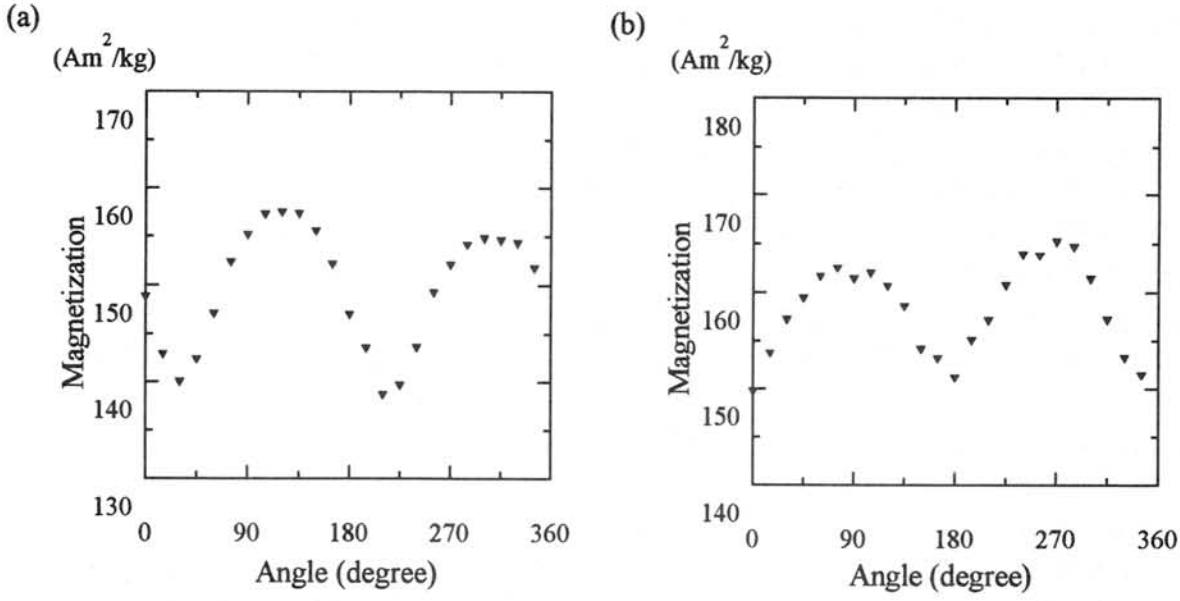

Fig.3 The anisotropy of spontaneous magnetizations in the 0.5 T external magnetic field during the sample rotated. (a): Gibeon and (b): Toluca.

PRELIMINARY STUDY OF SHOCK-INDUCED MAGNETIZATION (SIM) at 10 and 20GPa on GIBEON IRON METEORITE

M. Funaki[1], Y. Shono[2], T. Yamauchi[3] and P. Wasilewski[4]
1: National Institute of Polar Research, Tokyo
2: Tohoku University, Sendai Japan
3: Shinshu University, Matsumoto Japan
4: Goddard Space Flight Center, NASA

1. Introduction

Every meteorite has experienced shocks when their parent bodies were crushed by hypervelocity-collision among asteroids. We have, however, almost no information that the natural remanent magnetization (NRM) acquired on the primordial asteroid can survive by the shocks. In order to estimate a possibility of shock-induced magnetization (SIM) for iron meteorite, two disks prepared from the Gibeon iron meteorite (octahedrite) were examined at 10 and 20GPa produced by explosive gun.

Projectile of aluminum or nonmagnetic stainless steel of 2.5cm in diameter collided with the target (10mm in diameter and 2mm thick) of Gibeon at 10GPa or 20GPa respectively. The magnetic field was 37.5μT (I=55.1, D=271.4) at the place of sample holder made of iron steel and cupper, although it could not be measured in the holder due to too narrow space. Shock was loaded toward the perpendicular with the disks. The samples were removed from the holder after shock loading using a lathe having the magnetization less than 5 Oe.

2. Experimental results

Two disk samples of A and B were demagnetized up to 100mT by AF demagnetization. Their NRM intensity decayed from 7.365×10^{-3} to 3.830×10^{-4} Am^2/kg for sample A and from 1.480×10^{-2} to 1.922×10^{-4} Am^2/kg for sample B. The shock of 10 and 20GPa were loaded to the sample A and B respectively. The magnetization increased consequently to $8.871 \times 10^{-3} Am^2/kg$ (I=-4.8, D=222.6) for the sample A and to $3.349 \times 10^{-2} Am^2/kg$ (I=5.2, D=347.4) for sample B, when the sample A was cut into 4 subsamples. Their directions of remanence scattered widely maintaining low inclination. This characteristic was also observed in the sample B. Figure 1 shows the intensity changes of the 3 subsamples against AF demagnetization of SIM, acquisition of IRM (isothermal remanent magnetization) and AF demagnetization of IRM, where the intensities were normalized by the maximum value of IRM (SIRM) of each subsample. The remanent intensities of subsamples were less than 0.12, 0.57 and 1.02 for 0, 10 and 20GPa respectively compared with their SIRM values. They were drastically demagnetized before 20mT. Almost all subsamples were seemed to be saturated before 0.2 T of the external magnetic field, but one of them at 20GPa showed no saturation at 0.8T. These unsaturated subsamples acquired larger SIM than IRM observed at 0.8T. In general, the SIM acquired at 20GPa is larger than that at 10GPa. The stability of IRM (SIRM) by AF demagnetization is variable among the non-shocked subsamples, but it is more homogeneous for shocked subsamples. It is clearly stable for the subsamples of 20GPa

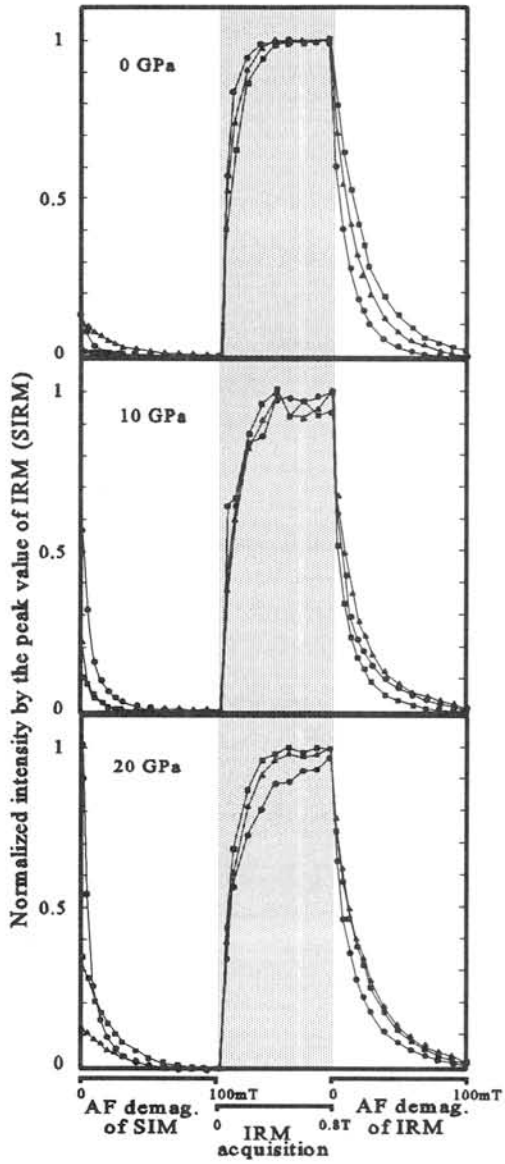

Fig. 1

Curves of AF demagnetization of SIM at 0, 10 and 20GPa, IRM acquisition and AF demagnetization of IRM for the 3 subsamples.

than those of 10GPa.

3. Discussion

The disk samples of Gibeon acquired SIM of 23.2 times by 10GPa for sample A and 174 ones by 20GPa loading for sample B compared with the demagnetized values. If the SIM is acquired referred to the ambient magnetic field in the sample holder triggered shock, the remanence should be directed toward the field direction. The scattered directions of SIM among the subsamples may suggest that the SIM was acquired disregarding the ambient magnetic field. However, The low inclination of SIM may be insignificant due to the shape anisotroy resulting disk shape. From these viewpoints, we concluded that the samples were acquired the SIM by hypervelocity shocks disregarding the ambient magnetic field.

Wasilewski (1975) reported that the stability of SIM decreases when α-iron (ferromagntic) transforms to ϵ-iron (antiferromagnetic): the phase transition starts from 13GPa and is accomplished before 20GPa for iron. Although our experiment was performed through the phase transition, the results do not agree to their results for the SIM stability. Fundamental magnetic properties should be investigated for understanding of this inconsistency.

References

Wasilewski (1976): Shock-loading meteoritic b.c.c metal above the pressure transition: remanent-magnetization stability and microstructure. Phy. Earth Plan. Int., **11**, 5-11.

UV-VIS-NIR ABSORPTION FEATURES OF HEATED PHYLLOSILICATES AS REMOTE-SENSING CLUES OF THERMAL HISTORIES OF PRIMITIVE ASTEROIDS. TAKAHIRO HIROI[1] AND MICHAEL E. ZOLENSKY[2], [1]Department of Geological Sciences, Brown University, Providence, RI 02912, USA, [2]SN2, NASA Johnson Space Center, Houston, TX 77058, USA.

1. Introduction

Reflectance spectra of primitive asteroids (C, G, B, and F types) were shown to have similar absorption bands to some carbonaceous chondrites, especially CMs [1]. Later, varying degrees of thermal metamorphism of primitive asteroids were suggested based on their UV absorption strengths and overall spectral profiles [2, 3], and later based on their 0.7 and 3 μm band strengths [4] in our previous studies based on comparison with reflectance spectra of CI and CM chondrites. Because Fe and OH in phyllosilicates are believed to be mainly responsible for the UV, 0.7 μm, and 3 μm absorption features, their changes due to the heating process are examined in this study in order to help detecting evidence of heating through remote sensing.

2. Heating Experiments of Phyllosilicates

Each of antigorite, lizardite, clinochrysotile, chlorite, and saponite samples was separated into five fractions for the heating experiments at 300, 400, 500, and 600°C. The pyrex tubes for the heating experiments were pre-cleaned, and the tubes for 300, 400, 500, and 600°C were preheated at 200, 300, 400, and 450°C for one hour, respectively, during which all the mineral samples were evacuated. The pre-heating was done to minimize oxidative effects of evolved volatiles. All tubes were sealed under vacuum and were heated to their final temperature for one week.

Despite these precautions, some considerable water was noted with chrysotile at 500°C, and lizardite and antigorite at 600°C. In addition, the saponite 600°C tube gave off a sulfur oxide smell upon opening. The chrysotile 600°C sample exploded, and the sample was recovered from the bottom of the furnace after the week was out. Although the explosion is believed to have occurred late in the run, the final heating for that one sample took place at least partly in air rather than inside a sealed capsule. This may have caused significantly more oxidization to the sample. In fact, the color of the 600°C chrysotile sample is much redder than those at other temperatures.

3. Reflectance Spectral Measurements

All the mineral samples were ground and dry-sieved into powders of <125 μm, and their UV-Vis-NIR diffuse reflectance spectra were measured at 30° incidence and 0° emergence angles at wavelengths from 0.3 to 2.6 μm using the RELAB bidirectional spectrometer. Reflectances were then divided by those of halon at the same viewing geometry and the ratios were corrected based on absolute reflectances of halon. Biconical IR diffuse reflectance spectra of the samples were measured at 30° incidence and emergence angles at wavelengths from 1.8 to 26 μm using the Niclet 740 FT-IR spectrometer with diffuse gold as the standard.

Antigorite samples show only small changes in their overall spectral shapes except for the 600°C sample which shows very blue and rounded visible spectrum and a sharp 2.7 μm band. Brightness, if it is measured by the reflectance at 0.55μm, decreases until 500°C and increases again at 600°C. The 1.4 μm band and the complex bands around 2.3-2.5 μm steadily decrease as the heating temperature increases, while the 2.7 μm band strength stays about the same.

Lizardite samples show very systematic changes as heating temperature increases. The brightness decreases until about 400°C and increases again. The 0.7, 0.9, and 1.1 μm bands keep weakening until they disappear around 400°C. The 1.4 and 2.3-2.5 μm bands steadily decrease, while the 2.7 μm band weakens only slightly before 600°C where the band weakens dramatically and becomes very sharp. The 1.4 μm band seems to disappear at 600°C. The 600°C spectrum shows a very blue and smooth visible profile, similar to the antigorite 600°C sample.

Clinochrysotile samples also show very systematic changes except for the 600°C sample, which may be due to the explosion of the container and the consequent oxidization. The 0.7, 0.9, and 1.1 μm bands disappear around

400°C, the 1.4 and 2.3-2.5 μm bands steadily decrease until 500°C, and the 2.7 μm seems to become sharper. The brightness keeps decreasing until 500°C.

Chlorite samples do not show much systematic change. The brightness seems to decrease until 400°C and begins increasing again. Visible spectral slope seems to have changed at 400°C but has reversed at 500°C. Strengths of other bands do not seem to have changed through the heating process up to 600°C.

Saponite samples show drastic and systematic changes. The brightness decreases until 400°C and begins increasing again. The 1.4, 1.9, 2.3, and 2.4 μm bands keep weakening steadily, and the 2.7 μm band keeps sharpening. The UV-visible spectral profile keeps flattening.

4. The Albedo and the UV, 0.7-μm, and 3-μm Absorption Strengths

In order to quantify and compare the above spectral features with telescopic measurements of primitive asteroids, the albedo and the UV and 0.7-μm absorption strengths are defined by simulating the filters used in the eight-color asteroid survey [5]. And the 3-μm band strength is defined so that even low-quality IR spectra of asteroids could be used. More concretely, the albedo and the absorption strengths are defined in the same way as in [4]:

Albedo : $R(0.550)$

UV absorption strength : $\ln R(0.337) - \ln R(0.550)$

0.7-μm band strength : $\ln R(0.701) - \left[0.152 \ln R(0.550) + 0.151 \ln R(0.853)\right] / 0.303$

3-μm band strength : $\ln R(2.9 \sim 3.0) - \ln R(2.3 \sim 2.5)$

The above four quantities for all the phyllosilicate samples were calculated and plotted against heating temperatures in Fig. 1. As clearly seen in the figure, the albedo tends to decrease until 300~500°C and begin increasing again. Only saponite shows a clear trend of decreasing UV absorption strength as the heating temperature becomes higher. The 0.7-μm band for some samples disappear around 400°C, whereas that of chlorite sample survived until 600°C. Saponite and lizardite show steady decrease of the 3-μm band strength as they are heated at higher temperatures. The correlation between the UV and 3-μm absorption strengths claimed in [4] is examined in Fig. 2. The correlation is very clear for saponite samples because saponite show a very positive correlation between the heating temperature and both the UV and 3-μm absorption strengths. Lizardite also show a slight correlation between the UV and 3-μm absorption strengths, and the other phyllosilicate samples do not show any clear correlation.

5. Discussion

The results that the albedo decreases until 300~500°C and begins increasing afterward and that the 0.7-μm band disappears around 400°C are in accordance with our previous studies concerning the heated Murchison samples [2, 3]. It should be further investigated whether differences in spectral change among the phyllosilicates studied here are realistic in simulating asteroidal heating processes or they can be changed by changing some experimental conditions such as the concentration of the released volatiles or adding carbon to simulate carbonaceous chondrites.

Acknowledgments: T. H thanks Dr. J. Akai for a comment concerning saponite at the past symposium. Reflectance spectra of the above meteorite samples were measured at RELAB in Brown University. RELAB is a multiuser facility operated under NASA grant NAG5-3871.

References: [1] Vilas F. and Gaffey M. J. (1989) *Science* **246**, 790-792. [2] Hiroi T., Pieters C. M., Zolensky M. E. and Lipschutz M. E. (1993) *Science* **261**, 1016-1018. [3] Hiroi T., Pieters C. M., Zolensky M. E. and Lipschutz M. E. (1994) *Proc. NIPR Symp. Antarct. Meteorites* **7**, 230-243. [4] Hiroi T., Pieters C. M., Zolensky M. E. and Lipschutz M. E. (1996) *Meteoritics Planet. Sci.* **31**, 321-327. [5] Zellner B., Tholen D. J. and Tedesco E. F. (1985) *Icarus* **61**, 355-416.

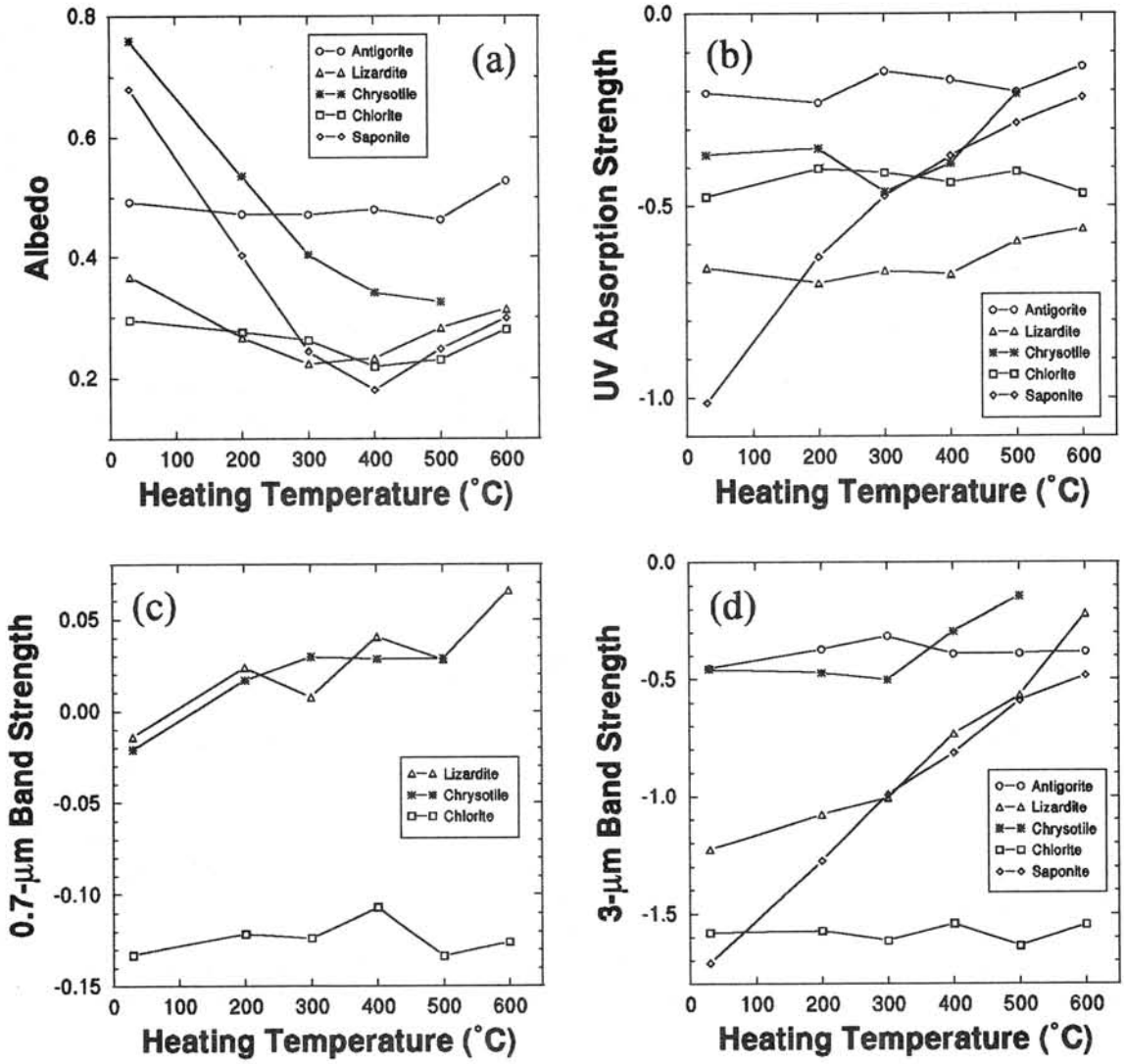

Fig. 1. Plots of albedo and UV, 0.7-μm, and 3-μm absorption strengths of unheated and heated phyllosilicates samples. Data for the chrysotile 600°C sample are not included because of its possible oxidization in the ambient air.

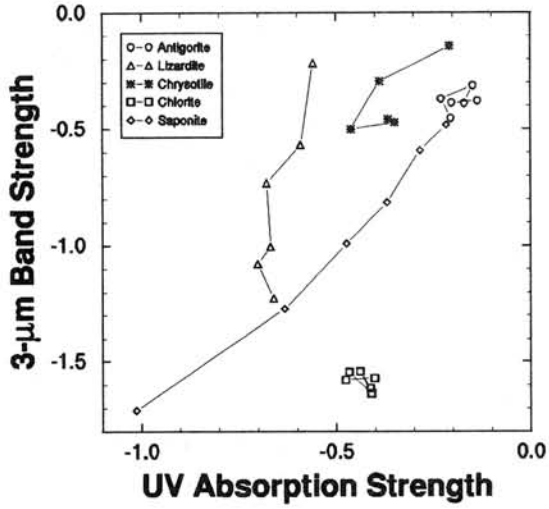

Fig. 2. Plot between the UV and 3-μm absorption strengths for the unheated and heated phyllosilicate samples. Data for the chrysotile 600°C sample are not included.

An ion microprobe study of oxygen isotopes in Yamato-86009 (CV3) chondrite: discovery of ^{16}O-rich olivine inclusions

Hajime HIYAGON[1] and Akihiko HASHIMOTO[2]

1) Department of Earth and Planetary Physics, The University of Tokyo, Bunkyo-ku, Tokyo 113, JAPAN.
2) Department of the Earth and Planetary Sciences, Hokkaido University, Sapporo 060, JAPAN.

1. Introduction

Since the work of Clayton et al. [1,2], it has been well recognized that Calcium-Alminium-rich inclusions (CAIs), most commonly observed in carbonaceous chondrite groups (CV, CM and CO), have anomalous oxygen isotopic compositions with both $\delta^{17}O$ and $\delta^{18}O$ values down to ~-40‰. This ^{16}O-rich anomaly cannot be explained by mass dependent fractionation and its origin is still under debate: whether it is derived from a carrier having anomalous oxygen isotopes [1,3] or from non-mass dependent fractionation caused by some kind of chemical reactions [4,5,6].

Recent development of ion microprobe techniques has enabled *in situ* analyses of oxygen isotopes with a spacial resolution of 10-20μm and a precision approaching ~1‰ level (see, e.g., [7]). Using this technique, Hiyagon [8] recently found in the Allende meteorite that (a) diopside in the Wark-Lovering rim [9,10] of a type-A inclusion has a large oxygen isotope anomaly with $\delta^{17}O$ and $\delta^{18}O$ down to ~-45‰, indistinguishable from the spinel values, and (b) some olivine grains in the accretionary rims [11] of two type-A CAIs also have rather high anomalies with $\delta^{17}O$ and $\delta^{18}O$ down to ~-30‰. This suggests that both Wark-Lovering rims and accretionary rims formed in the same process (and/or environment) as that for the CAI bodies which they enclose, with regards to oxygen isotopic composition.

In order to better understand the origin of oxygen isotopic anomalies, it is critical to determine distributions of oxygen isotopes in various petrographic components inside various types of meteorites. In the present study, we performed an *in situ* ion microprobe analysis of oxygen isotopes for Yamato-86009 (CV3) chondrite. We report here discovery of the high ^{16}O enrichments in olivine grains inside olivine-rich inclusions in this meteorite.

2. Samples and Experimental Procedures

Four olivine-rich inclusions (A, B, C, and D), one spinel-pyroxene-feldspar aggregate (E), and one chondrule (F) have been analyzed in a thin section of Yamato-86009 (CV3) chondrite. Inclusion (E) is a large (600μm x 1100μm) fine-grained aggregate (typical grain size <20μm) consisting of spinel, pyroxene, and a feldspar-like phase. Pyroxene is fassaitic to diopsidic with variable Al contents; the feldspar-like phase appears to be a mixture of anorthitic feldspar and grossular, presumably an alteration product of melilite. Because of its fine-grained texture, individual phases could not be analyzed from inclusion E without some overlap to other phases, except for one spinel grain. Two spinel grains (a single spinel grain and a spinel-fassaite mixture), one fassaite-diopside-rich phase, and four feldspar-rich phases were analyzed. The olivine-rich inclusions (A, B, C, and D), ranging from 100μm x 150μm to 200μm x 320μm in size, consist mostly of Mg-rich olivine with Mg# (i.e., Mg/[Mg+Fe] mol%) >99 for (A) and (C),

and Mg# =97-98 for (B) and (D). These olivine-rich inclusions are different from other olivine-rich aggregates and chondrules, in that they contain miniature Ca-Al-rich inclusions inside them, which are made mostly of fassaite or diopside with spinel (A and C) or without spinel (B and D), and that they have many void spaces (<1μm to a few μm in size) both in olivine and Ca-Al-rich portions. From their outlook they are probably amoeboid olivine aggregates. Analyzed phases were olivine (8 points) and fassaite-diopside-rich phases (3 points). The chondrule (F) consists of enstatite (Mg#>99), forsterite (Mg#>99), diopside and glass. Rounded forsterite grains are poikilitically enclosed by enstatite, which in turn is rimmed by euhedral diopside that protrudes into the glass. Cromium was detected in all of the phases inside the chcondrule. The grain sizes were large enough for probing; two forsterite, one enstatite and one diopside grains were analyzed.

In situ oxygen isotope analyses were performed using a CAMECA ims-6f ion microprobe at the University of Tokyo. Analytical conditions were similar to those described in [8]. The size of the Cs^+ primary beam was~15μm in diameter except for one spot (an olivine grain inside the chondrule, which was analyzed by a ~30μm dia. beam). San Carlos olivine ($\delta^{17}O_{SMOW}$= +2.44‰ and $\delta^{18}O_{SMOW}$= +4.70 ‰ [7]) was used as a standard and was analyzed repeatedly before and after the period of sample runs under the same probe condition All the data were normalized to the averaged valule of the standard analyses. The reproducibility of the data (1σ) was ±2.1‰ for $^{18}O/^{16}O$ and ±1.5‰ for $^{17}O/^{16}O$, respectively.

3. Results and Discussion

The present results are shown in the oxygen three-isotope diagram (Fig.1). All four olivine-rich inclusions analyzed in the present study are highly anomalous, with $\delta^{17}O$ and $\delta^{18}O$ values down to ~-50‰. This is the first observation that olivine also has oxygen isotopic compositions at lower ends of the slope~1 correlation line which was defined by many analyses of Allende CAI minerals [1,2]. Another important fact is that these olivine-rich inclusions are not rare, at least in this meteorite; at least 5 more olivine-rich inclusions of similar morphologies are observed in this particular thin section. Since olivine is the most abundant mineral in chondrites except enstatite chondrites, the present result implies a possibility that the oxygen isotopic anomaly was ubiquitous in the nebula when chndrite materials formed. It is not certain for the moment whether Y-86009 is a pristine (or rare) type of chondrite that kept anomalous oxygen isotopic compositions intact, or an *in situ* isotopic study of other chondrites will turn up similar anomalies in olivine. Further studies are required to confirm this point.

All three phases (forsterite, enstatite, and diopside) inside the chondrule show $\delta^{18}O$ values around -10‰; the data points exactly lie on the slope~1 correlation line. It is notable that an euhedral diopside grain, which must have grown last from liquid (now glass), shows the ^{16}O enrichment similar to those of forsterite and enstatite which crystallized earlier. This indicates that isotope equilibration was established throughout the crystallization process. If a smaller degree of oxygen isotopic anomaly (-10‰) of the chondrule relative to those (-50‰) of olivine-rich aggregates was caused by isotopic re-equilibration between chondrule precursors and an isotopically normal nebular gas, isotope exchange at the liquid/gas interface must be slower than isotope diffusion inside the liquid and mineral phases; otherwise an isotopic heterogeneity would result inside the chondrule. Alternatively, the nebular gas had -10‰ local anomaly in oxygen isotopes as a result of complete isotopic homogenization between gas and solid.

This is only the beginning of extensive survey on various types of petrographic components from different meteorites. We believe that *in situ* isotopic studies will provide unprecedented information regarding not only the cause of oxygen isotopic anomalies, but also the origin of CAIs, olivine-rich inclusions, chondrules, and their relationships.

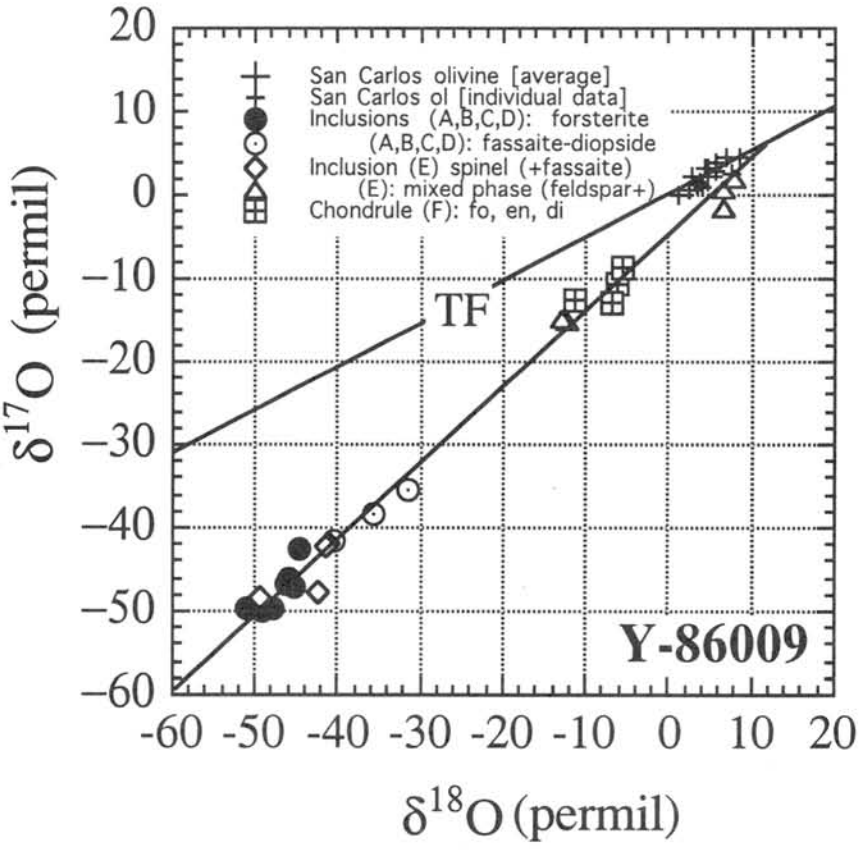

Fig.1 Oxygen isotopic compositions in various phases of Y-86009 (CV3) chondrite. Note that four olivine-rich inclusions (A, B, C, D) show extremely high anomalies with $\delta^{17}O$ and $\delta^{18}O$ values down to ~-50 ‰. The slope~1 line is a regression line for all the data points of Y-86009, which is essentially identical to the Allende mixing line [1,2].

References: [1] Clayton, R.N., Grossman, L. and Mayeda, T.K. (1973) *Science* **182**, 485-488. [2] Clayton, R.N., Onuma, N. and Mayeda, T.K. (1976) *Earth Planet. Sci. Lett.* **30**, 10-18. [3] LattimerJ.M, Schramm, D.N. and Grossman, L. (1978) *Astrophys. J.*, **219**, 230-249. [4] Thiemens, M.H. and Heidenreich III J.E. (1983) *Science* **219**, 1073-1075. [5] Thiemens, M.H. (1996) in *Chondrules and the Protoplanetary Disk* (eds. Hewins, R.H., Jones, R.H. and Scott, E.R.D.) Cambridge Univ. Press, Cambridge, pp.107-118. [6] Hahimoto, A. and Takahashi, T. (1997) *NIPR Symp. on Antarctic Meteorites* **22** (abstract), 49-51. [7] Hiyagon, H. (1997) *Antarctic Meteorite Res.* **10**, 249-274. [8] Hiyagon, H. (1998) *Lunar Planet. Sci.* **29** (abstract), 1582-1583. [9] Wark, D.A. and Lovering, J.F. (1977) *Proc. Lunar Sci. Conf.* **8**, 95-112. [10] MacPherson, G.J., Grossman, L., Allen, J.M. and Beckett, J.R. (1981) *Proc. Lunar Sci. Conf.* **12B**, 1079-1091. [11] MacPherson, G.J., Hashimoto, A. and Grossman, L. (1985) *Geochim. Cosmochim. Acta* **49**, 2267-2279.

Petrology of the Asuka-881931 Ureilite

Y. Ikeda
Dept. of Material & Biological Sciences, Ibaraki Univ., Mito, Japan

Introduction

Ureilites are a complex primitive achondrite group, consisting of olivine, pigeonite, and carbonaceous materials (mainly graphite). The number of known meteorites in this group has expanded drastically in recent years, including some polymict ureilites, with most of them having been recovered from Antarctica. There are mainly two types of hypotheses for the origin of the olivine-pigeonite assemblage in the ureilites (Goodrich, 1992); one is the crystal cumulative hypothesis (Berkley et al., 1980; Mittlefehldt, 1986; Goodrich et al., 1987) in which the ureilite assemblages were produced as cumulates settled from basaltic or ultramafic magmas. The other is the partial melting residue hypothesis (Takeda, 1987; Rubin, 1988; Warren and Kallemeyn, 1992; Scott et al., 1993; Walker and Grove, 1993) wherein the assemblages were produced as residues of the partial melting or smelting of chondritic materials. Detailed petrological study of ureilites may be a key to solve this problem stated above.

Petrography of Asuka-881931

The A-881931 meteorite is a typical monomict ureilite consisting mainly of olivine and pigeonite with a coarse-grained equigranular texture. Their grain sizes are about 0.5-1.0 mm across. The modal composition of the meteorite is; equigranular olivine (72.1 areal%), equigranular pigeonite (16.5 %), metal(now, limonite)-troilite veins (4.3 %), fine-grained silicate-metal aggregates (7.0 %), and interstitial glass (probably 0.1 %).

[Equigranular Olivine and Pigeonite]: Cores of equigranular olivine and pigeonite grains are homogeneous in composition, and they are $Fo_{77-78}Fa_{22-23}$ for olivine and $En_{70-73}Fs_{18-20}Wo_{9-10}$ for pigeonite. Equigranular olivine shows reverse zoning up to $Fo_{99}Fa_{1}$ at the rims with widths of several tens of μm. Equigranular pigeonite is sometimes replaced at the rims or along cracks within grains by high-Ca enstatite having Wo_{3-7} contents often in close association with silica-rich glass and small metal.

[Metal and Troilite]: Metal-troilite veins, with various widths up to 100 μm, occur at grain boundaries between equigranular olivine and pigeonite and along cracks in the grains. Metal is predominant in the veins although most of the metal has altered to limonite. Small ellipsoidal or irregular metal-troilite grains, several to a few tens of μm across, occur sometimes within equigranular olivine and pigeonite, and they are kamacite with 1-5 wt% of Ni. Small spherulitic metal, several μm in diameter, often occurs within interstitial glass, and is kamacite with less than 1 wt% of Ni.

[Fine-grained Silicate-metal Aggregates]: There are two types of fine-grained silicate-metal aggregates, forsterite-metal and enstatite-metal aggregates. The former, up to a few hundreds of μm across, occurs between equigranular olivine and pigeonite grains, and consists mainly of fine-grained forsterite with $Fo_{90-99}Fa_{1-10}$ and metal. The forsterite-metal aggregates are often surrounded by high-Ca enstatite grains having Wo 3-7 contents and minor diopside with Wo_{30-40}. The enstatite-metal aggregates, several tens of μm across, replace equigranular olivine near the grain boundaries in close association with the forsterite-metal aggregates. They consist mainly of low-Ca enstatite with $Fs_{2-10}Wo_{0.3-2.0}$ and abundant small metal.

[Interstitial Glass]: Interstitial glass occurs between equigranular olivine or pigeonite grains. The chemical compositions of the glass vary according to the occurrence; interstitial glass which is just in contact with olivine has higher Al_2O_3 (19-23 wt%) and Na_2O (5.5-6.5 wt%) contents and lower SiO_2 (60-66 wt%), and that in contact with metal-troilite veins or high-Ca enstatite is poorer in Al_2O_3 and Na_2O contents and enriched in SiO_2 more than 66 wt%. The Al-Na-rich glass in contact with olivine is surrounded by olivine, fassaite, and Al-rich enstatite, and chromian spinel rarely occurs within the glass. The Al-Na-rich glass has a composition near the ternary peritectic point of the albite-forsterite-silica system. The Si-rich glass in contact with metal or enstatite never contacts with olivine, and that in contact with metal is often enriched in SiO_2 more than 80 wt%. The Si-rich glass has chemical compositions between the Al-Na-rich glass and silica glass. Sometimes a silica mineral (tridymite or crystobalite) occurs in contact with metal of the metal-troilite veins.

Discussion and Conclusions

The Asuka-881931 ureilite was originally a mixture of equigranular olivine (Fo_{87-88}) and pigeonite ($En_{70-73}Wo_{9-10}$) with minor amounts of interstitial Fe-S melts, silicate melts, and carbonaceous materials. The interstitial Fe-S and silicate melts may have been remnants of partial melts of chondritic materials and were in equilibrium with the equigranular olivine and pigeonite. Then, the silicate melts seem to have been reduced probably by graphite and have crystallized enstatite and minor diopside. Later, fassaite, Al-rich enstatite, and chromian spinel precipitated from the fractionated melts, which had chemical compositions near the ternary peritectic point of the Ab-Fo-Silica system and were finally quenched as interstitial glass. The silica-rich silicate melts also were produced by mixing of the fractionated Al-Na-rich melts with silica components that were supplied from Si-bearing Fe-S melts or from decomposition of equigranular olivine by reduction. The forsterite-metal aggregates formed from equigranular olivine by reduction and reaction with interstitial melts, and the enstatite-metal aggregates were also produced from equigranular olivine by reduction at temperatures lower than those for the forsterite-metal aggregates.

[References]: Goodrich (1992) Meteoritics 27, 327-352. Berkley et al. (1980) GCA 44, 1579-1597. Mittlefehldt (1986) GCA 50, 107-110. Goodrich et al. (1987) GCA 51, 2255-2273. Takeda (1987) EPSL 81, 358-370. Rubin (1988) Meteoritics 23, 333-338. Warren and Kallemeyn (1992). Scott et al. (1993) Geophy. Res. Lett. 20, 415-418. Walker and Grove (1993) Meteoritics 28, 629-636.

Oxygen isotope micro-analysis of CAI by Secondary ion mass spectrometry.

M. Ito[1], H. Yurimoto[2] and H. Nagasawa[1].

[1]Faculty of Science, Department of Chemistry, Gakushuin University, Mejiro, Toshima-ku, Tokyo 171-8588, Japan.

[2]Department of Earth and Planetary Sciences, Tokyo Institute of Technology , Ookayama, Meguro-ku, Tokyo 152-8551, Japan.

Introduction.

By using high mass resolution analysis technique of secondary ion mass spectrometry (SIMS), the isotope ratios in individual minerals in meteorites and terrestrial samples can be determined [e.g. 1, 2, 3, 4]. This technique is useful in geo- and cosmochemistry because the interesting parts of meteorite samples are too small for a conventional method of negative thermal ionization mass spectrometry (NTIMS) [e.g. 5, 6, 7] and gas mass spectrometry [e.g. 8].

Oxygen isotope distribution of 7R-19-1 (a), compact Type A CAI from Allende meteorite have been measured by SIMS with a high mass resolution technique. In this paper some new data, in addition to those reported in 29th LPSC [9], are presented and discussed.

2. Experimental Procedure.

2.1. Sample Description.

The sample used in this study was a polished thin section, 7R-19-1 (a) from 7R-19-1 coarse-grained compact Type A CAI in the Allende meteorite. Petrographically 7R-19-1 consists of melilite ($Åk_{13\text{-}30}$, roughly 60 ~ 70 %), fassaite (~ 10 %) and spinel (~ 10 %) grains and, the rim fringed with sodalite.

2.2. SIMS analysis.

The polished samples were coated with 30 nm gold film for SIMS analysis in order to eliminate the electrostatic charge on the sample surface. Oxygen isotope ratios were measured by the T.I.Tech ims CAMECA 1270 SIMS instrument with a high mass resolution technique. The primary ion beam was massfiltered positive ^{133}Cs ions accelerated to 10 keV and beam spot size of ~ 3 μm diameter. Negative secondary ions of ^{16}O tail, ^{16}O, ^{17}O, ^{16}OH and ^{18}O were detected by an electron multiplier (EM) operated in a pulse counting mode. A mass resolution power was set to ~ 6000, sufficient to completely eliminate hydride interference (Fig 1) in order to resolve ^{17}O from mass interference of ^{16}OH. The basic conditions for oxygen isotope measurement

are described in the previous work in detail [9].

The matrix effect which may cause inter-mineral systematic errors can be checked by comparing the analytical results for terrestrial analogues. The instrumental mass fractionation is another possible cause of systematic errors. For the purpose of estimating the matrix effect and instrumental mass fractionation, we measured oxygen isotope ratios of terrestrial standards with known oxygen isotopic ratios [3].

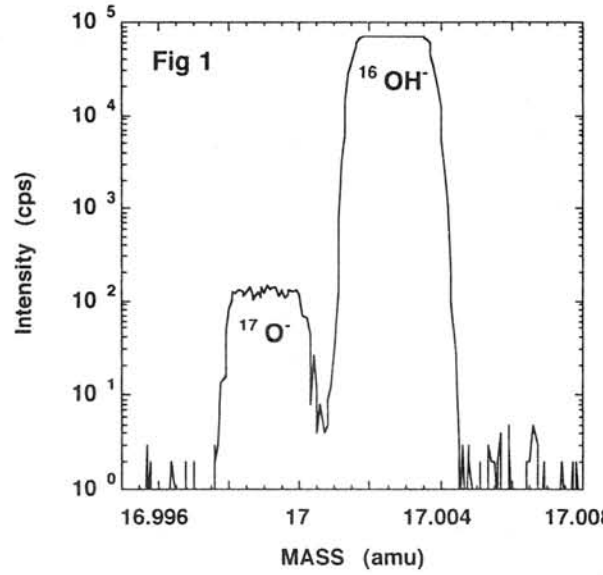

Fig 1. High resolution spectrum in the mass 17 region for SPU (spinel from Russia). The molecular hydrous ion interference of $^{16}OH^-$ is well separated from the $^{17}O^-$ peak at a mass resolving power of ~ 6000.

Results and Discussion.

For 7R-19-1 (a), the $\delta^{18}O$ and $\delta^{17}O$ values of the spinel measured range from -42.1 ± 2.3 ‰ to -27.3 ± 1.8 ‰, and -41.5 ± 3.3 ‰ to -28.0 ± 2.9 ‰ (all errors are 1 σ mean), respectively. This CAI has two melilite crystals; the $\delta^{18}O$ and the $\delta^{17}O$ values of the melilite #1 measured range from -12.7 ± 2.1 ‰ to -8.1 ± 2.1 ‰, and -13.4 ± 3.2 ‰ to -4.1 ± 3.5 ‰, respectively, and the $\delta^{18}O$ and the $\delta^{17}O$ values of the melilite #2 measured range from -50.8 ± 2.0 ‰ to -30.2 ± 2.0 ‰, and -49.6 ± 3.1 ‰ to -28.8 ± 3.4 ‰, respectively. The $\delta^{18}O$ and the $\delta^{17}O$ values of the blocky fassaite measured range from -18.5 ± 2.1 ‰ to -0.0 ± 2.1 ‰, and -24.3 ± 3.0 ‰ to 1.1 ± 3.1 ‰, respectively. The $\delta^{18}O$ and the $\delta^{17}O$ values of the fassaite grains in melilite #1 measured -16.5 ± 2.1 ‰, and -16.9 ± 3.3 ‰, respectively. The $\delta^{18}O$ and the $\delta^{17}O$ values of the fassaite grains in melilite #2 measured ranged from -36.3 ± 2.0 ‰ to -33.6 ± 2.0 ‰, and -37.8 ± 3.0 ‰ to -32.2 ± 3.1 ‰, respectively.

The results are plotted in a three isotope diagram which is shown in Fig 2. The values for 7R-19-1(a) fall on the carbonaceous chondrite anhydrous minerals (CCAM) line. However, in 7R-19-1 (a) all 3 minerals showed large negative anomalies with the order, spinel and melilite > fassaite, which is parallel to the crystallization sequence [10]. Nevertheless the order of the size of the oxygen isotope anomalies is different from that observed for normal type B1 CAI's, the lower limit values of ~ -40 ‰ is similar to the normal CAI's. ^{16}O excess in melilite was found in an Allende CAI [9, 11].

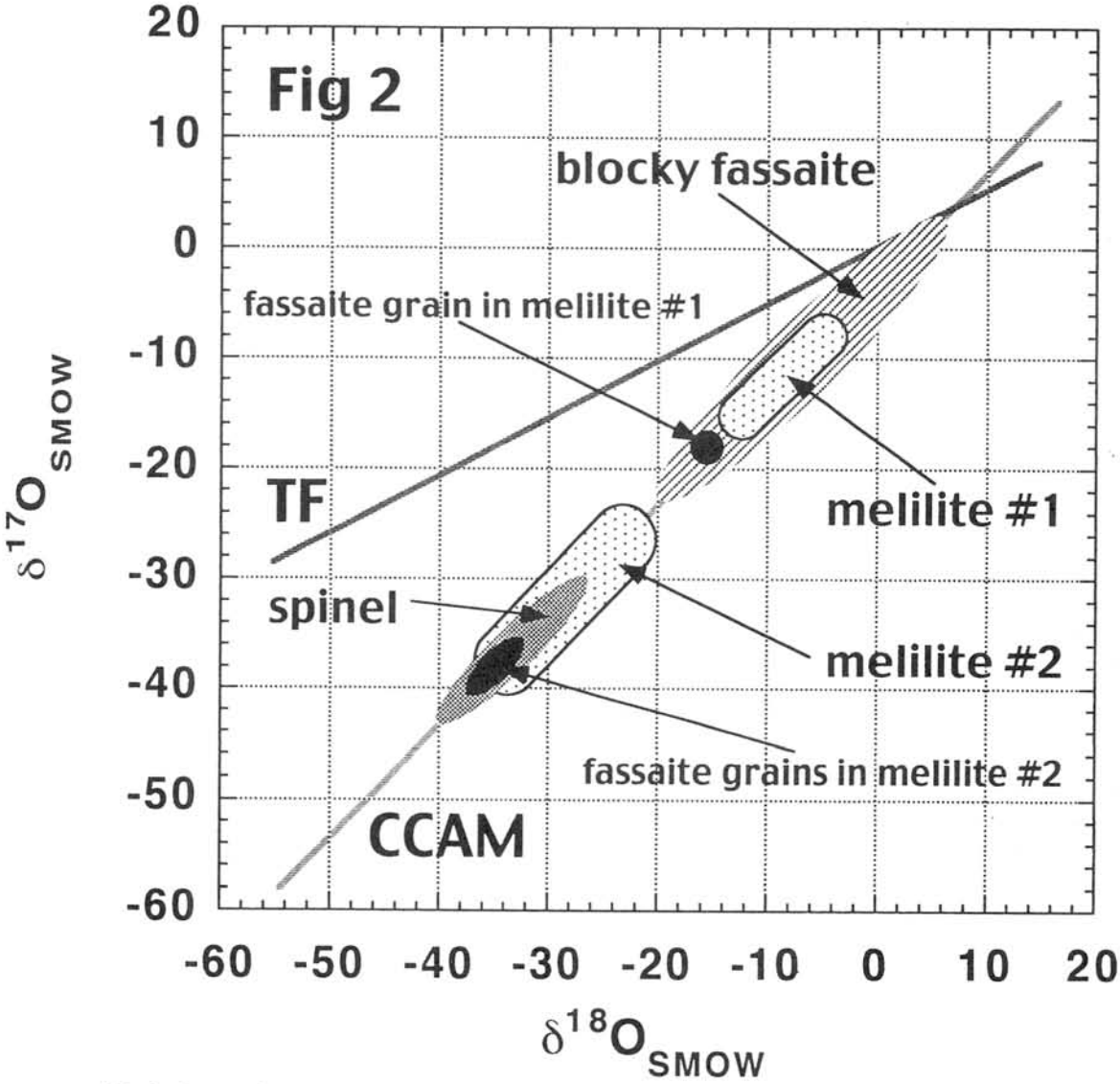

Fig 2. Oxygen isotope compositions of 7R-19-1 (a) from Allende meteorite. Terrestrial Fractionation (TF) line and carbonaceous chondrite anhydrous mineral mixing (CCAM) line defined by previous data [12] were presented.

References.

[1] Hervig, R. L. et al. (1992) Intl. J. Mass. Spec. Ion. Proc. **120**, 45-63. [2] Riciputi, L. R. and Paterson, B. A. (1994) American Mineralogist, **78**, 1227-1230. [3] Yurimoto, H. et al. (1994) EPSL, **128**, 47-53. [4] Leshin, L. A. et al. (1997) GCA, **61**, 835-845. [5] Heumann et al. (1989) Proc. 5th ASMS Conf. Mass. Spectrometry, 414-416. [6] Wachsmann and Heumann (1991) Intl. J. Mass. Spec. Ion. Proc. **108**, 75-86. [7] Holmden et al. (1997) GCA, **61**, 2253-2263. [8] Clayton, R. N. and Mayeda, T. K. (1977) Geophy. Res. Lett., **4**, 295-298. [9] Ito, M. et al. (1998) LPSC, **29**, #1556, CD-ROM. [10] Stolper, E. (1982) GCA, **46**, 2159-2180. [11] Kim, G. L., Yurimoto, H. and Sueno, S. (1998) LPSC, 29, #1344, CD-ROM. [12] Clayton, R. N (1993) Annu. Rev. Earth Planet. Sci., **21**, 115-149.

Na-BEARING Ca-Al-RICH INCLUSIONS IN FOUR CO3 CHONDRITES, KAINSAZ, ORNANS, LANCE, AND WARRENTON

Daisuke Itoh and Kazushige Tomeoka
Department of Earth and Planetary Sciences, Faculty of Science, Kobe University, Nada, Kobe 657-8501, Japan

INTRODUCTION

Ca-Al-rich inclusions (CAIs) in some CO3 [1,2] and CV3 [3-6] chondrites contain various amounts of low-temperature phases such as nepheline and sodalite. These phases were formed by replacing primary high-temperature phases like melilite and anorthite [6,7]. Most previous authors have interpreted that nepheline and sodalite formed by reaction with the solar nebula gas before accretion to the meteorites [1-6]. However, recently, some authors [8-10] suggested that they may have formed during secondary alteration processes that occurred on the meteorite parent body. Kojima et al.[9] compared alteration features in CAIs in three Antarctic CO3 chondrites and found that there are apparent correlations between the degree of alteration and the metamorphic grade of the host meteorites. Russel et al. [10] also found similar correlations in ten CO3 chondrites and concluded that CAIs in CO3 chondrites have experienced secondary alteration both before and after accretion. However, the number of CAIs studied in detail is still limited and much remains to be known as to whether the alteration of CAIs occurred before or after accretion or both. We here present the results of mineralogical and petrographic study of CAIs in four non-Antarctic CO3 chondrites, Kainsaz, Ornans, Lance and Warrenton. These meteorites were classified into petrologic type 3.1, 3.3, 3.4 and 3.6, respectively [11], spanning a wide range of metamorphic grades.

RESULTS

61, 54, 47 and 46 CAIs were found from each thin section of Kainsaz, Ornans, Lance and Warrenton, respectively. They range in diameter from 50 to 550 μm, and most are <200 μm. In order to compare the degree of alteration based on the modal contents of secondary phases, CAIs of approximately similar size ranging in diameter between 100 and 200 μm were selected. Consequently, 48 (Kainsaz), 41 (Ornans), 41 (Lance) and 37 (Warrenton) CAIs were selected and subjected to detailed investigation; they represent more than 75 % of the total inclusions found from each meteorite.

Most inclusions in all the four meteorites contain various amounts of nepheline. Nepheline commonly shows irregular contacts with melilite, fassaite and spinel, which indicates that the nepheline was formed by replacing these minerals. For comparison of degree of alteration, the inclusions were divided into four types based on the modal contents of nepheline, i.e., very lightly altered (<10 modal%), lightly altered (10-25 modal%), moderately altered (25-50 modal%), and heavily altered (>50 modal%). The results of modal analysis are shown in Fig. 1.

Kainsaz (type 3.1)

Among the 48 inclusions studied, 30 are single concentric objects or aggregates of concentric objects; each object has a core of spinel, mantled by bands of nepheline, melilite and aluminous diopside. Anorthite occasionally occurs immediately inside of the pyroxene rims. The spinel core commonly contains tiny grains of perovskite and hibonite. These inclusions resemble the "nodular" and "banded" spinel-pyroxene inclusions described by MacPherson et al. (1983) from the Murchison CM chondrite. 18 inclusions are rimmed objects which have an internal area composed of interlocking melilite and Fe-free or -poor spinel containing small grains (<10 μm in diameter) of perovskite. The rims consist of aluminous diopside. These rimmed objects correspond to the melilite-spinel-rich inclusion (Y17-21) described by Tomeoka et al. (1992) from the Yamato-791717 CO3 chondrite.

Among the inclusions in the four meteorites, those in this meteorite show the lowest modal contents of nepheline and the highest melilite contents; approximately 50 % of all the inclusions contain <25 modal% of nepheline (Fig.1). Nepheline commonly occurs as fine grains (<5 μm in diameter) and forms porous aggregates with fine grains (<2 μm in diameter) of troilite. Occasionally small amounts of Cl were detected from nepheline, which indicates that minor amounts of sodalite are probably intermixed with nepheline. Spinel shows a wide range of Fe content (1.7-64 mol% $FeAl_2O_4$) (Fig. 2) and weak Fe-Mg zoning. There is an apparent tendency that the inclusions with melilite contain less amounts of Fe-rich spinel than those without melilite (Fig. 2). Perovskite is common, whereas ilmenite is rare; ilmenite is found only

in five heavily altered inclusions.

Ornans (type 3.3)

Among the 41 inclusions studied, 19 are concentric objects and 22 are rimmed objects. Their internal textures are similar to those in Kainsaz, although they generally show higher modal contents of nepheline (Fig. 1) and lower modal contents of melilite than those in Kainsaz. There is also a tendency that the inclusions with melilite contain less amounts of Fe-rich spinel than those without melilite. Most nepheline occurs as porous aggregates with tiny troilite grains. Spinel shows a wide range of Fe content (0-69 mol% $FeAl_2O_4$) and is generally more enriched in Fe (Fig. 2) and shows more developed Fe-Mg zoning than that in Kainsaz. Perovskite is common, but in heavily altered inclusions, perovskite is partly replaced by ilmenite.

Lance (type 3.4)

Among the 41 inclusions studied, 27 are concentric objects and 14 are rimmed objects. In general, the inclusions contain higher modal contents of nepheline and lower modal contents of melilite than those in Ornans (Fig.1). Spinel shows a wide range of Fe content (0.6-65 mol% $FeAl_2O_4$), but in general, a higher proportion of spinel grains than those in Ornans are enriched in Fe (Fig. 2). Approximately 56 % of the inclusions have interiors composed largely of Fe-rich spinel, nepheline and troilite. There is also a tendency that the inclusions with melilite contain less amounts of Fe-rich spinel than those without melilite. In very lightly or lightly altered inclusions perovskite is common, while in heavily altered inclusions ilmenite is more common than perovskite.

Warrenton (type 3.6)

Due to extensive formation of nepheline and absence of melilite, it was difficult to distinguish between concentric objects and rimmed objects. Among the 37 inclusions, 22 have diopside rims. In general, the modal contents of nepheline are much higher than those in the meteorites described above (Fig.1). More than 90 % of the inclusions contain >25 modal% of nepheline, and there is no inclusion classified into very lightly altered type. In contrast to the inclusions in the other meteorites, nepheline crystals are commonly well developed and show smooth surfaces, and most are free of troilite grains. All spinel is enriched in Fe and very homogenized (47-53 mol% $FeAl_2O_4$). Anorthite occurs in close association with nepheline. In highly altered inclusions, even spinel is replaced by nepheline. Ilmenite is common, but perovskite is not observed.

DISCUSSION

The present study reveals that the inclusions in the four non-Antarctic CO3 chondrites have similar overall textures; most are concentric and rimmed objects. However, the internal mineralogy shows great variations between meteorites. The rimmed objects in Kainsaz generally contain major amounts of melilite and minor amounts of nepheline, while those in Ornans, Lance and Warrenton contain, progressively in this order, less melilite and more nepheline. From texture and mineralogy, it is probable that the rimmed objects in Ornans, Lance and Warrenton were originally rich in melilite and had texture similar to the rimmed objects in Kainsaz, but during alteration, melilite was preferentially consumed to form nepheline. Therefore, the differences in mineralogy between the inclusions in the four CO3 chondrites probably reflect different degrees of alteration.

Previous workers [6,7,9] showed that there are considerable differences in resistance to alteration among the primary minerals in CAIs. Melilite is the most susceptible to alteration to nepheline, and as the alteration proceeds, fassaite and even spinel are subjected to alteration. However, diopside, which commonly constitutes inclusion rims, is the most resistant to alteration. Along with the formation of nepheline, troilite is formed, spinel is enriched in Fe, and perovskite is replaced by ilmenite. All of these alteration features are observed in the CAIs in the four CO3 chondrites studied. Comparison of mineralogy before and after alteration suggests that considerable amounts of Na, Fe and S were added to CAIs, while some amounts of Ca and Mg were lost during alteration.

Based on the modal contents of nepheline (Fig. 1), we conclude that the relative degrees of alteration in CAIs are as follows: Kainsaz < Ornans < Lance < Warrenton. This order is the same as the increasing order of metamorphic grades of the host meteorites. The relationship between the modal content of nepheline and the metamorphic grade of the host meteorites resembles that observed in the CAIs in the three Antarctic CO3 chondrites, Y81020 (petrologic type 3.0), Y82050 (type 3.1) and Y790992 (type 3.3-3.5) [9]. Therefore, these results, taken together,

suggest that the alteration, especially the formation of nepheline, in CAIs in the CO3 chondrites was related to the metamorphism of the host meteorites that occurred on the CO meteorite parent body.

REFERENCES

1. Kurat G. (1975) Tschermaks Min. Petr. Mitt. 22, 38-78.
2. Davis A.M. (1985) Lunar Planet. Sci. 16, 165-166 (Abstr.).
3. Wark D.A. and Lovering J.F. (1977) Proc. Lunar Sci. Conf. 8th, 95-112.
4. MacPherson G.J. and Grossman L. (1984) Geochim. Cosmochim. Acta 48, 29-46.
5. Wark D.A. (1986) Earth Planet. Sci. Lett. 77,129-148.
6. Hashimoto A. and Grossman L. (1987) Geochim. Cosmochim. Acta 51, 1685-1704.
7. Tomeoka K., Nomura K. and Takeda H. (1992) Meteoritics 27, 136-143.
8. Greenwood R.C., Hutchison R., Huss G.R. and Hutcheon I.D. (1992) Meteoritics 27, 229 (Abstr.)
9. Kojima T., Yada S. and Tomeoka K.(1995) Proc. NIPR Symp. Antarct. Meteorites 8, 79-96.
10. Russell S.S., Huss G.R., Fahey A.J., Greenwood R.C., Hutchison R. and Wasserburg G. J. (1998) Geochim. Cosmochim. Acta, in press.
11. Scott E.R.D. and Jones R.H. (1990) Geochim. Cosmochim. Acta 54, 2485-2502.

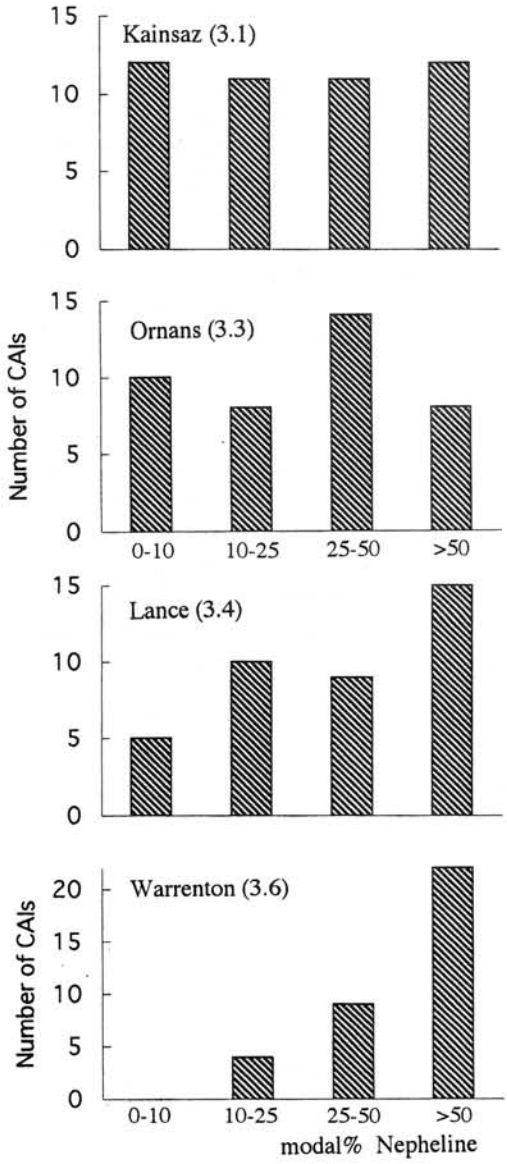

Fig. 1 Modal contents of nepheline in inclusions in the four CO3 chondrites.

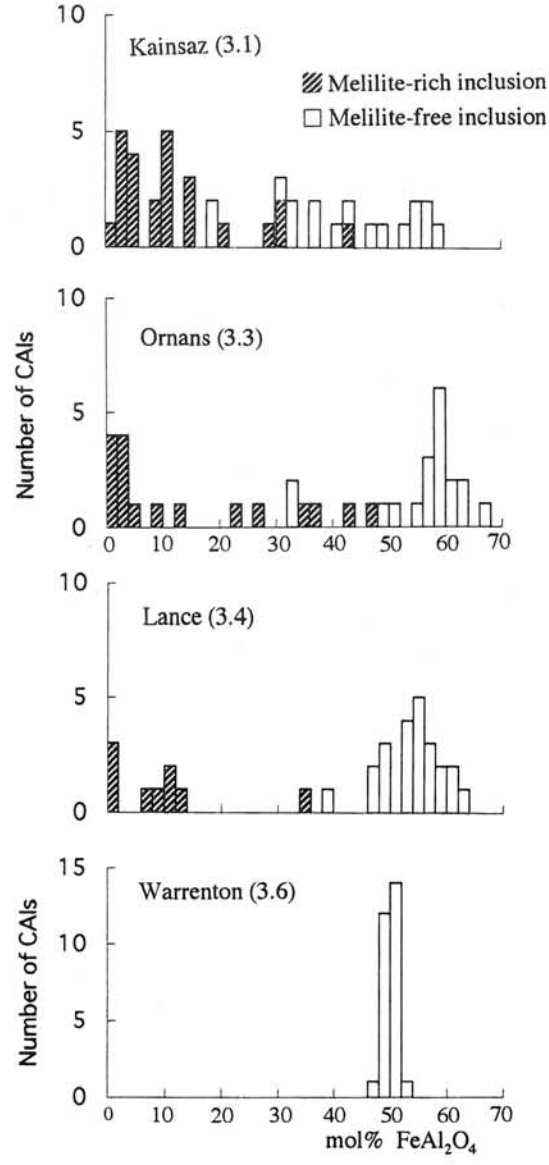

Fig. 2 Hercynite ($FeAl_2O_4$) contents of spinel in inclusions in the four CO3 chondrites.

Petrology of unique Fe-Ni metal bearing cumulate eucrite EET92023

K. Kaneda [1] and P. H. Warren [2]

1: Mineralogical Institute, Graduate School of Science, University of Tokyo, Tokyo 113-0033, Japan
2: Institute of Geophysics and Planetary Physics, UCLA, Los Angeles, CA 90095-1567, USA

Introduction: EET92023 is a brecciated cumulate eucrite that superficially resembles Moore County, but contains a high proportion (>1.3 vol%) of opaque phases. Siderophile concentrations are also extraordinarily high in EET92023, and based on an INAA study Mittlefehldt et al. [1] tentatively suggested that it might be a clast from a mesosiderite rather than a normal cumulate eucrite. The siderophile elements are presumably concentrated mainly in Fe-Ni metal phases. Most eucrites contain very little metal, and even those metals that occur are typically extremely depleted in Ni and other siderophile elements [2, 3]. The Fe-Ni metal phases observed in this meteorite may be parts of a Fe-Ni metal containing meteorite that fell on the surface of the HED parent body, and this unique eucrite may provide information about the formation environment of the HED crust. We have studied its texture and mineralogy, and used INAA and RNAA to determine a larger suite of siderophile elements.

Petrography and mineralogy: EET92023 shows gabbroic structure, mainly composed of pyroxene (~59.1%), plagioclase (~38.9%), iron sulfide (~0.8%), Fe-Ni metal (~0.5%), silica (~0.5%), phosphate (~0.1%), chromite (<0.1%) and ilmenite (<0.1%). Mesostasis was not observed.

Plagioclase: Plagioclase grains are typically euhedral, rectangular with rounded edges, and show comparatively strong chemical zoning. Typically, an euhedral high-Ca (~An95) core has been preserved, and at the grain edge a thin irregular Na-rich rim (An ~ 80) partly covers the higher Ca area (Fig. 1). Composition of the most Na-rich rim shows An ~68. Large plagioclase grains usually include pyroxene spherules, up to 130 μm in diameter, between the high-An core and Na-rich rim.

Pyroxene: Pyroxene crystals are subhedral and medium ~ coarse grains, up to ~2.0 mm in maximum dimension. They have fairly thin augite exsolution lamellae, generally <0.5 μm wide, spaced several micrometers apart. Small to medium size pyroxenes (~<300 μm) show almost constant *mg* value (Mg/(Mg+Fe)) ~0.51, but in large pyroxenes *mg* decreases from core (~0.58) to rim (~0.51). Large grains also retain a remnant of Ca zonation, with augite lamellae increasing in thickness toward rim. Pyroxene spherules included in plagioclases also have augite lamellae, and their average composition is very close to that of the medium-sized pyroxenes.

At the rims of some pyroxenes, especially near FeS and Fe-Ni metal, discrete augite and low-Ca pyroxene dominated regions (50-100 μm across) are observed (Fig. 2). On a plot of Al_2O_3 vs. Wo in pyroxene (Fig. 3), these regions show lower Al contents than normal EET92023 pyroxenes (poorly exsolved pigeonites) of similar Wo. Contents of Cr and Ti are also unusually low in these regions. Most of the augite and low-Ca pyroxene in this rock clearly formed by exsolution from primary-igneous pigeonite, but these regions might have formed as primary-igneous augite + low Ca pyroxene after the crystallization of the normal pyroxenes. Primary augite does not seem to be present in any other cumulate eucrite [e.g., 2]. In three-pyroxene assemblages among terrestrial andesites, wt% Al_2O_3 is usually slightly higher in opx than in pigeonite, and ~2× higher in augite than in pigeonite [4]. However, oxygen fugacity (and thus the ferric/ferrous iron ratio) is vastly higher during genesis of andesite than it was in the case of EET92023.

Phosphates: Both whitlockite and apatite are present. The whitlockite contains 1.0-1.3 wt% Na_2O. The apatite is very Na-poor, and is usually enveloped, or partially enveloped, by coarser whitlockite.

Fe-Ni metal: The most characteristic feature of this eucrite is its high abundance of Fe-Ni metal (up to ~300 μm in size). Like metal observed in ordinary chondrites and iron meteorites, Fe-Ni metal in this eucrite has two main

phases, Ni-poor (kamacite) and Ni-rich (taenite), and shows chemical zoning in taenite (Fig.4, 5). At the edges of taenite phases, Ni contents exceed ~48 wt% and there is a compositional discontinuity, suggesting the presence tetrataenite and outer taenite rim (OTR) [5]. The composition of kamacite is almost constant (~4.8 wt% Ni) and there might be very weak chemical zoning toward taenite phase. Both kamacite and taenite grains are anhedral but equigranular, unlike the irregular xenomorphic metal seen in mesosiderites. Boundaries between kamacite and taenite are sharp and linear, and a Ni-rich (>48 wt%) rim invariably surrounds the taenite phase. Therefore, the observed Fe-Ni metal structures were formed by reheating or annealing.

Other minerals: Chromite and ilmenite are generally small (<100 μm) and rare. Only one large chromite grain (~300 μm) with fine ilmenite lamellae (<5 μm wide) was observed. Silica generally fills gaps between plagioclase grains.

Estimated cooling rate from Fe-Ni metal: Because, as noted above, the boundary between kamacite and taenite phase is sharp and linear, we applied a planar diffusion model to the observed Ni zoning profile in taenite to estimate the approximate cooling rate of Fe-Ni metal. In this eucrite, Ca-phosphates are scattered and some are situated near metal phase, so the effects of P on diffusion coefficients were considered when the simulation was performed [6]. The Fe-Ni phase diagram adopted in this study was determined by investigation of Fe-Ni metal phases in meteorites [7]. Estimated cooling rate of Fe-Ni metal in EET92023 from computer simulation is ~4°C/My from ~700°C to ~300°C. This cooling rate is very slow even for cumulate eucrites.

RNAA and INAA analysis: Our analyses of two powder samples from a 600-mg chip confirm a strong bulk-compositional similarity to Moore County, except for siderophile elements. The siderophile contrast is even more dramatic than suggested by [1], who reported results in terms of EET92023/MC ratios, e.g., Ir = 100×. Our results (averaged, in μg/g) for Ni, Ge, Re, Os, Ir and Au are 1230, 1.41, 0.0053, 0.046, 0.050 and 0.015. As EET92023/MC ratios, using Moore County data from [8], the Re result is 2400× and the Os result is 15000×. These data hint at possible kinship with mesosiderites, because CI-normalized Re/Ir (1.3×) and Ge/Ir (0.40×) resemble, in dampened form, similar fractionations in mesosiderites. However, Ge/Ir is also much less than chondritic in howardites and polymict eucrites [9; also unpublished UCLA data].

Discussion: Although the zoning profile of Ni in taenite grain indicates very slow late-stage cooling, thin augite exsolution lamellae (<0.5 μm) in pyroxene and chemical zoning preserved in large pyroxene grains imply a quite fast cooling history, by cumulate eucrite standards. Even the discrete augites at the edges of pyroxene grains show weak chemical zoning of Al, Ti and Cr. Therefore, this eucrite should not be classified as a normal cumulate eucrite. The presence of Fe-Ni metal and high abundance of siderophile elements imply this meteorite originated from an impact melt, and the fast pyroxene cooling suggests that it originally crystallized at a relatively shallow depth. The slower cooling from ~700°C to ~300°C determined by Ni zoning profile of taenite suggests that the rock was relocated to a slower cooling environment while still at roughly 700°C. This transition of cooling rate might have been caused by burial, under impact ejecta, or perhaps under a massive effusion of lava. Another possibility, if the mesosiderite clast model is correct, is involvement in the general reheating of mesosideritic materials at ≥ 4.47 Ga, or their localized reheating at 4.5~3.9Ga [10]. However, the Fe-Ni metal and siderophile elements enrichments and fractionated Re/Ir and Ge/Ir ratios (i.e., the only evidence for a possible close relationship with mesosiderites) must have been preserved in EET92023 since its initial igneous crystallization.

References: [1] Mittlefehldt et al. (1996) Meteoritics, 31, A90. [2] Lovering J. F. (1975) *Meteoritics*, *10*, 101-114. [3] Palme H. et al. (1988) *Meteoritics*, *23*, 49-57. [4] Ishii T. (1981) *Initial Reports of the Deep Sea Drilling*

Project, *LIX*, 693-715. [5] Yang et al. (1997) GCA 61, 2943-2956. [6] Saikumar V. et al. (1988) GCA, 52,715-726. [7] Yang et al. (1996) J. Phase Equilibria, 17, 522-531. [8] Morgan et al. (1978) GCA, 42, 27-38. [9] Chou C.-L. et al. (1976) *Proc. Lunar Planet Sci. Conf. 7th*, 3501-3518. [10] Rubin and Mittlefehldt (1993) Icarus, 101, 201-212.

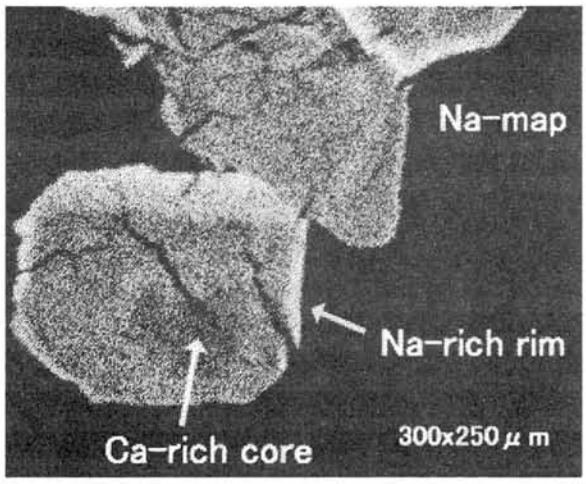

Fig. 1 : Chemical zoning of plagioclases.

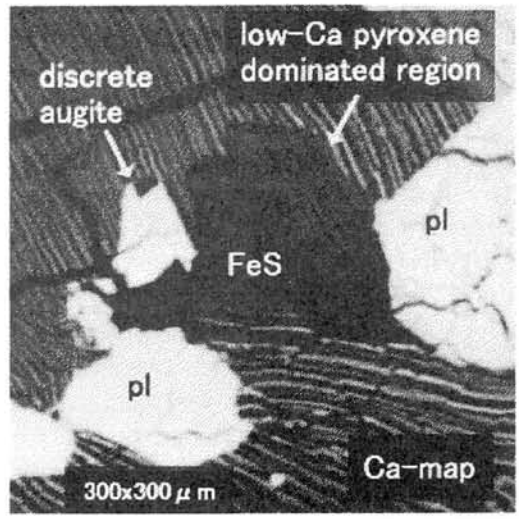

Fig. 2 : Discrete augite : considered to be primary-igneous origin.

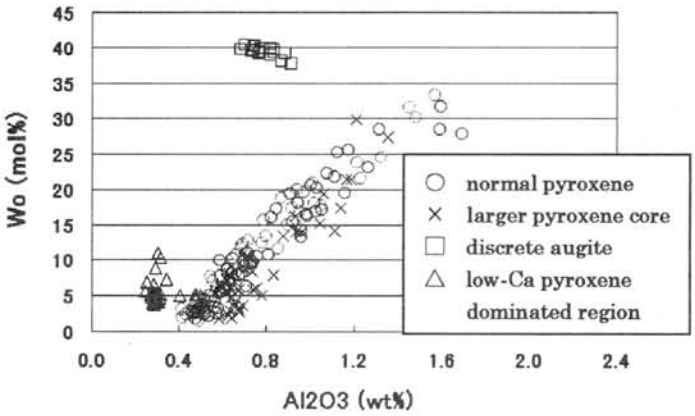

Fig. 3 : Discrete augites and low-Ca dominated regions show lower Al contents.

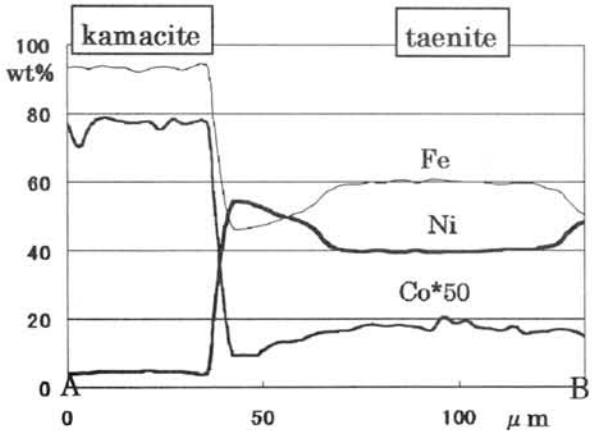

Fig. 5 : Zoning profile between kamacite and taenite. Co content is ×50.

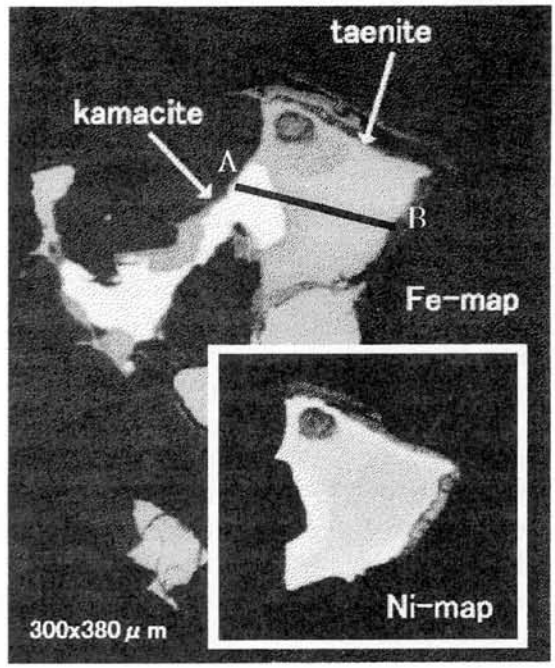

Fig. 4 : Fe-map and Ni-map of metal in EET92023. Zoning profile between A-B is shown in Fig. 5.

Petrological and mineralogical study of enstatite chondrites with reference to their thermal histories.

M. Kimura[1] and Y. Lin[2], 1) Ibaraki University, Mito 310-8512, Japan, 2) Guangzhou Institute of Geochemistry, Chinese Academy of Sciences, Guangzhou 510640, China.

Introduction

Enstatite chondrites are the most reduced chondrites, and some of them were once melted [1]. Lin and Kimura [2] noticed that four Antarctic enstatite chondrites are EH melt rocks. However, mineral chemistry of these meteorites revealed the complicated thermal histories; Three meteorites (Y-8404, Y-8414 and Y-86004) cooled rapidly near the surface of the parent body, whereas Y-82189 experienced slow cooling. Y-82189 contains the first occurrence of F-phlogopite in enstatite meteorites.

In order to explore the thermal histories of enstatite chondrites, here we report petrological and mineralogical features of 8 enstatite chondrites, compared with the results of our previous work [2].

Petrography

We studied ALH-77156 (EH3), Abee (EH melt breccia, [1]), Y-791510, Y-791790, Y-791810, Y-791811, Y-793258 and Y-86760 from the NIPR collection. Y-791790, Y-791810 and Y-791811 have abundant recrystallized chondrules and characteristic minerals of EH chondrites, *e.g.*, niningerite, indicating that they are EH4 chondrites. These three chondrites contain roedderite grains. Y-791790 has a glassy vein including eutectic intergrowth assemblages of kamacite and troilite, suggesting that this meteorite was partially melted.

Y-86760 includes no any chondrules and their relics, and shows typical melt rock texture predominantly consisting of euhedral orthoenstatite, 20-200 μm in size. The euhedral enstatites protrude into and/or are enclosed in Fe-Ni metal and troilite. Y-86760 is an EH melt rock. Y-791510 also seems to be a melt rock consisting of euhedral orthoenstatite. However, this meteorite severely experienced terrestrial weathering to lose most of opaque minerals. Y-793258 is well recrystallized and has alabandite grains. It is an EL6 chondrite.

The modal compositions of the samples were measured using a microanalyzer by the method of Lin and Kimura [2]. The EH3-4 and melt rocks including Y-8404 and others, contain 60-70 vol% and 50-60% enstatite, respectively. The abundance of plagioclase plus silica mineral is 6-12% in the EH3-4 and 14-28% in the melt rocks. On the other hand, the EH3-4 and melt rocks contain 9-16% and 3-16% Fe-Ni metal, and 5-13% and 12-21% total sulfides, respectively.

Mineralogy

One of the characteristic features of E-chondrites is diversity of minerals containing alkali metal and halogen elements; Plagioclase occurs in all samples. On the other hand, roedderite occurs only in the EH3-4 chondrites, and not in the EH melt rocks, except a tiny inclusion in Fe-Ni metal in Abee [3]. Djerfisherite and phases A and B, the unidentified alkali-bearing chromium sulfides, also exclusively occur in the EH3-4 chondrites, except for a melt rock, Y-82189, which also contains phlogopite.

Atomic Na/Na+K ratios of plagioclase are different between the EH3-4 (0.97-0.99) and melt rocks (0.94-0.95). It seems that the occurrence of djerfisherite (the Na/Na+K ratio: 0.11-0.27) and roedderite (0.50-0.70) compensates for almost K-free plagioclase in the case of the EH3-4 chondrites.

Thermal history

The diagram of FeS-MgS-MnS system [4] and FeS contents (~50-55 mol%) of niningerites in the EH melt rocks indicate closure temperatures of ~800°C, which agree with those of the other melt rocks, but are much higher than that of Y-82189 (~430°C) [2]. Such high temperatures suggest fast cooling of the melt rocks.

The modal compositions of the melt rocks indicate an enrichment of plagioclase, silica mineral and sulfides relative to enstatite, in comparison with the EH3-4 chondrites (Fig. 1). Yugami *et al.* [5] suggested that some differentiation processes including segregation and migration of partial melts of plagioclase component, occurred in primitive achondrites. It could be possible that similar differentiation processes also took place in the EH melt rocks.

References: [1] Rubin and Scott (1997) *GCA*, **61**, 425-435. [2] Lin and Kimura (1998) *Meteorit. Planet. Sci.* **31** (in press). [3] Kimura and El Goresy (1988) *Meteoritics* **23**, 279-280. [4] Skinner and Luce (1971) *Am. Mineral.* **56**, 1269-1297. [5] Yugami *et al.* (1997) *Antarctic Meteorites* **XXII**, 220-222. [6] Weisberg *et al.* (1995) *LPS* **26**, 1481-1482.

Fig. 1 Modal compositions of enstatite chondrites.

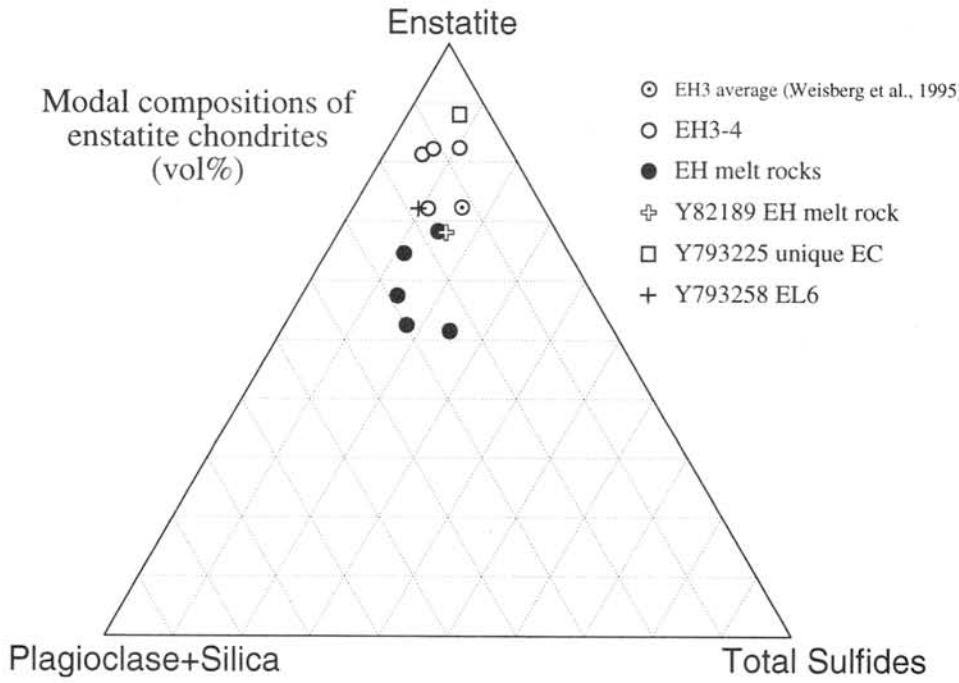

A DARK INCLUSION IN THE MURCHISON CM CARBONACEOUS CHONDRITE

Koji Kiriyama and Kazushige Tomeoka

Department of Earth and Planetary Sciences, Faculty of Science, Kobe University, Nada, Kobe 657-8501, Japan

INTRODUCTION

The CM chondrites consist largely of hydrous phyllosilicates and show abundant evidence of aqueous alteration that probably occurred on the meteorite parent body [e.g.1-3]. In contrast, type 3 carbonaceous chondrites (CV3 and CO3) contain little or no hydrous minerals and have been widely believed to have escaped major degree of aqueous alteration. However, it has been suggested recently that some dark inclusions (DIs) in CV3 chondrites were affected by extensive aqueous alteration and subsequent dehydration on the meteorite parent body [4-7]. The DIs are likely lithic clasts of the host CV3 chondrites [4-7]. This implies that there was a local region (or regions) in the CV parent body that at one time was involved in aqueous alteration and dehydration. DIs are common in CV3 chondrites, and to date, they have been mostly reported from this type of carbonaceous chondrites. We found an unusual inclusion from the Murchison CM chondrite; it is distinctly darker in color than the already dark host meteorite, thus it has an appearance resembling the DIs in CV3 chondrites. We here present the results of detailed mineralogical and petrographic study of this dark inclusion in Murchison.

MATERIAL AND METHODS

Two polished thin sections were made from the sample. The DI is subrounded in shape and approximately 10×8 mm and 7×6 mm in size on the thin sections. They were examined by an optical microscope, a scanning electron microscope equipped with an energy-dispersive X-ray spectrometer (EDS), and an electron-probe microanalyzer (EPMA).

RESULTS

The DI is composed mainly of chondrules embedded in a matrix. The chondrule size distribution and the modal content of matrix in the DI are similar to those in the host meteorite, although the modal content of chondrules in the DI (~18%) is slightly smaller than that (~20%) in the host meteorite. The matrix in the DI also has a composition similar to that of the host meteorite, thus probably consisting largely of Mg-Fe serpentine and tochilinite. PCP is also present. This DI contains a Ca-, Al-rich inclusion (CAI) (~350 μm in diameter) that consists of spinel, perovskite and Fe-rich serpentine. Thus, the DI is probably a CM clast or a clast of Murchison itself. However, our study reveals many significant differences in detailed mineralogy and petrography between the DI and host Murchison.

Chondrules in the DI generally contain more abundant Mg-Fe serpentine than those in the host meteorite; texture indicates that serpentine is produced by replacing not only mesostasis but also olivine and pyroxene phenocrysts. Approximately 95% of all the chondrules are surrounded by characteristic rims that consist mainly of serpentine and tochilinite, while ~69 % of all the chondrules have rims in the host meteorite. The chondrule rims in the DI are generally thicker (50-200 μm) than those in the host meteorite (mostly <100 μm), and ~42 % of them show a double-layer structure, while only ~7 % show a double-layer structure in the host meteorite; the rest of the chondrule rims in both DI and host show a single-layer structure.

The defocused electron beam analysis indicates that the matrix is slightly higher in Mg/Fe content than that in the host meteorite. In the matrix of the host meteorite, fine isolated grains (<10 μm in diameter) of olivine and pyroxene are dispersed, while in the matrix of the DI no such grains are present; instead, fine grains (<5 μm) of troilite are widespread. Fe-metal also occurs as isolated grains (~20 μm in diameter) in the matrix of the host meteorite, but no

metal is observed in the matrix of the DI.

PCP (type II) in the host meteorite is a rounded to irregularly shaped aggregate (10-100 μm in diameter) that occurs in the matrix; it is an intimate intergrowth of tochilinite and cronstedtite [2]; the proportion of these phases varies widely within and between grains. In contrast, most type-II PCPs in the DI show a characteristic core-rim structure with the rim being composed of troilite.

DISCUSSION

Individual CM chondrites were affected by various degrees of aqueous alteration [2,3,8], which probably occurred in situ on the regolith of the meteorite parent body. The different degrees of aqueous alteration are reflected in textures of chondrules and matrix, proportions of constituent minerals in matrix, and matrix compositions. It has been interpreted that as the alteration advances, magnesian olivine and pyroxene that constitute chondrules are consumed to form serpentine, and Fe-metal and Fe-sulfide are converted to tochilinite [2-3]. Simultaneously, cronstedtite in the matrix reacts with the newly formed serpentine, altering to ferroan serpentine. Thus the CM matrix is increasingly enriched in Mg with alteration.

The present study reveals that the DI in Murchison is most likely to be a clast of Murchison itself. However, chondrules in this DI are generally more intensely replaced by serpentine than those in the host meteorite, which suggests that the DI was affected by a higher degree of aqueous alteration than host Murchison. This is consistent with the high Mg/Fe ratio of the DI matrix and the absence of fine grains of olivine, pyroxene and Fe-metal in the matrix. The high abundance of fine grains of troilite in the matrix and the presence of troilite-rich rims in type-II PCPs suggest that the DI was affected by heating and dehydration after the aqueous alteration. Tochilinite is known to be thermally transformed to troilite at relatively low temperature (245°C) [9]. The texture of the matrix indeed resembles that in the unusual CM chondrites that have been thermally dehydrated [10-11].

Therefore, we conclude that this DI in Murchison has probably experienced a higher degree of aqueous alteration than the host Murchison meteorite and subsequent dehydration. The results suggest that the CM parent body was heterogeneous in the extent of not only aqueous alteration but also thermal metamorphism. The sequence of secondary processes, i.e. aqueous alteration and subsequent thermal metamorphism, resembles the processes that have been experienced by the dark inclusions in the CV3 chondrites [4-7]. Therefore, these results further suggest that the sequence of secondary processes was a common event that occurred on the C-chondrite parent bodies.

REFERENCES

1. Bunch, T.E. and Chang, S. (1980) Geochim. Cosmochim. Acta 44, 1543-1577.
2. Tomeoka, K. and Buseck, P.R.(1985) Geochim. Cosmochim. Acta 49, 2149-2163.
3. Browning, L.B., McSween, H.Y. and Zolensky, M.E. (1996) Geochim.Cosmochim.Acta 60, 2621-2633.
4. Kojima, T., Tomeoka, K. and Takeda, H.(1993) Meteoritics 28, 649-658.
5. Krot, A.N., Scott, E.R.D. and Zolensky, M.E. (1995) Meteoritics 30, 748-775.
6. Kojima, T. and Tomeoka, K. (1996) Geochim. Cosmochim. Acta 60, 2651-2666.
7. Krot, A.N., Scott, E.R.D. and Zolensky, M.E. (1997) Meteor. Planet. Sci. 32, 31-49
8. McSween, H.Y. (1979) Geochim. Cosmochim. Acta 43, 1761-1770.
9. Fuchs, L.H., Olsen, E. and Jensen, K.J. (1973) Smithson. Contrib. Earth Sci. 10, 1-39.
10. Tomeoka, K., McSween, H.Y. and Buseck, P.R. (1989), Proc. NIPR Symp. Antarct. Meteorites 2, 221-234.
11. Tomeoka, K. (1990) Proc. NIPR Symp. Antarct. Meteorites 3, 40-54.

IN-SITU SIMS U-PB ANALYSES OF APATITES FROM ORDINARY CHONDRITES.

Noriko T. Kita, Shigeko Togashi, and Yuichi Morishita
(Geological Survey of Japan)

Introduction: The U-Pb system is assumed to be the most reliable chronometer for meteoritic samples because (1) closure temperature is high, (2) the high precision of the age (in the order of 1 million years or smaller), (3) later disturbance to the chronometer is easily recognized by the discordant behavior between ^{238}U-^{206}Pb and ^{235}U-^{207}Pb systems. For ordinary chondrites, phosphate separates from several H chondrites showed the good correlation between the petrologic types and the U-Pb ages, indicating the "onion shell model" for the H chondrite parent body [1]. Thus, U-Pb chronometers are useful chronometer for understanding the thermal history of asteroidal bodies. Although the highly precise ages are obtained from the conventional U-Pb technique, phosphates are minor constituents in chondrites and grain sizes are as small as 10 μm, so that mineral separation is difficult and requires large amount of samples (10-20g bulk chondrites to obtain several mg phosphates). Furthermore, shocked or brecciated samples are not used because mineral separate becomes a mixture of grains with different thermal history. For this reasons, we have been trying to develop analytical method of in-situ U-Pb analyses using SIMS [2].

SIMS analyses: We used Cameca IMS-1270 at Geological Survey of Japan for the SIMS analyses. The analytical condition is very similar to that of terrestrial zircon dating. We used 20 μm spot for the phosphate analyses. In our previous preliminary results on Y792770 (H6) [2] have shown that (1) among the two phosphate minerals, apatite and whitrockite, apatite contains higher amount of U than whitrockite, (2) the precision of the radiogenic $^{206}Pb/^{207}Pb$ ratio of each analysis was 2%, (3) plagioclase analysis in the same meteorite is useful to determine non-radiogenic Pb composition for correcting apataite data, and (4) the Pb-Pb isochron age of Y792770 was obtained from 7 analyses of 3 apatite grains and the mean value of 5 plagioclase analyses to be 4505 ± 12 (2σ) Ma, which is similar to other published H6 U-Pb ages.

Improving Precision: Although the error of 12 million years is good enough to distinguish the ages between H4 (~ 4560 Ma) and H6 (~4500 Ma), the precision of 1 to 3 million years is required to understand thermal evolution of chondritic parent body. In order to improve precision, we need to measure numbers of apatite from a single meteorites. The polished section of Y792770 used in the previous work [2] was small (6mm x 6mm) and we could find only 3

large apatite grains for the analyses. In this work we prepared larger thin sections of Kernouve (H6) and Forestvale (H4) with the size of 10 mm x 5 mm. The precise U-Pb ages for these meteorites were obtained by Göpel et al (1994) [1], so that we can calibrate our SIMS results.

For H6 Kernouve, phosphates are course enough to identified by Back Scattered Electron image with the lower magnification (x 20) using JMS-6400 SEM. We found 8 apatites among 34 phosphate grains of the size between 10 μm to 200 μm. Some apatites are contained in the mixture of apatite and whitrockite (Fig. 1). For H4 Forest Vale, we used elemental mapping of P, Ca, and Cl to identify apatite grains using JXA-8800R EPMA. Although most phosphate grains are as small as 10 μm, some of phosphate grains are larger than 100 μm and they all appeared in the matrix phase. A half of the phosphates are found to be apatites.

In our previous work, we used 20 μm beam diameter for the SIMS analyses. However, according to the complex texture and small grain sizes of apatites in these chondrites, we should use beam diameter of 10 μm. We have tested the analytical condition using 10 μm beam for isotopic analyses of Ni and found to be successful. Therefore, such a smaller beam will be used for further Pb isotopic analyses, and the additional data will be reported at the meeting.

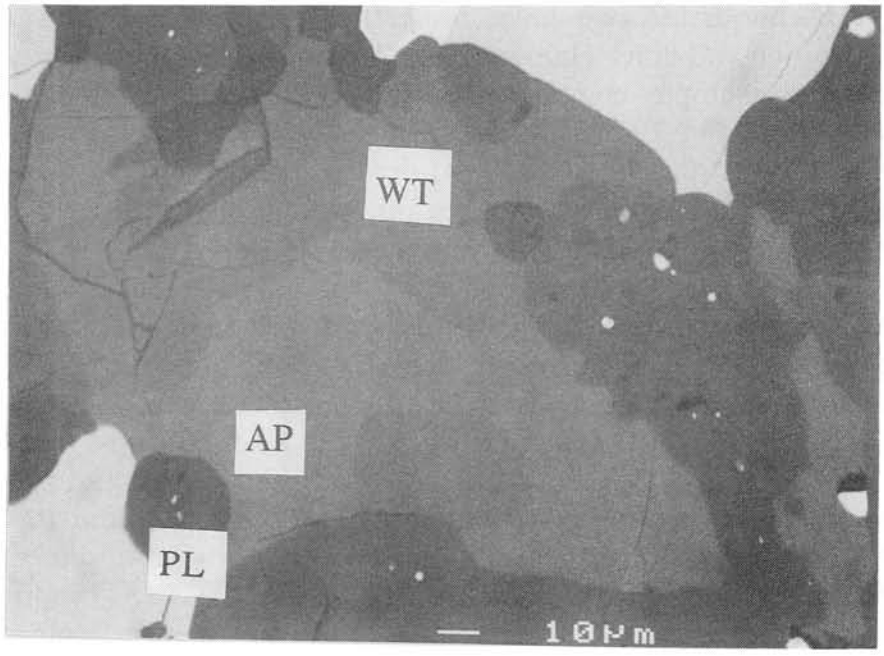

Fig. 1: An example of apatite grain in Kernouve H6 chondrite.

[1] Göpel C. et al. EPSL, 121, 153-171. [2] Kita N. T. et al. Meteorit. Planet. Sci. 32 Suppl. A72

CONSORTIUM STUDIES OF FIVE ANTARCTIC RUMURUTI CHONDRITES

H. Kojima[1], N. Imae[1], S. Sawada[2], N. Nakamura[2], R.N. Clayton[3], T.K. Mayeda[3], K. Yanai[4] & N. Morikawa[2]

[1]Department of Antarctic Meteorites, National Institute of Polar Research, Kaga 1, Itabashi, Tokyo 173, Japan, [2]Department of Earth & Planetary Sciences, Faculty of Science, Kobe University, Nada, Kobe 657, Japan, [3]Enrico Fermi Institute, University of Chicago, IL 60637, USA, [4]Department of Environmental and Planetary Sciences, Iwate University, Ueda, Morioka, Iwate 020, Japan

Rumuruti (R) group chondrites have been known as Carlisle Lakes-type chondrites and found to be a new grouplet which has bulk compositional similarities to the ordinary chondrites but with more oxidized features[1,2] and distinctive oxygen isotopic compositions [3]. Yanai et al. [4] first suggested that Y-79302 was classified as a new group of chondrites. This early suggestion has been substantiated by latter works [1,2]. Including Y-79302, several unique (Carlisle Lakes-type) chondrites have been identified in the NIPR collection [4]. Majority of the R-chondrites in NIPR is less than 10g in weight and have not been sufficiently investigated yet for their chemical, petrological and isotopic characteristics. In order to obtain better understanding of the origin and evolution of R-chondrites, we have undertaken (mini) consortium studies of petrography, major and trace element chemistry, Rb-Sr isotopic systematics, rare gas and oxygen isotopic compositions for five R-chondrites in NIPR. Two meteorites (A-881988, Y-791827) have not been reported yet and other three (Y-75302, Y-79575, Y-82002) have been studied previously[1,2,5]. We report here preliminary results of petrographic examinations, wet chemical and isotope dilution analyses of major and minor (partly trace) elements.

Results are presented in Table 1 and Fig. 1-3, It is noted that Sr, Ca, Fe as well as Mg are quite similar to averag ordinary chondrites but Al, Cr, Na and Rb are more variable in most R-chondrites studied. Parts of variations may be due to small sample sizes, however, systematic Na~K/Rb fractionations first observed in this work may be real. A-881988 is classified as subtype 4.0 and has the lowest mean Fa compositions among five chondrites and other R-chondrites previously reported[3]. Although Al is too high, other lithophile abundances are least fractionated relative to mean ordinary chondrites. Y-791827 appeared more weathered and overall PTS becomes red to brown colored, matrix recrystallization proceeds optically tranparent under the optical microscopes (subtype classification; 4.0). It shows generally variable lithophile abundances with high Na but low Rb. Isotopic analyses are in progress.

References: [1] Rubin A.E. & Kallemeyn G.W. (1989), GCA 53, 3035-3044, [2] Weisberg M.K. et al. (1991), GCA 55, 2657-2669, [3] Kallemeyn G.W. (1996), GCA 60, 2243-2256, [4] Yanai K. et al. (1985) Meteoritics 20, 791 (abstr.) [5] Nakamura T. et al. (1993), Profc. NIPR Symp. Ant. Arct Met. 6, 171-185.

Table 1 Bulk chemical compositions of R-chondrites

	Y-791827*1)	Y-793575*1)	Y-793575*1)	Y-82002*1)	A-881988*2)
SiO_2	34.99	33.31	33.98	34.61	34.65
TiO_2	0.08	0.08	0.07	0.11	0.13
Al_2O_3	2.87	3.93	3.46	2.21	4.19
Fe_2O_3	8.42	5.85	5.52	9.23	8.62
FeO	19.25	19.62	18.51	17.61	11.19
MnO	0.26	0.23	0.25	0.34	0.34
MgO	22.37	22.36	22.54	23.74	22.98
CaO	2.08	2.23	1.69	1.67	1.63
Na_2O	1.21	0.89	0.91	0.78	0.88
K_2O	0.10	0.10	0.09	0.09	0.10
H_2O (-)	0.29	0.14	0.15	0.40	1.02
H_2O (+)	1.00	1.20	1.10	1.10	1.10
P_2O_5	0.52	0.43	0.45	0.13	0.30
Cr_2O_3	0.38	0.25	0.35	0.47	0.50
FeS	5.92	6.76	9.61	6.80	10.45
Fe	< 0.1	1.08	< 0.1	0.00	0.55
Ni	0.69	1.30	1.18	0.89	1.19
Co	0.041	0.040	0.037	0.044	0.041
Total	100.62	99.80	100.08	100.22	99.77
Total Fe	24.71	24.71	24.46	24.47	21.92

*1) Yanai and Kojima (1995)
*2) Unpublished

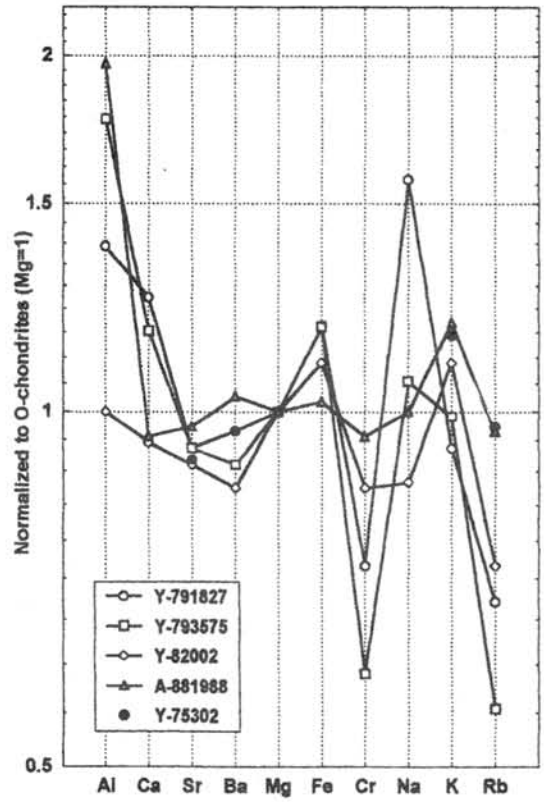

Fig. 1 Lithophile element abundnace patterns for 5 R-chondrites. Aluminum abundances are more variable and tend to be higher, Rb to be lower than typical ordinary chondrites

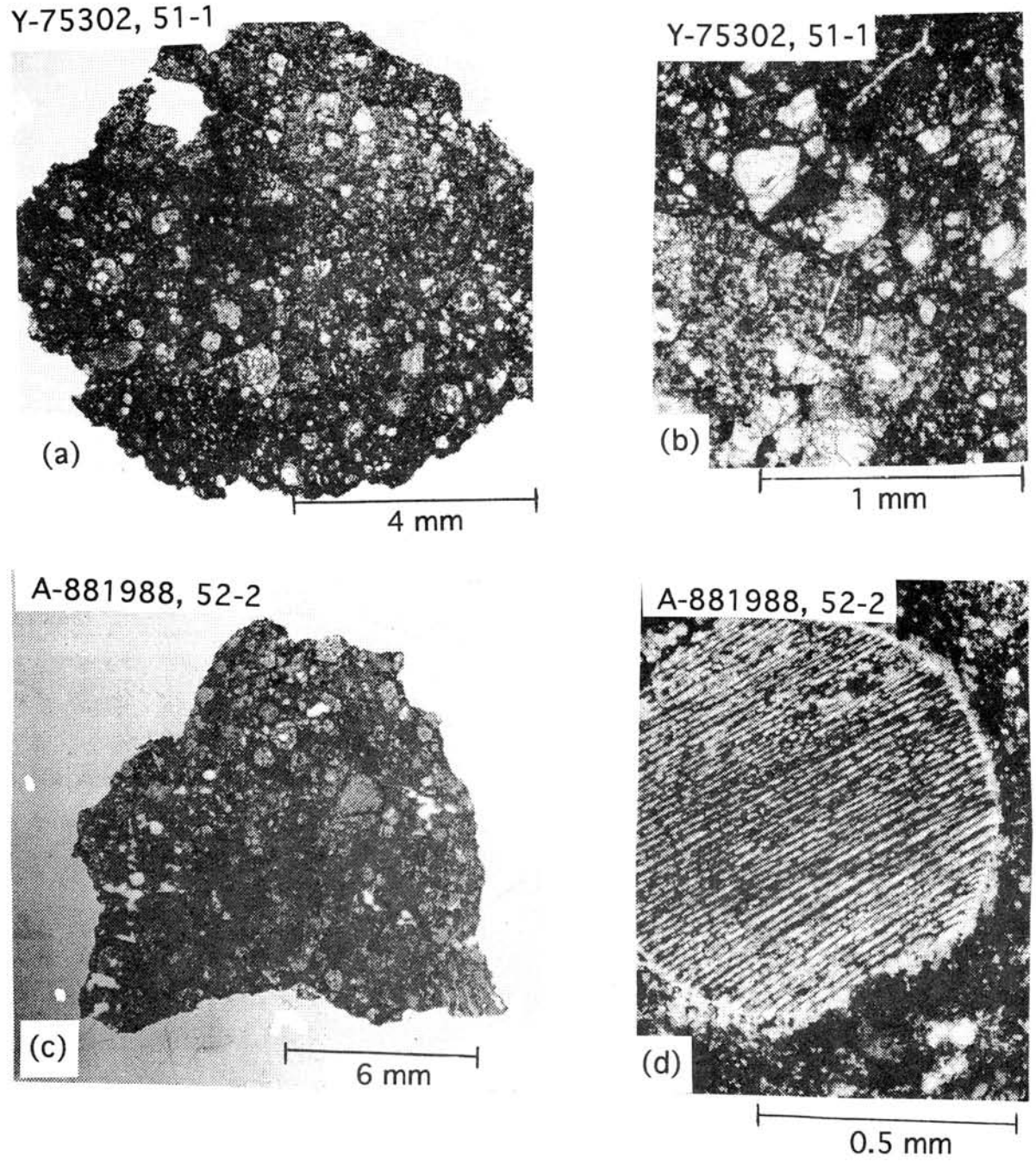

Fig. 2 Photomicrographs of the thin sections of Antarctic R-chondrites. (a) Yamato-75302, 51; The chondrule textures of PO and BO can be observed but RP can not be seen. The matrix is recrystalized (subtype 3.9). (b) The brecciated textures are noted. (c) Asuka-881988, 52-2; The matrix recrystalliztion proceeds transparent. (subtype 4.0). (d) Average chondrule sizes are largest among five R-chondrites examined in this work. Mean Fa compositions are lowest (Fig. 3) among five studied and other R-chondrites (Kallemeyn et al.1996).

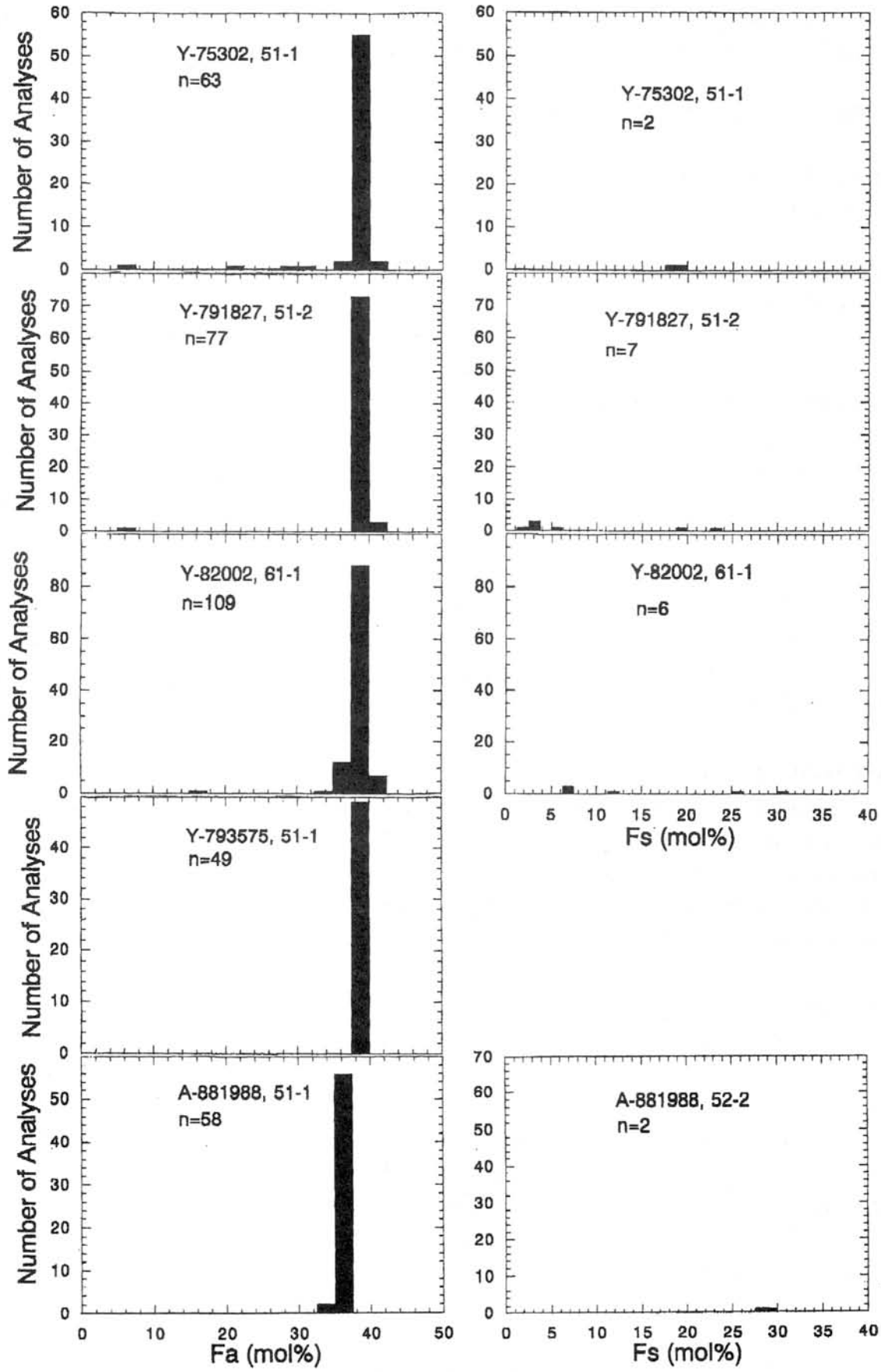

Fig. 3 Compositional distributions of olivine and low-Ca pyroxene of R-chondrites. For Y-793575, low-Ca pyroxene is not detected by random analyses.

HYDROTHERMAL ALTERATION OF THE ALLENDE CV3 CHONDRITE WITH NEUTRAL WATER: COMPARISON TO ALTERATION WITH ACIDIC WATER

Tomoko Kojima and Kazushige Tomeoka

Department of Earth and Planetary Sciences, Faculty of Science, Kobe University,
Nada, Kobe 657-8501, Japan

INTRODUCTION

CV3 chondrites are commonly believed to have escaped major degrees of aqueous alteration and thermal metamorphism on the meteorite parent body, and thus to be petrologically the most primitive of the known chondrite types. However, some CV3 chondrites contain considerable amounts of phyllosilicates that probably formed during alteration on the parent body [1-5]. Recent studies of dark inclusions in CV3 chondrites [6-10] also showed evidence that they have experienced various degrees of aqueous alteration and subsequent dehydration. In order to understand the alteration processes and conditions that these meteorites have experienced, we believe experimental studies are a promising approach. Previously we reported the results of hydrothermal experiments of the Allende CV3 chondrite performed with 1-N HCl [11]. The experiments produced remarkable alteration textures and mineralogy that are similar to those observed in naturally altered CV3 chondrites. We here present the results of hydrothermal experiments performed with neutral water and compare the results with the previous ones.

EXPERIMENTALS

Samples of Allende (0.1-0.2 g) were sealed in gold tubes with neutral water, then heated in a reactor vessel at 450°C and 800 bar for 7 weeks. Thin sections were made from the run products, and they were examined with an optical microscope, a scanning electron microscope (SEM) equipped with an energy-dispersive X-ray spectrometer and an electron-probe microanalyzer (EPMA).

RESULTS

Macroscopically the alteration products show little change in appearance; no significant amount of by-product is produced, which contrasts with the alteration with 1-N HCl [11]. However, the optical microscope observations indicate that the internal areas of most chondrules and Ca-, Al-rich inclusions (CAIs) are replaced by brownish-to-greenish phyllosilicate. The phyllosilicate also fills fractures in matrix, forming a network of veins (~10 μm wide and ~500 μm long). These features are similar to those observed in the products altered with 1-N HCl. The SEM observations reveal that the phyllosilicate shows characteristic fibrous texture. All the phyllosilicates in chondrules, CAIs and matrix contain major Si, Mg, Fe and Al (36-44 wt% SiO_2, 18-25 wt% MgO, 4-14 wt% FeO, 6-12 wt% Al_2O_3) and have compositions similar to Fe-rich saponite. They are similar in composition to the saponite in the products altered with 1-N HCl, although they show slightly higher Al contents than the latter. They are also similar in composition to the saponite in the Mokoia [1] and Kaba [2] CV3 chondrites. The high-Al phyllosilicate (HAP), which occurred in the products altered with 1-N HCl, is rare in the present run products.

The mesostases of chondrules are extensively replaced by saponite; numerous tiny grains (<1 μm in diameter) of an Fe-rich phase, probably magnetite or Fe-hydroxide, are intimately mixed with saponite. Olivine and low-Ca pyroxene grains in chondrules are also partly replaced by saponite; some low-Ca pyroxene grains show linear intergrowths with saponite and lath-shaped inclusions of Fe-rich olivine. However, the extent of alteration of olivine and pyroxene is much lower than that in the products altered with 1-N HCl. Mg-rich olivine grains are commonly rimmed by Fe-rich olivine, but it is difficult to determine whether the Fe-rich olivine rims were produced during the experiments or not. In CAIs, melilite and anorthite are partly replaced by relatively Al-rich saponite (<12 wt% Al_2O_3), but diopside, which commonly constitutes inclusion rims, and andradite remain unaltered.

Compared to the chondrules and CAIs, the matrix shows relatively minor effects of alteration. Most olivine grains in the matrix remain unaltered and show the original lath- to spindle-shape morphologies, although they show less sharp edges than those in the matrix of natural Allende. Saponite occurs in minor amounts mostly filling the narrow interstices between olivine grains. Although relatively large (10-50 μm in diameter) aggregates of saponite occur in the matrix of the products altered with 1-N HCl, no such aggregate is observed in the present products. Rounded aggregates composed of Ca-rich pyroxene and andradite remain unaltered. In general, the texture and mineralogy in the matrix are very similar to those in the matrix of Mokoia. The defocused electron beam analysis indicates that the matrix shows no significant differences in major element contents from the matrix of natural Allende.

DISCUSSION

By comparison of the abundance and the texture of phyllosilicates, it is evident that the extent of alteration is much lower in the products altered with neutral water than in those altered with 1-N HCl. This is probably related to the differences in dissolution rates of constituent minerals in an acidic solution and a neutral solution, because alteration reactiveness is considered to be generally dependent on dissolution rates of reactants, which in turn depend on solution pH [12]. Many of the ortho-, ino- and tecto-silicates show higher dissolution rates in an acidic solution than in a neutral solution [13]. The effect of dissolution is especially remarkable in the alteration of Ca-rich silicates and glass with 1-N HCl. In that alteration, most Ca^{2+} in these phases leached out and most of them are replaced by phyllosilicates. However, in the alteration with neutral water, diopside and andradite mostly remain unaltered. In CAIs in CV3 and CO3 chondrites, diopside is generally among the most resistant to alteration.

There are significant differences in phyllosilicate mineralogy between the products altered with 1-N HCl and those altered with neutral water. In the products altered with 1-N HCl, both saponite and HAP are produced [8]; saponite replaces mainly olivine and pyroxene in chondrules and matrix, while HAP replaces Ca-Al-Si-rich phases in chondrules and CAIs. However, the phyllosilicate produced in the alteration with neutral water is almost exclusively saponite. This is probably also related to differences in dissolution rates of reactant minerals in solutions of different pH. Therefore, the present experimental results suggest that pH in solution is an important factor to control phyllosilicate mineralogy. Such differences in phyllosilicate mineralogy are observed in some CV3 chondrites; Mokoia contains both saponite

and HAP [1], while Kaba contains only saponite [2]. The present results suggest that Mokoia was altered with a relatively acidic solution, while Kaba was altered with a neutral solution.

Some previous authors [e.g., 14] argue against an *in situ* parent-body origin for the phyllosilicates in CV3 chondrites based on the observation that olivine grains in the matrix have a relatively fresh appearance; where olivine and saponite coexist, euhedral olivine laths are enclosed by saponite. They imply that olivine and saponite formed separately in the nebula and were mixed during accretion. However, the present hydrothermal experiments reveal that although substantial areas of chondrules and CAIs are replaced by phyllosilicate, fine-grained matrix shows only very minor effects of alteration; most of micron-size olivine grains remain little altered and retain their original morphologies. The overall similarities in mineralogy and texture between the hydrothermally altered Allende samples and the naturally altered CV3 chondrites strongly suggest that the aqueous alteration of the CV3 chondrites occurred after accretion on the meteorite parent body.

REFERENCES

[1] Tomeoka K. and Buseck P. R. (1990) Geochim. Cosmochim. Acta 54, 1745-1754.

[2] Keller L. P. and Buseck P. R. (1990) Geochim. Cosmochim. Acta 54, 2113-2120.

[3] Keller L. P., Thomas K. L., Clayton R. N., Mayeda T. K., DeHart J. M. and McKay D. S. (1994) Geochim. Cosmochim. Acta 58, 5589-5598.

[4] Lee M. R., Hutchison R. and Graham A. L. (1996) Meteorit. Planet. Sci. 31, 477-483.

[5] Brearley A. J. (1997) Science 276, 1103-1105.

[6] Kojima T., Tomeoka K. and Takeda H. (1993) Meteoritics 28, 649-658.

[7] Krot A. N., Scott E. R. D. and Zolensky M. E. (1995) Meteoritics 30, 748-776.

[8] Kojima T. and Tomeoka K. (1996) Geochim. Cosmochim. Acta 60, 2651-2666.

[9] Krot A. N., Scott E. R. D. and Zolensky M. E. (1997) Meteorit. Planet. Sci. 32, 31-49.

[10] Buchanan P. C., Zolensky M. E. and Reid A. M. (1997) Geochim. Cosmochim. Acta 61, 1733-1743.

[11] Tomeoka K. and Kojima T. (1995) Papers presented to 20th Symposium on Antarctic Meteorites 251-253.

[12] White A. F. and Brantley S. L. (1995) Rev. Mineral. 31, 1-583.

[13] Oelkers E. H. (1996) Rev. Mineral. 34, 131-191.

[14] Cohen R. E., Kornacki A. S. and Wood J. A. (1983) Geochim. Cosmochim. Acta 47, 1739-1757.

LL CHONDRITES AND PRIOR'S RULES.

M. Komatsu[1] and A.M. Reid[2]

[1]Mineralogical Institute, Graduate School of science, University of Tokyo.
[2]Department of Geosciences, University of Houston, Houston TX 77204-5503

Introduction

The LL chondrites show enough range in composition to allow the search within the group for systematic trends in mineral compositions and abundances. In particular we are looking for changes that correlate with the petrographically expressed differences between petrologic types 4 through 7. We have checked and in a few cases have amended the classification from the Antarctic Newsletter. In doing so we have used only the petrographic criteria of Van Schmus and Wood [1], avoiding the use of any quantitative non-petrographic criteria (e.g. [2]). Some 42 LL chondrites from the collection at Johnson Space Center and National Institute of Polar Reserch have been studied to date.

Analytical Methods

Mineral compositions were determined using the Cameca SX100 electron microprobe at the Johnson Space Center and JEOL Superprobe 733 II at Geological Institute, University of Tokyo. All silicate and oxide analytical runs, and all metal and sulfide analytical runs were made under identical operating conditions. Reproducibility for repeat runs on the same highly equilibrated LL chondrite is cited in [3].

Variability in mineral composition within the LL group

Within the range of samples from LL4 to LL7 the variability in mineral composition decreases with increasing petrologic type [3]. For most samples of LL chondrite, other than the LL3s, the silicate compositions are remarkably homogeneous. This is particularly striking for the minimally recrystallized samples, the LL4s, which retain abundant textural indications of rapid cooling. Exceptions occur where relict olivines and pyroxenes of contrasting composition are partly preserved in LL4s.

Variations in olivine and pyroxene composition with petrologic type.

Within each petrologic type there are ranges in olivine and orthopyroxene composition. However the average iron content in olivine and orthopyroxene increases with the extent of recrystallization (Figure 1 and 2). These changes, noted by several authors [4-7], are consistent with the suggestion [7] that the progression to higher petrologic types is also a sequence of progressive oxidation.

Prior's Rules

Prior [8] observed that as metal decreases in abundance, it becomes more nickel-rich, and the silicates become more iron-rich. We have attempted to investigate whether Prior's Rules describing the mineralogical relationship among the H, L, and LL chondrites, are applicable within the LL group. If bulk compositions, other than oxygen, are essentially constant within the LL group, then any increase in iron in the silicates derives from oxidation of metal and/or sulfides. A test of Prior's Rules within the LL group is to determine whether in the sequence LL4 to LL7 there is also a progressive change in metal composition, in metal and sulfide abundance, in silicate abundance, and in olivine/pyroxene ratio.

Mineral Abundances

It is relatively easy, with modern electron microprobes, to determine mineral abundances either by multiple analyses on a grid system, or by constructing element abundance maps and deriving mineral abundances from the appropriate elemental images. Metal and sulfide abundances can even be derived

from back-scattered electron images because of the high contrasts in average atomic number. We have done this type of modal analysis on a number of LL chondrites. However the data are only of value for the surface areas of the individual thin sections analyzed and are of limited applicability to the bulk meteorites. The heterogeneity in size, shape and distribution of metal and sulfide grains within these meteorites makes it impossible to extrapolate modal data from individual thin sections. Reliable estimates of modal mineral abundances will have to be determined on significantly larger sample sizes than single thin sections.

Metal Compositions

The alternative approach is to determine metal compositions as a function of petrologic type. In LL chondrite, kamacite is the less abundant metal phase, particularly in the higher petrologic types where there are relatively few kamacite grains. The more abundant taenite increases in average Ni and in Co abundance from type 4 through type 7. Coexisting kamacite shows an increase in Co with petrologic type with little change in Ni content. There is an overall increase in both average Ni and Co for the bulk metal in LL chondrites, that correlates with increasing degree of recrystallization. Silicate and metal compositions are compared in Figure 3, which is a plot of FeO content in olivine, the major silicate, against Ni content of taenite, the more abundant metal phase. Increase in the iron contents in the coexisting metal, and the correlation appears to be a function of petrologic type.

Conclusions

Most LL chondrites are breccias and it is not uncommon for a single meteorite to contain clast with contrasting textures. Using the dominant textures to classify indivisual meteorites with respect to petrologic type, it is possible to demonstrate a correlation between mineral compositions and textures.

Over a significant range of compositions within the LL chondrites the iron content of the major silicates increases with petrologic type and this increase correlates with a change in the composition of coexisting metal grains which become progressively richer in Ni and Co. These mineralogical changes within the LL group are consistent with Prior's Rules. Prior's Rules are more commonly cited in describing the relationship that exists between the major ordinary chondrite groups, a relationship that may have been established prior to the accretion of chondrite parent bodies. The limited application of Prior's Rules described here for, a single cohesive group of ordinary chondrites, is associated with the textural and mineralogical changes that are generally considered to result from metamorphic processes occurring within the LL parent body.

The mineral data indicate that the sequence from LL4 to LL7 is an oxidation sequence [7] and may be accompanied by minimal change in bulk composition. These data and the limited presence of relict silicates in LL4 chondrites imply that the source material for the LL4 chondrites was a more reduced assemblage containing some highly magnesian silicates.

Acknowledgments

This work has been supported by NASA grant NAGW-3623 and by the LPI Summer Intern Program.

References

[1] Van Schmus W.R. and Wood J.A. (1967) Geochim. Cosmochim. Acta 31, 747-765. [2] Scott E.R.D., Taylor G.J. and Keil K. (1986) Proc. Lunar Planet. Sci. Conf. 17th, E115-123. [3] Reid A.M. (1997) Workshop on Parent-body and Nebular Modification of Chondritic Materials, LPI Tech. Rept. 97-12 Part 1, pp. 50-51. [4] Fredriksson K., Nelen J. and Fredriksson B.J. (1968) in Origin and Distribution of the Elements (L.H. Ahrens, ed.),pp. 457-466 . [5] Heyse J.V. (1978) Earth Planet. Sci. Lett. 40, 365-381. [6] McSween H.Y. and Patchen A.D. (1989) Meteoritics 24, 219-226. [7] McSween H.Y. and Labotka T.C. (1993) Geochim.Cosmochim. Acta 57, 1105-1114. [8] Prior G. T. (1916) Mineral. Mag. 17 , 33-38.

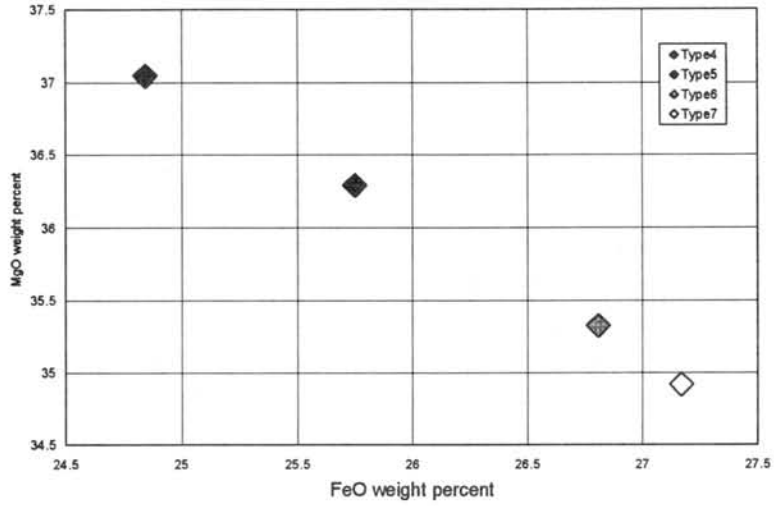

Figure 1. Average Olivine Compositions by Petrologic Type.

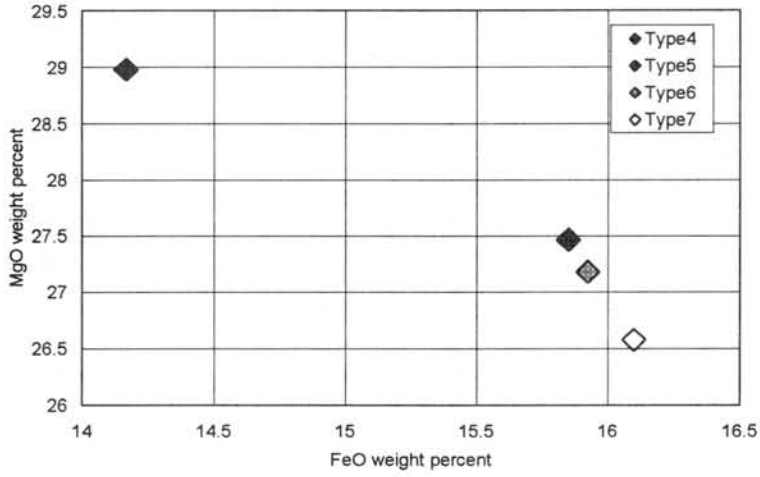

Figure 2. Average Orthopyroxene Compositions by Petrologic Type.

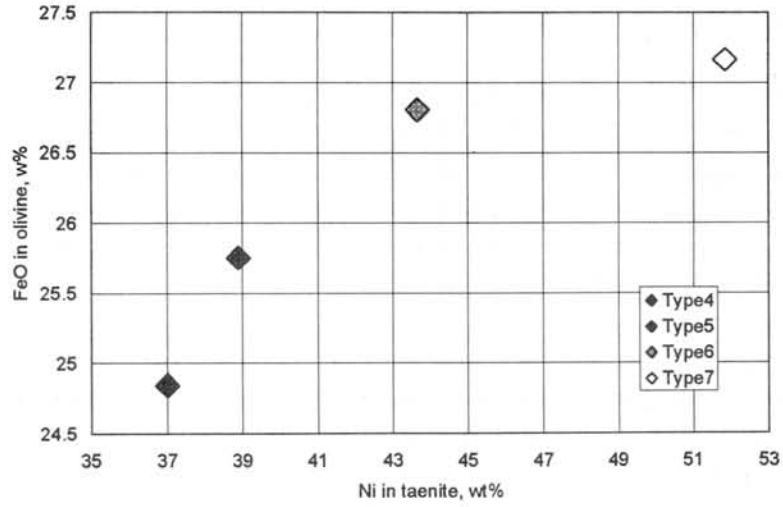

Figure 3. FeO in olivine versus Ni in taenite.

Noble Gases in 20 Yamato H-Chondrites: Comparison with Allan Hills Finds and Modern Falls.

Thomas Loeken and Ludolf Schultz
Max-Planck-Institut für Chemie, D-55020 Mainz/GERMANY

On the basis of concentration differences of trace elements it has been suggested that H-chondrites found at the Allan Hills in Antarctica and Modern Falls represent members of different extraterrestrial populations with different thermal histories [1,2,3]. It was also concluded that H-chondrites found in Victoria Land (Allan Hills) differ chemically from those found in Queen Maud Land (Yamato Mountains). This effect could be caused by different distributions of terrestrial ages and could imply a change of the meteoroid infall onto the Earth on a timescale of several 10^5 years. However, this topic is discussed controversially [4,5,6], one reason being the similar noble gas record of different H-chondrite populations. H-chondrites (Modern Falls) have several characteristic features, e.g. a major cluster of exposure ages at about 7 Ma. A close similarity between the exposure age distribution of Allan Hills finds and Modern Falls has been shown [4,6].

We report here the results of noble gas analyses of 20 Yamato H-chondrites which were selected with the aim to exclude pairing. Concentration and isotopic composition of He, Ne, Ar, Kr, and Xe have been determined in bulk samples (sample weights about 100 mgs). Apparatus and procedures of measurements were similar to those given in [7]. The results are presented in Tab.1. Uncertainties of gas concentrations are believed to be less than ±5%, those of isotope ratios are generally less than ±1%. Tab.2 contains the cosmogenic isotope ratios $^3He/^{21}Ne$ and $^{22}Ne/^{21}Ne$ together with exposure ages, calculated from the cosmogenic nuclides ^3He, ^{21}Ne, and ^{38}Ar using methods given in [8]. Included in Tab. 2 are ^4He-U,Th and K-Ar gas retention ages, calculated with mean H-chondritic values for K, U and Th.
The exposure age distribution of H-chondrites from the Yamato ice fields and Modern Falls shows no pronounced difference. This similarity of the exposure age distribution of Antarctic and non-Antarctic L- and H-chondrites has been noted earlier [4,9,10]. Both distributions show a characteristic clustering around 7 Ma. Other similarities between Antarctic H-chondrites and Modern Falls include the concentrations of radiogenic ^4He and ^{40}Ar and calculated gas retention ages. The concentration of radiogenic isotopes is influenced by thermal events in the history of the meteoritic material, but no difference is seen between Antarctic and non-Antarctic chondrites. Also, no correlation is observed between exposure ages and terrestrial ages for Antarctic meteorites from different locations.

From the agreement of exposure age distributions and thermal history indicators it becomes evident that a change in the H-chondrite meteoroid population reaching the earth during the recent 10^5 years is not corroborated from the noble gas record of these meteorite groups.

Acknowledgements: We thank the National Institute of Polar Research, Tokyo, for making available the meteorite samples.

References:
[1] J.E. Dennison, D.W. Lingner & M.E. Lipschutz, Nature 319, 390-393 (1986). [2] S.F. Wolf & M.E. Lipschutz, J. Geophys. Res. 100, E3297-E3316 (1995). [3] S.F. Wolf & M.E. Lipschutz, J. Geophys. Res. 100, E3335-E3349 (1995). [4] L. Schultz, H.W. Weber & F. Begemann, Geochim. Cosmochim. Acta 55, 59-66 (1991). [5] G.W. Kallemeyn, A.N. Krot & A.E. Rubin, Meteoritics 28, 377 (1993). [6] T. Loeken & L. Schultz, in LPI Techn. Rep. Nr. 95-02, 45-47 (1995). [7] T. Loeken, P. Scherer, H.W. Weber & L. Schultz, Chem. Erde 52, 249-259 (1992). [8] O. Eugster, Geochim. Cosmochim. Acta 52, 1649-1682 (1988). [9] N. Takaoka, K. Saito, Y. Ohba & K. Nagao, Mem. Natl. Polar Inst. (Tokyo), Spec. Issue 20, 264-275 (1981). [10] T. Loeken, P. Scherer & L. Schultz, LPSC XXIV, 889-890 (1993).

										Trapped gases		
	Class	^{3}He	^{4}He	^{20}Ne	^{21}Ne	^{22}Ne	^{36}Ar	^{38}Ar	^{40}Ar	^{84}Kr	^{132}Xe	^{129}Xe/^{132}Xe
Yamato					(in 10^{-8}cm^{3}STP/g)					(in 10^{-10}cm^{3}STP/g)		
790269	H4-5	11.43	1520	1.69	1.72	2.04	1.00	0.45	6000	0.99	1.87	1.29
790445	H6(-5)	25.33	1720	3.75	3.83	4.61	1.16	0.81	6299	0.84	1.25	1.27
790746	H6-5	12.80	119	2.97	2.87	3.09	2.24	0.77	273	2.70	2.94	1.11
791027	H5	11.28	1320	1.85	1.91	2.23	1.00	0.46	6400	1.24	1.44	1.18
791604	H5-4	8.21	1180	13.36	1.85	3.05	1.10	0.45	3674	0.72	0.98	1.19
791820	H4-5	84.78	1950	16.22	17.73	19.50	2.30	3.13	5957	0.46	0.81	1.16
791861	H6-5	12.45	1210	1.44	1.41	1.79	0.56	0.39	5992	0.45	0.75	1.09
791905	H5	63.08	1350	12.68	13.76	15.50	2.00	2.28	5700	0.74	1.56	1.26
791926	H5	3.25	1000	0.87	0.94	1.01	0.86	0.30	5831	1.07	1.83	1.26
792764	H5-4	5.15	1410	1.44	1.57	1.71	1.55	0.46	5580	1.71	3.23	1.29
792771	H5	14.26	1560	2.22	2.26	2.70	1.07	0.59	5350	0.99	1.77	1.31
792935	H5	62.87	1270	11.97	12.64	14.70	1.98	2.18	5683	0.94	2.06	1.29
793167	H5	59.41	1200	8.14	8.07	10.10	3.29	1.94	6735	4.05	1.63	1.21
793222	H5	11.03	1390	1.24	1.21	1.56	0.80	0.37	6320	1.00	1.71	1.49
793251	H5	5.83	740	1.35	1.38	1.63	1.11	0.42	4507	1.20	2.10	1.26
793409	H5	10.60	1410	1.75	1.80	2.12	0.93	0.48	5394	1.16	1.77	1.38
793501	H4-5	11.73	1290	1.69	1.62	2.05	1.06	0.47	5682	1.21	2.49	1.29
793510	H4-5	4.37	344	1.38	1.37	1.49	0.90	0.35	1908	0.97	1.80	1.31
793514	H5	9.85	1280	1.55	1.53	1.87	0.77	0.41	5228	1.11	1.74	1.22
81012	H5	1.67	45	0.91	0.96	1.06	0.77	0.28	431	0.93	1.41	1.32

Tab.1: Concentration of He, Ne and Argon and selected isotopes of Kr and Xe in 20 Yamato H-chondrites.

			Exposure age			Gas retention age	
	^{3}He/^{21}Ne	^{22}Ne/^{21}Ne	T(^{3}He)	T(^{21}Ne)	T(^{38}Ar)	U,Th-^{4}He	K-^{40}Ar
Yamato				[Ma]		[Ga]	
790269	6.65	1.186	7.4	7.5	7.8	3.95	4.40
790445	6.61	1.203	16.4	17.6	18.3	4.15	4.49
790746	4.45	1.075	8.0	7.8	8.6	0.20	0.71
791027	5.91	1.168	7.3	7.8	7.9	3.70	4.50
791604	4.45	1.110	5.2	6.0	6.4	*3.40*	3.63
791820	4.78	1.100	53.5	54.8	70.0	4.10	4.40
791861	8.80	1.266	8.2	7.8	9.9	3.40	4.40
791905	4.58	1.126	40.1	47.8	51.5	3.20	4.32
791926	3.46	1.078	2.0	2.6	3.5	3.10	4.36
792764	3.27	1.087	3.2	4.6	4.2	3.85	4.33
792771	6.32	1.196	9.2	10.1	11.8	4.05	4.22
792935	4.97	1.163	40.3	50.6	51.8	3.00	4.33
793167	7.36	1.252	39.1	42.7	44.6	2.90	4.61
793222	9.14	1.292	7.3	7.1	8.0	3.75	4.51
793251	4.23	1.183	3.8	5.9	6.3	2.40	3.95
793409	5.89	1.178	6.8	7.6	9.1	3.80	4.24
793501	7.22	1.263	7.7	8.9	9.2	3.60	4.33
793510	3.19	1.088	2.7	4.0	4.5	1.20	2.65
793514	6.45	1.225	6.4	7.5	8.4	3.60	4.19
81012	1.73	1.099	1.1	3.0	3.6	0.15	1.02

Tab.2: Exposure ages and gas retention ages of 20 Yamato H-chondrites.

ORIGIN OF ALH84001 ANTARCTIC METEORITE

A.A.Marakushev*, A.V.Bobrov**

**Institute of Experimental Mineralogy, Russian Academy of Sciences, Chernogolovka, Moscow District, 142432 Russia; **Chair of Petrology, Geological Department, Moscow State University, Vorob'evy Gory, 119899 Moscow, Russia*

The ALH84001 meteorite attracted the public attention by a find of carbonaceous matter. The unique features of its morphology gained the illusion of organic origin of this matter (Gibson et al., 1997). According to the oxygen isotope composition it was attributed to the group of so-called Martian (SNC) meteorites (Clayton and Mayeda, 1996). This point of view cannot be justified, because the age of ALH84001 is 4.5 billion years, and SNC meteorites are relatively young with an age of 1.0–1.3 billion years (Wood and Ashwal, 1981).

In fact ALH84001 should be attributed to the ordinary chondrite family, in which it enters into the group of igneous inclusions. It shows a good fit to them by an isotopic composition *(figure)* and an age of 4.56 billion years according to the data of (Mayeda et al., 1987; Nakamura et al., 1994).

Igneous inclusions are clearly distinguished from host chondrites (L and H) by a lower $\delta^{17}O$-value, as it is shown in *figure* by tie-lines, whereas the oxygen isotope compositions of igneous inclusions lie near the H-chondrite field. Such a position of igneous inclusions definitely shows, that the belt of asteroids is a source of them and also ALH84001 meteorite.

The problem of ALH84001 meteorite origin may be solved only if it is considered together with igneous inclusions in ordinary chondrites, as it is attributed to their genetic group. The find of a relic barred olivine chondrule in the core of the inclusion of L-chondrite Y–793241 (Nakamura et al., 1994) provides a key to the solution of that problem: the origin of igneous inclusions may be considered in connection with the formation of the barred olivine chondrules – typical elements of both ordinary and carbonaceous chondrites. In Allende chondrite barred chondrules form a regulary row from the carbonaceous (C3) chondrites to barred olivine chondrules of H-chondrites according to the oxygen isotopic composition *(see figure)*, iron number of olivine (from 0 to 12), K/Ca and Na/Ca ratios (Nakamura et al., 1990), and other petrochemical characteristics.

As it was shown in our previous papers (Marakushev, 1997_{1-2}), separation of barred chondrules in chondritic melts took place on the early stages of development of parent chondritic protoplanets under the high hydrogen pressure of their fluid envelopes in

progressively increasing reduced environment. As a whole, the process may be characterized by a reaction in terms of conventional symbols of normative minerals: $2Mg_{1.5}Fe_{0.5}SiO_4$ (initial oxygen) + H_2 = Fe + Mg_2SiO_4 (anomalous light oxygen) + $MgSiO_3$ (anomalous light oxygen)+ +H_2O (anomalous heavy oxygen). The high hydrogen pressure initiated production of water phase which accumulated anomalous heavy oxygen isotopes $\delta^{17}O$=7.5‰, $\delta^{18}O$=5.6‰ (Clayton et al., 1976). In ordinary chondrite melts with $\delta^{17}O$=3.55‰ and $\delta^{18}O$=4.53‰ (Y–75097, Nakamura et al., 1994), it resulted in formation of barred chondrules and igneous inclusions of light oxygen isotopic composition $\delta^{17}O$=3.05‰, $\delta^{18}O$=4.54‰, and in that number corresponding to ALH84001 meteorite (Clayton and Mayeda, 1996): $\delta^{17}O$=2.58‰, $\delta^{18}O$=4.53‰.

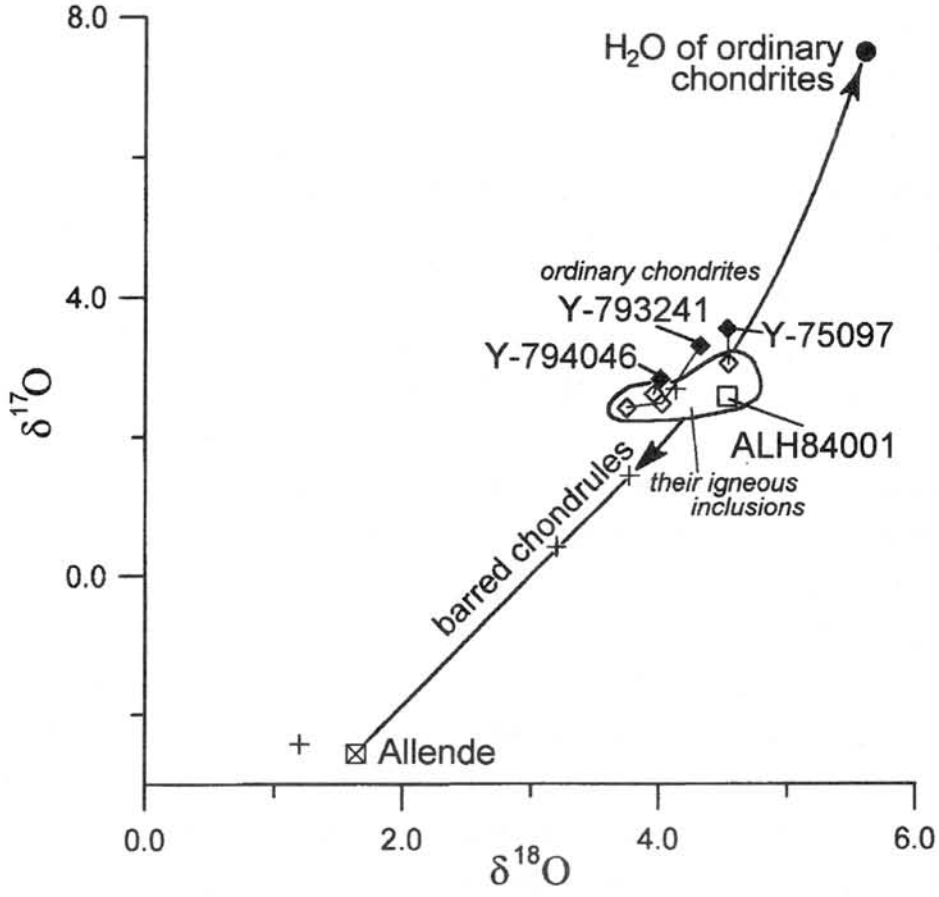

Oxygen isotopic composition (‰) of ALH84001 meteorite (Clayton and Mayeda, 1996) in relation to ordinary chondrites (Y–75097, Y–793241, and Y–794046) and their igneous inclusions (Mayeda et al., 1987; Nakamura et al., 1994).
Trend of oxygen isotope anomal fractionation is shown with the arrows. It is caused by the anomalous extraction of heavy oxygen isotopes from chondritic melts and their accumulation in water phase under the hydrogen pressure; it moves the compositions of ordinary chondrites towards igneous inclusions in them and barred chondrules of carbonaceous chondrites (Clayton and Mayeda, 1977).

The next stage of evolution of chondrite melts inside their parental fluid planets reflects the transition of chondrite magmatism from the ordinary chondrites to forsterite and then carbonaceous (C3) chondrites. This transition is seen in the row of barred chondrules from the Allende meteorite (Clayton et al., 1977): $\delta^{17}O$=1.45‰, $\delta^{18}O$=3.77‰→$\delta^{17}O$=–2.42‰, $\delta^{18}O$=1.20‰. Increase of hydrogen influence in this row *(see figure)* results in anomalous lightening of oxygen isotopic composition, decrease of silicate iron number, and enrichment of melts with carbon, hydrocarbons, and H_2O by the reactions: $CO+H_2=C+H_2O$, $CO+3H_2=CH_4+H_2O$, $3CO+H_2=CO_2+2C+H_2O$. All these reactions are directed to the right as the temperature decreases. It is a specific feature of carbonaceous chondrites (C3–C2–C1), and it is also seen in transitional to them meteorites of the H–C3 row, and ALH84001 in that number *(see figure)*. This meteorite contains carbonate globules and hydrocarbon matter. The segmented morphology and composition of them is similar to that of carbonaceous chondrite (Vdovykin, 1967), nonbiological origin of which is well-known.

References: **Clayton, R.N. and Mayeda, T.K.** Oxygen isotope studies of achondrites. – Geochim. Cosmochim. Acta. 1996. Vol. 60. No. 11. P. 1999–2017. **Clayton, R.N., Onuma, N., Grossman, L., and Mayeda, T.K.** Distribution of the presolar component in Allende and other carbonaceous chondrites. – Earth Planet. Sci. Lett. 1977. Vol. 34. P. 209–224. **Clayton, R.N., Onuma, N., and Mayeda, T. K.** A classification of meteorites based on oxygen isotopes. – Earth Planet. Sci. Lett. 1976. Vol. 30. P. 10–18. **Gibson, E.K., McKay, D.S., Thomas-Keprta, K., and Romanek, Ch.S.** The case for relic life on Mars. – Sci. American. 1997. December. P. 36–41. **Marakushev, A.A.** Genetic meaning of oxygen isotopic variations of chondrules in chondrites. – Pap. presented to the 22nd symp. on Antarctic meteorites. Tokyo. 1997. P. 97–99. **Marakushev, A.A.** An essential flaw in the traditional theory of the solar system evolution. – Vestnik MGU, geol. series. 1997. No. 6. P. 3–13 (in Russian). **Mayeda, T.K., Clayton, R.N., and Yanai, K.** Oxygen isotopic compositions of several Antarctic meteorites. – NIPR Spec. Issue. 1987. No. 46. P. 144–150. **Nakamura, N., Matsuda, H., Yokoyama, S., et al.** Fractionated alkali metal abundances in Allende BO chondrules: a clue to melting processes. – Pap. presented to the fifteenth symp. on Antarctic meteorites. Tokyo. 1990. P. 147–148. **Nakamura, N., Morikawa, N., Hutchison, R., et al.** Trace element and isotopic characteristics of inclusions in the Yamato ordinary chondrites Y–75097, Y–793241 and Y–794046. – Proc. NIPR Symp. Antarct. Meteorites. 1994. No. 7. P. 125–143. **Vdovykin, G.P.** Carbon matter of meteorites. – Moscow: Nauka. 1966. 271 p (in Russian). **Wood, C.A. and Ashwal, L.D.** SNC meteorites: igneous rocks from Mars? – Proc. Twelfth Lunar Planet Sci. 1981. Vol. 12. Pt. I.

Multiple primordial components of Xe in the Mugura IAB iron

Teruyuki Maruoka[1], Jun-ichi Matsuda[1], and Gero Kurat[2]

1. Department of Earth and Space Science, Graduate School of Science, Osaka University, Toyonaka, Osaka 560-0043, Japan
2. Naturhistoriches Museum, Postfach 417, A-1014 Viene, Austria

Introduction

Mathew and Begemann [1] observed an unknown isotopic composition of Xe derived from schreibersite and graphite in the El Taco IAB meteorite, whereas a typical planetary Xe was observed in the silicate inclusions. The unknown xenon component was designated as "El Taco Xe". Based on their data, Maruoka [2] recently showed that "El Taco Xe" is a mixture of a Xe-HL-rich planetary Xe and a mass-fractionated solar Xe and that the isotopic data of high temperature fractions can be explained by mixture of these two components. These observations indicate that different primordial components are present in different phases of IAB irons. This means that IAB irons did not undergo the high temperatures which spoiled the isotopic un-equilibrium.

In order to make additional constraints for physico-chemical process, such as heating and shock, which occurred on the IAB parent body, we analyzed isotopic compositions of noble gases derived from the Magura IAB iron by stepwise heating method.

Samples and Experiments

The analyzed sample is the bulk metal of Magura meteorite with visible graphite inclusions. The stepwise heating technique (800, 1200, and 1600°C) was applied in the gas-extraction. The sample heated in a single crystal MgO crucible which was specially prepared for the metal samples. Noble gases have been analyzed with VG5400, a sector-type mass spectrometer at Osaka University.

Results and Discussion

Trapped Xe component of 800°C is dominated by the mass-fractionated solar Xe, whereas those of high temperature fractions (1200, 1600°C) are the mixtures of a mass-fractionated solar Xe and Q-Xe (Fig. 1). Such a relationship between the extraction temperature and the isotopic compositions is observed in graphite nodule of the Bohumilitz IAB iron [3]. The diagrams such as $^{131}Xe/^{132}Xe$-$^{136}Xe/^{132}Xe$ (Fig. 2) and $^{134}Xe/^{132}Xe$-$^{136}Xe/^{132}Xe$ (Fig. 3) show that the data point of 800°C fraction is explained by the addition of Xe-HL component (~4% for ^{132}Xe) to a mass fractionated solar Xe. This addition cannot be evaluated from the Fig. 1 because the isotopes such as ^{130}Xe and ^{131}Xe are not enriched in the Xe-HL component. The Xe-HL component does not appear in the high temperature fractions. This suggests that the abundance ratios between the components (e.g., Xe-HL/Q-Xe) varied with the extraction temperatures. Therefore, the sites including Xe-HL, a mass fractionated solar Xe, and Q-Xe are different from each other. The mean isotopic ratio obtained from all temperature fractions is located near the line

extending from a mass-fractionated solar Xe to Xe-HL (Fig. 2). This nature enriched in Xe-HL is observed in the El Taco IAB iron [1, 2]. This characteristic prefers the link with shock events for the IAB genesis because Nakamura et al. [4] reported that HL-component remained, although Q-component was lost, by the strong shock compression.

Acknowledgements

This study was supported in part by Research Fellowships of the Japan Society for the Promotion of Science for Young Scientists.

References

[1] Mathew and Begemenn (1995) Geochim. Cosmochim. Acta 59, 4729-4746; [2] Maruoka (1998) Geochim. Cosmochim. Acta, submitted; [3] Maruoka et al. (1998) LPS XXIX; [4] Nakamura et al. (1979) Antarctic Meteorites XXII, 135-136; [5] Ozima and Podosek (1983) Noble Gas Geochemistry. Cambridge Univ. Press; [6] Wieler and Baur (1994) Meteoritics 29, 570-580; [7] Podosek et al. (1971) Earth Planet. Sci. Lett. 10, 199-216; [8] Wieler et al. (1992) Geochim. Cosmochim. Acta 56, 2907-2921; [9] Huss and Lewis (1994) Meteoritics 29, 791-810

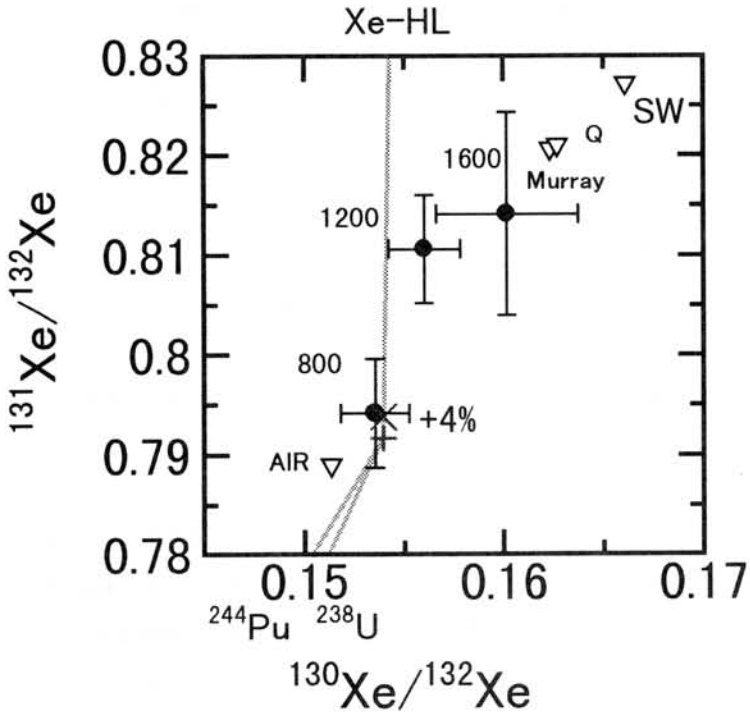

Fig. 1 $^{130}Xe/^{132}Xe$ vs. $^{131}Xe/^{132}Xe$. Air Xe, ^{244}Pu and ^{238}U fissiogenic Xe are from Ozima and Podosek [5], solar-wind (SW) Xe from Wieler and Baur [6], Murray Xe from Podosek et al. [7], Q-Xe from Wieler et al. [8], Xe-HL from Huss and Lewis [9]. The numerical values near the data symbols show temperature steps at the noble gas measurements. The cross symbol represents the mass-fractionated solar Xe determined in Maruoka [2]. Diagonal crosses represents the isotopic compositions with 4% of Xe-HL and 96% of mass-fractionated solar Xe (^{132}Xe basis).

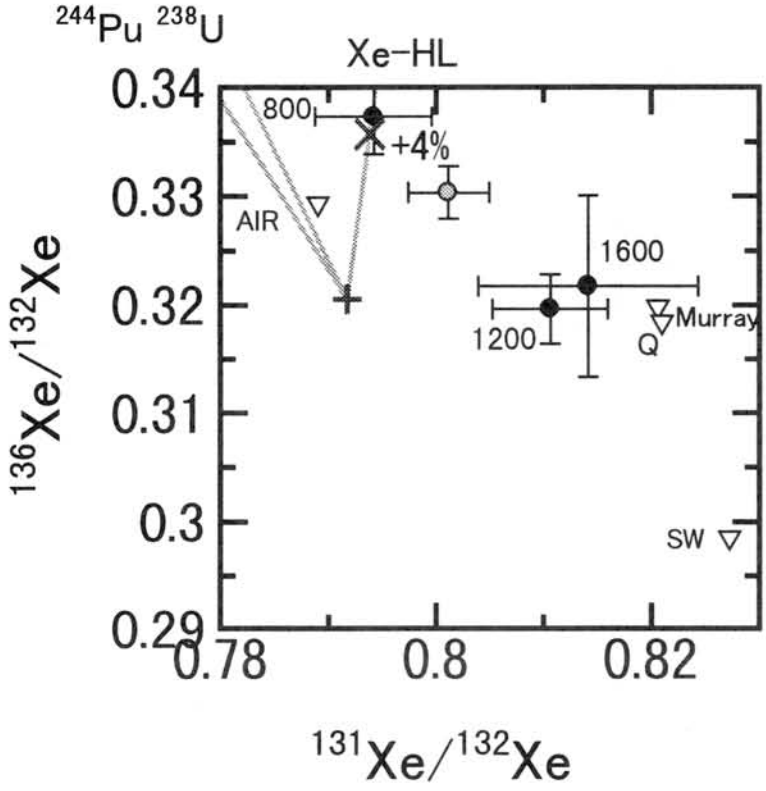

Fig. 2 $^{131}Xe/^{132}Xe$ vs. $^{136}Xe/^{132}Xe$. Sources and symbols of the isotopic compositions are the same as in Fig. 1. Gray symbol represents the mean isotopic ratios obtained from all temperature fractions.

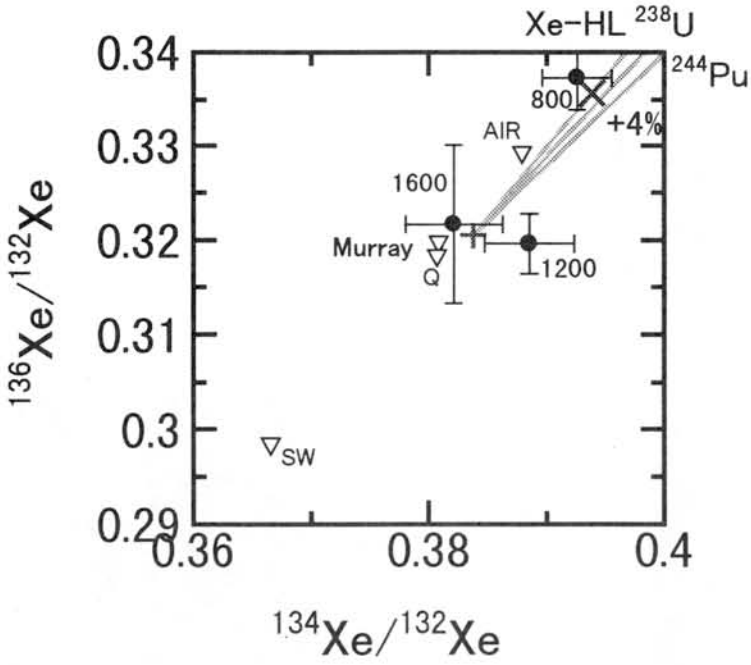

Fig. 3 $^{134}Xe/^{132}Xe$ vs. $^{136}Xe/^{132}Xe$. Sources and symbols of the isotopic compositions are the same as in Fig. 1.

Refractory mineral-bearing chondrules in the Allende meteorite.

S. Maruyama[1], H. Yurimoto[2] and S. Sueno[3], [1]Venture Business Laboratory, University of Tsukuba, Tsukuba Ibaraki 305-8573, Japan (e-mail:maruyama@arsia.geo.tsukuba.ac.jp), [2]Earth and Planetary Sciences, Tokyo Institute of Technology, Meguro, Tokyo 152-8551, Japan (e-mail: yuri@geo.titech.ac.jp). [3]Institute of Geoscience, University of Tsukuba, Tsukuba, Ibaraki 305-8571, Japan (e-mail: sueno@arsia.geo.tsukuba.ac.jp).

INTRODUCTION Carbonaceous chondrites such as the Allende CV3 meteorite are composed of abundant ferromagnesian chondrules and Ca, Al-rich inclusions (CAIs) embedded in a fine-grained matrix. These major constituents of chondrites could have formed compound objects among the same constituents [1]. No compound chondrule-CAI objects have been recognized, although trace element analyses of individual chondrules from carbonaceous chondrites suggest that chondrules and CAIs are genetically related [2]. Recently Misawa and Fujita [3] found a barred-olivine chondrule in the Allende meteorite contains a coarse, subhedral spinel grain including fassaite and a Ca, Al-rich phase and refractory platinum metals nuggets. This spinel grain may be a relict phase because the composition is similar to those of CAIs. The evidence indicates that some CAIs and ferromagnesian precursor materials of chondrules coexisted in the same region of the solar nebula. However, the relationship between chondrules and CAIs is not completely obvious yet. In fact, O isotope composition of spinel in Al-rich chondrules does not show large ^{16}O-enrichment such as CAI spinel [4].

Here we present *in-situ* O isotopic measurements on two chondrules including spinel grains of the Allende meteorite. The results show that the O isotopic compositions of spinel grains included in these chondrule plotted on the carbonaceous chondrite anhydrous minerals (CCAM) line. Spinel grains of one chondrule show CAI-like O isotope composition, but those of the other one do not. Preliminary results has been reported in [5].

SAMPLE DESCRIPTION A1-2b-1 (Fig. 1) is a typical barred-olivine chondrule (BOC). A1-2b-1 mainly consists of olivine, mesostasis, spherules of Fe-Ni metal or sulfide. The core part (~1.7mm diameter) is surrounded by the porphyritic olivine rim (200-500μm width). A coarse, euhedral spinel grain (up to 300μm in size) is embedded in the core part. Olivine bars in the core part are forsteritic (Fo99). The composition of the core of the spinel grain is the almost pure $MgAl_2O_4$, whereas the rim of the spinel grain is rich in Fe (FeO~7.4wt.%, 4-60μm width) and Cr (Cr_2O_3~3.2wt.%, ~30μm width). The mesostasis is dominated by the feldspathic phase. The fassaitic phase and Fe, Ca-rich assemblages are among the feldspathic phase.

AL95-2-1-CDL.1 compound chondrule, which may be classified into independent consorting compound chondrules of [6] (Fig. 2). The left spheroidal body may be a primary chondrule and the left itself is categorized into an independent enveloping compound chondrule which consist of a porphyritic olivine primary enveloped by porphyritic pyroxene secondary. The right spheroidal body is a secondary chondrule which can be categorized as a plagioclase-olivine inclusion (POI)

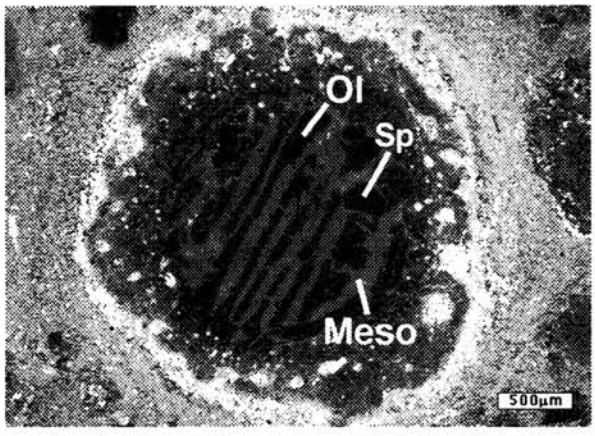

Fig.1. The BSE image of A1-2b-1 BOC.

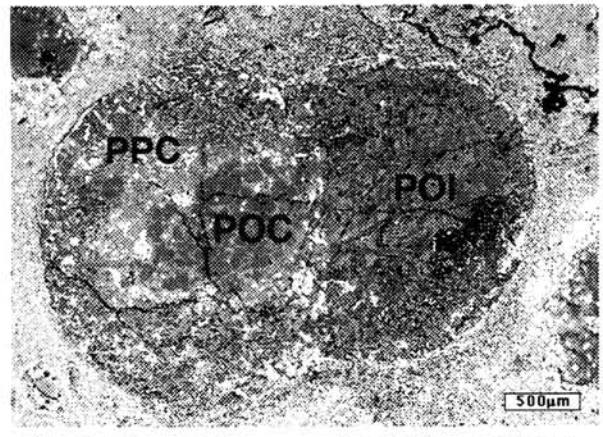

Fig.2. The BSE image of AL95-2-1-CDL.1.

[7].

The porphyritic olivine chondrule (POC) mainly consistent of porphyritic olivine grains (Fo98, ~80vol%) and interstitial mesostasis (~20vol%). The enveloping porphyritic pyroxene chondrule (PPC) mainly consist of abundant Ca-rich pyroxene lath (90-370μm length) and porphyritic Ca-poor pyroxene (40-70μm diameter). Olivine (Fo85, ~50μm diameter) with Fe-rich rim is minor phase. The interstitial space among the minerals is filled by mesostasis which contains Na and Cl components.

The POI is sub-ophitic texture and consists of Ca-rich pyroxene (34vol%, small Ca-poor pyroxene core exist), plagioclase (25vol%, An88-100), olivine (4vol%, Fo90-95), spinel (4vol%) and nepheline (30vol%). Olivine and spinel grains are poikilitically enclosed by the plagioclase assemblage. The spinel grains exhibit corroded or serrated character, and this feature strongly suggests that the spinel grains are the relict phase. These mineral characteristics indicate the POI categorized into Group 2 POI of [7]. From textural observation nepheline is apparently the secondary phase as a result of the alteration of plagioclase or exists as matrix surrounding other phases.

EXPERIMENTAL Oxygen isotopic measurements were performed with the TiTech Cameca ims 1270 SIMS instrument using a ~5μm diameter Cs^+ beam and an electron flood gun to compensate for electrostatic charging on sample surface. The mass resolution power was set to ~6000 to resolve ^{17}O from the interference of ^{16}OH. Secondary ion signals were detected with an electron multiplier (EM). Measurements were made by magnetic scanning through the following mass sequences; the tail of $^{16}O^-$ (15.9915amu), $^{16}O^-$, $^{17}O^-$, $^{16}OH^-$, and $^{18}O^-$. Measurements of the tail of ^{16}O and ^{16}OH were performed for correction of the ^{16}OH contribution on ^{17}O peaks. This correction is always less than 0.5‰. Data were corrected for deadtime and the instrumental mass fractionation by utilizing a terrestrial spinel standard.

RESULTS and DISCUSSION The data of O isotopic analysis for the major phases in A1-2b-1 BOC are plotted along the CCAM line (Fig. 3). The O isotopic composition of olivines in the core part distribute along the CCAM line. The mean δO values of olivines ($\delta^{17}O_{SMOW}$ = -9.9±1.0‰; $\delta^{18}O_{SMOW}$ = -8.2±1.1‰) are similar to those of individual olivine grains in the Allende meteorite [8, 9]. The O isotopic compositions of the core of the spinel grain ($\delta^{17}O_{SMOW}$ = -13.5±1.1‰; $\delta^{18}O_{SMOW}$ = -13.7±1.2‰) are close to those of coexisting olivines, and are quite different from those of spinels in CAIs. The spatial distribution of the δO values of the rim of the spinel grains displays no systematic pattern, and the mean δO values ($\delta^{17}O_{SMOW}$ = -13.6±2.3‰; $\delta^{18}O_{SMOW}$ = -14.4±2.1‰) are very close to those of the core of the A1-2b-1 spinel grain. It is certain that the spinel grain is the primary phase which crystallized just before (or almost simultaneously with) olivines.

The O isotopic compositions of the feldspathic mesostasis in the core part of A1-2b-1 distribute along the CCAM line. The mean δO values of the mesostasis ($\delta^{17}O_{SMOW}$ = 1.7±1.7‰; $\delta^{18}O_{SMOW}$ = 4.4±1.5‰) are similar to those of melilites and anorthites in CAIs [10].

The data of each measurement for AL95-2-1-CDL.1 are plotted along the CCAM line (Fig. 4). The O isotopic compositions of olivines in the POI distribute over the slightly wide range ($\delta^{17}O_{SMOW}$: -25.1 ~ -13.4‰; $\delta^{18}O_{SMOW}$: -19.4 ~ -9.5‰). The O isotopic compositions of Ca-rich pyroxenes ($\delta^{17}O_{SMOW}$ = -10.5±0.8‰; $\delta^{18}O_{SMOW}$ = -9.9±1.1‰) and Ca-poor pyroxenes ($\delta^{17}O_{SMOW}$ = -9.1±1.8‰; $\delta^{18}O_{SMOW}$ = -7.3±1.6‰) in the POI are essentially equal to those of olivine ($\delta^{17}O_{SMOW}$ = -14.2±3.1‰; $\delta^{18}O_{SMOW}$ = -10.8±2.1‰) and pyroxenes ($\delta^{17}O_{SMOW}$ = -11.3±1.6‰; $\delta^{18}O_{SMOW}$ = -10.0±1.5‰) in the primary chondrule. Small degree of ^{16}O-enrichment of the ferromagnesian minerals in primary and secondary chondrules is good agreement to those of individual olivine grains [8, 9], and olivine in POC [11] from Allende meteorite. The agreement of O isotope composition of ferromagnesian minerals suggests that the POC, PPC and POI are the same genetic relationship in spite of an independent compound chondrule. The oxygen isotopic compositions of the spinel grains in the POI part are $\delta^{17}O_{SMOW}$ = -32.7±1.3‰, $\delta^{18}O_{SMOW}$ = -29.6±1.8‰ and are similar ^{16}O-excess to those of CAI spinels [10]. This is the evidence that the spinel grains did not equilibrate with the melt crystallized ferromagnesian minerals. This is consistent to the textural observation of the spinel

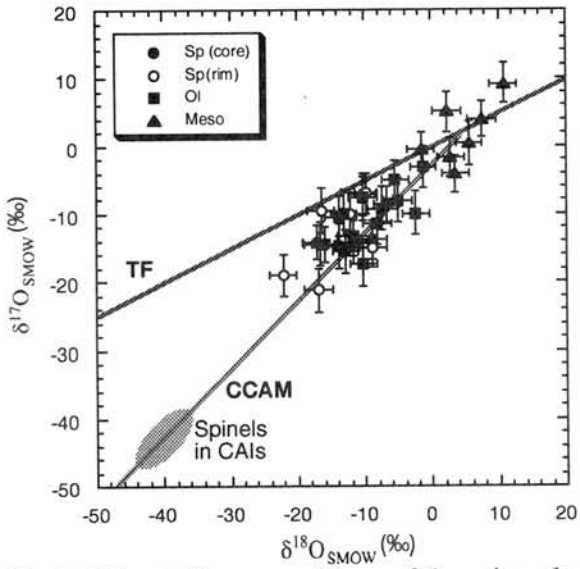

Fig.3. O isotopic compositions of the minerals in A1-2b-1 BOC.

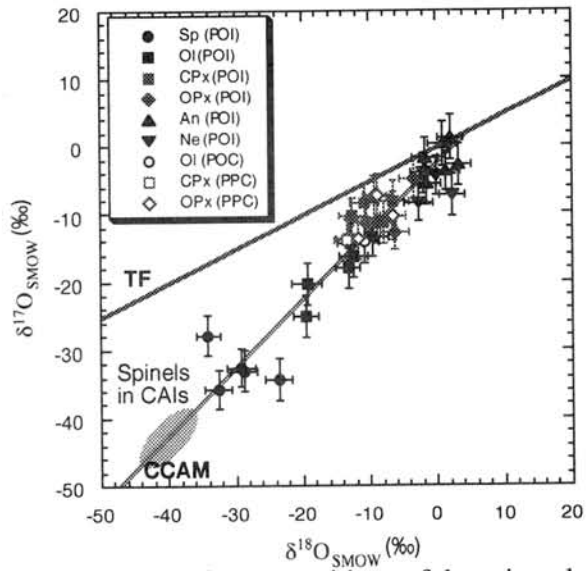

Fig.4. O isotopic compositions of the minerals in AL95-2-1-CDL.1 compound chondrule.

(TF = Terrestrial Fractionation, CCAM = Carbonaceous Chondrite Anhydrous Minerals.)

shape and supports the model that spinel grains in POIs are the relict phase that survived the chondrule-forming event [7]. The origin of the spinel grain may be directly related to CAI precursors or CAIs itself from the similarity of ^{16}O-enrichment.

The O isotopic compositions of plagioclase ($\delta^{17}O_{SMOW}$ = -2.0±1.0‰; $\delta^{18}O_{SMOW}$ = 0.7±0.8‰) and nepheline ($\delta^{17}O_{SMOW}$ = -6.0±1.1‰; $\delta^{18}O_{SMOW}$ = 0.6±1.1‰) in the POI are less enriched in ^{16}O, which values are similar to those of anorthites and melilites in CAIs [10]. Nephelines are the anhydrous alteration products which may have formed by the replacement of plagioclases by reactions with the nebular gas [12]. The nebular gas may have had normally O isotopic composition. If this assumption is correct, then O composition of late stage melt of the chondrules was in equilibrium with the nebular gas because the texture of plagioclase indicates melt origin.

The compound chondrule AL95-2-1-CDL.1 is igneous origin and the O isotopic composition changed from ^{16}O-rich to ^{16}O-poor through crystallization, at least during olivine, pyroxenes and plagioclase crystallization. The crystallization sequence of the A1-2b-1 core part is spinel, olivine and then feldspathic mesostasis. The O isotopic composition of each phase in A1-2b-1 also changed from ^{16}O-rich to ^{16}O-poor through solidification. This trend is parallel to an exchange scenario of ^{16}O-rich solids with ^{16}O-poor gas [13]. One model adapted to the scenario is that the O isotope exchange between chondrule liquid and the surrounding gas of normal O composition was gradually progressed during chondrule crystallization. An alternative model is that O isotopic composition of the surrounding gas gradually changed from ^{16}O-rich to ^{16}O-poor during chondrule crystallization even if the O isotopic composition of liquid always achieved in equilibrium. The condition may also be realized in heterogeneous O isotopic nebular gas if the chondrule moved in the nebular.

References: [1] Rubin A. E. (1994) *Science* **368**, 691. [2] Misawa K., Nakamura N. (1988) *Nature* **334**, 47-50. [3] Misawa K., Fujita T. (1994) *Nature* **368**, 723. [4] Russell S.S., Leshin L.A. McKeegan K.D. MacPherson G.J. (1997) *Meteoritics Planet. Sci.* **32,** A111. [5] Maruyama S., Yurimoto H. and Sueno S. (1998) *LPSC XXIX*, 1342. [6] Wasson J.T., Krot A.N., Lee M.S., Rubin A.E. (1995) *G.C.A.* **59,** 1847. [7] Sheng Y. J., Hutcheon I.D., Wasserburg G. J. (1991) *G.C.A.* **55**, 581. [8] Hervig R.L., Steele I.M. (1992) *LPSC XVII*, 364. [9] Weinbruch S., Zinner E.K. El Goresy A., Steele I.M., Palme H (1993) *G.C.A.* **57,** 2649-2661. [10] Clayton R. N., Onuma N., Grossman L., Mayeda T. K. (1977) *Earth Planet. Sci. Lett.* **34**, 209. [11] Hiyagon H. (1996) *Meteoritics Planet. Sci.* **31,** A62. [12] Ikeda Y., Kimura M. (1995) *Proc. NIPR Symp. Antarct. Meteorites* **8**, 97-122. [13] Clayton R.N., Mayeda T.K., Goswami J.N., Olsen E.D. (1991) *G.C.A.* **55,** 2317.

Additional Petrographic Features of Martian Meteorite ALH84001

G. A. McKay[1], C. S. Schwandt[2], and T. Mikouchi[3]
[1]*SN4, NASA Johnson Space Center, Houston TX 77058, USA*
[2]*Lockheed-Martin, 2400 NASA Road 1, Houston TX*
[3]*Mineralogical Institute, Graduate School of Science, University of Tokyo, Tokyo 113, Japan*

Introduction. ALH84001, originally classified as a diogenite, was subsequently recognized by [1] as a Martian meteorite. It differs from other Martian meteorites in that it is a coarse-grained orthopyroxene cumulate containing ~1% carbonate [1,2]. It has attained enhanced importance as a result of the recent announcement of possible evidence for relict biogenic activity, especially in the carbonates [3]. The issue of biogenic activity is of great philosophical and scientific importance, and yet remains highly controversial. Understanding the origin of these carbonates is a key to resolving the controversy surrounding this issue. However, such understanding has proved elusive, in part because this sample has had a complex history involving multiple impacts [e.g., 2,3,4,5], granulation, pervasive fracturing, and shock melting of one or more components. We are studying ALH84001 using petrographic, SEM, and microprobe techniques to elucidate the relative timing and possible genetic relationships between carbonate formation and shock events.

Fig. 1. Ca map showing reaction rim of augite (medium gray) between apatite (Light gray) and Orthopyroxene (dark gray). Width of image is 250 μm.

The general petrography of ALH84001 was described by [2,3], and many workers have studied the petrography and chemical compositions of carbonates [e.g., 4-7,9]. The sample was initially formed as an igneous orthopyroxene and chromite cumulate with interstitial plagioclase. Subsequently, the sample suffered mechanical granulation along sheared zones (probably from shock), possible recrystallization of the granular material (there is no general agreement on this), and at least one shock event after the recrystallization. The plagioclase was converted to feldspathic glass, but this glass may not be a simple product of shock-induced solid-state transition to a disordered state [8]. At some point during these events, carbonates were introduced into the sample. However, the age of the carbonates is not yet well understood [10,11], and even the timing of their formation relative to other events affecting this sample is unclear, as is the mechanism of carbonate formation. This abstract presents data that provide additional clues to the origin and history of this sample.

Samples and analytical methods. We have studied ten polished thin sections of ALH84001 that were allocated by the Meteorite Working Group to a round-robin study among many investigators. We used optical microscopes, electron microprobes for elemental mapping and quantitative analyses, and electron microprobes and FEG-SEMs for BSE imaging.

Results and Discussion. We present several new observations that provide information about the complex history of ALH84001.

Augite reaction rims on apatite. Figure 1 shows an augite reaction rim between apatite and orthopyroxene. Such rims are common wherever apatite abuts orthopyroxene. The reaction must have occurred in an open system, because there is no indication of remaining excess P, Fe, or Mg. It is not clear whether this reaction occurred during cooling or during subsequent alteration of this sample.

Shocked feldspar-silica intergrowths. Fig. 2A shows a patch of feldspathic glass that contains several silica-rich areas ranging up to ~20 μm in size. The feldspar is K-rich, suggesting this area might

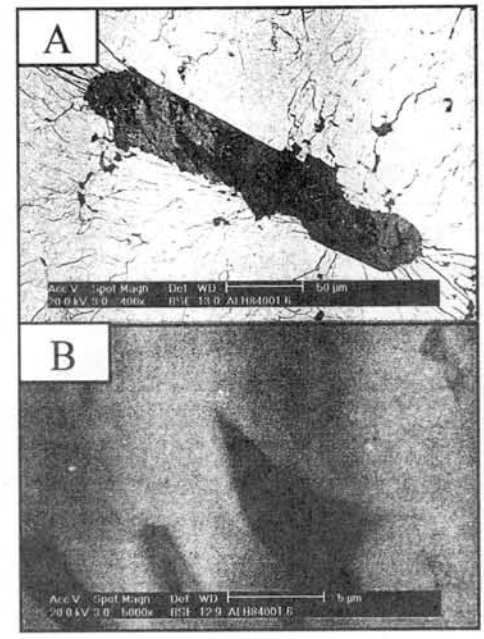

Figure 2A. BSE image of patch of feldspathic glass (medium gray) containing irregular blebs of SiO_2 (darker gray) up to ~20 μm in size. Scale bar is 50 μm. Many fractures in orthopyroxene (light gray) around glass patch are filled with shock-injected glass. B. Enlargement of central region of glass patch. Dark regions in center of silica blebs are voids. Scale bar is 5 μm.

represent primary mesostasis. However, the Al_2O_3 content of the silica is around 0.1 wt%, suggesting that the silica was originally quartz rather than tridymite. Boundaries of some silica areas are indistinct, suggesting melting and mixing with feldspathic melt during shock.

Granulated feldspar with interstitial silica. Fig. 3A is a BSE image of ALH84001 showing a granulated band running from top to bottom. This band cuts across both pyroxene and feldspar. Fig. 3B shows a high-contrast BSE image of the region within the rectangle near the top center of 3A. The feldspathic glass shows a pervasive network of low-Z material. High-resolution SEM images show this network to be a set of web-like veins about 1 μm in thickness occupying the interstices between feldspar fragments [12]. A Si map of a similar region (Fig. 3C) illustrates that the vein material is silica. It is clear that the feldspar has been granulated, with textures and grain sizes similar to granulated pyroxene (Fig. 3B). The interstices have been filled with SiO_2 subsequent to granulation. The origin of the interstitial SiO_2 is uncertain. [13,14] proposed that SiO_2 veins in pyroxene are shock-injected melts. However, SiO_2 is ubiquitous throughout granulated regions of the sample, suggesting that the source material should be common. Yet abundant primary magmatic SiO_2 has not been reported in ALH84001. The silica in Fig. 2 is the only candidate for primary silica we have seen in more than 8 thin sections, but it is not characteristic of primary igneous silica in other martian meteorites, which is typically a high-temperature polymorph with much more Al_2O_3. Furthermore, the delicate and pervasive nature of the SiO_2 vein networks in the granulated feldspar seems more consistent with deposition from fluids percolating through fractures created by the granulation event than with injection of shock-melted primary igneous SiO_2. Based on radial fractures around feldspar grains (e.g., Fig 2A) and the lack of fractures in feldspar (in contrast with all other phases in the sample), [8] proposed that the feldspar glass was completely melted by shock. Yet it clearly must have consisted of solid fragments at the time the SiO_2 was introduced. Thus it is likely that subsequent to deposition of the SiO_2, the sample was subjected to an impact strong enough to melt the feldspar, and possibly the interstitial SiO_2. However, the sharp boundaries between the SiO_2 veins and the feldspathic glass [12] indicate that heating was too brief for significant diffusive mixing, although there is some suggestion of such mixing in Fig. 2. It may have been this impact that fractured and disrupted the carbonate globules [6].

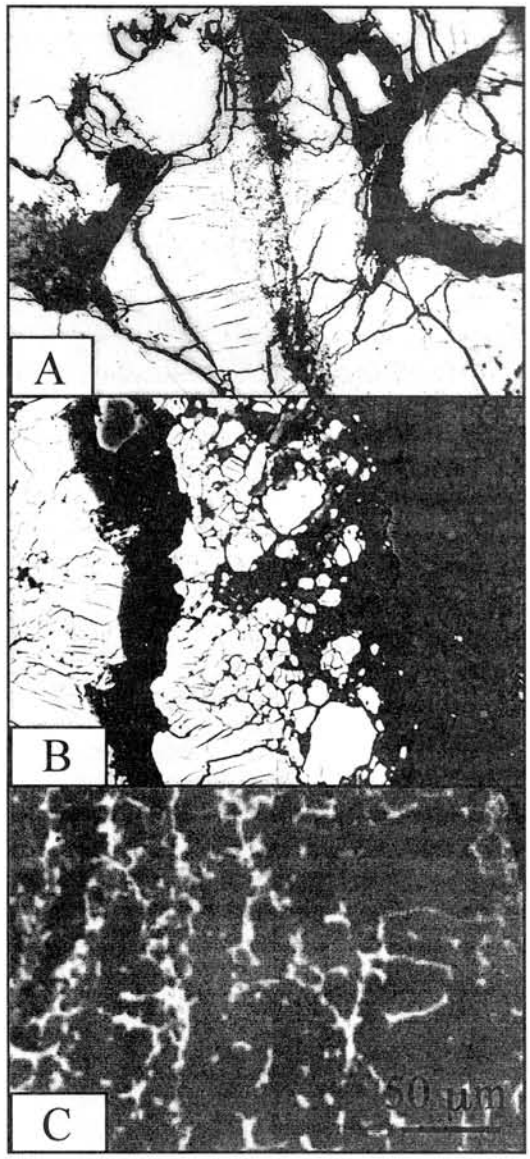

Figure 3A. BSE image showing granulated zone running diagonally from top to bottom near center of image. Width of image is 2490 μm. B. High-contrast BSE image of region in rectangle near top center of A. Dark gray = feldspathic glass, medium gray = orthopyroxene, white = chromite. Dark veins between granulated feldspar fragments are SiO2. Width of field is 150 μm. Width of image is 150 μm. C. Si map of area similar to B. Interstitial material is SiO_2.

It is clear that this complex rock reveals its history very reluctantly. Every new thin section yields previously unseen features. Continued study is required to understand the formation of the carbonates.

References: [1] D. Mittlefehldt (1994) Meteoritics 29, 214-221. [2] A. Treiman (1995) Meteoritics 30, 294-302. [3] D. McKay *et al.* (1996) Science 273, 924-930. [4] R. Harvey and H. McSween (1996) Nature 382, 49-51. [5] J. Bradley *et al.* (1996) GCA, 60, 5149-5155. [6] G. McKay and G. Lofgren (1997) LPS XXVIII, 921-922. [7] E. Scott *et al.* (1997) LPS XXVIII, 1271-1272. [8] A. El Goresy *et al.* (1997) LPS XXVIII, 329-330. [9] D. Kring *et al.* (1997) Conference on Early Mars. [10] M. Wadhwa and G. Lugmair (1997) Conference on Early Mars. [11] G. Turner *et al.* (1997) Geochim. Cosmochim. Acta 61, 3835-3850. [12] McKay G. et al. (1998) LPS XXIX, #1944, CD-ROM. [13] Scott E.R.D. et al. (1997) Nature 387, 366-379. [14] Scott E.R.D. and Krot. A. (1998) LPS XXIX, # 1786, CD-ROM.

Shocked plagioclase in martian and lunar meteorites: Textures, chemical compositions, Raman spectra, and implications for their post-shock thermal histories

Takashi Mikouchi[1], Masamichi Miyamoto[1], and Gordon A. McKay[2]

[1]*Mineralogical Institute, University of Tokyo, Hongo, Bunkyo-ku, Tokyo 113-0033, Japan*

[2]*SN2 Planetary Science Branch, NASA Johnson Space Center, Houston, TX77058, USA*

1. Introduction

Among more than 10,000 meteorites recovered, only 12 stones are known to have originated from the planet Mars [*e.g.*, 1] and 14 stones are known to come from the Moon [*e.g.*, 2,3]. Most of these meteorite types experienced severe shock effects when they were ejected from their parent bodies. Plagioclase is one of the major minerals in both martian and lunar meteorites and is often used to estimate their shock degrees because plagioclase is known to show variable properties according to increasing shock pressures [*e.g.*, 4]. The shock range of 30-55 GPa on plagioclase produces a diaplectic glass by a shock-induced solid-state transformation and more extensive shock produces shock fused glass [*e.g.*, 4]. "Maskelynite" is understood as a diaplectic plagioclase glass and is first identified in the Shergotty martian meteorite [5]. Recently, El Goresy *et al.* [6] proposed that maskelynite in Shergotty was melted during shock and is a true melt. Bunch *et al.* [8] reported that annealing of Shergotty maskelynite at 1150 °C for only 1 hour caused partial transformation to crystalline plagioclase. Thermal annealing of the experimentally shocked plagioclase also reproduces crystalline plagioclase, but recrystallization rates and textures depend upon its initial structure state (diaplectic glass or fused glass) [7]. In this study we analyze textures, chemical compositions and Raman spectra of plagioclase within them in order to estimate post-shock thermal histories of martian and lunar meteorites in conjunction with annealing experiments of "maskelynite" in the Zagami martian meteorite.

2. Samples and Methods

We analyzed six martian meteorites (Zagami, EETA79001, QUE94201, ALH77005, Y-793605, and ALH84001) and two lunar meteorites (Y-793169 and Asuka881757 (A-881757)) by optical microscope, electron microprobes (JEOL JXA 8900L electron microprobe at Geological Inst., Univ. of Tokyo and JEOL Superprobe 733 electron microprobe at Ocean Research Inst., Univ. of Tokyo), and micro Raman spectrometer (JASCO micro Raman spectrometer). The Raman analytical method is generally similar to that of [9].

Small chips of Zagami (0.5-1 mm in size) were heated at 900 °C in a CO_2-H_2 gas mixing furnace for 1, 4, 8, 24 and 72 hours at the oxygen fugacity of two log units above the iron-wüstite buffer (IW+2) in order to study mineralogical properties of thermally annealed "maskelynite" in martian meteorites. The heated products were polished into thin sections and they were first observed with an optical microscope. "Maskelynites" within them were then analyzed by the same electron microprobes and the micro Raman spectrometer as used for analyzing the meteorite samples.

3. Martian meteorites

Textures

Almost all plagioclase in the martian meteorites studied is isotropic glass through an optical microscope. They have been considered as a diaplectic glass produced by intense shock and have been termed as "maskelynite" [*e.g.*, 5]. Plagioclase glass in Zagami, EETA79001, QUE94201, ALH77005, and Y-793605 preserves relict grain boundaries and twin planes. QUE94201 contains large impact melt areas which contain plagioclase glass showing flow textures. Plagioclase glass in ALH84001 does not have such textural properties and suggests multiple complex shock and impact history [*e.g.*, 10]. As is suggested by [11], plagioclase glass in ALH77005 contains many vesicles, and recrystallizing rims are observed in some grains. Such rims have clear extinction through an optical microscope.

Chemical compositions

Although El Goresy *et al.* [6] suggested that the original chemical composition of Shergotty plagioclase glass was modified during shock melting, plagioclase glass in the martian meteorites studied preserves original igneous chemical zoning. Plagioclase glass in EETA79001 even preserves sector zoning that is clearly of igneous origin (Fig. 1). As is stated before, ALH77005 contains crystalline plagioclase rims. These rims show growth zoning from the original plagioclase walls, producing a sharp contact against the inner plagioclase glass [11]. Generally, chemical composition of martian plagioclase (glass) is around An_{50}.

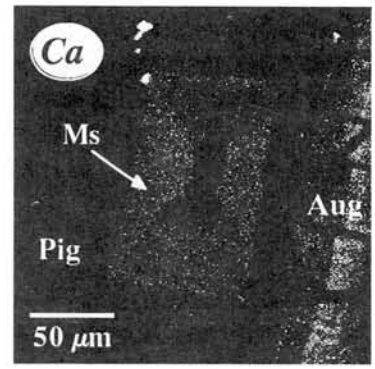

Fig. 1. Ca distribution map of the lithology B of EETA79001. The field of view is 200 μm. Note that an euhedral "maskelynite" grain showing sector zoning is present in the center. Ms: "maskelynite". Pig: pigeonite. Aug: augite.

Raman spectra

Micro Raman spectra of plagioclase glass in the martian meteorites studied give only broad emissions in the Raman shift range of 200-1000 cm^{-1}, which is

consistent with the result of [12]. The crystalline plagioclase rim in ALH77005 has Raman peaks near 500 cm^{-1} that is characteristic in plagioclase [13].

4. Annealing of Zagami maskelynite

Texture

"Maskelynite" in Zagami that was heated for 1 hour did not show clear evidence for recrystallization and "maskelynite" is still optically isotropic glass. "Maskelynite" heated for 4 and 8 hours has partial birefringence at the rims of the original grains. "Maskelynite" heated for 24 and 72 hours almost completely converts to polycrystalline plagioclase (Fig. 2). The recrystallizing plagioclase is microlitic in texture and usually shows a radiating lath shape from the grain boundary. Vesicles are rarely found within recrystallizing plagioclase. Individual microlites have different optical orientations from one another, suggesting that original atomic ordering has been lost. It is also noted that the devitrification texture of annealed Zagami "maskelynite" is similar to those produced by heating of experimentally shock-melted labradorite up to 45 GPa [7].

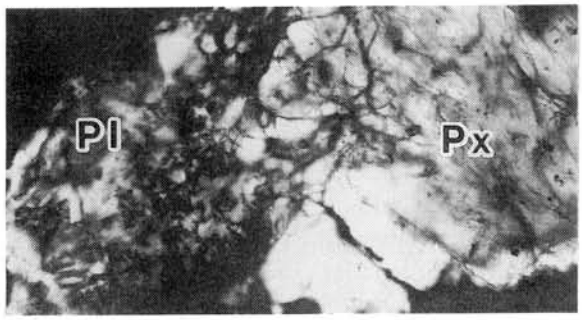

Fig. 2. Photomicrograph of the heated Zagami "maskelynite" for 72 hours (crossed polarizers). The original maskelynite converts to polycrystalline plagioclase (left). The field of view is about 550 μm. Pl: plagioclase. Px: pyroxene.

Chemical compositions

Ca and K in the heated "maskelynite" for 4 and 8 hours show unique distributions. Because recrystallization usually starts from the rims of the original maskelynite, glass areas are still present at the inner parts. These inner glass areas are enriched in K (up to 3 wt% K_2O for "maskelynite" heated for 8 hours) that is consistent with the content estimated from the reported partition coefficient of K between plagioclase and melt [14]. In contrast, "maskelynite" heated for 24 and 72 hours shows enrichment of K near the rims, like that of unheated "maskelynite" and their compositions are not different from that of unheated "maskelynite".

Raman spectra

"Maskelynite" in unheated Zagami did not show any Raman peaks and shows only broad emissions (Fig. 3). As is consistent with the optical microscopic observation, the sample heated for 1 hour shows no Raman peaks, whereas "maskelynite" heated for longer than 4 hours shows Raman peaks near 510 cm^{-1} (Fig. 3) Generally, "maskelynite" heated for a longer time has narrower full width at half maximum (FWHM) than that heated for a shorter time, indicating that the former has better crystallinity.

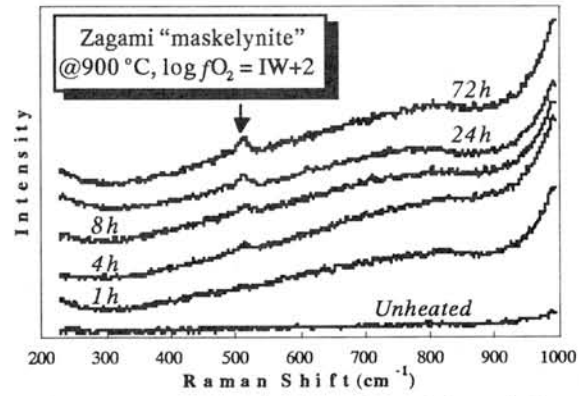

Fig. 3. Raman spectra of unheated and heated Zagami "maskelynite".

5. Lunar meteorites

Texture

Y-793169 and A-881757 are the only non-brecciated basaltic lunar meteorites [*e.g.*, 15]. Plagioclase in Y-793169 are composed of fine-grained microlitic crystals within an original plagioclase grain (Fig. 4). Some of such microlitic plagioclase show fibrous growth from the surrounding pyroxene walls. Generally, the optical orientation of these microlites is parallel to one direction within the same original plagioclase grain, probably preserving the original overall optical orientation. There are abundant spherical to irregular vesicles within the original plagioclase. In contrast, plagioclase in A-881757 is completely isotropic through an optical microscope and is similar to "maskelynite" in martian meteorites.

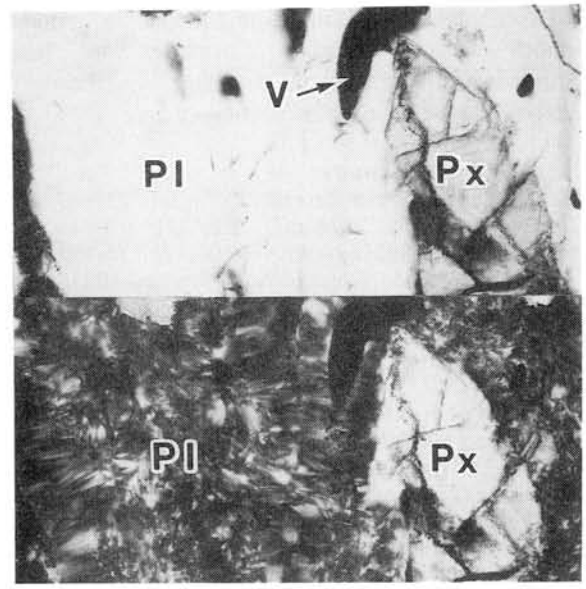

Fig. 4. Photomicrographs of Y-793169 lunar meteorite. Note that plagioclase shows a polycrystalline texture, some showing needle-like growth from the grain boundaries. Pl: plagioclase. Px: pyroxene. V: vesicle. The field of view is about 1 mm, respectively. A: transmitted light. B: crossed polarizers.

Chemical compositions

Plagioclase in lunar meteorites is much more An-rich than that of martian meteorite and is about An_{90}. Although plagioclase in Y-793169 recrystallizes to fine microlites, the overall chemical zoning of plagioclase is similar to that for normally-zoned igneous plagioclase. A-881757 also shows normal zoning from core to rim.

Raman spectra

Raman spectra of Y-793169 plagioclase give clear Raman peaks of plagioclase at 487, 507, and 560 cm^{-1}, while those of A-881757 plagioclase glass give only broad emissions (Fig. 5), which are similar to those of the martian "maskelynites".

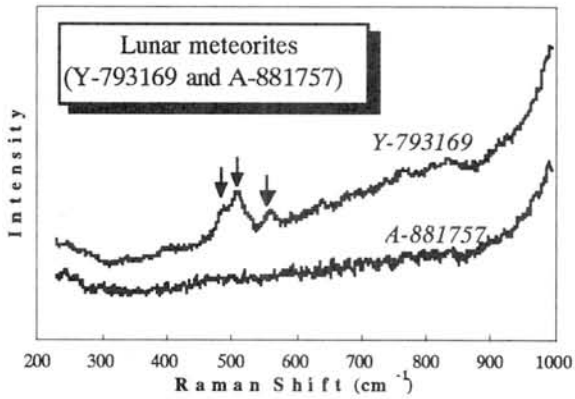

Fig. 5. Raman spectra of plagioclase (glass) from Y-793619 and A-881757 lunar meteorites.

6. Discussion

This study shows that shocked plagioclase glass in the martian meteorites and the A-881757 lunar meteorite is isotropic glass without Raman peaks, but preserves original igneous chemical zoning. This means that they are melting glass as suggested by [6,12] and were rapidly quenched without permitting recrystallization. The preservation of igneous chemical zoning suggests that even small-scale atomic diffusion was not achieved during melting and subsequent cooling. Because viscosity of plagioclase glass seems extremely low in such shock-melted plagioclase glass as is suggested by the presence of "euhedral"-shaped grain in the impact melt of QUE94201, nucleation of plagioclase for recrystallization may be difficult after shock melting. It should be noted that there is no mineralogical difference between martian and lunar "maskelynite" in spite of different chemical compositions.

This study also reveals that "maskelynite" in Zagami easily converts to polycrystalline plagioclase by thermal annealing like Shergotty [7]. The devitrification texture of annealed Zagami "maskelynite" is similar to that observed in the heated fused glass that is experimentally produced by shock, but is different from that observed in the diaplectic glass [8]. This result further suggests that "maskelynite" in Zagami is not a diaplectic glass, but is a melt glass. Because "maskelynite" easily converts to crystalline phases by annealing, it is obvious that "maskelynite"-bearing meteorites (Zagami, EETA79001, QUE94201, Y-793605, ALH84001 and A-881757) have not experienced high temperature after they were elected from each parent body.

Unlike these meteorites, the Y-793169 lunar meteorite and ALH77005 martian meteorite contain crystalline plagioclase, showing clear Raman peaks of plagioclase at 500-510 cm^{-1}. We suppose that plagioclase in Y-793169 formed by annealing of both diaplectic glass and shock melted glass. This is because the a recrystallizing texture of Y-793169 is similar to that of annealed plagioclase (diaplectic glass) after the shock experiment [8] Preservation of the overall optical orientation in Y-793169 plagioclase microlites also supports annealing of diaplectic glass. Nevertheless, it is also likely that some plagioclase microlites were recrystallized from the shock-melted plagioclase glass because some plagioclase grains indicate volume expansion by quenching of melting glass (*e.g.*, radiating fractures [6] and bent pyroxene twin). This is probably because that the peak shock pressure in Y-793169 was locally heterogeneous and both melting glass and diaplectic glass were present at the same time. It is not clear why some ALH77005 plagioclase glass contains crystalline rims despite that the other martian meteorites are completely absent in such crystalline plagioclase. We consider that ALH77005 cooled slightly more slowly than the other martian meteorites after the shock, and which caused partial recrystallization at the rim during cooling.

Acknowledgment

We thank Prof. H. Takeda and Drs. A. Yamaguchi and T. Kogure for discussion. We also thank The National Institute for Polar Research and The Meteorite Working Group (NASA Johnson Space Center, Houston, USA) for the samples. This work was partially supported by The Moritani Scholarship Foundation, which is gratefully acknowledged.

References

[1] McSween H. Y. Jr. (1994) *Meteoritics* **29**, 757-779. [2] Bischoff A. and Weber D. (1997) *Meteoritics & Planet. Sci.* **32**, Suppl., 13A-14A. [3] McBride K. and Mason B. (1998) *Antarct. Meteorite Newsl.*, **21**, No. 1, 12. [4] Bischoff A. and Stöffler D. (1992) *Eur. Jour. Mineral.*, **4**, 707-755. [5] Tschermak G. (1872) *Sitzber. Math.-Naturw. Classe. Akad. Wiss. Wien*, **65**, 122-146. [6] El Goresy A. *et al.* (1997) *Meteoritics & Planet. Sci.*, **32**, Supple., 214A. [7] Bunch T. E. *et al.* (1969) *American Mineral.*, **52**, 244-253. [8] Ostertag R. and Stöffler D. (1982) *Proc. LPSC 13th*, in *JGR*, **87**, Suppl., A457-A463. [9] Miyamoto M. and Ohsumi K. (1995) *Geophys. Res. Lett.*, **22**, 437-440. [10] McKay G. *et al.* (1997) *Meteoritics & Planet. Sci.*, **32**, Supple., A87-A88. [11] Ikeda Y. (1994) *Proc. NIPR Symp. Antarct. Meteorites*, **7**, 9-29. [12] Treiman A. and Toreado P. (1998) *LPS XXIX*, abst. #1196 (CD-ROM). [13] Heymann D. and Hörz F. (1989) *Phys. Chem. Minerals*, **17**, 38-44. [14] McKay G. and Weill D. F. (1977) *Proc. LSC 8th*, 2339-2355. [15] Takeda H. *et al.* (1993) *Proc. NIPR Symp. Antarct. Meteorites*, **6**, 3-13.

X-ray diffraction study of shocked plagioclase in martian and lunar meteorites with the micro-area Laue method using synchrotron radiation

Takashi Mikouchi[1], Takanobu Osaka[1], Kentaro Kaneda[1], and Kazumasa Ohsumi[1,2]

[1]*Mineralogical Institute, Graduate School of Science, University of Tokyo, 7-3-1 Hongo, Bunkyo-ku, Tokyo 113-0033, Japan*

[2]*Photon Factory, High Energy Accelerator Research Organization, 1-1 Oho, Tsukuba, 305-0801, Japan*

1. Introduction

"Maskelynite" is understood as a diaplectic plagioclase glass produced by a shock-induced solid-state transformation and is often observed in martian meteorites. Maskelynite is known to be optically isotropic and amorphous to X-ray (*e.g.*, Steele and Smith, 1982). Recently, El Goresy *et al.* (1997) proposed that "maskelynite" in the Shergotty martian meteorite was melted during shock and therefore is a true melt. Since it is a very significant issue for isotopic aging to determine whether "maskelynite" is a true melt or not, understanding of mineral property of shocked plagioclase is important. In this study we employed the micro-area Laue method using synchrotron radiation (SR) (Ohsumi *et al.*, 1991; 1994; Mikouchi *et al.*, 1995) for analyzing a small-area (1.6 μm) X-ray diffraction property of shocked plagioclase in martian and lunar meteorites. The analyzed samples were thin sections of six martian (Zagami, QUE94201, ALH77005, Y-793605, Nakhla, and ALH84001) and two lunar (Y-793169 and Asuka881757 (A-881757)) meteorites. Similar study was only performed on olivines in chondrites by using the almost same technique (Ohsumi *et al.*, 1994).

2. Methods

Shocked plagioclase in the thin sections of martian and lunar meteorites was analyzed by SR at BL-4B$_1$ of the Photon Factory (PF), High Energy Accelerator Research Organization (KEK), Tsukuba, Japan. The Laue method was used to record the diffraction patterns with an imaging plate (IP; Fuji Co., Ltd.) of a two-dimensional detector coated by storage phospheres with a micro-pinhole set just behind the optical system which was installed in the beamline. The diffraction apparatus (Ohsumi *et al.*, 1991) was used to generate micro-beam at the sample position. The micro-region 20 x 20 μm in size of a thin section was set to the SR beam position by an optical microscope with a CCD (charged coupled device) camera mounted on the diffraction equipment. The Laue diffraction pattern was recorded on an IP from -60 to 165° in the 2θ range with a cylindrical camera radius of 100 mm. The uniformity of the beam at the sample position was confirmed by an image recorded on Radcolor film. The actual beam size was measured using the signal from an ion chamber with a slit in the front side by scanning stepwise in the vertical direction and a minimum beam diameter of 1.6 μm was employed by using the micro-pinhole of 1.6 μm diameter set on a goniometer-head placed just after an X-ray collimator. The Laue patterns of the shocked plagioclase were taken with 3-5 minutes exposures, with the storage ring current at around 250 mA and a ring energy at 2.5 GeV. The IP moves to the readout position and is read by the system using a laser. A computer software system developed for an analysis of submicrometer-sized single crystals (Hagiya *et al.*, 1994) has been revised and used for data reduction. A more detail description of the method is in Ohsumi *et al.* (1994).

3. Results

3. 1. Martian meteorites

ALH77005 and Nakhla are the only samples that give X-ray diffraction for shocked plagioclase among the martian meteorites studied. Shocked plagioclase in the other samples (Zagami, QUE94201, Y-793605, ALH84001 and plagioclase glass of ALH77005) does not give any diffraction patterns as far as been analyzed in this study. This result is consistent with the micro Raman spectroscopic study of the same region, suggesting that they are glass (Mikouchi *et al.*, 1998). The Laue spots of the crystalline plagioclase

rims in ALH77005 ($An_{53}Ab_{46}Or_1$) (Ikeda, 1994; Mikouchi *et al.*, 1998) are fairly sharp (Fig. 1). As is suggested from the optical microscopic observation, the 1.6 μm X-ray beam analysis shows diffraction from a single crystal.

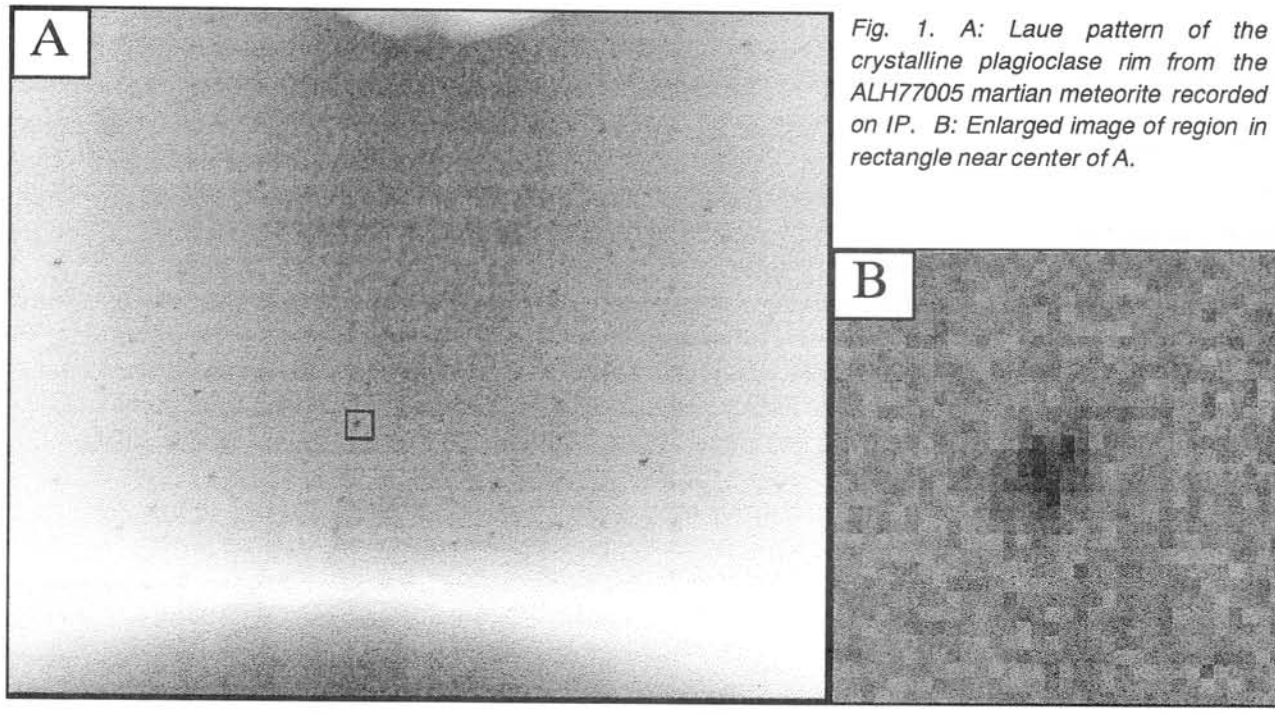

Fig. 1. A: Laue pattern of the crystalline plagioclase rim from the ALH77005 martian meteorite recorded on IP. B: Enlarged image of region in rectangle near center of A.

Nakhla is a clinopyroxenite and is not as extensively shocked as the other martian meteorites (shergottites) (*e.g.*, McSween, 1994). Nakhla contains crystalline plagioclase and K-feldspar (in mesostasis that comprises of ~10 vol.% of the sample (*e.g.*, Bunch and Reid, 1975). They are lath-shaped reaching ~1 mm in length. No "maskelynite" is observed. The Laue spots of Nakhla plagioclase ($An_{32}Ab_{64}Or_4$) are fairly clear , but faint streaks are observed between the neighbor spots along the intense zone axes (Fig. 2).

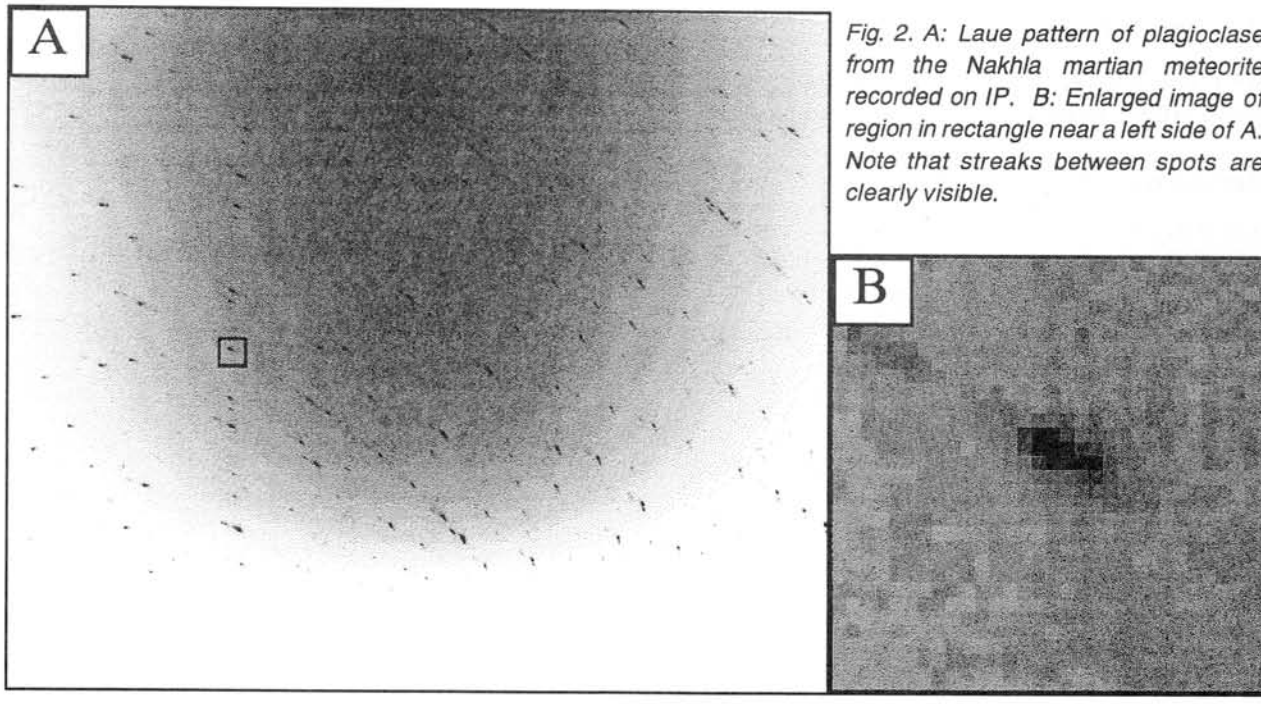

Fig. 2. A: Laue pattern of plagioclase from the Nakhla martian meteorite recorded on IP. B: Enlarged image of region in rectangle near a left side of A. Note that streaks between spots are clearly visible.

3. 2. Lunar meteorites

Like "maskelynite" in martian meteorites, shocked plagioclase glass in A-881757 did not give any diffraction patterns. Y-793169 shows a polycrystalline microlitic texture that is recrystallized by thermal annealing after shock (Mikouchi *et al.*, 1998). However, almost no diffraction pattern was obtained and only a few faint obscure spots were visible. Although we also analyzed recrystallized plagioclase in Y-793169 without micro-pinhole (The X-ray beam was about 50 μm in diameter), no Laue spots were obtained.

4. Discussion

This study shows that "maskelynite" in martian and lunar meteorite is amorphous to X-ray even in a small range of as small as 1.6 μm in diameter.

ALH77005 martian meteorite contains crystalline plagioclase rims showing fairly non-distorted Laue spots (Fig. 1). This may suggest that the rims have not experienced shock effects after they crystallized. This is consistent with the interpretation by Ikeda (1994) and Mikouchi *et al.* (1998) that the crystalline rim formed during cooling after the final shock. Plagioclase in the Nakhla martian meteorite also has sharp Laue spots, but they are slightly elongated and show streaked textures (Fig. 2). This may be caused by distortion of the crystal lattice that affected Nakhla when it was ejected from Mars although shock effects in Nakhla is extremely uncertain (Bischoff and Stöffler, 1992).

Y-793169 lunar meteorite clearly shows a recrystallizing texture (Mikouchi *et al.*, 1998), but the micro-area Laue analysis in this study did not give clear diffraction spots. We consider the reason is that we analyzed the areas showing needle-like textures where microlites are composed of very small domains and their crystal orientations are not uniform. This is supported by the observation that each microlite shows undulatory extinction through an optical microscope.

This study reveals that the micro-area Laue method by SR is very useful to obtain crystallographic data of crystalline shocked plagioclase. However, it seems difficult to give quantitative estimates of shock degrees although Ohsumi *et al.* (1994) suggests that the same technique has a potential to estimate shock degrees of olivine in chondrites. The reason may be that plagioclase behaves distinctly from olivine against shock.

At present, indexing of the Laue spots obtained from ALH77005 and Nakhla plagioclases is in progress and detailed profile analysis of the Laue spots may give further information about shock effects observed in shocked plagioclase in martian and lunar meteorites.

5. Acknowledgment

We thank The National Institute for Polar Research and The Meteorite Working Group (NASA Johnson Space Center, Houston, USA) for the samples.

References

Bischoff A. and Stöffler D. (1992) *Eur. Jour. Mineral.*, **4**, 707-755.
Bunch T. E. and Reid A. M. (1975) *Meteoritics*, **10**, 303-315.
El Goresy A. *et al. (1997) Meteoritics & Planet. Sci.*, **32**, Suppl., A87-A88.
Hagiya K. *et al.* (1994) *Acta Cryst.*, **A49**, Suppl., 57.
Ikeda Y. (1994) *Proc. NIPR Symp. Antarct. Meteorites*, **7**, 9-29.
McSween H. Y. Jr. (1994) *Meteoritics*, **29**, 757-779.
Mikouchi T. *et al.* (1995) *American Mineral.*, **80**, 585-592.
Mikouchi T. *et al.* (1998) *Antarctic Meteorites*, **XXIII**, this volume.
Steele I. M. and Smith J. V. (1982) *Proc. 13th Lunar Planet. Sci. Conf.* (*Jour. Geophys. Res.*, **87**, Suppl.), A375-A384.
Ohsumi K. *et al.* (1991) *Jour. Appl. Cryst.*, **24**, 340-348.
Ohsumi K. *et al.* (1994) *Proc. of NIPR Symp. on Antarct. Meteorties*, **7**, 244-251.
Ostertag R. and Stöffler D. (1982) *Proc. 13th Lunar Planet. Sci. Conf. (Jour. Geophys. Res*, **87**, Suppl.), A457-A463.

THE INCORPORATION OF RADIOGENIC LEAD COMPONENTS INTO PLAGIOCLASE DURING SHOCK METAMORPHISM

Keiji Misawa[1,2], Fumie Yamazaki[1], Noboru Nakamura[1,2], and Toshimori Sekine[3]
[1] Graduate School of Science & Technology, [2] Department of Earth & Planetary Sciences, Kobe University, Nada, Kobe 657, Japan
[3] National Institute for Research in Inorganic Materials, 1-1 Namiki, Tsukuba, Ibaraki 305, Japan

Because of the key role of plagioclase in the U-Th-Pb systematics of meteorites and lunar rocks, it is important to understand the mobility of volatile Pb in plagioclase during shock metamorphism. With increasing shock intensity, plagioclase transforms into maskelynite (diaplectic glass) which is commonly observed in shergottites, lunar highland rocks, and brecciated meteorites. The maskelynitized plagioclase fractions from the Asuka-881757 lunar meteorite lie above the 3.94 Ga isochron (*i.e.*, ^{207}Pb-rich), indicating open-system behavior owing to a disturbance in the U-Pb system [1]. Whether Pb from older lunar highland rocks was incorporated into plagioclase during shock events or the plagioclase separates still partly contaminated and should have been leached more is an issue of importance in evaluating the evolution history of this new type of mare basalt. As an initial step in understanding the disturbance in the U-Pb system of lunar meteorites, we have carried out shock experiments on plagioclase, over the pressure range 21-34 GPa, by using a propellant gun and measured Pb isotopes of maskelynitized plagioclase.

Anorthite (Tarumaeyama) and olivine (Kilbourne Hole or San Carlos) were crushed in a stainless steel mortar. From the coarse fraction (ϕ>60μm), grains without inclusions were handpicked. Samarskite (Luster pegmatite, South Platte district, Colorado) was crushed in an agate mortar. After sieving, ϕ>60μm- and 60μm<ϕ<150μm-sized fractions were used. The projectile is a 4-mm thick plate made of stainless steel bedded at the front of a high density polyethylene sabot. The target is a layered assemblage (anorthite + olivine + samarskite) encapsulated in a cylindrical container made of stainless steel SUS304. For several runs, a 50μm-thick Mo sheet was placed between olivine and samarskite layers in order to avoid mechanical mixing of anorthite with samarskite during compression. Before encapsulating into a container, the starting materials were washed with ethanol, leached in dilute HCl, and washed with distilled water. Because the peak pressure depends on the initial porosity of the material, samples were pressed at 100-200 kg/cm^2. The experimental conditions are presented in Table 1.

Shock-loaded anorthite was separated from each recovered sample by handpicking under a microscope in addition to magnetic separation using a Frantz isodynamic separator equipped with an ethanol-filled chute. The Pb isotopic compositions of the starting materials (anorthite and samarskite) as well as stainless steel (SUS304) and Mo sheet were measured. In order to remove any laboratory Pb contamination, anorthite (maskelynite) separated from run products were washed with acetone and ethanol, and leached in HBr and HNO_3. Samples were decomposed in a mixture of HNO_3 and HF in PFA Teflon screw-cap jars. Chemical procedures for separation of Pb from other elements are similar to those described previously [1]. Analytical blanks for Pb were 150~200 pg. Isotopic compositions of Pb were measured on a Finnigan MAT 262 mass spectrometer equipped with five Faraday collectors and an ion counting system. The raw data were corrected for instrumental mass fractionation of 0.91± 0.29 ‰ per mass unit (2σ) for Pb as determined by measurement of the NBS 981 standard. The Pb isotopic compositions of leachates and residues of the starting materials and the anorthite (maskelynite) are shown in ^{207}Pb/^{206}Pb *vs.* ^{204}Pb/^{206}Pb diagrams (Figs. 1-4).

Starting materials: To provide a check on possible inhomogeneity of the starting materials, we measured different sized anorthite (89.3mg, 92.3mg, and 121.0mg) and samarskite (48.7mg and 78.8mg). Leachates and residues of the anorthite show Pb isotopic compositions close to that of modern terrestrial lead (MT) [2]. The Pb isotopic compositions of the acid residue of anorthite are

homogeneous and non-radiogenic. The Pb of the residue of samarskite is radiogenic ($^{206}Pb/^{204}Pb$ = 68.4 and 112), indicating that the samarskite is old enough (1040-1070 Ma [3]) and contains sufficient radiogenic Pb. The samarskite's Pb is not homogeneous in the 50-80 mg-sized samples (Fig. 1).

Run products: The Pb isotopes of the acid residue of anorthite (#570) shocked to 34 GPa without samarskite were not different from those of the starting material (Fig. 2), indicating that the Pb isotopes of anorthite were not affected by olivine or stainless steel even if transformation into maskelynite occurred (> 26 GPa [4]). Anorthite (#575) isolated from samarskite by a Mo sheet and shocked to 31 GPa with samarskite was first leached three times in 0.1M HBr (L1), three times in 1M HNO_3 (L2), and finally twice in 7M HNO_3 (L3) for 5 min each time. The first leachate is the most radiogenic and the second and third leachates are getting less radiogenic (Fig. 3). Anorthite (#569) shocked to 31 GPa was leached twenty times in 7M HNO_3 for 5 min each time. We assume that the laboratory Pb contamination, including adhering samarskite, if existing, might be removed by repeated 7M HNO_3 treatments. Leachates were combined after each five steps (L1-L4). The Pb of leachates is getting radiogenic with increasing leaching steps (Fig. 4). In both cases (#569 and #575) the data points of acid leachates fall on a tie line connecting the anorthite data with data for samarskite, suggesting that the acid leaching treatments effectively removed surface Pb components. The Pb isotopic compositions of the residues of shock-loaded anorthite are radiogenic and different from those of unshocked anorthite but rather similar to those of samarskite. Because we can rule out the possibility of samarskite contamination especially in #569, the radiogenic nature of the shock-loaded anorthite is considered to be indigenous.

Although there are large differences between the shock metamorphism which took place in meteorite parent bodies and the artificial shock compression (*e.g.*, shock duration time, cooling rate, and mechanism of volatile transportation), the present results suggest that radiogenic Pb components could be incorporated into the maskelynite without isotopic fractionation during shock events.

TABLE 1 Experimental conditions

Run No.	anorthite (mg)	olivine (mg)	samarskite (mg)	Mo sheet	Pressure (GPa)	Porosity (%)
#569	407	150	52	no	33	28
#570	403	154	no	no	34	25
#575	392	157	127	yes	31	32
#579	398	157	104	yes	21	34

REFERENCES: [1] Misawa K. *et al.* (1993) *GCA*, **57**, 4687-4702. [2] Stacy J.S. & Kramers J.D. (1975) *EPSL* **26**, 207-221. [3] W.R. Premo (1997) personal communication. [4] Stöffler D. *et al.* (1988) in *Meteorites and the Early Solar System* pp. 165-202. Univ. of Arizona Press.

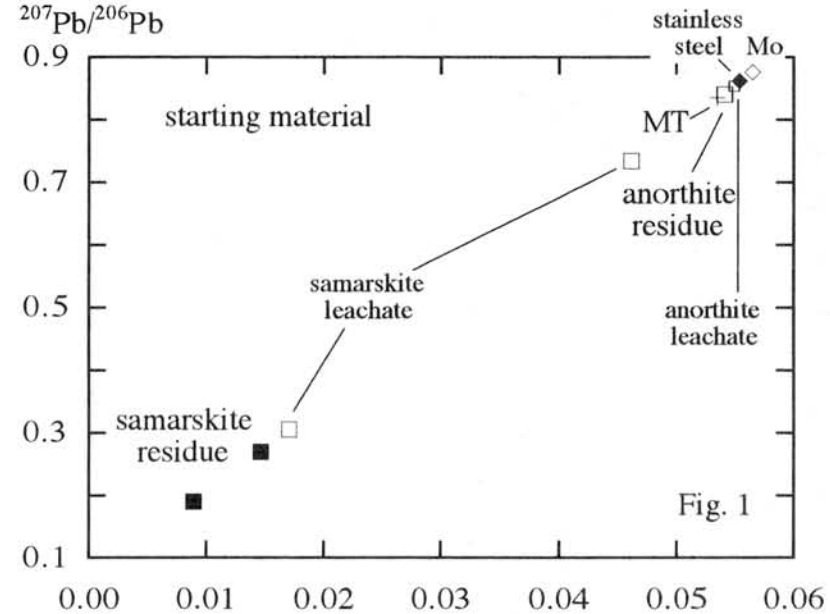
$^{207}Pb/^{206}Pb$
0.9
0.7
0.5
0.3
0.1
0.00
0.01
0.02
0.03
0.04
0.05
0.06
stainless steel
Mo
MT
starting material
anorthite residue
samarskite leachate
anorthite leachate
samarskite residue
Fig. 1

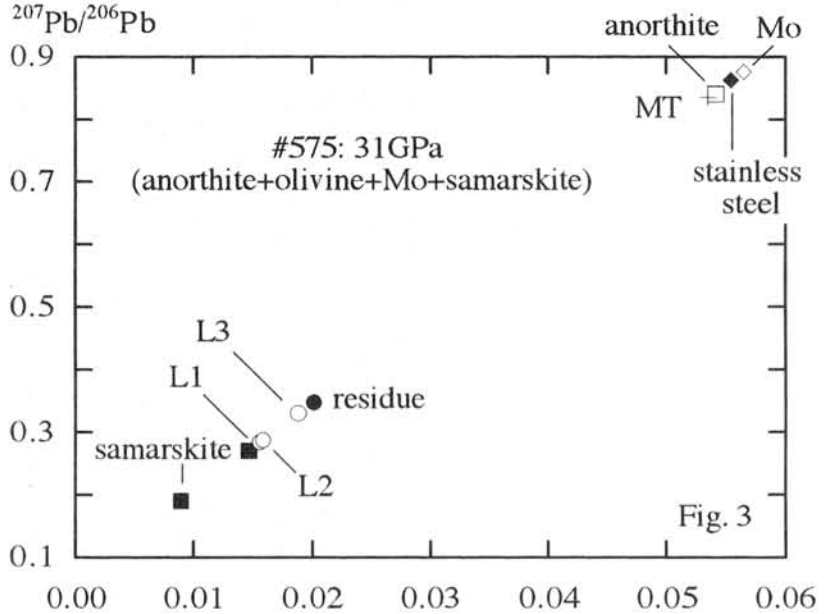
$^{207}Pb/^{206}Pb$
0.9
0.7
0.5
0.3
0.1
0.00
0.01
0.02
0.03
0.04
0.05
0.06
anorthite
Mo
MT
#575: 31GPa
(anorthite+olivine+Mo+samarskite)
stainless steel
L3
L1
residue
samarskite
L2
Fig. 3

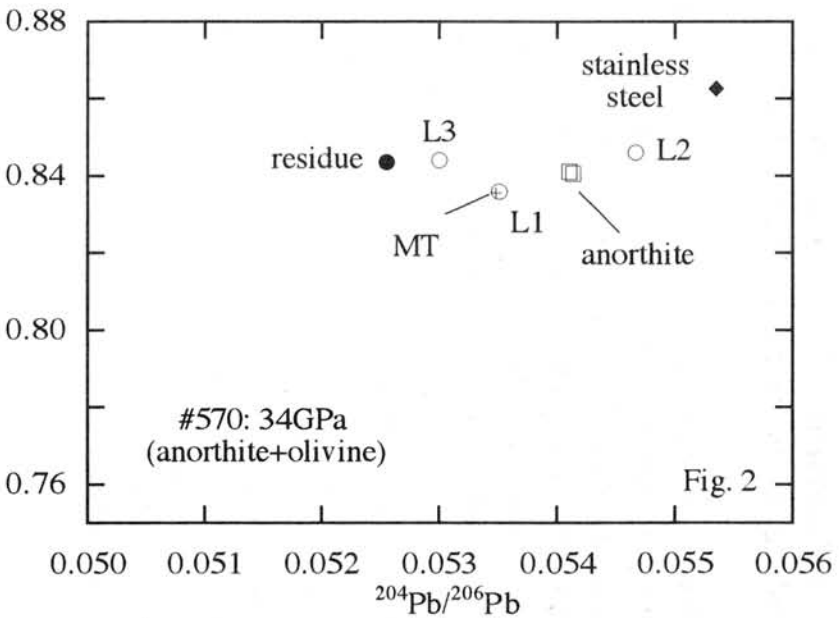
0.88
0.84
0.80
0.76
0.050
0.051
0.052
0.053
0.054
0.055
0.056
$^{204}Pb/^{206}Pb$
stainless steel
L3
residue
L2
MT
L1
anorthite
#570: 34GPa
(anorthite+olivine)
Fig. 2

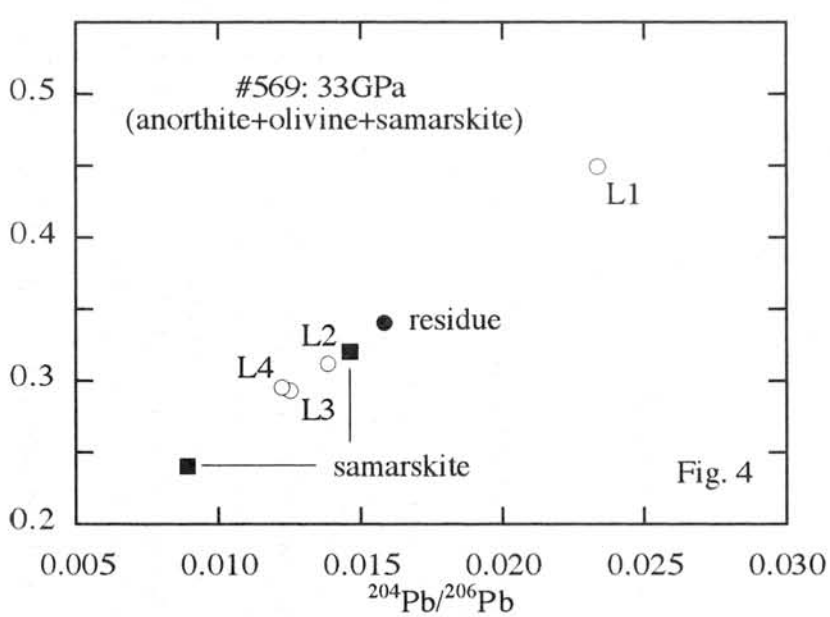
0.5
0.4
0.3
0.2
0.005
0.010
0.015
0.020
0.025
0.030
$^{204}Pb/^{206}Pb$
#569: 33GPa
(anorthite+olivine+samarskite)
L1
residue
L2
L4
L3
samarskite
Fig. 4

MELT OR VAPOR COMPOSITIONS FROM IRON-NICKEL METALS AFTER IMPACT

Miura Y., Fukuyama S. and Gucsik A.
Dept. of Earth Sciences, Yamaguchi Univ., Yamaguchi ,753,-8512 Japan.
yasmiura@po.cc.yamaguchi-u.ac.jp

Introduction: Material evidences for impact are existence of (a) high-pressure phases of stishovite, coesite and diamond, (b) mixings of iron meteoritic compositions of platinum group elements (PGE) including Ir, and (c) shock metamorphosed materials of shocked quartz, graphite and calcite which are relict of high pressure (cf.Miura et al., 1994, 1995, 1997). As it is difficult to find so easily on impact materials on active planet of the Earth, the other indicator of impact should be established so well. One of the candidates of other impact materials is mixing with iron meteorite (projectile) and terrestrial evolved rock (target rock), especially melt and vapor compositions from Fe-Ni metals of meteorites after impact (Miura et al., 1997). The main purpose of the present paper is to elucidate compositional characteristics of Fe-Ni metals after impact.

Compositional change of impact process: Impact reaction consists of three reactions of solid (main on target rocks), melt-liquid (both on target and projectile) and vapor (both on target and projectile)., though dynamic process of impact reaction is difficult to describe as static reaction with sharp boundary of three reactions. Mixed texture of impact is one of characteristics of melt-vapor reaction of impact. In fact, Fe-Ni metals of meteorite can be mixed with target rock under impact condition.

Fe-Ni metal of impact craters and spherules: Fe-rich mixed impact fragments of the Barringer meteorite crater (USA) and Wolf Creek meteorite crater (Australia) reveal that fragmental particles with Fe-Ni system in composition formed at long crystallization in the planetesimals can remain with Fe-Si mixing after impact process which are found as melted brecciated grains. However, fragmental particles with the Fe-Ni system in composition cannot be found as crystallized particles with Fe-Ni system under vapor-melt condition of impact where Fe-Si system in composition are found in vein of impact grains or spherules as major phases. Widmannstaetten texture of Fe-Ni iron meteorites formed in slow-cooling rate (several degrees per million years) cannot formed anymore after short impact reaction with high temperature and pressure conditions to form Ni-rich, Fe-rich, or Fe-Si mixing in composition. We found the similar fragmental grains of Fe-Si system from Odessa meteorite crater, Texas, U.S.A. at field investigation on March,,19-22,1998, and from Lappajarvi crater, Finland (Table 1). Spherules formed at meteoritic showers of Mezo-Madaras and Mocs meteorites, Romania, which were formed by impact reaction during collision with meteorites and atmosphere, shows Fe-Si system in major composition.

Fe-Ni mixings by artificial impact experiments: In order to obtain Fe-Ni-Si system in composition after artificial impact experiments, Barringer meteorite was broken by

railgun impact apparatus(ca.7km/sec), ISAS, Japan. Highest Ni content in this experiment is 47.1%Ni after impact. Silica is also mixed with 8 wt.%. Higher chlorine from iron meteorite is also concentrated to 2.9%Cl as Ni content increases (Table 2). It is found in this study that (a) Fe element is easily enriched in Si (as Fe-Si system in composition), whereas Ni element is relatively enriched with light elements of Cl or S, and (b) Ni content inreases from 7% Ni (kamacite) to 49% Ni after impact experiment.

Table 1. Compositions of impact materials from two terrestrial impact craters and spherules of Mezo-Madaras and Mocs meteorite showers..

Samples	Odessa-M1	Lappajarvi-M1	Mezo Madaras-S1		Mocs-S1	
Oxides						
SiO2	11.0	11.2	4.2	39.3	6.0	11.4
Fe	82.4	87.3	30.2	19.9	93.9	78.4
Ni	6.6	0.8	0.5	1.6	0.0	0.0

Table 2. Compositions of artificial impact materials from Barringer meteorite.

Samples	Barringer-high Fe-Si	Barringer-high Ni-Cl	Barringer (Original)
Oxides			
SiO2	8.0	0.0	0.0
Cl	0.7	2.3	(0.0)
Fe	79.3	50.5	93.4
Ni	12.0	47.1	6.6

Indicator of impact to the Earth: Among these fragmental grains, Ni element is considered to be significant indicator of extraterrestrial origin, though Fe element cannot distinguish from terrestrial or extraterrestrial origin. Thus Ni ore deposit on the Earth indicates (a) probable location of impact site of small iron meteorite on the continent, (b) impact site of large iron meteorite with mixing evolution in the interior of the Earth, and (c) hot or cold plume site of mantle convection which transports some of Ni-bearing materials from original iron meteorite source penetrating to the upper mantle.

Ni separation from Fe-Ni phase of kamacite mineral can be obtained by impact reaction mainly on ocean floor (with thin crust layer) to penetrate to mantle layer where it mixes and separates to Ni-rich phases as Ni-bearing materials of awaruite, or to make Ni-rich ore deposit on the present surface of the crust. Major Ni elements found at Sudbury crater, Ontario, Canada, can be explained as such impact induced crater with Ni deposite, where impact evidences are proved from shattercone, breccias with Ir anomaly , and shocked quartz.

Summary: The present results indicate as follows:

(a) grains of Fe-Ni system in major composition can remain under solid (or melt)-solid impact reactions,

(b) those of major Fe-Si system can be formed under vapor condition of impact, and

(c) those with Ni-Cl-S system in composition are formed under vapor condition of impact.

References

Miura Y. et al. (1994): Shock Waves, 3, 293-298.
Miura Y. et al. (1995): Shock Waves Proc., 19, 399-410.
Miura Y. et al. (1997): Proc. Int.Conf. High-Pressure Sci. and Tech (in press).

CARBON SOURCE FROM TARGET-ROCK OF LIMESTONE BY IMPACT REACTION AT K/T BOUNDARY

Y. Miura, H.Kobyashi S.Fukuyama , M.Okamoto and A.Gucsik
Department of Chemistry and Earth Sciences, Faculty of Science
Yamaguchi University, Yoshida, Yamaguchi 753-8512 Japan.
yasmiura@po.cc.yamaguchi-u.ac.jp

Introduction: Alvarez et al. (1980) [1] reported that main origin of Cretaceous-Tertiary (K/T) geological boundary is considered to be formed by iron meteorite with ca.10km in size hit to the Earth. Main reason of iron meteorite hit on K/T boundary is anomalous amount of Ir content, many shocked materials of shocked quartz, tektites, microtektites, stishovite, Ni-rich spinels and platinum-group elements (PGE) found at the K/T boundaries in the world by many researchers[1,2]. Recently buried large impact crater was found Chicxulub impact crater, Yucatan Peninsula,Mexico as main impact crater of meteorite hit on the K/T boundary [2], though there is possible explanation of multiple impacts around the K/T boundary [3,4,5,6,7]. However large amount of carbon at the K/T boundary is explained by wildfires [8,9].Miura et al. [10] reported that carbon can be acuumulated from target-rock of limestone by meteoritic impacts found at natural meteoritic impact craters and artificial impact experiments. The main purpose of this study is to elucidate new source of carbon from limeston of the K/T boundary.

Probable carbon source around the K/T geological boundary: Wolbach et al. (1985) explained [8,9] that main source of carbon of the K/T boundary is (a) extra-terrestrial origin of meteorite itself, (b) target rock of fossil organic carbon, or (c) wildfires as most plausible source. However Miura et al. [10] reported that large carbon blockes around the Barringer meteorite crater , Arizona, U.S.A. can be formed from Kaibab limestone by impact reaction including vaporization because it contains Si from Coconino sandstone and Ca from limestones on the target rocks. Similar carbon materials can be found at impact craters with limestone target rock, such as Ries, Germany, and Odessa,Texas, U.S.A as shown in Table 1. Artificial impact experiment supported that shocked graphite carbon can be found after railgun impact on limestone by X-ray diffractometer [10] (cf.Table 1).

Caculation of carbon content. Average content of carbon at the K/T boundaries of Denmark, New Zealand and Spain, 0.021 (g/cm^2), shows total amount of carbon as 1.0×10^{17}(g) on the world, which is larger than that of wildfires reported by 0.7×10^{17}(g) [11], though wildfires with reduction condition started from small fire around 10^3km of meteorite impact near middle America covered by ocean water is difficult to explain all carbon content in the world. In this meaning carbon formed by reduction condition can easily be found at impact reaction within vapor plume without oxidation.The present model of limestone contribution for carbon shows that all evaporation carbon from limestone (with 3km in depth and 40km in diameter) is 6.2×10^{17}(g) of carbon. From data of the previous craters, solid carbon formed under reduction condition of impact is from ca.12% (in total) to 0.1% of total carbon from limestone. This suggests that carbon from limestone by impact can explain carbon content of the K/T boundaries.

Impact model of K/T boundary : Based on the above-mentioned carbon source the following impact model mainly for impact materials is proposed [7,10,11] (Table 1).

1) Single Fe-rich asteroid of ca.10 to 15 km in size are collided to the Earth finally after splitting to many fragments near the Earth.
2) The Main fragment with ca.8 to 10 km in size finally hits to limestone of shallow water of present Yucatan Peninsula,Mexico, though Tertiary limestone can be found after formation of crater to produce present buried crater.

Table 1. Carbon formation at various impact events [7,10,11].

Impact event	Carbon materials
1) Barringer crater, U.S.A.	Graphite, Moissanite (diamond)
2) Ries, Germany	Graphite,. Lonsdalite
3) Odessa, Texas, U.S.A.	Graphite, Moissanite
4) Impact experiment (on limestone)	Graphite
5) K/T boundaries	Carbon

Conclusions: The following results can be summarized as follows[10].

1) Amount of carbon from limestone by impact can explain anomalous data of carbon at the various K/T boundaries.
2) Extraterrestrial objects of the K/T bolides are explained by iron-rich meteorite because it hits to limestone target rock with carbon. Comets and carbon-rich chondritic meteorite is considered to be broken before making large impact crater on hard rock of the Earth with thick atmosphere. This conclusion can support that Ir-anomaly is maily from iron meteorite source.
3) Carbon evaporated from target rock by impact reaction is found as carbon solid materials, though it is difficult to find it in melted or solid fragments of impact as tekite or spherule by melt condition.

References

[1] Alvarez, W.L. et al. (1980): Sci.Am., 263, 78-84.
[2] Hildebrand, A.R. et al. (1991): Geology, 19, 867-871.
[3] Miura, Y. et al., (1985): ESR Dating and Dosimetry (Japan), 1, 469-476.
[4] Miura, Y. (1989): Meteoritics, 24, 305; 25, 387.
[5] Miura, Y. (1991): Shock Waves, 1, 35-41.
[6] Miura, Y. et al. (1992): Meteoritics, 27, 261.
[7] Miura, Y. et al. (1997): Proc. ISAS LPS (Sagamihara,Japan), 30, 227-229.
[8] Wolbach, W.S. et al.(1985): Science, 230, 167-170.
[9] Wolbach, et al. (1988): Nature, 334, 665-669.
[10] Miura, Y. et al.(1996): Proc.ISAS LPS (Japan), 29, 293-296.
[11] Miura, Y. et al. (1998): (in press).

Rb-Sr ISOTOPIC SYSTEMATICS AND REE-PATTERN OF THE Y-793605 LHERZOLITIC SHERGOTTITE. N. Morikawa, G. Kondorosi, N. Nakamura and K. Misawa Dpt. of Earth & Planetary Sciences, Faculty of Science, Kobe University, Rokkodai 1-1, Nada, Kobe, 657 Japan

Introduction Y-793605 is a lherzolitic (peridotitic) shergottite, a member of the Martian meteorite clan and has close petrological and geochemical ties to the other two lherzolitic shergottites (ALH77005 and LEW88516), especially to the former one [e.g. 1-5].

As part of the consortium study organized by the NIPR [1] we have undertaken isotopic and LIL trace element studies. The results on the U-Th-Pb isotopic systematics of Y-793605 were already reported at the NIPR symposium in 1997 [6]. We present here the results of the Rb-Sr isotopic studies carried out on residues and leachates of mineral fractions and LIL trace element (typically REE) abundances obtained for a whole rock split of the meteorite.

Sample and Analytical Procedures A few fragments (about 0.4 g in weight) of the meteorite sample were allocated to us by the NIPR. The sample was crushed and sieved at <63 μm, 63-150 μm and 150-300 μm. Mineral fractions of olivine (OL), two types of pyroxene (PX1, PX2) and plagioclase (i.e. maskelynite) (PL) were separated by hand-picking and using a Frantz isodynamic separator. The finest fraction was analyzed as whole rock (WR) with the exception of a 3.3 mg powder split which was later used for the LIL trace element (2.2 mg) and an independent whole rock analyses. The mineral separation was followed by a three-step leaching procedure on all mineral phases and WR using 0.01M HBr, 0.1M HBr and 1M HNO_3, sequentially. After spiking and separating the U-Th-Pb fraction, the Rb and Sr fractions were also separated and used for this study.

The mineralogical separation and the chemical procedures are discussed in more detail by [6]. The LIL and REE trace element analysis was carried out by direct loading IDMS [7].

Results and Discussion

Rb-Sr Analysis of Residues and Leachates The leaching procedure, primarily intended for the purposes of the U-Th-Pb study, resulted in preferential leaching of Sr over Rb in all mineral phases and the WR, causing Rb/Sr (and, also, Sr isotopic) fractionation in the leachates compared to the residue phases.

The analysis of the residue phases (OL, PX1, PX2, PL and WR) yields an age of 164±10 Ma with an initial $^{87}Sr/^{86}Sr$ ratio of 0.71043±7. The PX1 and PL plots are slightly offset from the isochron. Excluding them from the isochron compilation, the remaining three data points (OL, PX2 and WR) indicate an age of 174±8 Ma with I_{Sr} of 0.71032±7.

Data points obtained by the analysis of the Rb-Sr systematics of the leachates scatter, in a relatively small cluster, around the isochron established based on the residue data, having considerably lower $^{87}Sr/^{86}Sr$ ratios than the corresponding residue phases. Leachate-data obtained from samples of the first and second leaching steps tend to plot above, while those of the third leaching step below the isochron with the exception of OL,2 , being the only second-step leachate plotting together with the third-level leachates below the isochron. Regardless of this tendency, the analysis of data for the leachates and their corresponding mineral residue fractions, and that of between the leachate fractions themselves, could not reveal further relationships.

Recombination of the residue and leachate data of the same mineral fractions and that of the WR resulted in a basically similar overall scheme as discussed above for the residue phases. The age obtained in this way is 170±13 Ma with I_{Sr} of 0.71042±7. Again, PL and PX1 plot slightly off from the isochron. An isochron based exclusively on the WR, PX2 and OL data gives an age of 183±8 Ma and I_{Sr} of 0.71032±7 (Fig.1).

Within error limit, the obtained ages and initial $^{87}Sr/^{86}Sr$ ratios are remarkably similar to those reported earlier for ALH77005 by [8] (183±12 Ma, 0.71037±5) and recently for LEW88516 by [10] (183±10 Ma, 0.710518±60). Considering the highly disturbed U-Th-Pb systematics reported and the data obtained by [6] for Y-793605, and comparing our Rb-Sr data with those published previously on the Rb-Sr and U-Th-Pb systematics of lherzolitic shergottites by other workers [e.g 8-10], we suggest that if the above mentioned age is the crystallization age of Y-793605, later processes such as metasomatism and/or impact and/or terrestrial weathering might greatly disturb its U-Th-Pb systematics while caused little disturbance in its Rb-Sr scheme. The slightly disturbed Rb-Sr systematics observed in PL and PX1 may be attributed to shock process(es) /these were the mineral phases that showed pronounced shock induced features by petrological studies, too/.

LIL Trace Element Abundances In Fig.2, the CI-normalized LIL-pattern obtained for Y-793605 is compared with those of other lherzolitic and basaltic shergottites. Some previous results on Y-793605 are also indicated [5,11]. The Yamato-lherzolite indicates very similar REE-pattern to that of ALH77005. Our data are in good agreement with those obtained by [5] but are significantly higher than those reported by [11], suggesting that our sample might contain more trapped melt.

Model-calculations indicate that the obtained REE-pattern is consistent with the derivation of the Y-793605 parent material by small degree (<0.5%) of partial melting of a mantle source with significant LREE-depletion (Sm/Nd < 1.19), which might contain minor (<1%) amount of garnet. The partial melting was followed by fractional crystallization of ~50%.

References: [1] Kojima, H. et al. (1997) Antarctic Meteorite Research 10, 3-12; [2] Mikouchi, T. & Miyamoto, M. (1997) Antarctic Meteorite Research 10, 41-60; [3] Wadhwa, M. et al. (1997) Antarctic Meteorites XXII NIPR, 197-199; [4] Nagao, K. et al. (1997) Antarctic Meteorite Research 10, 125-142; [5] Warren, P. H. & Kallemeyn, G. W. (1997) Antarctic Meteorite Research 10, 61-81; [6] Misawa, K. et al. (1997) Antarctic Meteorite Research 10, 95-108; [7] Nakamura, N. et al. (1989) Anal. Chem. 61, 755-762; [8] Shih C.-Y. et al. (1982) GCA 46, 2323-2344; [9] Chen, J. H. & Wasserburg G. J. (1986) GCA 50, 955-968; [10] Borg, L. E. et al. (1998) LPSC XXIX, 1233-1234; [11] Ebihara, M. et al. (1997) Antarctic Meteorite Research 10, 83-94.

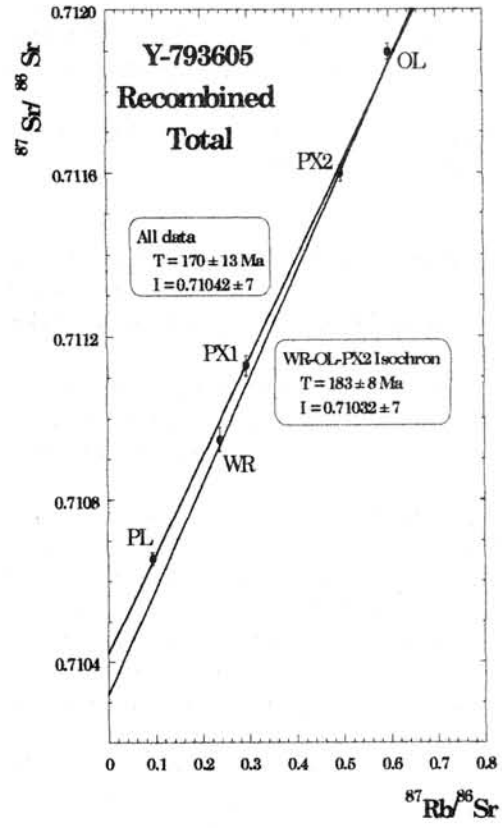

Fig. 1. Rb-Sr isochrons based on recombined total data (residue + leachates) of the mineral phases and WR. The obtained ages are only slightly higher than those obtained exclusively based on the residue phases and are within error limit. The age and initial $^{87}Sr/^{86}Sr$ values show close resemblance to those reported earlier for ALH7705 by [8].

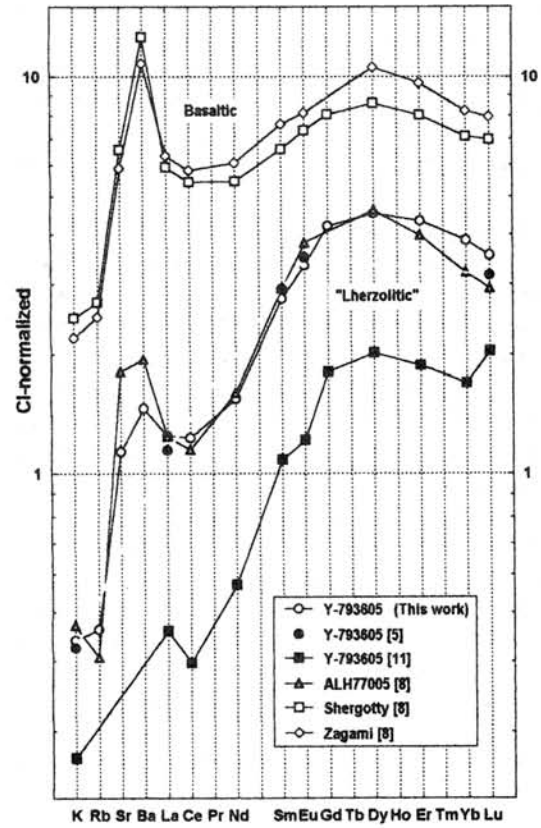

Fig.2. Comparision of CI-normalized LIL-element abundances for various shergottites. The REE-pattern obtained for Y-793605 by our group using DL-IDMS shows close similarity to that of ALH77005 reported by [8] utilizing IDMS. Two earlier results for Y-793605 are also shown. INAA measurement results by [5] plot together with the two IDMS patterns described above, while the ICP-MS data by [11] show systematically lower REE-(and K-) abundances indicating lower trapped melt content in that sample fragment of Y-793605.

FLUORESCENT ORGANIC MATTER IN CARBONACEOUS CHONDRITES

Tatsushi MURAE

Department of Earth and Planetary Sciences, Faculty of Science, Kyushu University,
Hakozaki, Fukuoka 812-8581

The presence of fluorescent carbonaceous matter in carbonaceous chondrites has been noticed more than 35 years ago [1,2]. Briggs detected three types of fluorescent organic compound in the hot-water extract of powdered Mokoia meteorite [1]. Two of them are strongly fluorescent (yellow) in the short ultra-violet. These strongly fluorescent compounds were differentiated each other by paper chromatography. The fluorescence of both these compounds is unaffected by pH. The fluorescent properties of these compounds suggest some conjugated ring system; while the water-solubility of all indicate the presence of polar groupings, such as carboxyl and hydroxyl. The third compound was weakly fluorescent.

Claus and Nagy reported the existence of many particles showing fluorescence (yellow) in ultraviolet light in crumbled grains of Orgueil and Ivuna [2]. The fluorescent particles did not show birefringence in polarized light. The fluorescent particles were absent in noncarbonaceous chondrites, Holbrook and Bruderheim. Acid treatments using hydrofluoric acid and hydrochloric acid did not seriously affect the morphology of these particles [3]. Significant portion of these fluorescent particles showed relatively high density (densities between 2.3 and 2.4). Certain organic solvents appear to affect, but not to dissolve, these particles eliminating the possibility that they are composed of sulfur, hydrocarbons, or of aggregates of low molecular weight organic compounds.

Deamer reported the observation of numerous yellow fluorescent particles in the micrometer size ranging from limit of resolution to ~10 μm as well as larger structures with deep red fluorescence in a Murchison meteorite sample immediately after fracture, and after gentle smoothing by a diamond-coated polishing disk [4]. The yellow fluorescent particles were substantially reduced in number following a brief chloroform rinse, and these presumably represent the *in site* appearance of the organic components of the Murchison chondrite.

I have reported the observation of fluorescent particles using a fluorescence microscope in powdered samples of carbonaceous chondrites, Y-791198, Y-74662, and Murchison [5]. Most of the fluorescent particles showed yellow color in ultra-violet right. I also observed fluorescent particles showing similar yellow color in C3 carbonaceous chondrites samples, ALH-77307, Y-791717, and Allende, after carbon enrichment by acid treatments. The mean size of fluorescent particles was smaller than those in above CM2 carbonaceous chondrites.

The acid treatments contain extraction with organic solvent, precipitation by centrifugation, and dissolution of minerals with hydrofluoric and hydrochloric acids. Therefore, the fluorescent particles observed in these meteorites are hardly soluble in water and organic solvent. The solubility of these fluorescent particles is somewhat different from those reported in Orgueil by Briggs [1] and in Murchison by Deamer [4]. The

fluorescent particles in my case precipitated in water by centrifugation to suggest the grater density than water.

These properties are closely resembled to those reported by Nagy *et al.* [3] for confirmation that the fluorescent particles are microfossils of extraterrestrial algae. However, I do not have any evidence that the fluorescent particles in my case originate from life activity. The whole part of the particles emitted fluorescence without any staining. This fact may suggest that the all part of the particles be constructed with fluorescent molecules such as fused aromatic ring system.

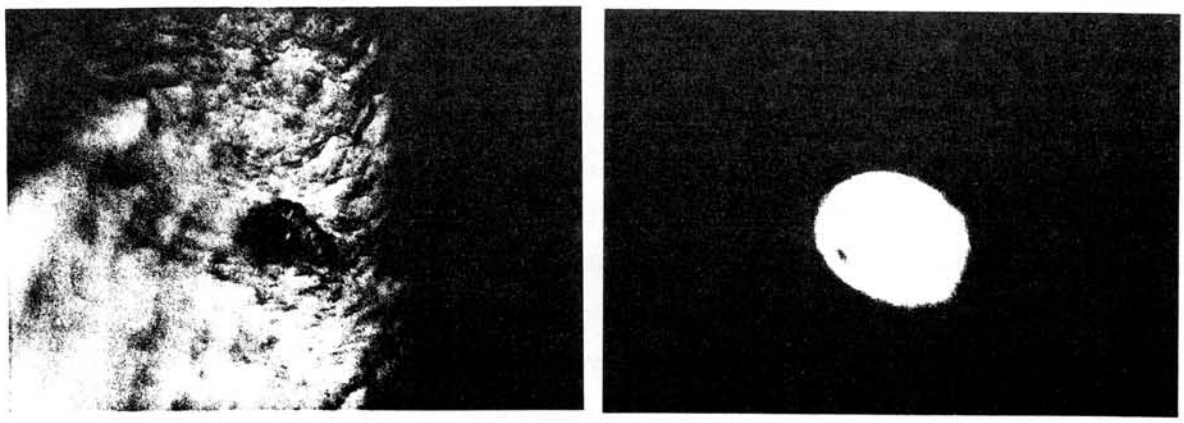

A B

Fig. 1. Photograph of a fluorescent particle observed in residues after acid treatment of Allende.
A: under day light, **B**: under ultra-violet light

References:
[1] M. H. Briggs, *Nature*, **191**, 1137-1140 (1961).
[2] G. Claus and B. Nagy, *Nature*, **192**, 594-596 (1961).
[3] B. Nagy, G. Claus, D. J. Hennesy, *Nature*, **193**, 1129-1133 (1962).
[4] D. W. Deamer, *Nature*, **317**, 792-794 (1985).
[5] T. Murae, *Abstract of symposium on Antarctic meteorites XXII*, 124-125, (1997).

ANTARCTIC MICROMETEORITE DATABASE: CONSTRUCTION OF A WWW BASED DATABASE SYSTEM

Toshio Murakami[1], Tomoki Nakamura[2], Naoya Imae[3], Izumi Nakai[4], Takaaki Noguchi[5], Hajime Yano[6], Kentaro Terada[7], Takaaki Fukuoka[8], Ken-ichi Nogami[9], Hideo Ohashi[10], Wataru Nozaki[2], Mai Hashimoto[2], Nahoko Kondo[4], Hiroyuki Matsuzaki[11], Osamu Ichikawa[3], and Rie Ohmori[9]

[1]Computer Center, Gakushuin Univ., 1-5-1 Mejiro, Toshima, 171-8588, Japan, [2]Earth and planetary Sci., Fac. of Sci., Kyushu Univ., Hakozaki, Fukuoka 812-8581, Japan, [3]Nat. Inst. of Polar Res., 1-9-10 Kaga, Itabashi, Tokyo 173-8515, Japan, [4]Dept. of Applied Chemistry, Fac. of Sci., Sci. Univ. of Tokyo, Kagurazaka, Shinjuku, Tokyo 162-0825, Japan, [5]Dept. of Materials and Biological Science, Ibaraki Univ., Bunkyo 2-1-1, Mito 310, Ibaraki, Japan, [6]Earth Sci. and Solar System Exploration Division, NASA/JSC, SN2, Houston, TX 77058, U.S.A. [7]Dept. of Earth and Planet. System Sci., Fac. of Sci. Hiroshima Univ., 1-3-1 Kagamiyama, Higashi-Hiroshima 739-8526, Japan, [8]Dept. of Environmental Systems, Fac. of Geo-environmental Sci., Rissho Univ., 1700 Magechi, Kumagaya, Saitama 360-0194, Japan, [9]Dep. of Physics, Dokkyo Univ., School of Medicine, Mibu, Tochigi 321-0293, Japan, [10] Dept. of Ocean Sci., Tokyo Univ. of Fisheries, Kounan, Minato, Tokyo 108, Japan, [11]Res. Center for Nuclear Sci. and Tech., Univ. of Tokyo, 2-11-16 Yayoi, Bunkyo, Tokyo 113-0032, Japan.

ANTARCTIC MICROMETEORITE (AMM) DATABASE consists of selected physical and chemical data for individual micrometeorites collected from water tanks in the Antarctic Dome Fuji station [1]. The database is published on the World Wide Web [URL: http://dust.cc.gakushuin.ac.jp/] via the Internet. The selected data set is listing below.

CONTENTS AND SUMMARY SHEET OF
"ANTARCTIC MICROMETEORITE DATABASE"

Name	micrometeorite name
Size	size in μm
Shape	optical characteristic according to [2,3]
Transparency	optical characteristic according to [2,3]
Color	optical characteristic according to [2,3]
Luster	optical characteristic according to [2,3]
Mg/Si	concentration ratio of major elements
S/Fe	concentration ratio of major elements
Analytical Method	EDS / WDS /XRF
Comments	comments
SEM / Optical image	SEM / Optical microscope image
X-ray energy Spectrum	X-ray energy spectrum according to analytical method

Individual AMM entries 18

Recently, information services on the Internet are getting very popular. There are some methods (e.g. Telnet, FTP, WWW) to retrieve some information through the Internet. There are the following restrictions for the services using Telnet. Only the character based data can be offered. An account in the server is needed to use the information service. The operation to use the database is complex because many commands are needed. Therefore, the distribution of the database on this technique has decreased now. FTP is also one of the data publishing methods. The user who wants to use the data must retrieve all the data by FTP. The data distributor should offer the data with an administration software corresponding to various platforms. Moreover, when the data is updated, it is necessary to acquire the data again. The problem with this technique is that obtaining the database is impossible in fact when the data becomes huge. One of the popular techniques is WWW. All users can use the database on any platforms in case of being in the environment for which WWW browser can be used. Because the WWW based database has graphical user interface, the operation is comparatively easy. Moreover, not only character data but also the image data can be distributed at the same time. The WWW based database has increased from the advantage of such a user side recently. The result of our preliminary investigation will be opened to the public in this technique.

The database that is opened to public on WWW needs various user-friendly interfaces, such as an easy-operating search menu, on the server side. The search method to take out the target data becomes important for a large amount of the data. The AMM DATABASE is prepared some search categories such as a name, an optical characteristic, the analysis method, and the chemical composition.

When information is distributed through WWW, it is usually necessary to describe information with HTML. Only static information can be described in this HTML. Dynamic information, such as a real-time accessible database, will distribute another method. The interface with the external program called "Common Gate Interface (CGI)" is prepared in the WWW server for above-mentioned function. The Microsoft Internet Information Server 3.0(IIS3) which operated on Microsoft Windows NT Server 4.0 is used for the WWW server program in this work. The IIS3 provides database connectivity to any ODBC-compliant database and a comparatively high-speed database search engine. The Microsoft Access, one of ODBC-compliant database, is also used as database management software in this work. The IIS3 provides database connectivity by two functions, one is Active Server Pages and the other is Internet Database Connector (IDC). The former provides a Web programming environment with database connectivity. The latter enables the arbitrary data to be taken out of the

database by describing the SQL. Fig.1 shows a part of this database access interface described with SQL.

A search result by above-mentioned IDC is provided in the form of the table (Fig.2). Information on individual AMM is provided by the Adobe PDF file (Fig.3). AMM DATABASE only provides information on the sample. The environment to request for distribution of AMMs that the researcher needs for scientific study through WWW is scheduled to be established in the future.

Reference: [1] Nakamura T. et al., in this volume, (1998). [2] CDPET, Cosmic Dust Catalog, NASA/JSC, **1-14**, (1981-1994). [3] Planetary Materials Curation (Stratospheric Dust), http://www-curator.jsc.nasa.gov/curator/dust/dust.htm.

```
Datasource: dust
Template: sresult.htx
SQLStatement:
+SELECT * FROM "Dust Catalog"
+          WHERE (NOT (%sh% = 'ALL' AND %trans% = 'ALL' AND %color% = 'ALL' AND %luster% = 'ALL' AND %equip% = 'ALL')
+                                    AND (
+                                    SHAPE LIKE %sh% AND TRANSPARENCY LIKE %trans% AND COLOR LIKE %color%
+                                    AND LUSTER LIKE %luster% AND EQUIPMENT LIKE %equip%
+                                    )
+                         )
+                         OR
+                                    (%sh% = 'ALL' AND %trans% = 'ALL' AND %color% = 'ALL' AND %luster% = 'ALL' AND %equip% = 'ALL')
+                         OR
+                         ((%sh% = 'ALL')
+                                    AND (
+                                    TRANSPARENCY LIKE %trans% AND COLOR LIKE %color%
+                                    AND LUSTER LIKE %luster% AND EQUIPMENT LIKE %equip%
+                                    )
+                         )
+                         OR
+                         ((%trans% = 'ALL')
+                                    AND (
+                                    SHAPE LIKE %sh% AND COLOR LIKE %color%
+                                    AND LUSTER LIKE %luster% AND EQUIPMENT LIKE %equip%
+                                    )
+                         )
```

Fig.1. A part of search program described with SQL

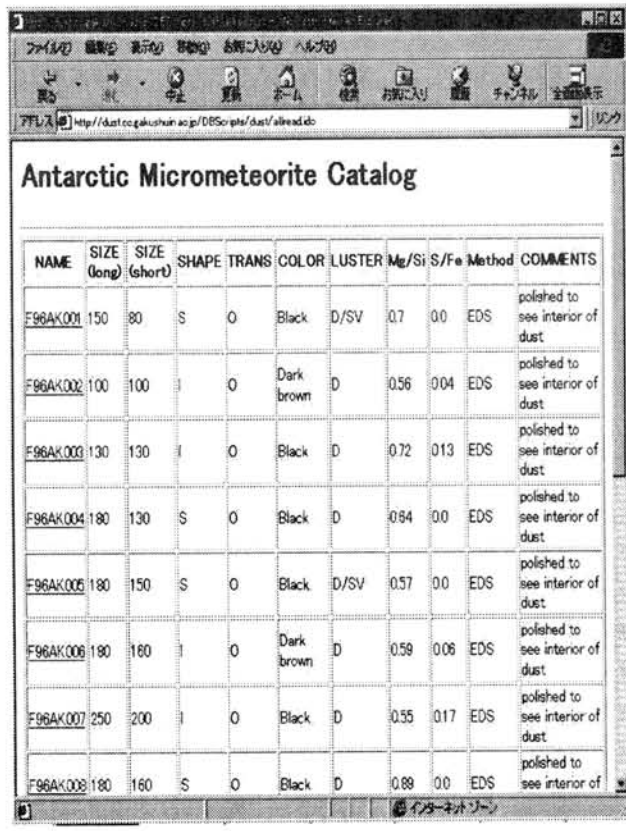

Antarctic Micrometeorite Catalog

NAME	SIZE (long)	SIZE (short)	SHAPE	TRANS	COLOR	LUSTER	Mg/Si	S/Fe	Method	COMMENTS
F96AK001	150	80	S	O	Black	D/SV	0.7	0.0	EDS	polished to see interior of dust
F96AK002	100	100	I	O	Dark brown	D	0.56	0.04	EDS	polished to see interior of dust
F96AK003	130	130	I	O	Black	D	0.72	0.13	EDS	polished to see interior of dust
F96AK004	180	130	S	O	Black	D	0.64	0.0	EDS	polished to see interior of dust
F96AK005	180	150	S	O	Black	D/SV	0.57	0.0	EDS	polished to see interior of dust
F96AK006	180	160	I	O	Dark brown	D	0.59	0.06	EDS	polished to see interior of dust
F96AK007	250	200	I	O	Black	D	0.55	0.17	EDS	polished to see interior of dust
F96AK008	180	160	S	O	Black	D	0.89	0.0	EDS	polished to see interior of

Fig.2. Search result of AMM DATABASE

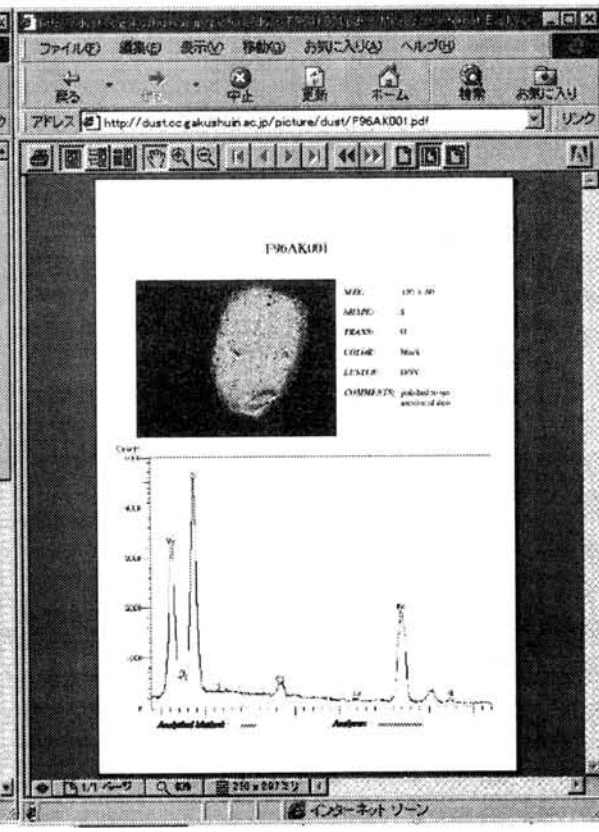

Fig.3. Example of a PDF file

CHEMICAL AND ISOTOPIC FRACTIONATION DURING EVAPORATION OF A MULTI-COMPONENT SYSTEM : (1) EXPERIMENTS IN THE OLIVINE SYSTEM. H. Nagahara[1] and K. Ozawa[2]: (1) Geol. Inst., Univ. Tokyo, hiroko@geol.s.u-tokyo.ac.jp, (2) Inst. Study Earth's Interior, Okayama Univ., ozawa@misasa.okayama-u.ac.jp

Introduction: Evaporation is one of the major processes that caused chemical fractionation in the solar system, which may be responsible for planetary and meteoritical compositions. Evaporation is a time-dependent kinetic process, and requires an experimental study to obtain the reaction rate and understanding of the dependence of kinetic factors on the physical and chemical conditions of the system. Previous work [1-3] has stressed that degree of chemical and isotopic fractionation is limited by evaporation rate (J), fractionation factor (K), and diffusion rate (D) of the species in the condensed phase. Furthermore, the three kinetics should have anisotropy when the condensed phase is a crystalline material [4]. In order to understand the role of those kinetics on chemical fractionation from a multi-component system, evaporation experiments in the olivine system was conducted as a first step. The olivine system was chosen because Si, Mg, and Fe are the most abundant cations among all the elements in the solar system, and their fractionation behavior at high temperature should be most liable for planetary fractionation. Phase relations at low pressures of the olivine system has been studied by [5], which stressed stoichiometric nature of evaporation and the large Mg/Fe distribution between coexisting solid and gas.

Experiments: Single crystals of olivine from San Carlos (Fo 91.8, FeO 8.2 wt%, NiO 0.37 wt%, CaO 0.065 wt%) were cut into crystallographically oriented parallelepipeds. Crystallographically oriented to (100) , (010), or (001) and flattened samples were prepared with weight of 30 to 40 mg. No chemical or physical treatment was operated for the surface. Experiments were conducted in a vacuum furnace at the Geological Institute of the University of Tokyo. The experimental temperature was 1400 ℃, 1450 ℃, and 1500 ℃. Experiments were conducted under continuous evacuation, and the pressure measured with an ionic gauge at a port of the vacuum chamber was about 10^{-4} Pa. Experimental duration ranged from 6 to about 210 hours. After experiments, the weight loss was measured, and surface of the samples were observed with an SEM. Chemical composition of the surface was measured with an EPMA. Then, they were cut perpendicular to the flattened surface, and compositional profile of the interior was measured along the crystallographic axes.

Experimental results: The residue is stoichiometric but more magnesian than the initial composition, suggesting stoichiometric and incongruent evaporation of olivine at a kinetic condition as well as an equilibrium condition. The average evaporation rate estimated from the weight loss decreases with time. Fig. 1 shows an example of the average evaporation rate along the c-axis at 1400 ℃, which decreases from 0.33 mm/hour in 10 hours to 0.15 mm/hour at 100 hours. Each crystallographic surface develops characteristic microstructures, which differ from those observed in synthetic forsterite [4], probably due to difference in type and density of dislocation. Surface composition changes with time and temperature, becoming enriched in MgO and CaO and depleted in FeO and NiO (Fig. 1). The surface composition changes with time depending on the crystallographic orientation (Fig. 2). The FeO and NiO contents decrease and the MgO and CaO content increase, and the degree of FeO- and NiO-depletion and MgO- and CaO-enrichment are largest in the (001) surface and smallest in (100). The results show that the olivine looses FeO quickly by evaporation. Interior of a grain is strongly zoned, and the pattern is shallowest along the c-axis and steepest along the a-axis.

Discussion: Nagahara and Ozawa [2] showed that the development of isotopic fractionation from a congruently evaporating material is controlled by the evaporation rate, grain size, and diffusion rate, with the dimensionless parameter, $\beta(=Jr/D)$. In the case of the present study, fractionation factor between solid and gas (K) should be one of another important factors that governs the reaction. We have developed equations that describe the process by three parameters, J, D, and K [6]. J and D are composition dependent, which in turn means that they are time dependent. By using the equations, the experimental results were fitted. The parameters obtained are summarized in Table 1. The change of composition of an olivine grain with an intermediate composition was investigated with an assumption of a sphere with parameters estimated by the experiments.

References: [1] Wang, J. *et al.* (19941) *LPSC* **XXII**, 1461-1462, [2] Nagahara, H. and Ozawa, K. (1997) *LPSC* **XXVIII**, 997-998, [3] Tsuchiyama, A. *et al.* (1995) *LPSC* **XXVI**, 1423-1424, [4] Nagahara, H. and Ozawa, K. (1996) *LPSC* **XXVII**, 989-990, [5] Nagahara, H. et al. (1994) *GCA* **58**, 1951-1963, [6] Ozawa, K. and Nagahara, H. (1998) *This volume.*

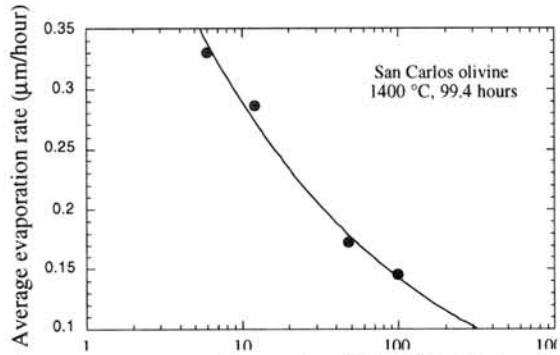

Fig. 1 Average evaporation rate of Fo 92 olivine in vacuum.

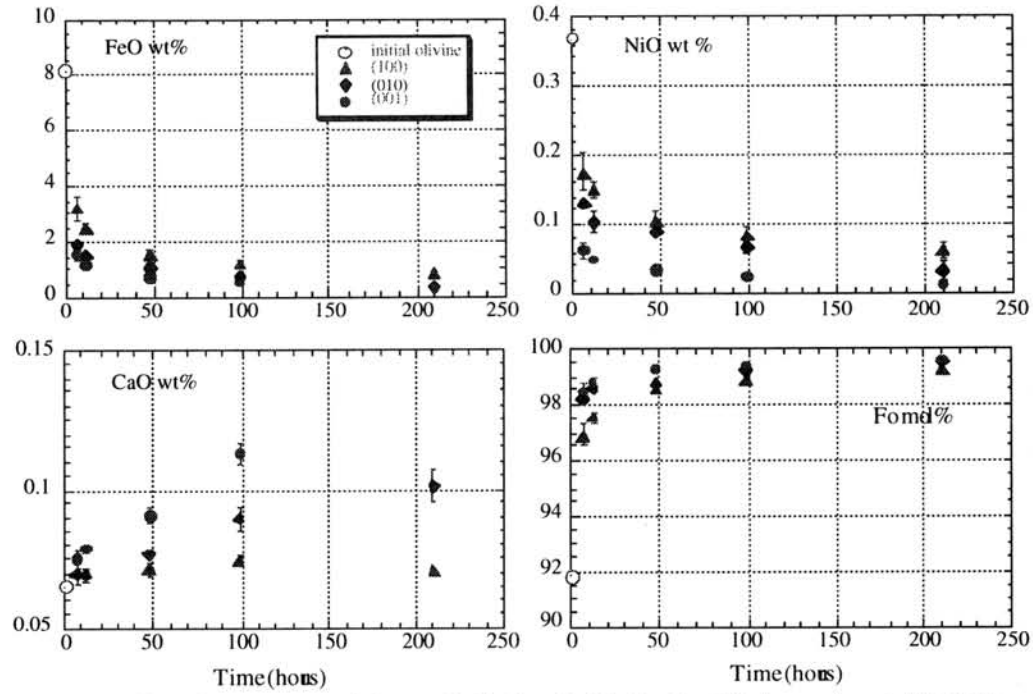

Fig. 2 Change of surface compositions of olivine (initially Fo 92) heated at 1400 ℃ in vacuum.

Table 1 Optimized parameters for evaporation of Fo91.8 olivine.

axis		a	b	c
K		0.035	0.028	0.019
J(Fo=0.918)	(mm/hour)	1.4×10^{-4}	4.7×10^{-4}	8.2×10^{-4}
D(Fo=0.918)	(cm^2/sec)	1.5×10^{-11}	3.1×10^{-11}	8.0×10^{-11}

Errata

Program No. 31

Authors: Nagao, Okazaki, Sawada and Nakamura
Title: Noble gas study on the five Yamato Rumuruti-group chondrites.

1) Meteorite name:

Yamato-881988 → Asuka-881988

2) Title:

Noble gas study on the four Yamato and one Asuka Rumuruti-group chondrites.

Noble Gas Study of the Five Yamato Rumuruti-group Chondrites

Keisuke NAGAO[1], Ryuji OKAZAKI[2], Shinobu SAWADA[3] and Noboru NAKAMURA[3]

1) Laboratory of Earthquake Chemistry, Graduate School of Science, University of Tokyo, Hongo, Tokyo 113-0033, Japan
2) Department of Earth and Planetary Sciences, Faculty of Science, Kyushu University, 33, Hakozaki, Fukuoka 812-81, Japan
3) Graduate School of Science and Technology, Kobe University, Nada-ku, Kobe 657, Japan

Rumuruti-like chondrite group (R-chondrites) comprises about 10 individual specimens [1]. Only a few noble gas data for the R-chondrites are available. According to the reported data, Acfer217 and Carlisle Lakes showed cosmic-ray exposure ages of about 35 and 7 Ma, and K-Ar ages of 3.9 and 3.4 Ga, respectively [2]. Acfer217, ALH85151, PCA91002/241 and Rumuruti contain solar noble gases, whereas Carlisle Lakes does not [2, 3]. Four R-chondrites Acfer217, ALH85151, and paired meteorites PCA91002/241 show similar cosmic-ray exposure ages of 39±3 Ma, and the ages of Rumuruti and Carlisle Lakes are 18 and 7 Ma, respectively [3]. ALH85151 with most abundant solar gases indicates trapped Ne isotopic ratio of $^{20}Ne/^{22}Ne=13.0\pm0.2$ [3]. R-chondrotes are also characterized by a relatively high $^{129}Xe/^{132}Xe$ ratios (~2) compared with those of ordinary chondrites [2].

We investigated noble gas isotopic compositions of five R-chondrites, Y-75302, Y-791827, Y-793575, Y-82002, and Y-881988, for which noble gas data have not reported yet. K concentrations for the aliquot samples have also been determined mass spectrometrically to calculate K-Ar ages for these meteorites. Here we present noble gas abundances, cosmic-ray exposure ages, and K-Ar ages for these specimens and discuss relationship with other known R-chondrites (see Tables 1 and 2).

Solar-type He and Ne are dominant in three meteorites Y-75302, Y-791827 and Y-82002. Trapped $^{20}Ne/^{22}Ne$ ratio estimated by extrapolation of a line connecting the data points for these samples is about 11.5, which is lower than the ratio of 13.0±0.2 determined for ALH85151 [3]. Solar gas component with higher energy such as SEP might have been implanted in our samples. The concentration of solar Ne are 120, 129 and 61 $x10^{-8}cm^3STP/g$ for Y-75302, Y-791827 and Y-82002, respectively, much lower than the highest value of 5500 $x10^{-8}cm^3STP/g$ observed for ALH85151 [3]. Ne isotopic ratios for Y-793575 and Y-881988 do not show a signature of solar Ne. High values of cosmogenic $^{22}Ne/^{21}Ne$ ratios, 1.22-1.23, suggest small preatmospheric masses for the two meteorites.

Cosmic-ray exposure ages calculated for Y-793575 and Y-881988 by cosmogenic Ne

are 9.0 and 24.5 Ma, respectively, where production rates were calculated by the formula presented in [4]. Exposure ages of 22, 25 and 18 Ma for Y-75302, Y-791827 and Y-82002, respectively, were calculated assuming the same production rate of cosmogenic ^{21}Ne by [3].

K concentrations, 695-912 ppm, measured for the 5 Yamato R-chondrites are in the range for ordinary chondrites [5]. K-Ar ages presented in Table 2 were calculated assuming 10% uncertainty for ^{40}Ar concentrations. Almost constant age of 4.2 Ga was obtained. Only one exception is Y-82002, for which slightly young age of 3.9 Ga was calculated. K-Ar ages for R-chondrites reported so far are 3.9 and 3.4 Ga for Acfer217 and Carlisle Lakes, respectively [2].

Kallemeyn et al. [1] discussed paring of three Yamato R-chondrites Y-75302, Y-82002 and Y-793575, and excluded paring for them with some ambiguity between the two, Y-75302 and Y-82002. Our noble gas data support the conclusion by them, i.e., Y-793575 does not contain solar noble gases but the gases are abundant in Y-75302 and Y-82002, and also in Y-791827. Based on our noble gas data and K-Ar ages, Y-75302 and Y-791827 probably be paired. It is still ambiguous to exclude Y-82002 from the Y-75302 and Y-79187 pairing, though slight differences in noble gas compositions and K-Ar ages are noticeable. Both Y-793575 and Y-881988 do not contain solar gases and have similar K-Ar ages, cosmogenic ^{22}Ne/^{21}Ne ratios, and have high ^{40}Ar/^{36}Ar and ^{129}Xe/^{132}Xe ratios. However, the two meteorites can not be paired because of their different cosmic-ray exposure ages, 9 and 25 Ma, respectively.

References: [1] Kallemeyn et al., G.C.A. **60** (1996) 2243-2256; [2] Bischoff et al., Meteoritics **29** (1994) 264-274; [3] Weber and Schultz, Meteoritics **30** (1995) 596 (Abstr.); [4] Eugster, G.C.A. **52** (1988) 1649-1662; [5] Kallemeyn et al., G.C.A. **53** (1989) 2747-2767.

Table 1. Trapped noble gas concentrations and characteristic isotopic ratios.

Meteorite	^{4}He	^{20}Ne	^{36}Ar	^{84}Kr	^{132}Xe	^{40}Ar/^{36}Ar	^{129}Xe/^{132}Xe	Ref.
	[10^{-8}cm^{3}STP/g]							
Y-75302	52000	119	8.78	0.026	0.027	640	2.06	
Y-791827	39900	119	7.82	0.022	0.022	559	2.24	
Y-793575	—	—	1.23	0.017	0.019	3810	3.74	
Y-82002	34000	60.5	5.28	0.023	0.022	867	1.96	
Y-881988	—	—	2.58	0.050	0.030	2300	1.99	
Acfer217	12100	23	4.36	0.030	0.067	1260	1.27	[2]
Carlisle Lakes	1072	—	2.30	0.030	0.027	1730	2.18	[2]

Table 2. Cosmic-ray exposure ages, K concentrations and K-Ar ages.

Meteorites	^{3}He [$10^{-8}cm^{3}STP/g$]	^{21}Ne [$10^{-8}cm^{3}STP/g$]	^{38}Ar [$10^{-8}cm^{3}STP/g$]	$(^{22}Ne/^{21}Ne)_c$	P_{21} [$10^{-8}cm^{3}STP/g/Ma$]	T_{21} [Ma]	K [ppm]	K-Ar age [Ga]	Ref.
Y-75302	19.6	6.30	0.966	—	0.281[1]	22.4	878	4.18±0.16	
Y-791827	15.7	6.98	0.955	—	0.281[1]	24.8	695	4.15±0.16	
Y-793575	10.3	1.65	0.230	1.236	0.184	9.0	738	4.17±0.16	
Y-82002	43.6	5.12	0.851	—	0.281[1]	18.2	869	3.87±0.16	
Y-881988	27.2	4.67	0.566	1.223	0.191	24.5	912	4.21±0.16	
Acfer217	(51.0)	9.44	1.51		0.276	34.2		3.9	[2]
Carlisle Lakes	(8.6)	2.44	0.32	1.08	0.317	7.7		3.4	[2]
Acfer217					0.281				[3]
ALH85151					0.281	39±3			[3]
PCA91002					0.281				[3]
PCA91241					0.281				[3]
Rumuruti						18			[3]
Carlisle Lakes						7			[3]

[1] assume same production rate by Weber and Schultz(1995).

ANTARCTIC MICROMETEORITES COLLECTED AT THE DOME FUJI STATION: INITIAL EXAMINATION AND CURATION

Tomoki Nakamura[1], Naoya Imae[2], Izumi Nakai[3], Takaaki Noguchi[4], Hajime Yano[5], Kentaro Terada[6], Toshio Murakami[7], Takaaki Fukuoka[8], Ken-ichi Nogami[9], Hideo Ohashi[10], Wataru Nozaki[1], Mai Hashimoto[1], Nahoko Kondo[3], Hiroyuki Matsuzaki[11], Osamu Ichikawa[2], and Rie Ohmori[9]

[1]Earth and planetary Sci., Fac. of Sci., Kyushu Univ., Hakozaki, Fukuoka 812-8581, Japan, [2]Nat. Inst. of Polar Res., 1-9-10 Kaga, Itabashi, Tokyo 173-8515, Japan, [3]Dept. of Applied Chemistry, Fac. of Sci., Sci. Univ. of Tokyo, Kagurazaka, Shinjuku, Tokyo 162-0825, Japan, [4]Dept. of Materials and Biological Science, Ibaraki Univ., Bunkyo 2-1-1, Mito 310, Ibaraki, Japan, [5]Earth Sci. and Solar System Exploration Division, NASA/JSC, SN2, Houston, TX 77058, U.S.A. [6]Dept. of Earth and Planet. System Sci., Fac. of Sci. Hiroshima Univ., 1-3-1 Kagamiyama, Higashi-Hiroshima 739-8526, Japan, [7]Computer Center, Gakushuin Univ., 1-5-1 Mejiro, Toshima, 171-8588, Japan, [8]Dept. of Environmental Systems, Fac. of Geo-environmental Sci., Rissho Univ., 1700 Magechi, Kumagaya, Saitama 360-0194, Japan, [9]Dep. of Physics, Dokkyo Univ., School of Medicine, Mibu, Tochigi 321-0293, Japan, [10] Dept. of Ocean Sci., Tokyo Univ. of Fisheries, Kounan, Minato, Tokyo 108, Japan, [11]Res. Center for Nuclear Sci. and Tech., Univ. of Tokyo, 2-11-16 Yayoi, Bunkyo, Tokyo 113-0032, Japan.

Micrometeorites (MMs) were found in the precipitated fine particles recovered from water tanks in the Antarctic Dome Fuji station. These MMs had been contained in the snow around the station. They are preliminary examined by different means for characterization of their micro-morphology and major-element concentration. A digital catalog on the internet for these MMs was planed to be established on the web site < *http://dust.cc.gakushuin.ac.jp/* >. Researchers who need the MMs for a scientific study will be able to request them via internet. MMs found in this study are the first Japanese extraterrestrial dust collection that will be distributed all over the world from NIPR like Antarctic meteorites. A series of works have been done to develop the methods and techniques applicable for the initial analysis and curation of MMs that are being collected by the 39th Japanese Antarctic Research Expedition (JARE) team.

The Antarctic Dome Fiji station is located at 77°19' degrees south latitude and 39°42' degrees east longitude. 400 liters of water that are used for the daily life of the residents are prepared every day from accumulated snow around the station. The snow is collected under the ground in the depth from 2.5 to 5.0 meters. These layers of snow is estimated to have fallen during 1950's and 1970's based on the rates of snow accumulation. The 37th JARE team collected precipitated material in the water tanks several times in 1996 and brought it back to National Institute of Polar Research (NIPR), Japan. The precipitated material is residues of melting of approximately 100 tons of snow. The material was kept frozen in the deep-freezer room in NIPR till the initial investigation. The Antarctic micrometeorite working group was organized and started the examination after NIPR has entrusted us with the precipitated material.

Optical microscope observations of the precipitated material showed that it consists largely of natural and synthetic terrestrial particles such as fragments of wood, iron, paints, volcanic ashes, and various kinds of minerals. Prior to selection of MMs we separated the precipitated material into 9 fractions by grain size, magnetic property, and sedimentation rates in pure water to make a MM-enriched fraction. The fraction enriched in MMs was a magnetic fraction in the range of grain size less than 300 μm and has rapid sedimentation rates.

Approximately 1 g of the fraction was investigated for ^{26}Al-induced γ-ray with a counting time one month at Tanashi low-background laboratory in Institute for Cosmic Ray Research, Univ. of Tokyo. No detectable ^{26}Al γ-ray at 1809 KeV was observed, suggesting low concentration of extraterrestrial material in the magnetic fraction. The main population of the fraction is irregularly or spherical shaped iron and iron-oxide, both of which contain a trace amount of Si and no Ni. Presence of Si and absence of ^{26}Al suggest that most iron spherules are not extraterrestrial and they were probably originated from evaporates of weldment of iron material.

In the next process we have done a direct hand-picking of MMs from the magnetic fraction under high-magnification binoscopes. We selected candidates of mainly two types of MMs: (1) irregularly shaped black particles that are candidates for unmelted to partially melted MMs and (2) gray to black spherules showing lineation on the surfaces so called stony-type (S-type) cosmic spherules. Optical characteristics of these candidates were determined using transmitted and reflected light of binoscopes based on a classification scheme of cosmic dust catalog published by NASA JSC [1]. Then the dust samples were investigated for major element composition and detailed morphology by various methods in 7 different sites in Japan: a low-vacuum scanning electron microscope with an energy dispersive spectrometer (LV-SEM/EDS) at Kyuhsu University, a LV-SEM/EDS at Tokyo Institute of Technology, a field-emission (FE-) SEM/EDS at Dokkyo University, a FE-SEM/EDS at Tokyo University for Fisheries, an original X-ray fluorescence spectrometer at Science University of Tokyo, an electron probe microanalyser with wave-length dispersive spectrometer at NIPR, and a desk-top X-ray Analytical Microscope at Hiroshima University. Along with the analyses of dust samples we measured several fine-grained matrix material of Allende CV3 and Murchison CM2 meteorites in order to calibrate X-ray energy spectra obtained by different analytical methods and to know the spectra of "solar system abundance". These elemental analyses revealed that approximately 10 % of the candidates were MMs, which was confirmed by similarities in elemental abundances of the MMs to those of carbonaceous chondrites. Abundance of MMs in the magnetic fraction is estimated to be less than 1 ‰. Table 1 shows a part of MM collection processed in Kyushu University.

A digital catalog of the MMs showing optical characteristics, images and X-ray energy spectra of individual MMs will be opened to the public on the web site stated above and detailed information of the catalog is reported in [2]. We continue to search MMs from the dust samples that we have and those being recovered by the 38th and 39th JARE teams. Based on the snow accumulation rates MMs found in this study are supposed to have fallen to Antarctica recently, thus they might provide us valuable information on the interplanetary space these days. Compared with blue ice on the Antarctic ice sheet where Euromet cosmic dust collection was recovered [3 and 4], snow layers around the Fuji station are apparently lower abundance of MMs. The abundance in the snow layers would represent an actual abundance of MMs in recent falling snow and the higher concentration in the blue ice would indicate some mechanism which enriches cosmic dust in the surface layers of the blue ice fields.

Acknowledgment: We greatly appreciate Dr. H. Yurimoto and his colleagues at the Tokyo Institute of Technology have kindly allowed us to use their LV-SEM/EDS.

Reference: [1] CDPET, Cosmic Dust Catalog, NASA/JSC, **1-14**, (1981-1994). [2] Murakami T. et al., in this volume, (1998) [3] Maurette M. et al., *Nature*, **351**, 44-46, (1991). [4] Maurette M. et al., *LPSC* **XXIII**, 85-86, (1992).

Table 1. Antarctic micrometeorites collected at the Dome Fuji station

ID	size (μm x μm)	shape	transparency	color	luster	type
F96AK001*	150 x 80	S (spherical)	O (Opaque)	Black	D (Dull)/SV (Subvitreous)	S-type spherule
F96AK002	100 x 100	I (Irregular)	O	Dark brown	D	Unmelted to partially melted micrometeorite
F96AK003	130 x 130	I	O	Black	D	Unmelted to partially melted micrometeorite
F96AK004	180 x 130	S	O	Black	D	S-type spherule
F96AK005	180 x 150	S	O	Black	D/SV	S-type spherule
F96AK006	180 x 160	I	O	Dark brown	D	Unmelted to partially melted micrometeorite
F96AK007	250 x 200	I	O	Black	D	Unmelted to partially melted micrometeorite
F96AK008	180 x 160	S	O	Black	D	S-type spherule
F96AK009	200 x 140	I	O	Dark brown	D	Unmelted to partially melted micrometeorite
F96AK010	120 x 120	S	O	Black	D	S-type spherule
F96AK011	250 x 200	S	O	Black	D/SV	S-type spherule
F96AK012	200 x 200	S	O	Black	D	S-type spherule
F96AK013	200 x 200	S	O	Dark green	SV	S-type spherule
F96AK014	210 x 150	I	O	Dark brown	D	Unmelted to partially melted micrometeorite
F96AK015	170 x 130	I	O	Gray to brown	D	Unmelted to partially melted micrometeorite
F96AK016	200 x 120	I	O	Dark brown	SV	Unmelted to partially melted micrometeorite
F96AK017	270 x 200	I	O	Dark brown	SV	Unmelted to partially melted micrometeorite
F96BK001#	90 x 60	I	O	Black	D	Unmelted to partially melted micrometeorite

*ID numbers of micrometeorites express collection sites and years, identities of precipitated material, and facilities performed the initial examination; F96AK001 means the MM was collected at Dome Fuji (F) in 1996 (96), contained in a magnetic fraction in 960423-1 precipitated material (A), and processed in Kyushu University (K).

#Abbreviation B means that the MM was found in a non-magnetic fraction of 960423-1 precipitated material.

X-RAY STUDIES OF IRON AND CARBON MINERALS IN THE KENNA UREILITE

Y. Nakamuta[1], T. Aoyagi [2] and Y. Aoki[1]

[1] Dept. Earth and Planetary Sciences, Faculty of Science, Kyushu University, Fukuoka 812-8581, Japan. [2]Kyushu Environmental Evaluation Association, Higashi-ku Syoukoudai 1-10-1, Fukuoka 813-0000, Japan.

The Kenna ureilite studied here is composed of xenoblastic olivine (~Fo_{78}), commonly rimmed by forsterite (~Fo_{90}), and pigeonite ($En_{71}Wo_{10}Fs_{19}$) set in a matrix of iron and carbon minerals. The matrix is interstitial between xenoblastic crystals with the width from 0.1-0.5 mm. Carbon minerals occur in general in the central part of the matrix with iron minerals at the margin of the matrix. Until now, iron and carbon minerals in a matrix were investigated by EPMA with polished thin sections and by an x-ray method with powdered samples separated from the matrix. Nickel-iron metal, troilite, and three carbon polymorphs (graphite, lonsdaleite, and diamond) have been reported for the Kenna ureilite (Berkley et al., 1976). In this study, x-ray powder patterns of iron and carbon minerals in the matrix of the Kenna ureilite were obtained with a small grain of minerals of about 50 μm by a Gandolfi camera after the analysis of chemical compositions by EPMA.

Fig. 1 shows the EDS spectra of carbon-rich (Fig. 1a) and iron-rich (Fig. 1b) parts of the matrix. The carbon-rich part of the matrix is mainly composed of carbon with minor amounts of silicon and iron (Fig. 1a) and the iron-rich part is mainly composed of iron with small amounts of carbon, oxygen and nickel (Fig. 1b). Fig. 2 shows the x-ray powder diffraction patterns of carbon-rich (Fig. 2a) and iron-rich (Fig. 2b) parts of the matrix. The carbon-rich part is composed of diamond and graphite, the amounts of which are nearly equal (Fig. 2a). Lonsdaleite as suggested by Berkley et al. (1976) cannot be found in the x-ray pattern of this study. The iron-rich part is composed of magnetite and goethite with small amounts of olivine (Fig. 2b). Goethite in the iron-rich part may have formed from magnetite by terrestrial weathering.

Iron minerals in the matrix of the Kenna ureilite have been thought to be iron-nickel metal and troilite (Berkley et al., 1976) and magnetite has not been reported in any ureilite. This may be partly due to the close resemblance between the x-ray patterns of chromite, being identified during x-ray investigations of ureilite (Vdovykin, 1970), and magnetite. In Fig. 1b, chromium is not detected in the iron-rich part of the matrix, then the x-ray peaks assigned

to magnetite in Fig. 2b can be unambiguously identified to those of magnetite.

Petrogenesis and origin of ureilites are controversial as reviewed by Goodrich (1992). In considering ureilite petrogenesis, the important role of fO_2 has been pointed out repeatedly (Goodrich, 1992). The iron-poor forsterite rim of olivine in the Kenna ureilite reveals that the Kenna ureilite has experienced a reducing condition after the crystallization of olivine. In the reducing condition, iron metal was stable in the matrix. The presence of magnetite in the matrix found by this study reveals that the iron metal in the matrix has been oxidized after the reduction of FeO to Fe in olivine-rim. This oxidizing condition following to the reduction of FeO to Fe in olivine-rim may suggest that the ureilite parent body had a high-fO_2 like as carbonaceous chondrites as suggested by Goodrich et al. (1987) and the oxidizing condition was attained due to the decrease of temperature, or that oxygen was injected into the Kenna ureilite from carbonaceous chondrite like impactor when the ureilite parent body was impacted.

References

J. L. Berkley, H. G. Brown IV, K. Keil, N. L. Carter, J-C. C. Mercier and G. Huss (1976) GCA **40**, 1429-1437. C. A. Goodrich, J. H. Jones and J. L. Berkley (1987) GCA **51**, 2255-2273. C. A. Goodrich (1992) Meteoritics **27**, 327-352. G. P. Vdovykin (1970) Space Sci. Rev. **10**, 483-510.

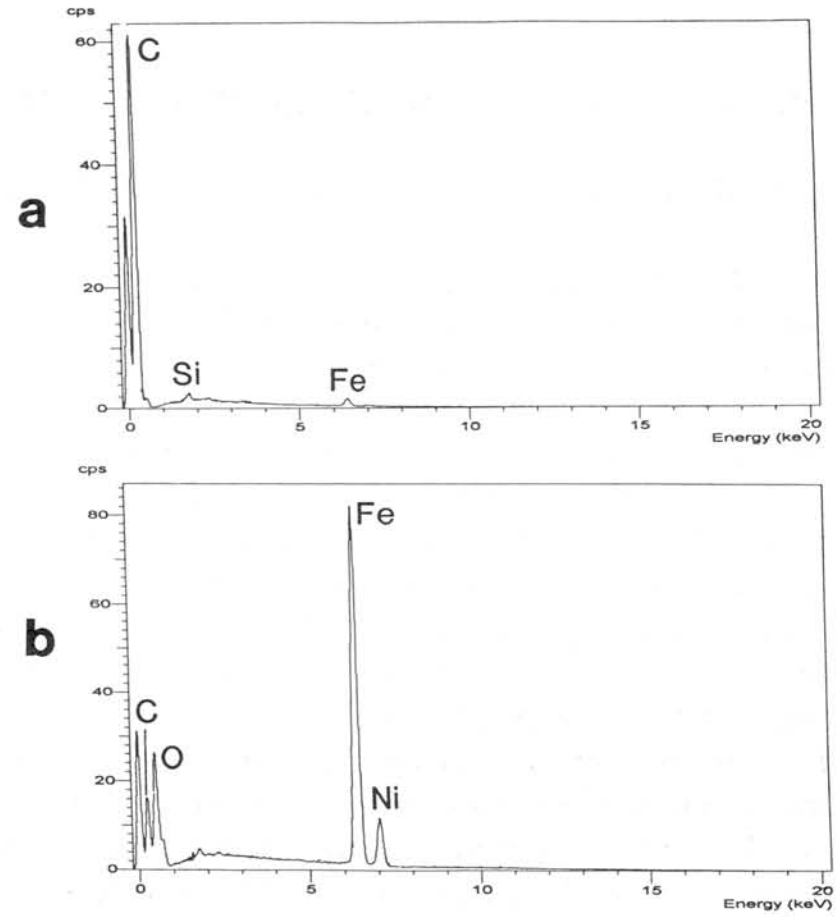

Fig. 1. EDS spectra of carbon-rich (a) and iron-rich (b) parts of the matrix.

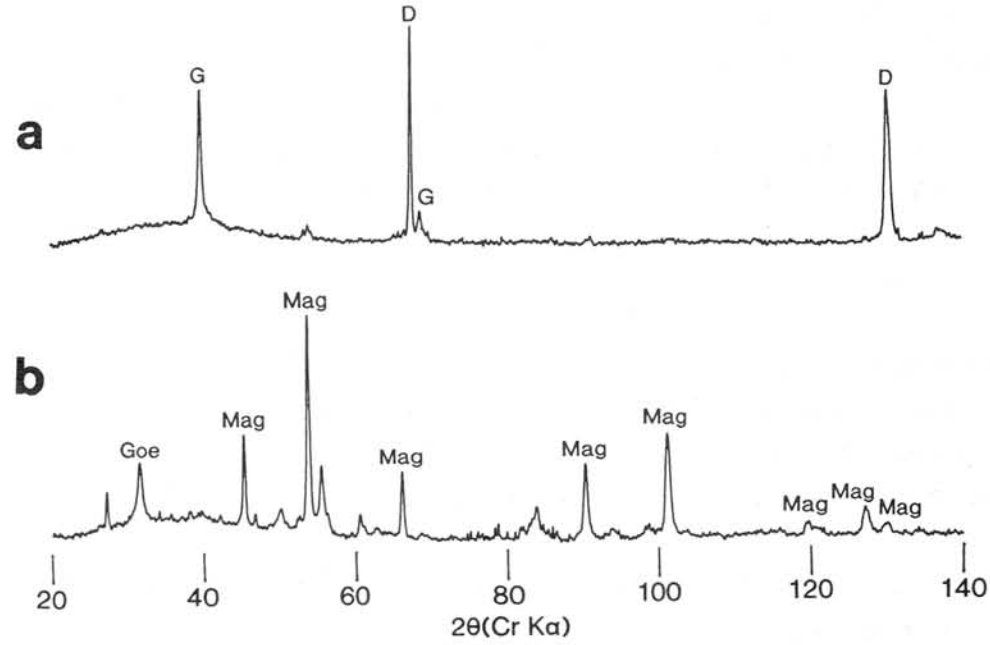

Fig. 2. X-ray diffraction patterns of carbon-rich (a) and iron-rich (b) parts of the matrix.
G: graphite, D: diamond, Goe: goethite, Mag: magnetite.

THERMOLUMINESCENCE OF JAPANESE ANTARCTIC METEORITES II

K. Ninagawa[1], H. Miyazaki[1], K.Soyama[1], N. Imae[2], Kojima[2], P.H. Benoit[3] and D.W.G. Sears[3]

[1] Department of Applied Physics, Okayama University of Science, 1-1, Ridai-cho, Okayama 700, Japan
[2] National Institute of Polar Research, 9-10, Kaga 1-chome, Itabashi-ku, Tokyo 173, Japan
[3] Department of Chemistry and Biochemistry, University of Arkansas, Fayetteville, AR 72701, USA

Natural TL (thermoluminescence), the luminescence of a sample that has received no irradiation in the laboratory, reflects the thermal history of the meteorite in space and on Earth. Natural TL data thus provide insights into such topics as the orbits of meteoroids, the effects of shock heating, and the terrestrial history of meteorites. Induced TL, the response of a luminescent phosphor to a laboratory dose of radiation, reflects the mineralogy and structure of the phosphor, and provides valuable information on the metamorphic and thermal history of meteorites. The sensitivity of the induced TL is used to determine petrologic type of type 3 ordinary chondrites.

Then the natural TL of meteorites, along with induced TL data and cosmogenic radionuclide (*e.g.*, ^{26}Al) and noble gas abundance data, have been used to identify potentially paired fragments of Antarctic ordinary chondrites. The TL criteria used by Benoit *et al.* (1992) [1] for pairing Antarctic meteorites were that for two meteorites to be paired 1) natural TL dose at 250 ℃ had to be within 10%, 2) TL sensitivity values had to be within a factor of two, 3) induced TL peak temperatures had to be within 10% and peak widths within 20%. These criteria, based on data for petrographically paired meteorites, were deliberately conservative. As more reliable pairing approach, TL properties within large chondrites were analyzed, taking advantage of the fact that serial samples from these meteorites are known to be paired [2]. Then another set of TL pairing criteria: 1) the natural TL peak height ratios, LT/HT, should be within 20%; 2) that ratios of raw natural TL signal to induced TL signal should be within 1.5; 3) the TL peak temperatures should be within 20 ℃ and peak widths within 10 ℃ was proposed. This new set of TL pairing criteria are less restrictive than previously used.

This time we applied these new TL pairing criteria to TL data of fifteen Japanese Antarctic unequilibrated chondrites, measured under Okayama TL instrument and measuring conditions. The data of them were listed in Table 1. Ratio of natural TL signal (raw data as number of counts) to Dhajala-normalized TL sensitivity vs. natural TL peak height ratio is plotted in Fig.1. Y-794064 and Y-794011 are potentially paired according to the new TL criteria.

The petrographic subtype of these unequilibrated ordinary chondrites were also determined from their TL sensitivity and Y-74660 (LL3) was found to have petrographic types under 3.3.

References: [1] Benoit *et al.* (1992): *J. Geophys. Res.*, **97**, 4629-4648. [2] Ninagawa *et al.* (1998): *Antarctic Meteorite Res.*, **11**, 1-17.

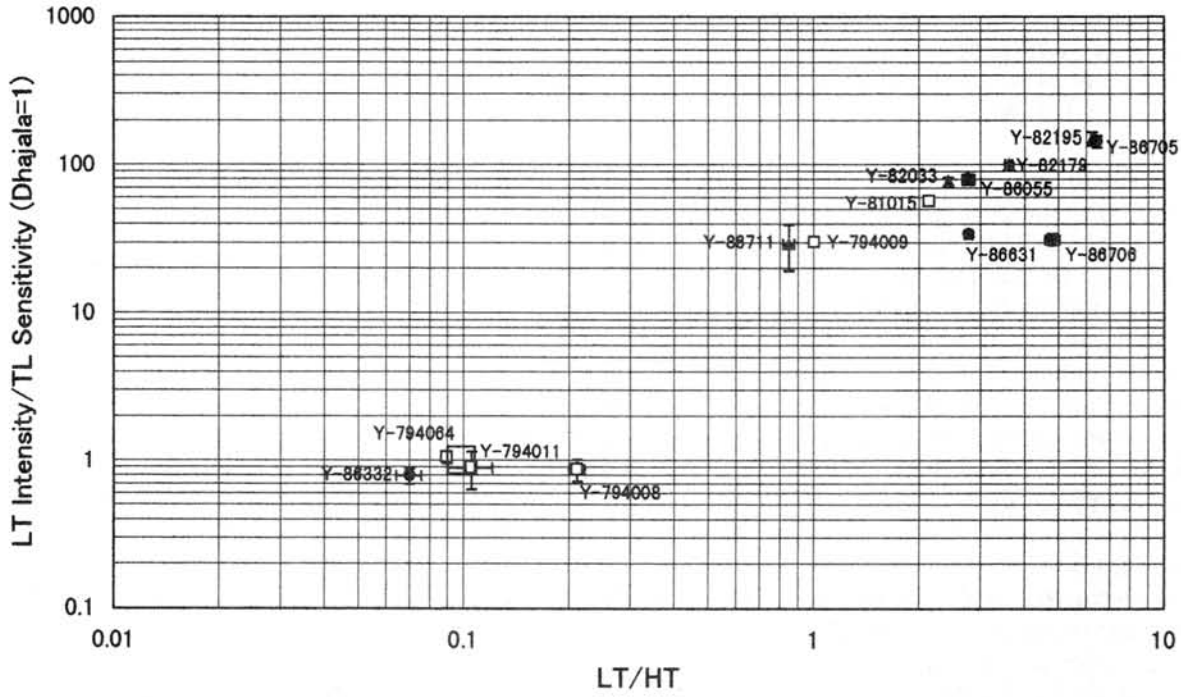

Fig. 1 Ratio of natural TL signal to Dhajala-normalized TL sensitivity vs. natural TL peak height ratio.

Table 1 TL data for fifteen Japanese Antarctic unequilibrated chondrites

Meteorite	Class	Natural TL		Induced TL				LT Int.	Pairing
		LT/HT	LT Intensity (10^3 counts)	TL Sensitivity* (Dhajala=1)	Peak Temp. (°C)	Width (°C)	TL Subtype	/TL Sens. ($x10^3$)	
Y-74660	LL3			0.0020 ± 0.0003	133 ± 0	148 ± 7	3.0		
Y-86711	LL3	0.85 ± 0.03	2.2 ± 0.7	0.08 ± 0.01	174 ± 6	150 ± 16	3.4-3.5	29 ± 10	
Y-82033	LL3	2.42 ± 0.01	78.4 ± 2.4	1.01 ± 0.05	167 ± 0	158 ± 0	3.7-3.8	78 ± 4	
Y-82179	LL3	3.61 ± 0.09	20.3 ± 0.1	0.201 ± 0.004	163 ± 0	146 ± 1	3.5-3.6	101 ± 2	
Y-82195	LL3	6.24 ± 0.05	146.8 ± 5.5	0.98 ± 0.09	166 ± 1	158 ± 0	3.7-3.8	150 ± 14	
Y-86332	L3	0.07 ± 0.01	0.3 ± 0.0	0.325 ± 0.009	143 ± 5	145 ± 1	3.6	0.8 ± 0.1	
Y-86055	L3	2.77 ± 0.11	55.0 ± 0.5	0.69 ± 0.05	162 ± 2	131 ± 2	3.7	80 ± 6	
Y-86631	L3	2.77 ± 0.07	16.3 ± 0.2	0.48 ± 0.01	120 ± 2	135 ± 2	3.7	34 ± 1	
Y-86706	L3	4.80 ± 0.24	27.2 ± 1.9	0.87 ± 0.06	102 ± 4	103 ± 1	3.7-3.8	31 ± 3	
Y-86705	L3	6.45 ± 0.02	41.1 ± 1.0	0.29 ± 0.02	151 ± 2	139 ± 0	3.6	144 ± 13	
Y-794064	H3	0.09 ± 0.00	0.5 ± 0.0	0.51 ± 0.02	153 ± 0	147 ± 1	3.7	1.0 ± 0.1	○
Y-794011	H3	0.11 ± 0.02	0.3 ± 0.1	0.38 ± 0.02	148 ± 1	147 ± 2	3.6	0.9 ± 0.3	○
Y-794008	H3	0.21 ± 0.01	0.4 ± 0.1	0.428 ± 0.006	155 ± 0	146 ± 1	3.6	0.9 ± 0.1	
Y-794009	H3	1.00 ± 0.00	38.0 ± 0.1	1.26 ± 0.04	154 ± 0	130 ± 1	3.8	30 ± 1	
Y-81015	H3	2.14 ± 0.02	27.1 ± 0.8	0.48 ± 0.02	162 ± 1	138 ± 8	3.6-3.7	57 ± 3	

* Intensity of Dhajala is supposed to be $5.9x10^3$ cps.

TEM study of matrix and some clasts in Vigarano (CV3) chondrite

Takaaki Noguchi
Department of Materials and Biological Sciences, Ibaraki University,
Bunkyo 2-1-1, Mito 310, Japan

Introduction Until recently, ubiquitous evidence for the aqueous alteration has been restricted to the case of the "oxidized" sub-group of McSween (1977). Lee and Graham (1992) and Lee et al. (1996) reported mineralogy of matrix of Vigarano which belongs to the "reduced" sub-group of McSween (1977). They found fibrous ferrihydrite and saponite in the matrix. Coarser ferrihydrite crystals fill the fractures of matrix minerals and saponite lines narrow channels within olivine (Lee et al., 1996). The author found some kinds of clasts which show distinct evidence for aqueous alteration predating the final agglomeration of Vigarano meteorite during a detailed SEM observation and microprobe analysis (Noguchi, 1997). Based on these data, some samples from these clasts and the host matrix were prepared for analytical electron microscopy (AEM). The samples were drilled and recovered from demountable thin sections. AEM samples were prepared by ultramicrotomy in order to minimize preferential thinning and decomposition of aqueous alteration products, which often occur during sample preparation by ion beam bombardment.

Petrography and chemical compositions of clasts investigated Matrix of the Vigarano meteorite contains at least two types of clasts which probably contain phyllosilicates. One is characterized by abundant magnetite. Another is characterized by laths of magnetite (Noguchi, 1997). One sample for AEM was prepared for each type of the clasts. Clast A contains aggregates of framboidal magnetite as well as fine-grained (less than 2-3 μm across) magnetite. Clast B contains laths of magnetite. Framboidal aggregates of fine-grained magnetite are not included in this clast.

Microprobe analyses of the host matrix, the matrices of clast A and clast B show that they have different compositions although there are overlaps among their compositions. Si/(Si+Mg+Fe) atomic ratios suggest that the host matrix is composed mainly of ferroan olivine, and that the matrix of clast A is composed mainly of ferroan olivine and serpentine (or ferroan olivine and minor saponite), and that the matrix of clast B is composed mainly of saponite and minor olivine (or mainly of saponite and serpentine and minor olivine).

TEM observation and analysis The matrix of clast A is composed of abundant olivine and magnetite, Fe sulfide, and fibrous minerals which fill interstices of anhydrous matrix minerals. Most of the anhydrous matrix minerals in this clast are < 200 nm across. The matrix of clast B is composed mainly of fine-grained phyllosilicate and Fe sulfide, Fe-Ni sulfide, and olivine. Fe sulfide is most abundant among the anhydrous matrix minerals. Most of Fe sulfide grains in the matrix of clast B are < 100 nm. In order to compare mineralogy, one area of the host matrix was also investigated. Host matrix is composed of abundant olivine and less abundant low-Ca pyroxene. One aluminous spinel was also found in the host matrix. The interstices of the anhydrous matrix minerals are filled by fibrous minerals and the materials with low crystallinity.

All of the TEM samples contain fibrous minerals. They are fine-grained and curved. Lattice fringes of these fibrous minerals are common among these three samples, from 1.0 to 1.2 nm. The lattice fringes suggest that these fibrous minerals are saponite. However, their sizes are different among these samples. In clast A, many saponite grains are from 5 to 20 nm wide normal to the fringe. In clast B, many saponite grains are from 5 to 30 nm across normal to the fringe. In the host matrix, most of saponite is < 5 nm wide normal to the fringe.

Individual fibrous mineral grains are too fine to get individual chemical compositions even by AEM. Therefore, only "bulk" compositions were acquired (beam diameters: 250-300 nm for clast A; 700-1000 nm for clast B; 150-200 nm for host matrix). Si/(Si+Mg+Fe) atomic ratios of "bulk" compositions of the fibrous minerals are similar to or higher than the ratios for serpentine in clast A and higher than those for serpentine in clast B. These mineral grains contain 2-3 Al_2O_3 wt % on average. Chemical compositions of fibrous minerals also suggest

that most of them are saponite. However, "bulk" compositions of fibrous minerals in the host matrix are different from those in clasts A and B. Their compositions are enriched in Fe. Their Si/(Si+Mg+Fe) ratios are even lower than those for olivine. Their compositions suggest that analyzed areas in the host matrix are composed mainly of Fe-rich materials and that saponite exist only a small amount in the areas. Interstitial materials among fine-grained fibrous mineral are probably Fe-rich materials.

Discussion Mineral species and amounts of hydrous minerals seem to be related to the extent of aqueous alteration which the host matrix, clast A, and clast B experienced. In the host matrix, hydrous minerals are least abundant among these samples. Therefore, the host matrix seems to experience the weakest aqueous alteration among these samples. Lee et al. (1996) indicated that the host matrix experienced aqueous alteration on the parent body. The host matrix contains Fe-rich material and a small amount of very fine-grained saponite. Lee et al. (1996) reported that electron diffraction spots from ferrihydrite. The author has not acquire obvious diffraction spots from ferrihydrite in the host matrix sample yet.

Clast A (a representative sample of fine-grained magnetite bearing clasts) contains framboidal aggregates of magnetite. Magnetite framboids have been found in CI and CM chondrites, and dark inclusions (DIs) in CR chondrites, and are regarded as aqueous alteration products on the meteorite parent bodies (e. g. Kerridge et al., 1979; Hyman et al., 1985; Weisberg et al., 1993). Therefore, clast A was also probably formed by aqueous alteration on the meteorite parent body. It is obvious that CI and CM chondrites and DIs in CR chondrites experienced heavier aqueous alteration than the host matrix of Vigarano. Therefore, it is reasonable that the extent of aqueous alteration of clast A is higher than that of the host matrix. In clast A, grain sizes of saponite are coarser than those in the host matrix. The matrix of clast A contains more abundant saponite than the host matrix, and lacks (or may contain a small amount of) ferrihydrite.

Coarse magnetite laths in the matrix of clast B (a representative sample of magnetite lath bearing clasts) have not been reported yet from any types of carbonaceous chondrites. Some magnetite laths seem to have nucleated on the kamacite spherules on the surface of a chondrule and to have grown in the matrix of clast A after accretion and during aqueous alteration (Noguchi, 1997). The abundant coarse saponite in the matrix of clast B suggest that this clast experienced heavier aqueous alteration on a parent body than the host matrix and clast A. Because microprobe data of the matrix of clast B tend to be more magnesian than the host matrix, the coarse magnetite laths in this clast were perhaps formed by consumption of ferrihydrite which is abundant in the host matrix and absent (or rare) in this clast.

Total wt % of microprobe data decrease with the increase of amounts of hydrous minerals. Because TEM observation shows that the amounts of hydrous minerals in the host matrix, the matrix of clast A, and that of clast B increase in this order, it is thought that total wt % of microprobe analyses decrease in this order. This expectation is consistent with the microprobe data of these samples (Noguchi, 1997). Because only the host matrix contains abundant ferrihydrite, the host matrix was perhaps experienced more oxidizing aqueous activity than clasts A and B. These materials with different degrees of aqueous alteration were probably accreted during final agglomeration of this meteorite.

References Graham, A. L. and Lee, M. (1992) Proc. 23rd LPSC, 435. Hyman, M. et al. (1985) Proc. 15th LPSC, C710-C714. Kerridge, J. F. et al. (1979) Science, 205, 395-397. Lee, M. R. et al. (1996) Meteoritics and Planetary Science, 31, 477-483. McSween, H. Y. (1977) Geochim. Cosmochim. Acta, 41, 1777-1790. Noguchi, T. (1997) Papers presented to the 22nd Symp. of Antarct. Meteorites, 156-159. Weisberg, M. K. et al. (1993) Geochim. Cosmochim. Acta, 57, 1567-1586.

TRACE ELEMENT CONCENTRATIONS IN IRON TYPE COSMIC SPHERULES DETERMINED BY THE SR-XRF METHOD

Wataru Nozaki[1], Tomoki Nakamura[1], Atsuo Iida[2], Kenji Matsuoka[1] and Nobuo Takaoka[1]

[1]*Depertment of Earth and Planetary Sciences, Kyushu University, Hakozaki, Fukuoka 812-8581, Japan.*
[2] *Photon Factory Institute of Materials Structure Science, High Energy Accelerator Research Organization, Tsukuba, Ibaraki 305-0801, Japan.*

Introduction

Iron type (I-type) spherules have been studied for more than one century (*e.g.*, Murray, 1891) and their extraterrestrial origin was confirmed by recent studies (*e. g.*, Nishiizumi *et al.*, 1983). They have simple mineralogy and major element abundance: dominant minerals are Fe oxide and FeNi metal containing Fe and Ni for major elements. This indicates that little evidence for the formation of I-type spherules can be obtained from mineralogy and major element composition. Origin and formation history of I-type spherules, therefore, can be elucidated from the signatures of trace element abundance, but there have been only a few reports on the analyses of trace elements (Ganapathy and Brownlee, 1978; Chevallier *et al.*, 1986). Small size range of spherules (up to 200 μm) makes it extremely difficult to determine the trace element concentrations. In this study we have applied an X-ray fluorescence method using synchrotron radiation (SR-XRF) to determine the trace element concentrations in I-type spherules.

Sample preparation and experimental techniques

We have collected I-type spherules from magnetic fractions separated from the deep-sea sediments that were dredged from 5800 m in depth offshore Hawaiian Islands. These I-type spherules were in a range of diameters from 50 to 200 μm and were polished to make thin sections with 30-μm thickness. Major element compositions and textual types of spherules were determined by an electronprobe microanalyzer (EPMA).

Trace element (Zn, Cu, Ga, Ge, Cr, Co, and Mn) compositions of the I-type spherule have been analyzed using a white X-ray microbeam with a beam size approximately 500 μm x 500 μm at the beamline 4A in the Photon Factory Institute of Materials Structure Science, High Energy Accelerator Research Organization. The samples were attached to nucleopore filters using an acetone-soluble bond. The background concentrations of the trace elements were measured repeatedly and were confirmed to be very low in the pore filters and the bond. Odessa 1A iron meteorite whose trace element concentrations are well known has been used for a standard sample. It was polished and cut to have 100 μm x 100 μm area and 30 μm thickness, which are similar area and thickness of the spherule samples, for accurate correction of X-ray absorption. X-ray fluorescence from samples were reflected by (001) planes of a graphite crystal and detected by a position sensitive proportional counter. Quantitative concentrations of the trace elements were obtained through X-ray intensity calibrations between spherules and standard sample and X-ray absorption corrections for differences in surface areas and material matrix of the samples. Minimum detection limits were approximately several ppm in the area of 100 μm x 100 μm.

Results and discussion

EPMA analyses showed that Ni concentrations in the spherule samples are variable ranging typically from 0.1 to 8.8 % and occasionally up to 32 %. We analyzed 43 I-type spherules by the SR-XRF method and also analyzed the Odessa iron meteorite in between the analyses of spherule samples. Cr and Co were detected from all spherules and concentrations are 700 and

200 ppm in average and range up to 9000 and 500 ppm, respectively. Ga, Ge, and Mn were detected from 8, 8, and 7 samples and average concentrations of these samples are 20, 15, and 25 ppm, respectively. Zn and Cu concentrations have not been determined yet.

The elemental abundance normalized to Odessa meteorite is shown in Figure 1. The relative abundance of elements decreases from left to right in the figure. Large excesses of Cr are observed in all spherules up to 1000. For Co and Ni, abundance in the spherules seems slightly lower than that in Odessa, and it scatters from 0.01 to 1. Ga and Ge abundances are apparently lower in the spherules than in Odessa. Assuming that precursor material of I-type spherule has contained similar amounts of trace elements to those of Odessa, the elemental abundance trend in figure 1 can be explained by differences of volatilities between elements. At temperatures and oxygen fugacity where liquid Fe_3O_4, the dominant compound in the spherules, is stable, Ga, Ge and Cr are in the form of oxide and Ni and Co are metallic. We calculated vapor pressures of Cr_2O_3, Co, Ga_2O_3, GeO_2, and Ni using literature data (JANAF, 1986). Volatilities of these elements and oxides at temperatures over 1650 K are in the order of Cr_2O_3 < Ni ~ Co < Ga_2O_3 < GeO_2 and this volatility trend shows a good agreement with relative elemental abundance trend in Figure 1.

According to Lamoreaux *et al.* (1986), vaporization rates of elements and oxides are expressed

$$\frac{dm}{dt} = 44.3 \left(\frac{M(M_b O_c)}{b} \right) \sum \left(\frac{p(i)x(i)}{[M(i)T^{1/2}]} \right)$$

where dm/dt is the mass loss rate in g $cm^{-2}s^{-1}$, M_bO_c is the formula of the condensed oxide, and x(i), M(i) and p(i) are the number of gram atoms of metal per mole, gram molecular weight of gas species and equilibrium partial pressure of vapor species i. Using vaporization rates of Cr_2O_3 and Co and average elemental ratios of Cr_2O_3 and Co in the spherule samples, we estimated thermal history and vaporization process of I-type spherule during atmospheric entry. For simplicity of model calculations, we made some assumptions: (1) I-type spherules have iron meteorite-like precursor material with Cr and Co concentrations of 20 ppm and 450 ppm, respectively, (2) The spherules have experienced heating at a constant temperature, and (3) during vaporization the size of the spherules is constant. The results of the calculation showed that, for instance, 50 μm I-type spherules with average Cr_2O_3 and Co concentrations have experienced atmospheric frictional heating for approximately 5 seconds at a temperature of 1800 K. The results are consistent with the results of numerical simulations reported by Yada *et al.* (1996).

Conclusions

Trace element analyses of I-type spherules by the SR-XRF method showed that there are remaining trace elements in I-type spherules and whose fractionation trend can be explained by the differences of volatilities among elements and oxides. A model calculation based on Cr_2O_3 and Co concentrations in I-type spherules and Cr and Co vaporization rates showed some features of the thermal history experienced by I-type spherules.

References

Chevallier P. *et al.* (1987): *Proc. Lunar. Planet. Soc.*, **92**, E649-656.
Ganapathy R. and Brownlee D. E. (1978): *Science*, **201**, 1119-1122.
Lamoreaux R. H. *et al.* (1986): *J. Phys. Chem. Ref. Data.* **16**, 419-443.
JANAF thermochemical tables (1985): (Eds. Chase M. W. et al.) 1985 Supplement, *J. Phys. Chem. Ref. Data.*
Murray J. and Renard A. F. (1891): *Deep-Sea Deposits*, 327.
Nishiizumi K. (1983): *Earth Planet. Sci. Lett.*, **63**, 223-228.
Yada T. et al. (1996): *Proc. NIPR Symp. Antarct. Meteorites*, **9**, 218-236.

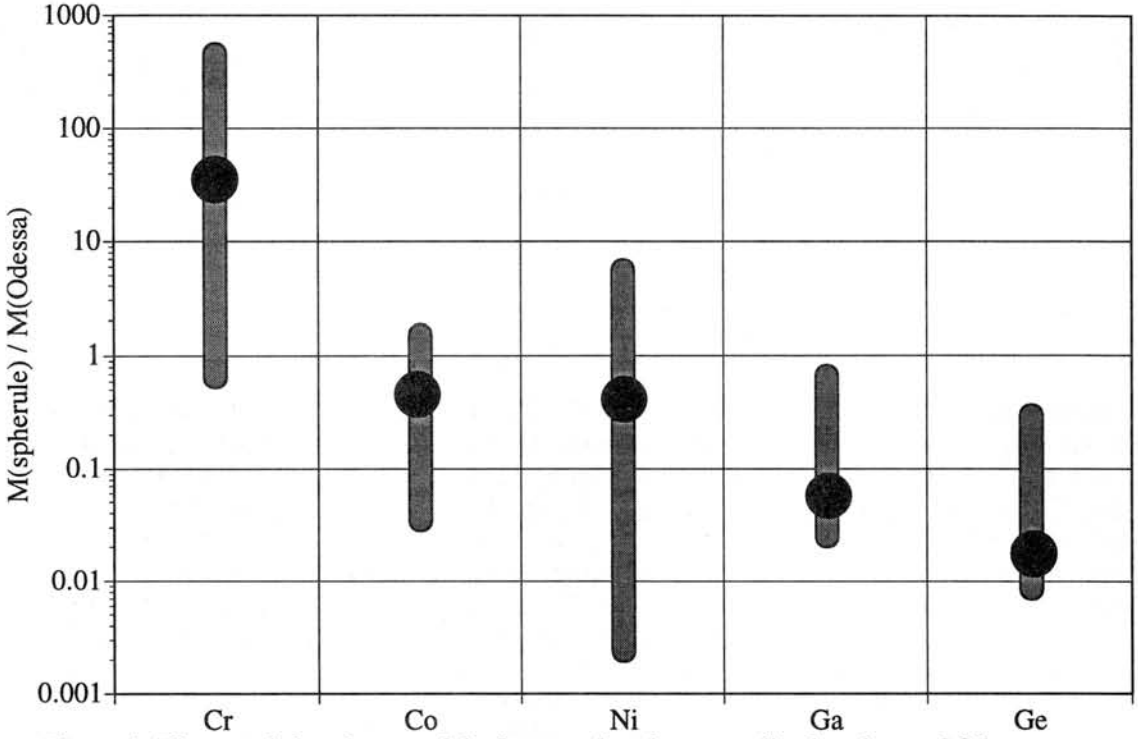

Figure 1. Elemental abundances of the I-type spherules normalized to those of Odessa iron meteorite. Average abundances and ranges of data distribution are shown as black marks and gray bars, respectively.

Exposure history of the H-chondrite Tsukuba

R. Okazaki[1, 2)], N. Takaoka[1)], T. Nakamura[1)] and K. Nagao[2)]

1) Department of Earth and Planetary Sciences, Faculty of Science, Kyushu University 33, Hakozaki, Fukuoka 812-8581, Japan
2) Laboratory for Earthquake Chemistry, Graduate School of Science, University of Tokyo, Hongo, Bunkyo-ku, Tokyo 113-0033, Japan

Introduction

Tsukuba meteorite is H5-6 chondrite that fell as a meteorite shower on 7th of January, 1996. 23 fragments with a total weight of about 800g were recovered in Tsukuba-city and thereabouts, in 38 days after fall [1, 2]. Petrographic observation showed that fragment No. 2, 6, 11 and 17 are breccias that exhibit characteristic dark-light structures [3]. In this paper, we report the results of noble-gas analyses in the dark and light portions of fragment No. 11 to elucidate the exposure history and the parent body process. The fragment No. 11 was carefully separated into the dark and light parts, and was analyzed for noble gases by heating stepwise at 600, 1000 and 1800 °C to investigate differences between these two portions. In addition, we have analyzed separated six dark parts of fragment No. 11 by a total melting method.

Results and discussion

The dark portion contains great amounts of light noble gases (^{4}He, ^{20}Ne and ^{36}Ar) compared with the light portion. Both isotopic and elemental compositions for the light noble gases evolved from the dark sample at 600 °C are solar. This suggests that the dark portion contains solar particles implanted into grain surfaces on the meteorite parent body. For radiogenic gases, both dark and light portions contain identical quantities of ^{40}Ar. With assumptions that all ^{40}Ar is radiogenic and K content is equivalent to that for H-chondrite average [4], we obtain about 4.3 Ga for the K-Ar age of Tsukuba chondrite. In addition, major element analyses of the dark and light portions by an electron microprobe in this study reveal that they have exactly same MgO/(FeO+MgO) ratios in olivine crystals (Fa_{17}). These chronological and mineralogical evidences suggest that both dark and light portions were derived from a common precursor rock, and the brecciation process producing the light-dark structure took place in the early stage of the solar system evolution.

On a three-isotope correlation diagram of Ne (Fig. 1), data for the dark and light portions could define two good correlation lines with different slopes. Both correlation lines give trapped ^{20}Ne/^{22}Ne=12.6 with trapped ^{21}Ne/^{22}Ne=0.033. For the cosmogenic isotopic ratios, the correlation lines for the dark and light portions give cosmogenic ^{21}Ne/^{22}Ne=0.67 and 0.82 with cosmogenic ^{20}Ne/^{22}Ne=0.82, respectively. The significantly low cosmogenic ^{21}Ne/^{22}Ne ratio for the dark sample indicates contribution of cosmogenic Ne produced by solar cosmic-rays (SCR) [5]. The SCR contribution is supported by a positive correlation between cosmogenic ^{21}Ne and trapped ^{20}Ne that is of solar wind (SW) origin on the isotopic ratio mentioned above (Fig. 2). The same correlation has been reported for Kapoeta meteorite [6]. In addition, the concentration of cosmogenic

^{21}Ne in the dark portion is higher than that in the light portion of fragment No. 11. It can be assumed that this difference is a reflection of SCR-produced Ne in the dark portion.

A large difference in cosmogenic gases between fragment No.1 and No.11 remains to be answered. The fragment No. 1, in which no dark portion was observed, contains ×2.1 and ×2.7 more abundant cosmogenic ^{3}He and ^{21}Ne, respectively [2], than the light portion of fragment No. 11 does. A cosmogenic ^{21}Ne/^{22}Ne ratio for No. 1 is larger than that for No. 11 (Fig. 1), suggesting a larger shielding depth for No. 1. There are three possible explanations for such differences: different shielding depths in the parent body and in the meteoroid that was parental for Tsukuba, and gas loss from fragment No. 11 that might have taken place at shock heating. The third possibility is out of consideration because it is inconsistent with solar gas retention in the dark sample. If the second possibility is the case, the Tsukuba meteorite should be much larger and it means that the main mass is missing. The first possibility seems to be plausible. However, other 21 fragments than No. 1 and No. 11 are not yet under investigation.

In summary, the Tsukuba meteorite is a brecciated stone consisting of 23 fragments that fell as a meteorite shower. The dark part of fragment No. 11 is composed of surface materials of the parent body. An impact shock disrupted the crust of the parent body, mixed stones from different depth of regoliths, and liberated a meteoroid compacted as a precursor of the Tsukuba meteorite. In order to evaluate the exposure history quantitatively, we need data on long-lived nuclides such as ^{10}Be and ^{53}Mn that can give the GCR exposure age for the meteoroid in the interplanetary space. Anyhow, the Tsukuba meteorite can give important constrains on surface processes induced by meteorite-impacts on the parent body, because it has complicated records of SCR and GCR-exposures and the records are very useful for deciphering those processes.

References

[1] Togashi S. et al. (1997) *Chishitsu News*, **509**, 7-15.

[2] Yoneda S. et al. (1996) *Meteoritics and Planet. Sci.*, **31**, A157-A158.

[3] Okuyama Y. K. et al. (1997) *Chishitsu News* **509**, 35-42.

[4] Wasson J. T. and Kallemeyn G. W. (1988) *Phil. Trans. R. Soc. Lond.*, **A 325**, 535-544.

[5] Garrison D. H. et al. (1995) *Meteoritics*, **30**, 738-747.

[6] Goswami J. N. and Wilkening L. L. (1984) *Space. Sci. Rev.*, **37**, 111-159.

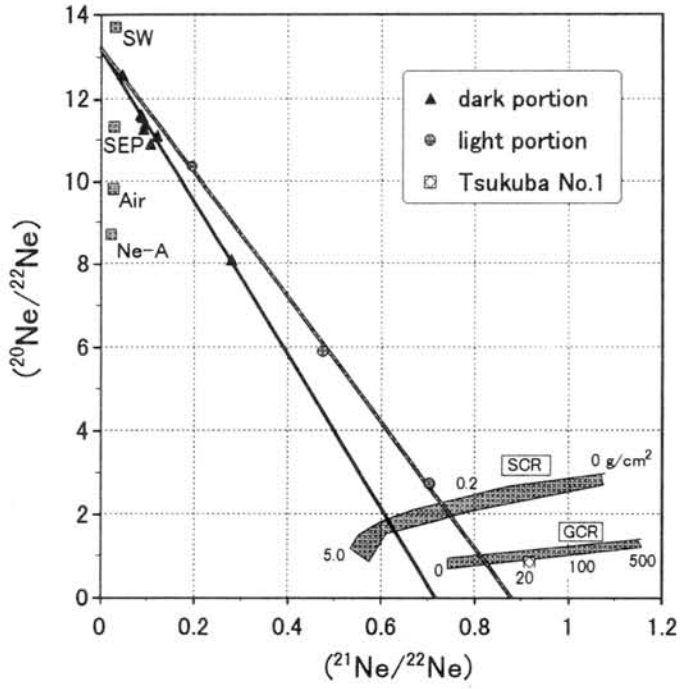

Fig. 1: Neon isotopic correlation plot for the dark and light portions of fragment No. 11, and No. 1 [2]. Ranges of cosmogenic Ne compositions produced by interactions of GCR and SCR are shown for different shielding conditions. The numerals near the shaded zones refer to shielding depths in g/cm^2.

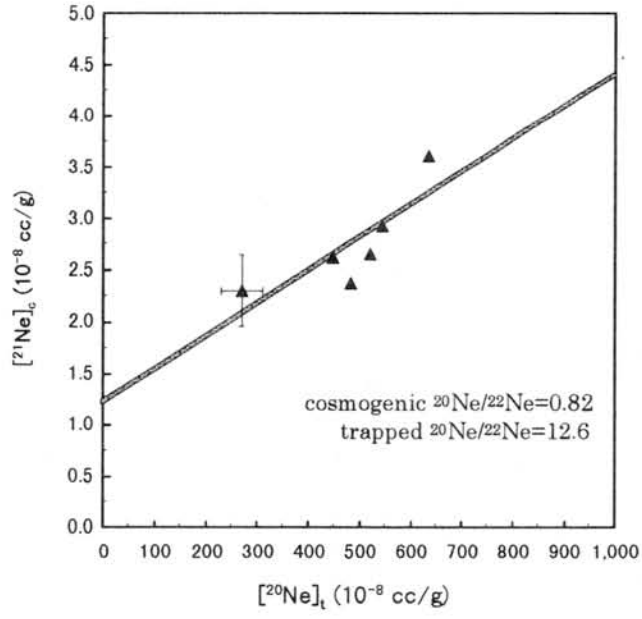

Fig. 2: Cosmogenic ^{21}Ne vs. trapped ^{20}Ne of the dark portion of fragment No. 11. Typical uncertainties of cosmogenic and trapped concentrations are shown for one sample.

Cosmogenic noble gases in E-chondrites

Ryuji Okazaki[1, 2)], Nobuo Takaoka[1)], Tomoki Nakamura[1)] and Keisuke Nagao[2)]

1) Department of Earth and Planetary Sciences, Faculty of Science, Kyushu University 33, Hakozaki, Fukuoka 812-8581, Japan

2) Laboratory for Earthquake Chemistry, Graduate School of Science, University of Tokyo, Bunkyo-ku, Tokyo 113-0033, Japan

Introduction

Energetic particle environments and irradiation histories of meteorites are recorded in concentrations and compositions of cosmogenic noble gases. We re-investigated noble gases in six E chondrites to elucidate conditions and duration of cosmic-ray exposures of these meteorites. Preliminary results of the six E chondrites have been reported in [1]. In this study, noble gases were analyzed in two different ways. One is total melt extraction, another is a newly developed method [2] that consists of a crushing and stepwise heating. There are large differences in noble-gas concentrations between the previous our data [1] and those obtained by this replicated analyses. This discrepancy is probably due to a fall in sensitivities of a mass spectrometer. Hence, we will revise our previous results and discuss cosmic-ray exposure histories for these E-chondrites based on the new results.

Results and discussion

Table 1 shows the revised cosmogenic noble-gas concentrations and cosmic-ray exposure ages. Ne-isotopic ratios of all samples were typically cosmogenic, except for Y-74370 (EH3), Y-82189 (EH6) (Fig. 1). In calculating cosmogenic gas concentrations, we assumed that all ^{3}He were cosmogenic, and isotopic compositions of trapped Ne and Ar were atmospheric. For the Y-82189, we will discuss below. All gas-concentrations obtained by the two methods are in good agreement within 20% for each meteorite, except for the ^{3}He-concentration of Y-74370. With production rates of ^{3}He, ^{21}Ne and ^{38}Ar calculated using equations given in [3], cosmic-ray exposure ages were obtained (Table 1). Significant differences are generally observed in our data between ^{3}He and ^{21}Ne ages, and ^{21}Ne and ^{38}Ar ages. For the differences between ^{3}He and ^{21}Ne ages, cosmogenic ^{3}He/^{21}Ne are plotted against cosmogenic ^{22}Ne/^{21}Ne (Fig. 2). Y-74370, Y-86004 and Ilafegh009 are plotted much lower than the correlation line observed for most chondrites, which is probably due to He losses from these meteorites. A difference between ^{21}Ne and ^{38}Ar ages for Y-793225 is possibly caused by a low concentration of Ca, which is a main target element producing ^{38}Ar via spallation reactions. Accordingly, we adopted the averages of the ^{21}Ne and ^{38}Ar exposure ages as representative exposure ages, except for Y-793225 for which ^{21}Ne age is adopted. Y-74370 and three E6 chondrites (Y-8414, Y-86004, and Y-82189) have short ages ($\leqq$10 m.y.). Only Y-793225 (E6) has a long age (35 m.y.). Two EH6 chondrites Y-8414 and Y-86004 show identical exposure ages, which suggests that the two meteorites could be pared. This is consistent with the petrological similarities between them [4].

The low ^{21}Ne/^{22}Ne ratios around 0.7 are observed in the low temperature fractions (600 and 800 °C) of Y-793225, reflecting the presence of sodium-rich phases such as plagioclase [e.g. 5, 6]. Regarding the Y-82189, irradiation condition seems to be different from other samples. Y-82189 shows the low ^{21}Ne/^{22}Ne ratios (=0.7) in every temperature fraction. We have inferred that such low ratios were caused by the presence of sodium-rich phases as is the case for Y-793225 [1]. Major element analyses by an electron microprobe in the present study, however,

show no enrichment in sodium in Y-82189. Therefore, we support the alternative explanation that the low $^{21}Ne/^{22}Ne$ ratios of Y-82189 were modulated by solar cosmic ray (SCR)-produced Ne. A typical $^{21}Ne/^{22}Ne$ ratio of SCR-produced Ne component is about 0.6 with a shielding condition of 2.0 g/cm^2 [7] for the chemical composition of EH-chondrite [8]. We calculated the exposure age of Y-82189 based on the Ne isotopic ratio and the production rates of GCR- and SCR-produced components with the shielding condition of 2.0 g/cm^2 [7, 9]. The depth of 2.0 g/cm^2 meets the condition that the exposure ages derived from SCR-produced Ne should not be longer than those from GCR-produced Ne. As a result, we obtain an approximately 2 m.y. for GCR and SCR-irradiation of Y-82189, which depends heavily on the assumption for the shielding condition. With a condition of large shielding, SCR-produced component would not be detectable because of the short range of SCR. Hence, it is suggested that Y-82189 was irradiated both by SCR and GCR on the outer layer of the meteorite parent body, and has a short GCR-exposure in space. Otherwise, Y-82189 has so small a preatmospheric size that SCR effects can be detectable. However, further discussion on Y-82189 would be subjected to a future investigation.

References

[1] Okazaki R. *et al.* (1997) *Symp. Antarct. Meteorites,* **XXII**, 160-163.
[2] Okazaki R et al. (1997) *Meteoritics & Planet. Sci.*, **32**, A102.
[3] Eugster O. (1988) *Geochim. Cosmochim. Acta,* **52**, 1649-1659.
[4] Lin Y. and Kimura M. (1998) *Meteoritics & Planet. Sci,*. **33**, in press
[5] Smith S. P. and Huneke J. C. (1975) *Earth Planet. Sci. Lett.*, **27**, 191-199.
[6] Wacker J. F. and Marti K. (1983) *Earth Planet. Sci. Lett.*, **62**, 147-158.
[7] Reedy R. C. (1992) *Lunar Planet. Sci.*, **23**, 1133-1134.
[8] Wasson J. T. and Kallemeyn G. W. (1988) *Phil. Trans. R. Soc. Lond.*, **A 325**, 535-544.
[9] Hohenberg C. M. et al. (1978) *Proc. Lunar Sci. Conf.*, **9**, 2311-2344.
[10] Zhang Y. and Sears D. W. G. (1996) *Meteoritics & Planet. Sci.*, **31,** 647-655.
[11] McCoy T.J. et al. (1995) *Geochim. Cosmochim. Acta,* **59**, 161-175.
[12] Nishiizumi K. et al. (1980) *Earth Planet. Sci. Lett.*, **50**, 156-170.

Table 1: Samples and cosmogenic-gas concentrations.

sample	weight (mg)	method	$[^3He]_c$ [1]	$[^{21}Ne]_c$	$[^{38}Ar]_c$	$(^{21}Ne/^{22}Ne)_c$	P_3	P_{21}	P_{38}	T_3	T_{21}	T_{38}	T_{ex} (Ma)
			($\times 10^{-9}$cm^3 STP/g)				($\times 10^{-9}$cm^3 STP/g/Ma)			(Ma)			
Y-74370	10.5	2)	10.6	4.20	0.882					0.69	2.27	2.26	
EH3[6]	107	3)	15.1	3.54	0.692	0.85	15.3	1.85	0.391	0.99	1.91	1.77	2.1[4]
mean			12.9	3.87	0.787					0.84	2.09	2.01	± 0.25
Y-8414	7.2	2)	134	20.4	3.10					8.78	11.2	8.00	
EH6[7]	105	3)	90	15.6	2.78	0.831	15.3	1.83	0.388	5.92	8.55	7.17	8.7[4]
mean			112	18.0	2.94					7.35	9.86	7.58	± 1.7
Y-86004	5.0	2)	101	18.0	2.77					6.66	10.6	7.46	
EH6[7]	114	3)	102	16.1	3.20	0.815	15.2	1.70	0.371	6.73	9.48	8.62	9.0[4]
mean			102	17.1	2.99					6.70	10.0	8.04	± 1.3
Y-82189	3.9	2)	8.61	5.29	0.696						2.6		
EH6[7]	106	3)	9.32	4.30	0.788			1.0			2.2		2
mean			8.97	4.80	0.742						2.4		
Y-793225	7.4	2)	562	101	9.67					35.4	39.7	25.8	
E6	103	3)	542	78.1	7.20	0.857	15.9	2.54	0.375	34.1	30.7	19.2	35[5]
mean			552	89.6	8.44					34.8	35.2	22.5	± 6.4
ILAFEGH009	13.3	2)	89.5	38.4	4.52					5.61	14.4	11.8	
EH7[8]	127	3)	71.9	29.8	3.27	0.925	15.9	2.67	0.384	4.51	11.2	8.5	11.5[4]
mean			80.7	34.1	3.90					5.06	12.8	10.2	± 2.4

1) All ^{3}He assumed to be cosmogenic. 2) Total melt extraction. 3) crushing and stepwise heating.
4) Average of ^{21}Ne and ^{38}Ar-ages. 5) Only ^{21}Ne-ages.
6) Ref. [10]
7) Ref. [4]
8) Ref. [11]

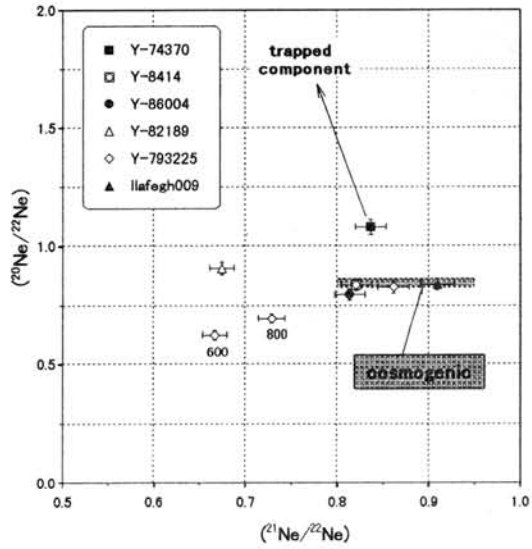

Fig 1. Ne three-isotope diagram for six E chondrites. The numerals near the data points refer to the temperature in °C. The shaded zone represents a typical range of isotopic composition of cosmogenic Ne produced by GCR are shown

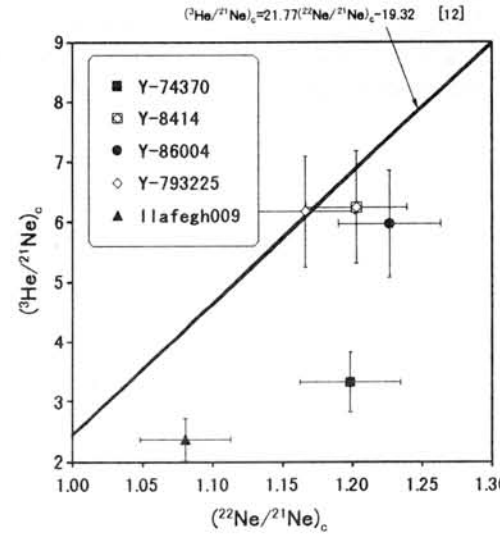

Fig. 2. Cosmogenic ^{3}He/^{21}Ne vs. ^{22}Ne/^{21}Ne. The correlation line proposed by [12] are shown.

Chemical composition of Asuka-881988, Yamato-75302 and Yamato-791827, Antarctic R chondrites.

Hiromasa Ozaki, Kazunori Shinotsuka, Gregory W. Kallemeyn and Mitsuru Ebihara
Department of Chemistry, Graduate School of Science, Tokyo Metropolitan University, Hachioji, Tokyo 192-0397, Japan.

Introduction The R chondrite group is now recognized as a new group of chondrites [1]. Since 1977 when the first recognized R chondrite, Carlisle Lakes, was discovered in Australia, more than 10 meteorites have been classified as R chondrites. Among them, Rumuruti is the only fall [2]. In the Japanese Antarctic meteorite collection, five meteorites have been identified as R chondrites; Asuka-881988, Yamato-75302, Yamato-791827, Yamato-793575 and Yamato-82002. Except for Asuka-881988, they are very small in size; Y-793575 is 25 g and the remaining meteorites are smaller than 10 g. Both Y-793575 and Yamato-82002 have been previously studied, but the others have not. A consortium study was formed to study the three previously unstudied Japanese R chondrites. In our study, we determined the chemical compositions of these R chondrites by using different analytical methods. In addition to the three meteorites from the consortium study, 7 other meteorites (8 samples) (Rumuruti, Carlisle Lakes, Yamato-793575, Yamato-82002, ALH 85151, PCA 91002, PCA 91241 and Acfer 217) were analyzed.

Experimental Chips of the meteorite samples were ground in an agate mortar. Because there are few metal grains in R chondrites, it was easy to powder the specimens. Samples (50 to 100 mg each) were each sealed in an FEP film and subjected to prompt gamma-ray analysis (PGA) using the cold neutron guided-beam at the Japan Atomic Energy Research Institute. After cooling, the same samples were used for INAA. Two successive irradiations of 100 s and 6 h were used for INAA analysis. After each irradiation, the samples were measured for their gamma-rays. After the 6 h irradiation, measurements were repeated three times following different cooling intervals. Using another aliquot of each specimen, REE, Th and U were measured by ICP-MS.

Results and discussion One of the advantages of PGA is its capability of determining Si non-destructively in rock samples [3]. Besides Si, 13 other elements (B, Na, Mg, Al, S, Cl, Ca, Ti, Cr, Mn, Fe, Co, Ni) were determined for the R chondrites by PGA. Five elements determined by PGA (B, Si, S, Cl, Ti) couldn't be determined by INAA. Nineteen elements (Na, Mg, Al, Ca, Sc, V, Cr, Mn, Fe, Co, Ni, Zn, As, Se, La, Sm, Os, Ir, Au) were determined by INAA.

Figure 1 shows the Mg-, CI-normalized elemental abundance patterns for mean R, H, L and LL chondrites. Refractory and moderately volatile lithophile element abundances for R chondrites are essentially ordinary chondrite-like. R chondrites are characterized by relatively high abundances of chalcophile elements. In this study, we confirmed that Se, Zn and S are enriched in R chondrites, including three small Antarctic meteorites. Kallemeyn et al. [1] reported an anomalously high Ca content (19.4 mg/g) in Carlisle lake. We also obtained a similarly high Ca value (19.3 and 18.6 mg/g by PGA and INAA, respectively). The three consortium meteorites yielded Ca contents of 13.2, 13.4 and 11.6, which are close to 11.8 mg/g for the only fall, Rumuruti. Despite the paucity of metal grains in R chondrites, siderophile element abundances are chondritic, or ordinary chondrite-like. CI-normalized abundances (Fig. 1) of refractory and moderately volatile siderophile elements are chondritic, being similar to those of H chondrites rather than those of L and LL chondrites.

It is well known that lithophile elements are systematically fractionated between carbonaceous and non-carbonaceous chondrites; refractory lithophile to Si ratios for carbonaceous chondrites are systematically higher than those for non-carbonaceous chondrites. Figure 2 shows the relationship of Ca/Si vs. Mg/Si. Like the Ca/Si ratio, the Mg/Si ratio varies systematically between carbonaceous and non-carbonaceous chondrites. R chondrites have a lower Mg/Si ratio than carbonaceous and ordinary chondrites. The

Mg-Si fractionation as well as the Ca (as a refractory lithophile element)-Mg fractionation must have taken place in the solar nebula at the time when the solar system formed. The fractionation of Ca and Si can be best explained in terms of the difference in their volatility. The fractionation between Mg and Si, however, cannot be explained by the same reason because the volatilities of Mg and Si are similar. The possibility that the Mg-Si fractionation was a function of heliocentric distance seems plausible among the carbonaceous, ordinary and enstatite chondrites. If the heliocentric variation in the Mg/Si ratio is extended to the R chondrites, then they possibly formed between the locations for the LL chondrites (or ordinary chondrites in general) and the enstatite chondrites.

Acknowledgments We thank the NIPR and Prof. Nakamura (consortium leader) for allocating the meteorite samples studied here. Drs. A. Bevan and Dr. H. Schulze are acknowledged for Carlisle Lake, Rumuruti and Acfer 217 meteorites, respectively. Meteorite Working Group of US is also thanked for Antarctic R chondrites, ALH 85151, PCA 91002 and PCA 91242. This work is supported in part by a Grant-in-Aid of the Ministry of Education, Culture and Science.

References [1] Kallemeyn G. W. et al. (1996) Geochim. Cosmochim. Acta **60**, 2243-2256. [2] Schulze H. et al. (1994) Meteoritics **29**, 275-286. [3] Latif S. K. et al. (1998) J. Radioanal. Nucl. Chem. (in press).

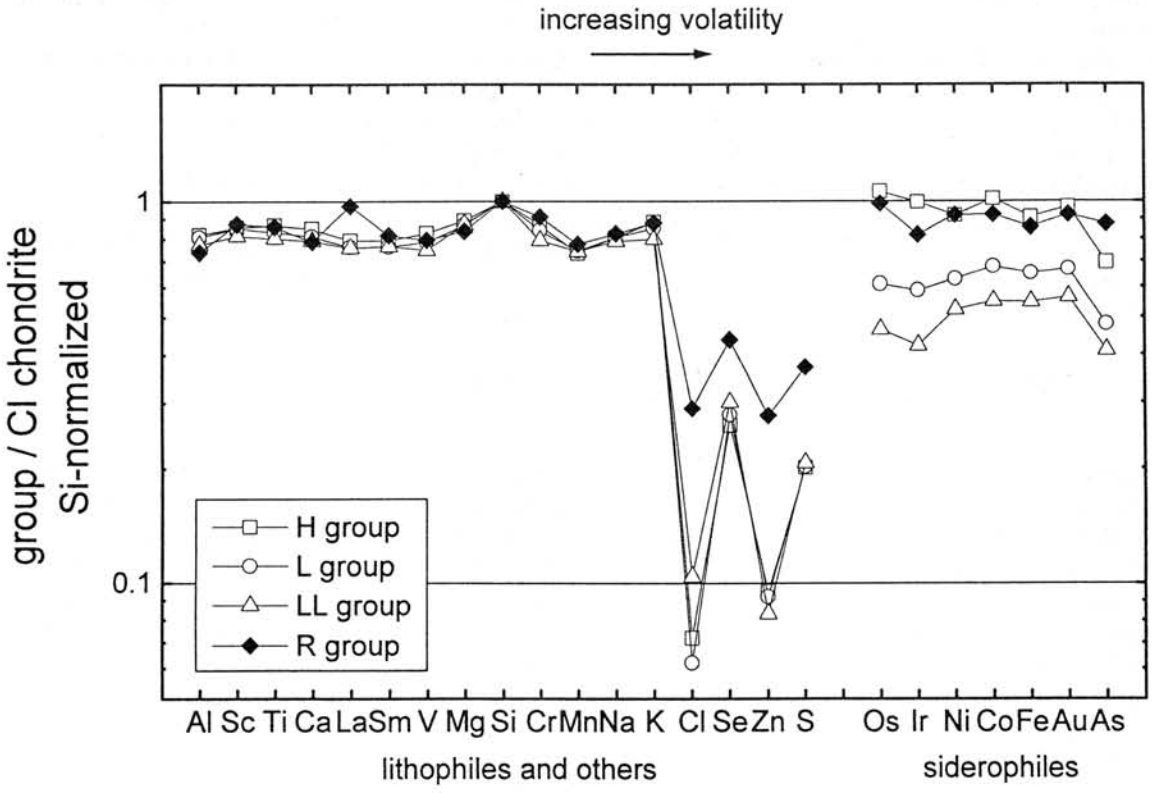

Fig. 1 Mg-, and CI chondrite-normalized elemental abundance pattern for mean R, H, L and chondrites.

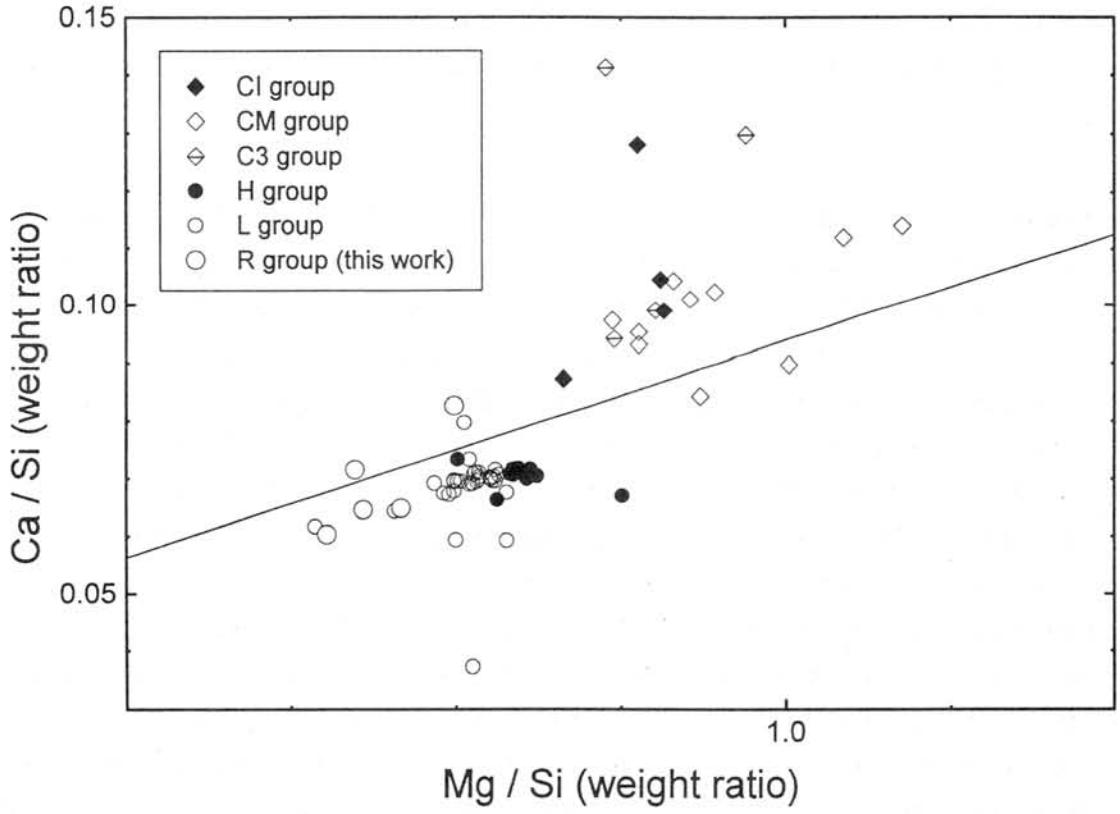

Fig. 2 Relationship of Ca/Si vs. Mg/Si for chondritic meteorites including R chondrites.

CHEMICAL AND ISOTOPIC FRACTIONATION DURING EVAPORATION OF A MULTI-COMPONENT SYSTEM : (2) GENERAL MODEL AND APPLICATION TO MG-FE OLIVINE K. Ozawa[1] & H. Nagahara[2]: (1) Inst. Study Earth's Interior, Okayama Univ., ozawa@misasa.okayama-u.ac.jp, (2) Geol. Inst., Univ. Tokyo, hiroko@geol.s.u-tokyo.ac.jp

Introduction: Isotopic fractionation during evaporation is a key to understanding evolution of stellar environments, which leads to the formation of planets. During evaporation, diffusion in condensed phases affects the degree of isotopic fractionation, which has been studied by Wang (1995), Tsuchiyama et al. (1995) and Nagahara and Ozawa (1997). Such studies treated stoichiometric pure end member minerals such as forsterite and SiO_2. These phases do not have solid solution and thus we do not need to care about chemical fractionation. However, this may not be the case for solution phases, such as olivine and silicate melt. In order to treat such diffusion-controlled isotopic fractionation in a multi-component system , a general model that takes the effect of chemical fractionation into consideration was developed. This model also can be applied to a problem of diffusion-controlled evaporation of solution phases.

If a condensed phase undergoing phase transition by a fractional process (such as free evaporation) is instantaneously homogenized, any pair of chemical components or isotopes during the maximum fractionation obeys the Rayleigh distillation law, in which the fraction of a component transferred across the phase boundary is used as a measure of the reaction extent. As far as we are concerned about the relative fractionation of a pair of elements or isotopes during maximum fractionation process, the Rayleigh law completely describes the phenomena even if a significant elemental fractionation takes place. However, if diffusive mass transfer in the reactant phase becomes a rate limiting factor or if we want to know the fractionation as a function of the total amount of a reactant transformed into a new phase, we need to treat explicitly the concentrations of chemical components or isotopes in the condensed phase.

Diffusion-controlled fractionation model: In the system consisting of N components, the diffusion equation and boundary conditions for a component at the interface between separating phase and reactant phase is given by

$$\frac{\partial \tilde{C}_s^i}{\partial t} = \left\{ \frac{\partial}{\partial r}\left(D_s^i \frac{\partial \tilde{C}_s^i}{\partial r} \right) + \frac{aD_s^i}{r}\frac{\partial \tilde{C}_s^i}{\partial r} \right\} \quad \text{----- (1)}$$

$$D_s^i \frac{\partial \tilde{C}_s^i}{\partial r}\Bigg)_{r=R(t)} + \frac{dR}{dt}\tilde{C}_s^i(R,t) = -J^i, \quad \text{------ (2)}$$

$$\frac{\partial \tilde{C}_s^i}{\partial r}\Bigg)_{r=0} = 0 \quad \text{----- (3)}$$

where a is the shape parameter (0 for plate, 1 for rod, 2 for sphere), r is the distance from the center of the reactant phase (radius in spherical symmetry), R is the half size of the grain, $\tilde{C}_s^i(R,t)$ is the concentration (in a unit volume) of the ith component in the reactant phase at the

interface with separating product $r = R$ at time t, D_s^i is the concentration dependent diffusion coefficient of the component, J^i is the evaporation flux of the ith component. The boundary condition (2) explicitly contains evaporation flux of a component, which is usually difficult to determine. In order to eliminate it, we introduce a chemical fractionation factor $\tilde{K}^{i,k}$, which is defined as follows

$$\tilde{K}^{i,k} = \frac{\tilde{C}_g^i}{\tilde{C}_g^k}\frac{\tilde{C}_s^k(R,t)}{\tilde{C}_s^i(R,t)} = \frac{J^i}{J^k}\frac{\tilde{C}_s^k(R,t)}{\tilde{C}_s^i(R,t)}, \text{ ------- (3)}$$

where $\tilde{C}_g^j$ is the concentration of the component in separating phase. $\tilde{K}^{i,k}$ depends on temperature, pressure, and composition of condensed phase. The second equality is only satisfied for perfect fractional case. By using (3), the boundary condition (2) for the ith chemical component becomes,

$$D_s^i \frac{\partial C_s^i}{\partial r}\Bigg)_{r=R(t)} = \frac{dR}{dt} C_s^i(R,t)\left\{\frac{1}{\left(C_s^i(R,t) + \sum_{k\neq i}^{N}\frac{C_s^k(R,t)}{\tilde{K}^{i,k}}\right)} - 1\right\} \text{ . ------ (4)}$$

For the pth isotope of the ith element ($\tilde{C}_s^{pi}$), the boundary condition (2) is also valid;

$$D_s^{pi}\frac{\partial \tilde{C}_s^{pi}}{\partial r}\Bigg)_{r=R(t)} + \frac{dR}{dt}\tilde{C}_s^{pi}(R,t) = -J^{pi}, \text{ ------ (5)}$$

where D_s^{pi} is the diffusion coefficient of the pth isotope of the ith element in the condensed phase, and J^{pi} is the evaporation flux of the isotope. Isotopic fractionation factor $\alpha^{p,q}$ of the pth isotope $\left({}^{p}i\right)$ relative to another isotope $\left({}^{q}i\right)$ is defined as follows

$$\alpha^{p,q} = \frac{\tilde{C}_g^{pi}}{\tilde{C}_g^{qi}}\frac{\tilde{C}_s^{qi}(R,t)}{\tilde{C}_s^{pi}(R,t)} = \frac{J^{pi}}{J^{qi}}\frac{\tilde{C}_s^{qi}(R,t)}{\tilde{C}_s^{pi}(R,t)}. \text{ ------ (6)}$$

By using the isotope fractionation factor, the boundary condition for the pth isotope of the ith element is obtained as

$$D_s^{pi}\frac{\partial C_s^{pi}}{\partial r}\Bigg)_{r=R(t)} = \frac{dR}{dt}C_s^{pi}(R,t)\left\{\frac{C_s^i(R,t)}{\left(C_s^i(R,t) + \sum_{k\neq i}^{N}\frac{C_s^k(R,t)}{\tilde{K}^{i,k}}\right)\cdot\left(C_s^{pi}(R,t) + \sum_{q\neq p}^{M_i}\frac{C_s^{qi}(R,t)}{\alpha^{p,q}}\right)} - 1\right\}. \text{ (7)}$$

Isotope fractionation between ${}^{p}i$ and ${}^{q}i$ isotopes can be calculated from $\tilde{C}_s^{pi}$ and $\tilde{C}_s^{qi}$, which were obtained by simultaneous integration of diffusion equation with boundary conditions of (4) and (7).

Application: The diffusion equation (2) is solved with boundary conditions (3), (4), and (7) for Mg-Fe fractionation and isotopic fractionation of binary olivine solid solution. The solution was applied to the evaporation experiments of olivine in order to determine evaporation rate, Mg-Fe fractionation factor, and interdiffusion coefficients. We have assumed the constant fractionation factor and optimize the composition dependence of evaporation rate and Mg-Fe interdiffusion coefficient. By using these parameters, time scale of evaporation of olivine and isotope fractionation are investigated.

Early evolution of the Earth inferred from $^{129}I/^{127}I$ - $^{244}Pu/U$ systematics.

M. Ozima[1,2] and F.A.Podosek[2]

(1) Dept. Earth Planet. Physics, University of Tokyo, Tokyo 113-8654, Japan, (diamond@gpsun01.geoph.s.u-tokyo.ac.jp)
(2) Department of Earth and Planetary Sciences, Washington University, St. Louis, MO63130-4889, USA

Extinct nuclides ^{129}I and ^{244}Pu or their isotopic and elemental ratios ($^{129}I/^{127}I$) and ($^{244}Pu/^{238}U$) have been yielding unique information as to the early chronology of meteorites. However, these data have not been fully exploited in the case of the Earth, primarily because of difficulty in estimating the abundance of these extinct nuclides. Earth's evolution would further complicate the interpretation of the extinct isotopic data, if obtained.

To tackle this problem, we adopt the "coherent degassing assumption" [1] in estimating the initial isotopic ratios $(^{129}I/^{127}I)_0$ and $(^{244}Pu/^{238}U)_0$ in the Earth. This assumes that iodine and uranium in the crust are the measures of the ^{129}I and ^{244}Pu associated with the atmospheric $^{129}Xe^*$ and $^{136}Xe_{sf}$. Hence, we infer the values of $(^{129}I/^{129}I)_0$ and $(^{244}Pu/^{238}U)_0$ in the Earth from the atmospheric excesses in ^{129}Xe and ^{136}Xe, and iodine and uranium contents in the crust. With I = 1.55 ppm [2], U = 0.91 ppm [3], excess ^{129}Xe = 6% [4} and ^{136}Xe = 2.8% [5], we estimate $^{129}I/^{127}I = 10^{-6}$ and $^{244}Pu/U = 2.4 \times 10^{-3}$ for the Earth.

The above estimated initial ratios are considerably smaller than values characteristic of meteorites, i.e., $^{129}I/^{127}I \approx 10^{-4}$ and $^{244}Pu/U \approx 7 \times 10^{-3}$. A formal interpretation would be that the Earth formed about 100 Ma later than meteorites. However, this conclusion should be examined with reference to other constraints on terrestrial xenon. Among such constraints, "missing Xe" seems to be most relevant. Both meteorites and the Earth (except for Xe) show systematic enrichment in heavier noble gases relative to the solar

abundance. This can be reasonably well understood if we assume that meteorites and the Earth trapped noble gases from the solar nebula; partition of noble gases between gas and solid generally results in enrichment of heavier noble gases in the solid objects. Comparative studies of meteorite and terrestrial noble gases support this view [6]. We therefore think that "missing Xe" is real, that is, the primordial terrestrial Xe must be much larger than the currently observed amount in the Earth's atmosphere. Recent studies of noble gas characteristics under high pressures (>5 GPa) suggest that considerable fraction of heavier noble gases, especially Xe, may be retained in deeper mantle or in the iron core [7]. Therefore, we examine $^{129}I/^{127}I$ - $^{244}Pu/U$ systematics taking account of missing Xe as an additional constraint.

We discuss the $^{129}I/^{127}I$ - $^{244}Pu/U$ systematics with the aid of a $^{129}I/^{127}I$ - $^{244}Pu/U$ diagram (Figure 1). Since $^{244}Pu/U$ is likely to be little affected by fractionation, the change in the values of $^{129}I/^{127}I$ and $^{244}Pu/U$ in meteorites and the Earth are essentially due to radioactive decay. Taking Bjurbole as a reference in the $^{129}I/^{127}I$ - $^{244}Pu/U$ diagram, we can then construct a growth curve corresponding to the time evolution of the isotopic and elemental ratios. Within the experimental uncertainties, we may argue that the Earth representative point corresponding to the above estimated terrestrial ratios lies on the growth curve. This might appear to suggest that the large difference in $^{129}I/^{127}I$ and $^{244}Pu/U$ between meteorites and the Earth is essentially due to the difference in the time of formation. However, if we accept the "missing Xe", this would further constrain the formation time interval of the Earth. For example, we see from Figure 1 that for 90% missing Xe, the formation of the earth may postdate Bjurbole by about 60 Ma.

[1] Schwartzman D. (1973) Nature Phys. Sci., *245*, 20. [2] Deruell et al., (1992) E.P.S.L, *108*, 217. [3] Taylor S.R. and S.M. McLenann, (1985) The continental crust: its composition and evolution. pp.312, Blackwell Sci. Publ., [4] Pepin R.O. (1991) Icarus *92*, 2. [5] Igarashi G. (1995) Proc. Conf. 341; Volatiles in the Earth and solar

system, ed. K.Farley, pp70-80. Amer. Inst. Physics. [6] Ozima M. et al. (1998) G.C.A.*62*, 301. [7] Jephcoat A. (1998) Nature (in press)

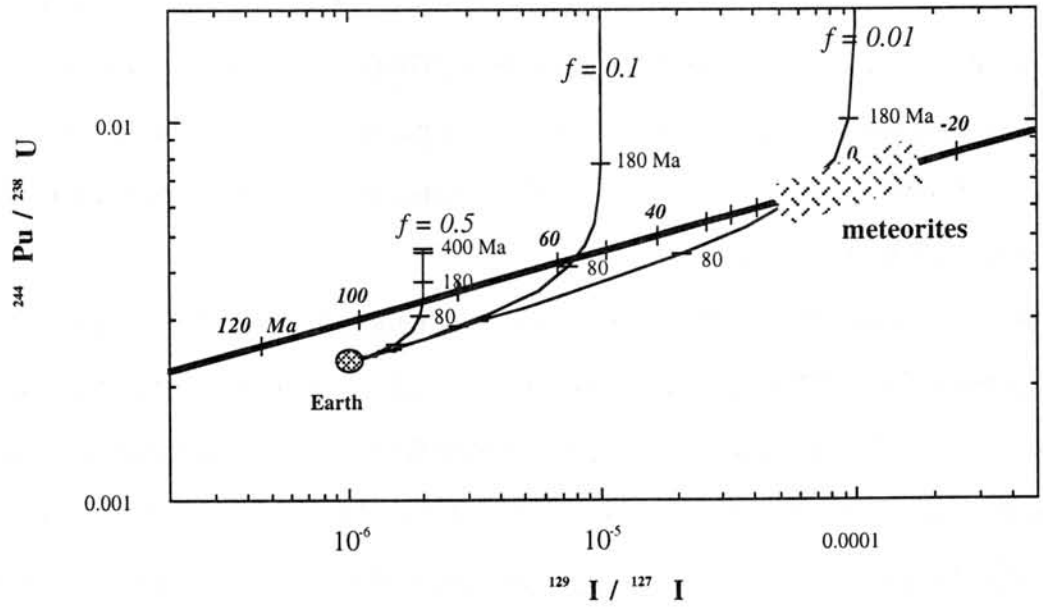

Figure 1. The thick curve indicates $^{244}Pu/^{238}U$-$^{129}I/^{127}I$ evolution in the solar system, where vertical ticks indicate the time (Ma) after the formation of Bjurbole meteorite. Thin curves represent trajectories on which putative primordial terrestrial Xe should lie if "missing Xe" took place in the Earth. The curves are shown for different values of f; f indicates the remaining fraction of Xe (now observed in the atmosphere) after the "missing Xe". The horizontal ticks on the curve correspond to the time (Ma after formation of the Earth) when the "missing Xe" event took place.

THE NOBLE GAS RECORD OF YAMATO 82102, 86009 AND 86751 AND A COMPARISON WITH OTHER ANTARCTIC CARBONACEOUS CHONDRITES

Peter SCHERER and Ludolf SCHULTZ
Max-Planck-Institut für Chemie, Abt. Kosmochemie, Postfach 3060, D-55020 Mainz, scherer@mpch-mainz.mpg.de.

Since 1969, Japanese, American and European search parties have recovered a considerable number of carbonaceous chondrites from Antarctic blue ice fields. Carbonaceous chondrites are subdivided according to their chemical and petrological properties into seven main groups - CI, CM, CO, CV, CK, CR and CH [1,2]. Some carbonaceous chondrites belong to small grouplets, others are still ungrouped. Noble gas studies are one means of providing clues to their origin and intergroup relationships among them and may contribute to a better understanding of this class. We have studied the noble gas abundance and isotopic composition of He, Ne, Ar as well as the concentrations of the major isotopes of Kr and Xe in Y 82102,73 (CK5), Y 86009,60 (CV3) and Y 86751,80 (CV3). Their noble gas contents (Tab. 1) are compared with other investigated Antarctic carbonaceous chondrites of CO, CV, CK and CR type.

Cosmic-ray exposure ages (CREA) were calculated as described by [3,4]. Production rates for the CK chondrite Y 82102 were evaluated using average bulk chemistry data for CK-chondrites. To correct for shielding we had to adopt an average value for cosmogenic $^{22}Ne/^{21}Ne$ of 1.11 for both CV3 chondrites because of abundant solar type noble gases which mask the true cosmogenic ratio. We obtain T21-Ne ages of 16.9 ± 2.5 Ma for Y 82102 and mean values of 5.6 ± 0.8 Ma and 22.3 ± 3.3 Ma for Y 86009 and Y 86751, respectively. The ages for all three meteorites lie within the range of other carbonaceous chondrite CREA of the corresponding type.

The Ne composition of Y 82102 is entirely dominated by the cosmogenic component like all other Antarctic and non-Antarctic CK-chondrites (Fig. 1). Both CV chondrites, however, contain solar type noble gases indicated by the high $^{20}Ne/^{22}Ne$ ratios of up to 10.74. Fitting a line through both bulk measurements of each sample yields a composition which lies in both cases between SEP (solar energetic particles) and SW (solar wind) with Y 86751 passing very close to the SEP endmember value. The Ar composition for the latter meteorite makes an additional contribution of planetary Ne very likely and stepwise heating experiments are in progress to study this in more detail. The planetary trapped noble gases ^{84}Kr and ^{132}Xe are correlated with the petrological type in carbonaceous chondrites. The lower the type, the higher the abundance of both nuclides (Fig. 2). The CO chondrites contain the highest amounts of trapped gases within the type-3 field. The CV chondrites are on average characterized by lower values. Both CV3 chondrites yield $^{84}Kr > 38 * 10^{-10}$ cm^3 STP/g and thus plot at the upper end of other CV3 values. The concentrations of trapped gases decrease with higher types 4, 5 and 6. Y 82102 fits between the C5/6 and C4 field with an ^{84}Kr of $\sim 1 * 10^{-10}$ cm^3 STP/g. The noble gases of all three samples are not influenced by terrestrial alteration because they fit on or slightly above the correlation line whereas weathered samples would drop below the line like some of the type 3 and type 4 meteorites indicated by the open symbols [5].

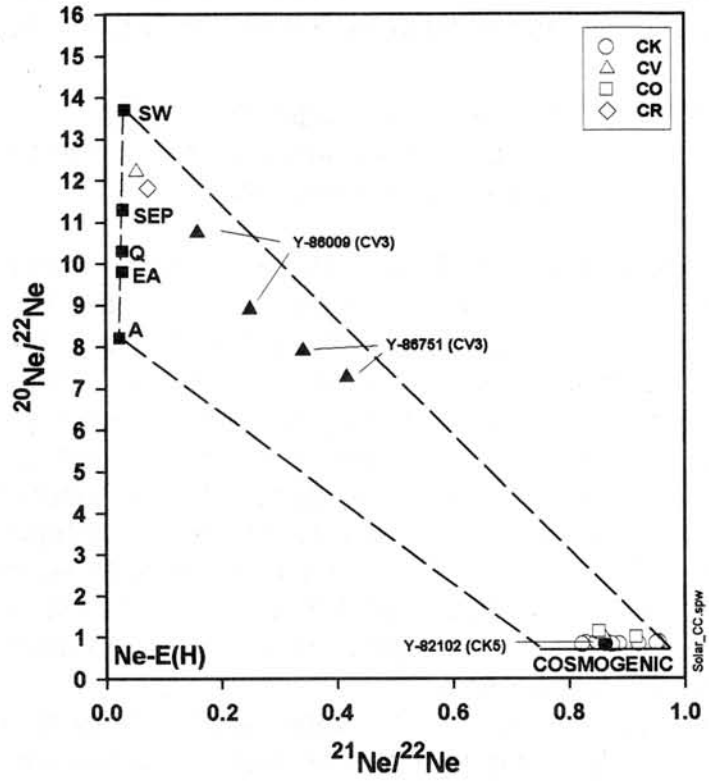

Fig.1: Neon-3-isotope plot with Yamato samples (filled symbols) and other investigated Antarctic carbonaceous chondrites (open symbols).

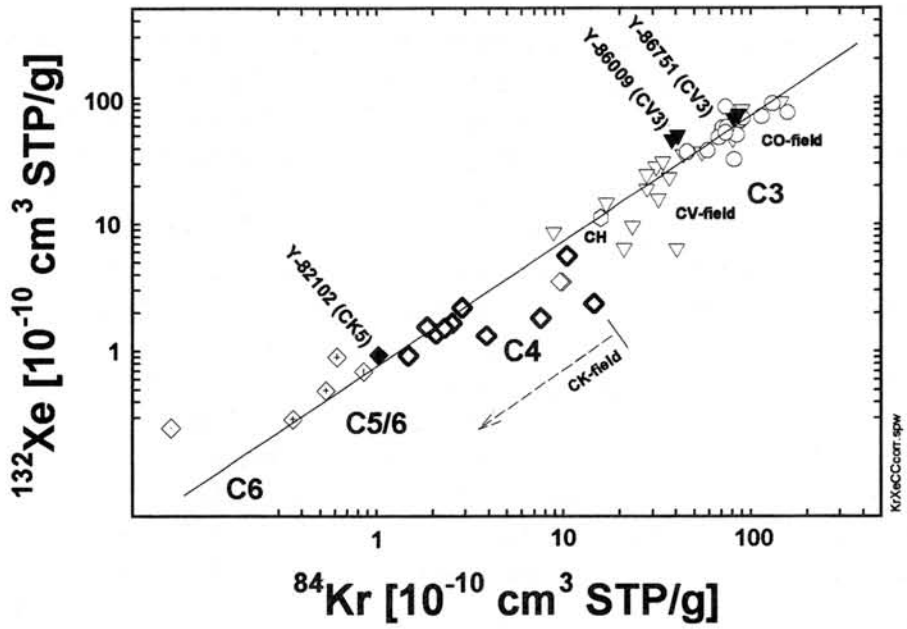

Fig.2: Planetary trapped noble gases in carbonaceous chondrites are correlated with their petrologic-chemical type. The lower the type, the higher the abundance of ^{84}Kr and ^{132}Xe.

Tab. 1: Measured noble gas nuclide concentrations (in units of 10^{-8} cm^3 STP/g for He, Ne, Ar and 10^{-12} cm^3 STP/g for Kr and Xe).

Name		^{3}He	^{4}He	^{20}Ne	^{21}Ne	^{22}Ne	^{36}Ar	^{38}Ar	^{40}Ar	^{84}Kr	^{129}Xe	^{132}Xe
Y-82102	CK5	25.87	1782	4.25	4.41	5.12	2.16	0.96	1886	103	457	93
Y-86009	CV3	12.88	23520	146.50	2.16	13.64	57.96	11.16	799	4090	5430	5010
		10.88	15550	70.04	1.96	7.86	53.06	10.44	767	3810	5120	4620
Y-86751	CV3	27.67	21340	137.90	7.92	18.98	169.30	33.40	1203	8620	9210	7330
		27.55	27200	163.50	7.05	20.69	155.40	30.89	1641	8110	9320	6800

Uncertainties are ± 5% for He, Ne and Ar and ± 12% for Kr and Xe.

Acknowledgments

We thank the National Institute of Polar Research for providing the samples for analysis.

References

[1] Kallemeyn, G.W. et al., *GCA* **55**, 881-892 (1991); [2] Rubin, A.E., *Meteorit. Planet. Sci.* **32**, 231-247 (1997); [3] Eugster, O., *GCA* **52**, 1649-1659 (1988); [4] Schultz, L. et al., *GCA* **55**, 59-66 (1991); [5] Scherer, P. et al., *Noble Gas Geochemistry and Cosmochemistry* (ed. by J. Matsuda), TERRAPUB, Tokyo, pp. 43-53 (1994).

THE ORIGINS OF CHONDRULES AND CHONDRITES.

Derek W. G. Sears, Cosmochemistry group, Department of Chemistry and Biochemistry, University of Arkansas, Fayetteville, Arkansas 72701.

Introduction

The question of the origins of chondrules and chondrites is two-hundred years old. The essential details are known; chondrites are as old as the solar system (4.6 Ga), have solar composition in all but the most highly volatile elements, and have unique textures that include chondrules [1]. Yet despite this there is considerable controversy as to the origin of the chondrites and the chondrules they contain [2,3]. A great many suggestions involving pre-solar, nebular and parent body processes have been discussed [4,5]. There are important clues. The nature of the chondrules, and their diversity, tell us something about conditions in the early solar system and accounts for many bulk properties of chondrites, as does their abundance in the various classes of meteorite [6]. The size and abundance of chondrules and metal grains tell us that sorting was important in making chondrites [7]. The peaks in the cosmic ray exposure age histograms and K-Ar ages tell us that most chondrites originated on very few parent bodies [8,9], and the spectral reflectivity of the asteroids tells us that very few asteroids are potential meteorite parent bodies [10]. Even if space weathering is a real and important process, less than 11% of the asteroids are potential meteorite parent objects. If space weathering is unimportant, then less than 1% of the known asteroids are potential parent bodies. We also know that the chondrites may be sorted into a number of discrete groups depending on bulk composition, the oxidation state of the iron, the relative abundance of metal, chondrules and matrix, and the relative abundance of the three isotopes of oxygen (Table 1). It seems likely that several of these are related through chondrule formation and the so-called metal-silicate fractionation. Finally, we know that surface processes have been important in the history of meteorites, since virtually all chondrites are brecciated, gas-rich regolith breccias occur in all classes, and many meteorites are now thought to be impact melt rocks [11,12]. In attempting to put all this together to identify an origin for chondrules and chondrites, I think two processes stand out as particularly important. These are the formation of the chondrules and the metal-silicate fractionation, and I think that there is a high likelihood that they were both processes that occurred on the surface of their parent bodies.

Table 1. The chondrite classes, particle sizes and metal abundances and certain compositional properties*.

	EH	EL	H	L	LL	CV	CO	CM	CI	
Physical properties										
Chondrule diam. (mm)	0.2-0.6	0.8	0.3	0.7	0.9	1.0	0.2-0.3	0.3	--	[13, 14]
Metal grain size (mm)	--	--	0.20	0.18	0.14	--	--	--	--	[7]
Chondrule abund. (vol %)	20-40	20-40	65-75	65-75	65-75	35-45	35-40	~15	0	[13, 14]
Metal abund. (wt %)	22	18	16	6	2	0-7	0-5	0	0	[15]
Matrix abund. (vol %)	<5	<5	10-15	10-15	10-15	40-50	30-40	~60	100	[13, 14]
Compositional properties										
Carbon (wt %)	0.42	0.32	0.11	0.12	0.22	0.43	0.38	1.82	2.8	[16]
Water (wt %)	1.9	1.6	0.22	0.46	0.71	0.25	3.3	10.4	16.9	[16]
Fe_m/Fe_t (a/a)	0.76	0.83	0.58	0.29	0.11	0-0.3	0-0.2	0	0	[15]
Fe/Si (a/a)	0.95	0.62	0.81	0.57	0.52	0.76	0.77	0.80	0.86	[15]
Mg/Si (a/a)	0.77	0.83	0.96	0.93	0.94	1.07	1.05	1.05	1.05	[15]
Ca/Si (a/a)	0.035	0.038	0.050	0.046	0.049	0.084	0.067	0.068	0.064	[15]
$\delta^{17}O$ (‰)	3.0	2.7	2.9	3.5	3.9	~-4.0	~-5.1	~4.0	~8.8	[15]
$\delta^{18}O$ (‰)	5.6	5.3	4.1	4.6	4.9	~0	~-1.1	~12.2	~16.4	[15]

* Major classes only. Small classes like CK, CH, CR, and R chondrites, the primitive achondrites and many anomalous chondrites are not considered here.

Chondrule classification

Attempting to understand objects as diverse as chondrules starts with their classification. The recently proposed compositional classification scheme for meteoritic chondrules divides the chondrules into groups depending on the composition of their two major phases; olivine (or pyroxene) and the mesostasis, both of which are genetically important [17, 18]. The scheme is described in Table 2. Compositional fields on

plots of CaO *vs.* FeO for olivine and normative quartz-albite-anorthote for mesostasis enable the identification of eight discrete classes, of which four are found in primitive (*i. e.* essentially unmetamorphosed) chondrites and

Table 2. Definition of the chondrule groups and frequency of occurrence in two primitive ordinary chondrites, Krymka (LL3.1) and Semarkona (LL3.0)*.

	Mesostases			Olivine		Frequency‡	
	CL	Composition†¥tab	CL	%FeO	%CaO	Krymka (51)	Semarkona (76)
A1	yellow	Pl(An>50%)	red	<2	>0.17	3.6	10.5
A2	yellow	Pl(An>50%)	none/dull red	2-4	0.1-0.2	0.0	25.0
A3	blue	Pl(An>50%)	red	<4	>0.2	33.3	0.0
A4	blue	Pl(An>50%)	none/dull red	>4	0.16-0.3	7.3	0.0
A5	blue	Pl(An<50%)	none	>4	<0.25	14.5	5.0
B1	none	>30% Qtz	none	4-25	0.08-0.3	0.0	56.9
B2	none	30-50% Qtz	none/dull red	10-25	0.08-0.3	36.4	0.0
B3	purple	15-30% Qtz	none	15-20	<0.08	0.0	2.6

* Phase compositions given as a guide, the group fields are not rectangular (see references [17, 18], for details). 'CL' refers to cathodoluminescence color.

†¥tab Normative composition (wt%) of the mesosotasis: Pl, plagioclase; An, anorthite; Qtz, quartz.

‡¥tab The figures in parentheses indicate the number of chondrules on which the statistics are based. Semarkona data from [19], Krymka data from [6].

four are found in metamorphosed chondrites and are the result of metamorphism of the primitive groups. Group A5 is unique in that it appears in both metamorphosed and unmetamorphosed chondrites, although the degree of compositional heterogeneity decreases with metamorphism. The compositional classification scheme for chondrules is compared with previous schemes in Table 3. The main advantage of the present scheme is that (aside from its suitability for rapidly classifying chondrules in a survey mode using their CL), the scheme relies entirely on the properties of the individual chondrules and avoids subjective descriptions and a knowledge of the petrographic type of the host meteorite. This is especially important for breccias. The CL of chondrules and relative abundance of chondrule classes is so sensitive to metamorphism that the scheme can be used to assign petrographic types to type 3 ordinary chondrites with a precision comparable to that of induced thermoluminescence [18].

Table 3. Comparison of the compositional classification scheme for chondrules with previously proposed schemes.

Compositional Class	Approximate previous equivalents
A1	Includes some of the droplet chondrules of Kieffer [20], some of the non-porphyritic pyroxene chondrules of Gooding and Keil [21], the type I chondrules of McSween [22], metal-rich microporhyritic chondrules of Dodd [23], and the type IA chondrules of Scott and Taylor [24].
A2	Includes the poikylitic pyroxene and type IB chondrules of Scott and Taylor [24] many of the type IAB chondrules of Jones [25, 26]
A5	There appear to be no previous observations of this chondrule group in unmetamorphosed meteorites.
B1	Dodd's [27] "lithic" or "clastic" chondrules and Dodd's [23] metal-poor microporphyritic chondrules are included in this group, as are the type II chondrules of McSween [22], Scott and Taylor [24] and Jones [28].

Diversity of chondrules, precursor mixing or reduction and evaporative loss during formation?

Many laboratory experiments have been performed that reproduce the textures observed in chondrules [28], stress the role of nucleation centers, and constrain temperatures and cooling rates of chondrules during formation [29, 30]. A great many potential processes might have occurred during the transient heating and cooling that was clearly the central feature of the processes, such as reduction by ambient gases and carbon, impact by dust, recondensation of volatiles as surface rims and diffusion of volatiles into the interiors of the chondrules [31, 32]. Most of these effects involve gas phases, but some will also involve liquid phases [33]. The major uncertainty, concerns whether chondrules acted as open or closed systems during formation [34, 35].

"Open-system" means that relatively volatile elements (like Fe, Na and K) were lost and the chondrules underwent chemical reactions with species in the environment during formation, while "closed-system" means that the various properties of the chondrules were inherited entirely from the precursors. Of course, both processes probably occurred, so the discussion really concerns the relative degree of the two processes. The refractory composition, low-FeO silicates, relatively high metal abundance and low-Ni content of the metal of group A1,2 chondrules are consistent with open-system behavior. A closed-system scenario would require that chondrule precursors were the products of earlier volatility-oxidation processes. The trend in the olivine to pyroxene ratio (which decreases from group B1 to A2 and then increases again in group A1), the smaller mean size of group A1 and A2 chondrules compared to group B1 chondrules, the relationships between oxygen isotope composition and chondrule size and peak temperature, diffusion of Na into chondrules, and the greater abundance of thick fine-grained rims around group A chondrules relative to group B chondrules are consistent with major evaporative loss, first of FeO and later SiO_2, accompanying the formation of groups A1 and A2 [6, 37]. These properties are difficult or impossible to understand in terms of closed-system behavior. It is concluded that while group A1 and A2 chondrules formed by reduction of FeO and major evaporative loss from precursors originally resembling those of CI chondrites, evaporative loss from group B1 chondrules was restricted to only the most highly volatile trace elements like Ga, Sb, Se and Zn. Thus the process that formed chondrules was capable of acting with a variety of intensities and was responsible for much of the redox differences that separate the chondrite classes.

Nebular origin of chondrules

The theories for chondrule origin involving condensation in the nebula require very high pressures, considerable subcooling, dust enrichments, or H_2 depletion and have difficulty explaining the abundance of the volatile elements and heterogeneity of certain chondrules [4, 5]. Thus they have not proved popular. Fusion of interstellar dust in the nebula by aerodynamic heating or chemical potential has not proved popular because of the "complimentary compositions" of matrix and chondrules, and other reasons [4, 5]. Fusion of nebula dust by lightning, impact or magnetic processes in the midplane and off-plane (with or without mechanical abrasion) has been the most popular idea in recent years, but requires what seem to be an alarmingly large number of non-nebular (or unusual nebular) conditions. These are:

- A high chondrule density. In some instances ~ 80 vol% of the meteorite is chondrules. However, ordinary chondrites might be over represented in the terrestrial meteorite collection, because of selection effects in ejecting meteorites from the asteroid belt and passing through the atmosphere. Spectral reflectivity data suggest that ordinary chondrites might be rare in the asteroid belt. Thus the process might be sometimes be highly efficient, but it only happens rarely.
- A $P(O_2)$ in the ambient gases that is enriched over the cosmic value by factors of about 1000. Some authors point out that increasing the dust-to-gas ratio by factors of ~1000 would have achieved the required high $P(O_2)$.
- Aerodynamic sorting requires high gas and dust densities.
- The "complimentary" composition of components suggests that the components were not separated during their chemical processing.
- Elemental and isotopic exchange during chondrule formation [38, 39] requires much higher gas densities than "nebula".
- Chondrule cooling rates were much slower than possible in the solar nebula; 1-1000 °C/h c.f. 10^6/h.
- Charged particle tracks are absent suggesting that the chondrules were not independent entities in the nebula [40].

Origin of chondrules by regolith impact

It appears that the difficulties of forming chondrules in a nebula setting are formidable. It is time to reconsider the possibility of that chondrules formed by impact. In fact, most of the objections raised twenty years ago to the formation of chondrules by impact on an asteroidal regolith [41] are no longer viable.
Impact velocities were not too low. Petrographic observations indicate that chondrule formation, accretion, metamorphism, and brecciation overlapped in time [42] and radiometric observations indicate that aggregation and lithification occurred up to ~4 x 10^6 years after the onset of accretion (marked by the formation of the refractory inclusions in carbonaceous chondrites) [43,44]. Since Jupiter formed very quickly (within ~10^5 years

of the onset of accretion, [45]) the asteroid belt was "stirred up" by resonances with proto-Jupiter (or the jovian core, [46]), so that mean relative velocities were ~5 km/s, prior to the formation of the chondrules and sufficient to produce impact melts.

Meteorite parent bodies were able to retain most of the impact ejector. Early work concerning impact on rocky asteroids suggested that ejecta velocities exceeded escape velocities [47]. However, prompted by observations that Phobos and Gaspra may have thick regoliths [48], recent work indicates that asteroids with lower strengths than that of solid rock used in earlier work would produce low ejecta velocities and 50-70% of the ejecta (depending mainly on impact velocity) that would return to the parent asteroid [49, 50]. ***Chondrule-(and other component) sorting could have occurred on the meteorite parent body.*** The evaporation of water and other volatiles from the regolith of the meteorite parent body would produce a temporary atmosphere that would "fluidize" the dust and create conditions suitable for aerodynamic and gravity sorting of chondrules. The flux and velocities of the fluids required are both surprisingly small because of the small size of the parent body. If chondrules formed in such a regolith, then the temporary atmosphere had an oxygen isotope composition near the terrestrial line on the oxygen three-isotope plot [38], similar to that of CI chondrites. ***There are lunar chondrules on the Moon's surface.*** The lack of chondrules on the lunar surface is often cited as an argument against impact origin for chondrules, yet lunar chondrules are present in Apollo 14 breccias in about the same abundance as CM chondrites (~10 vol %). Simple ballistic calculations show that crystallized impact spherules require long flight times and that only craters comparable in size to the target can achieve this. Thus most impacts on the Moon produce agglutinates or glass spherules [51]. As images of Gaspra, Ida, and Matthide demonstrate, such impacts can be important for certain asteriods and there will be bodies where chondrules dominate the local regolith.

Origin of Chondrites

If chondrules formed by impact into a regolith, and chondrules behaved as open systems during their formation, then the diversity of chondrule compositions presumably reflects the diversity in the intensity of impact. It is a small step to then assuming that the redox state of the resulatnt chondrite similarly depends on the violence of impacts locally. The remaining factor in forming chondrites concerns the matter of assembling the components, and producing small variations in the amount of matrix and metal in relation to the chondrules. The size and distribution of the chondrules and metal, that are characteristic of many classes of chondrites, suggests sorting before or during accumulation. Again, a great many mechanisms have been proposed for how this might have been achieved in the nebula, but I think it unlikely that this process occurred in the nebula because the meteorites managed to preserve compositions so close to cosmic and because aerodynamic sorting alone fails quantitatively. Density sorting is also required and this requires the presence of at least a weak gravity field. Some meteorite parent bodies must have experienced degassing in their early stage to turn CI compositions into ordinary chondrite compositions and may have had thick dusty surfaces that were easily mobilized by gases evolving from the interior. Density and size sorting may have occurred in the surface layers as the upward drag forces of gases (mainly water) acted against the downward force of gravity. This process is readily modeled quantitatively because it is analogous to the industrially important process of fluidization [52]. From fluid dynamics in porous media we calculate gas flow velocities and gas fluxes for the regolith of an asteroid-sized object heated by the impact of accreting objects and by ^{26}Al, and we find that both provide sufficient gas velocities and fluxes for fluidization (Table 4). The size and density sorting expected during this process can quantitatively explain metal and chondrule size-sorting and distribution in ordinary chondrites. This scenario is broadly in agreement with the major properties of chondritic meteorites (*i.e.*, redox state, petrologic type [53], cooling rate [54], matrix abundance, lithophile elemental ratio, etc.).

In summary, I think that most of the properties of chondrites are a result of processes occurring on the surfaces of asteroids, in a thick dynamic regolith. Chondrules are crystallized impact melt spherules, whose bulk composition and redox state depend on the severity of the impact process. Thus redox state of the chondrite was inherited largely from the chondrule-forming process, as suggested twenty years ago by Larimer and Anders [55]. Heating of a water-rich CI-like asteroid, possibly by internal radioactivities, probably by impact, produced large amounts of gaseous water that sorted the components, created the metal silicate fractionation, and removed fine-grained matrix by lifting grains clear of the surface in much the same way as dust is removed from comets [56].

Table 4. Calculated and observed metal abundances in H, L and LL ordinary chondrite meteorites.

Flow rate* u (mms^{-1})	$x_{LL} : x_L : x_H$ (weight ratio)
$1.3 \times u_{mf}$	1.0 : 2.1 : 3.9
$1.2 \times u_{mf}$	1.0 : 2.7 : 6.8
$1.1 \times u_{mf}$	1.0 : 4.5 : 7.4
(observed)	1.0 : 3.0 : 8.0

* u_{mf} refers to the minimum flow rate of LL chondrules, calculated from the Ergun equation.

References

[1] Kerridge J. F. and Mathews M. S. eds. (1988) *Meteoritics and the Early Solar System.* Univ. Arizona Press, Tucson. [2] King E. A. ed. (1983) *Chondrules and Their origins.* Lunar and Planetary Insitute, Houston. [3] Hewins R. H., Jones R. H. and Scott E. R. D., eds. (1996) *Chondrules and the Protoplanetary Disk.* Cambridge Univ. Press, Cambridge. [4] Grossman J. N. (1988) In *Meteoritics and the Early Solar System*, (Kerridge J. F. and Matthews M. S. eds.), 680-696. [5] Boss A. P. (1996) In *Chondrules and the Protoplanetary Disk*, (Hewins R. H., Jones R. H. and Scott E. R. D., eds.), 257-263. [6] Huang S., Lu J., Prinz M., Weisberg M. K., Benoit P. H. and Sears D. W. G. (1995) *Icarus* **122**, 316-346. [7] Dodd R. T. (1976) *Earth Planet. Sci. Lett.* **28**, 479-484. [8] Marti K. and Graf T. (1992) *Ann. Rev. Earth Planet. Sci.* **20**, 221-243. [9] Bogard D. D. (1994) *Meteoritics* **30**, 244-268. [10] Gaffey M. J., Burbin T. H. and Binzel R. P. (1993) *Meteoritics* **28**, 161-187.

[11] Keil K. (1982) In *Workshop on Lunar Breccias and Soils and the Meteoric Analogs* (G. J. Taylor and L. L. Wilkening, eds.) 65-83. [12] Rubin A. E. (1985) *Rev. Geophys.* **23**, 277-300. [13] Grossman J. N., Rubin A. E., Nagahara H., and King E. A. (1988) In *Meteoritics and the Early Solar System*, (Kerridge J. F. and Matthews M. S. eds.), 619-659. [14] Zhang Y., Benoit P. H. and Sears D. W. G. (1995) *Jour. Geophys. Res. (Planets)* **100**, 9417-9438. [15] Sears D. W. G. and Dodd R. T. (1988) In *Meteoritics and the Early Solar System*, (Kerridge J. F. and Matthews M. S. eds.), 3-31. [16] Jarosewich E. (1990) *Meteoritics* **25**, 122-145. [17] Sears D. W. G., Lu J., Benoit P. H., DeHart J. M., and Lofgren G. E. (1992) *Nature* **357**, 207-210. [18] Sears D. W. G., Huang S., and Benoit P. H. (1995) *Earth Planet. Sci. Lett.* **131**, 27-39. [19] DeHart J. M., Lofgren G. E., Jie L., Benoit P. H. and Sears D. W. G. (1992) *Geochim. Cosmochim. Acta* **56**, 3791-3807. [20] Kieffer S. W. (1975) *Science* **189**, 333-340. [21] Gooding J. L. and Keil K. (1981) *Meteoritics* **16**, 17-43. [22] McSween H. Y. (1977) *Geochim. Cosmochim. Acta* **41**, 1777-1790. [23] Dodd R. T. (1978) *Earth Planet. Sci. Lett.* **40**, 71-82. [24] Scott E. R. D. and Taylor G. J. (1983) *Proc. Lunar Planet. Sci. Conf. 14th, J. Geophys. Res.* **88**, B275-B286. [25] Jones R. H. (1992) *Lunar Planet. Sci.* **XXIII** 629-630. [26] Jones R. H. (1994) *Geochim. Cosmochim. Acta* **58**, 5325-5340. [27] Dodd R. T. (1981) Meteorites: A Petrologic Chemical Synthesis. Cambridge Univ. Press. [28] Jones R. H. (1990) *Geochim. Cosmochim. Acta* **54**, 1785-1802. [29] Hewins R. H. (1988) In *Meteoritics and the Early Solar System*, (Kerridge J. F. and Mathews M. S. eds.), 680-696. [30] Lofgren G. E. (1989) *Geochim. Cosmochim. Acta* **53**, 461-470. [31] Hewins and Connolly H. C. (1996) In *Chondrules and the Protoplanetary Disk*, (Hewins R. H., Jones R. H. and Scott E. R. D., eds.), 197-211. [32] Yu Y., Hewins R. H. and Zanda B. (1996) In *Chondrules and the Protoplanetary Disk*, (Hewins R. H., Jones R. H. and Scott E. R. D., eds.), 213-219. [33] Grossman J. N. (1996) *Lunar Planet Sci.* **XXVII** 467-468. [34] Wai C. M. and Wasson J. T. (1979) *Earth Planet. Sci. Lett.* **36**, 1-3. [35] Larimer J. T. and Anders E (1967) *Geochim. Cosmochim. Acta* **31**, 1229-1370. [36] Sears D. W. G., Huang S. and Benoit P. H. (1996) In *Chondrules and the Protoplanetary Disk*, (Hewins R. H., Jones R. H. and Scott E. R. D., eds.), 221-231. [37] Matsunami S., Ninagawa K., Nishimura S., Kubono N., Yamamoto I., Kohata M., Wada T., Yamashita Y., Lu J., Sears D. W. G. and Nixhimura H. (1993) *Geochim. Cosmochim. Acta* **57**, 2101-2110. [38] Clayton R. N., Mayeda T. K., Goswami J. N. and Olsen E. J. (1991) *Geochim. Cosmochim. Acta* **55**, 2317-2337. [39] Thiemens M. H. (1996) In *Chondrules and the Protoplanetary Disk*, (Hewins R. H., Jones R. H. and Scott E. R. D., eds.), 107-118. [40] Allen J. S., Nozette S. and Wilkening L. L. (1977) *Geochim. Cosmochim. Acta* **44**, 1161-1175. [41] Taylor G. J., Scott E. R. D. and Keil K. (1983) In *Chondrules and Their Origins.* (King E. A. ed.), 262-278. [42] Scott E. R. D., Lusby D. and Keil K. (1985) *Proc. Lunar Planet. Sci. Conf.* **16th**, D137-D148. [43] Podosek F. and Cassen P. (1994) *Meteoritics* **29**, 6-25. [44] Russell S. S., Srinivasan G., Huss G. R., Wasserburg G. J., and McPherson G. J. (1996) *Science* **273**, 757-762. [45] Cameron A. G. W. (1995) *Meteoritics* **30**, 133-161. [46] Davis D. R., Chapman C. R., Greenberg R., Weidenschilling S. J. and Harris A. W. (1979) In *Asteroids* (Gehrels T., ed.), 528-557. [47] Housen K. R., Wilening L. L., Chapman C. R. and Greenberg R. (1979) *Icarus* **39**, 317-351. [48] Chapman C. R., Davis D. R., Neukum G., Ververka J., Belton M. J. S., Johnson T. V., Morrison D., McEwen A. (1992) *Lunar Planet Sci.* **XXIII** 219-220. [49] Housen K. R. (1992) Lunar Planet Sci. XXIII 555-556. [50] Asphaug E. and Nolan M. C. (1992) Lunar Planet Sci. XXIII 43-44. [51] Symes S. J. K., Sears D. W. G., Akridge D. G., Huang S. and Beniot P. H. (1998) *Meteorit. Planet. Sci.* **33**, 13-29. [52] Huang S., Akridge G. and Sears D. W. G. (1996) *Jour. Geophys. Res. (Planets)* **101**, 29,373-29,385. [53] King E. A. (1972) *Proc. Third Lunar Sci. Conf.* 673-686. [54] Ackridge G., Akridge G., Benoit P. H., and Sears D. W. G. (1997) *Icarus* (in press). [55] Larimer J. W. and Anders E. (1967) *Geochim. Cosmochim. Acta* 31, 1239-1270. [56] Sears D. W. G., Huebner W. and Kochan H. (1998) *Meteorit. Planet. Sci.* (submitted).

H, C AND N ISOTOPIC COMPOSITIONS OF GRAPHITE IN SOME PRIMITIVE ORDINARY CHONDRITES. N. Sugiura and K. Kiyota, Department of Earth and Planetary Physics, University of Tokyo, Tokyo, Japan, sugiura@geoph.s.u-tokyo.ac.jp

Graphite in primitive ordinary chondrites has been reported to contain isotopically heavy nitrogen [1,2,3,4,5] and hydrogen [2,3]. It has been suggested that such graphite (or the precursor) originated in the interstellar molecular cloud [3]. Thus, it is expected that important information on the molecular cloud and the primitive solar nebula may be recovered from these graphite grains.

We examined graphite from four primitive ordinary chondrites; Dimmitt, Mezo Madaras, Yamato74191 and ALHA77167. By stepped combustion experiments of bulk samples, the former three chondrites are known to contain isotopically heavy nitrogen while the latter chondrite is known to contain a small amount of isotopically light nitrogen. Thick polished sections were prepared and examined with a SEM. Several tens of graphite grains were observed in a section of less than $1cm^2$ of these chondrites, except for Yamato74191 for which graphite grains are much more scarce. In many cases graphite is associated with metal, sulfide or oxide (magnetite). In the case of Dimmitt, graphite is almost always found in metal and/or magnetite grains. In the case of Mezo Madaras, a few graphite grains were found in chondrules. In the cases of Dimmitt and one of the Mezo Madaras samples, the polished sections were preheated to 300C for 30 minutes under high vacuum to remove terrestrial contamination. The Yamato74191 and ALHA77167 samples were not preheated. H, C and N isotopic compositions and H^-/C^- and CN^-/C^- ratios were measured in situ by SIMS using Cs primary ions.

ALHA77167

H, C and N isotopic compositions of graphite in ALHA77167 are nearly normal. H^-/C^- ratio ranges from 0.015 to 0.036, except for a high value (0.22) for a graphite grain in magnetite. CN^-/C^- ratio ranges from 0.0035 to 0.018, except for a high value (0.04) for the graphite grain in magnetite.

Dimmitt

N isotopic composition of graphite in Dimmitt is heavy. The highest delta ^{15}N value is about 570 permil, which is higher than the value (217 permil) observed by the stepped heating measurement. It is to be noted that this high value was obtained after repeated measurements on the same spot. During this repeated measurements, the CN^-/C^- ratio decreased from 0.045 to 0.016. This suggests that terrestrial nitrogen contamination is significant even though the sample has been preheated in vacuum. Similarly, the isotopic composition of H increased (the highest D/H is 2.42E-4) and H^-/C^- ratio decreased from 0.02 to 0.01 during repeated measurements on the same spot. Since we have not measured a standard graphite sample with known D/H ratio by SIMS, the D/H ratio cannot be translated to a delta D value. But if we assume that there is no instrumental fractionation, then it corresponds to about 630 permil. C isotopic composition of graphite in Dimmitt is not particularly anomalous.

Mezo Madaras

N isotopic composition of graphite in Mezo Madaras is heavy. Our highest delta ^{15}N value measured by SIMS is 297 permil [4] , while that reported by [3] is 275 permil. These values are fairly consistent with the 229 permil obtained by stepped combustion experiment of the bulk sample. Again, it is to be noted that the delta ^{15}N value usually increases by repeated measurements on the same spot, suggesting that terrestrial contamination is significant. It is observed, however, that the relationship between the delta ^{15}N and the CN^-/C^- ratio obtained from repeated measurements on the same spot is different from the relationship among different graphite grains. Therefore, it seems possible that each graphite grain has different indigenous nitrogen isotopic composition. CN^-/C^- ratio ranges from 0.0057 to 0.080. This is on the average larger than those for ALHA77167 and Dimmitt.

H isotopic composition of graphite in Mezo Madaras is heavy. The highest D/H ratio is 5.63E-4 which corresponds to delta D = 2800 permil, assuming no instrumental fractionation. This ratio is very large and exceeds the previously reported highest value of 1500 permil for graphite in Khohar [3]. H^-/C^- ratio ranges from 0.022 to 0.076, which is

on average larger than those for Dimmitt and ALHA77167. It is to be noted that the highest delta D was obtained for a preheated sample, an unheated sample also has heavy hydrogen. It is also to be note that the high value of D/H is accompanied by a relatively low delta ^{15}N value (less than 100 permil). C isotopic composition of graphite in Mezo Madaras is not particularly anomalous.

Yamato74191

The highest nitrogen isotopic anomaly measured by SIMS is about 300 permil while a bulk sample measured by stepped combustion showed an anomaly close to 1000 permil. The highest D/H ratio is about 1.7E-4. Contamination may be the main cause that produced these rather small isotopic anomalies.

Discussion

It appears that isotopic compositions and chemical compositions of graphite in primitive ordinary chondrites are quite diverse. Although difference in C isotopic compositions of graphite in three chondrites is small, the difference is probably significant [6]. Isotopic compositions of nitrogen of graphite in four chondrites seem to be significantly different. The present result on nitrogen in ALHA77167 and Yamato74191 may be dominated by terrestrial contamination. But there seems to be significant difference in the N isotopic composition between Mezo Madaras and Dimmitt. Hydrogen isotopic compositions of graphite in the four chondrites also seem to be different.

Hydrogen concentration (H^-/C^-) and nitrogen concentration (CN^-/C^-) in graphite are also somewhat different among these chondrites. There appear to be no clear correlation between H isotopic composition and H abundance among graphite of the four chondrites. This statement is correct if we neglect the trend observed by repeated measurements on the same spot, which can be interpreted as removal of terrestrial contamination. Also there appear to be no clear correlation between N isotopic composition and N abundance among graphite of the three chondrites. Again this statement is correct if we neglect the trend observed by repeated measurements on the same spot.

Even within a single chondrite, there may be graphite grains with different isotopic compositions as suggested by [3]. The number of graphite grains we analyzed is small at the moment. But there seem to be two types of graphite in Mezo Madaras.

Graphite in ALHA77167 is isotopically normal and contains relatively small amounts of nitrogen and hydrogen. If the nitrogen and hydrogen are not dominated by terrestrial contamination, this graphite could well be formed in the solar system.

Large isotopic anomalies of H and N are strong evidence for the presolar origin of the graphite in Dimmitt, Mezo Madaras and Yamato74191. However, so far, all the H and N isotopic compositions are heavy. Therefore, they could be, in principle, produced by fractionation from isotopically normal materials within the solar system. Their association with metal, sulfide and/or magnetite is rather unexpected for presolar grains. Further studies on the isotopic compositions and petrographic features of graphite on larger numbers of graphite grain are needed for confirmation of the presolar origin of the graphite.

References: [1] S. Mostefaoui et al. (1997) LPSXXVIII, 989-990. [2] S. Mostefaoui et al. (1997) Antarctic Meteorites XXVII,121-123. [3] S. Mostefaoui et al. (1997) Meteoritics & Planet. Sci. 32, A95. [4] N. Sugiura and K. Kiyota (1997) Antarctic Meteorites XXVII, 171-173. [5] N. Sugiura and K .Kiyota (1997) Meteoritics & Planet. Sci. 32, A126. [6] M.M. Grady (1989) Meteoritics 24, 147-154.

CUARTAPARTE METEORITE: A faulted ordinary chondrite.

G. Sánchez-Rubio*, J. Martínez-Reyes***, A.M. Reyes-Salas*, J. Robles-Camacho**, J.T. Vázquez-Ramírez*, and D. Flores-Gutiérrez****

*) Instituto de Geología (UNAM), Ciudad Universitaria, Apartado Postal 70-296, 04510 México, D.F.
**) Instituto Nacional de Antropología e Historia, México, D.F.
***) Estación Regional del Centro (Instituto de Geología, UNAM), Juriquilla, Qro.
****) Instituto de Astronomía, Ciudad Universitaria, México, D.F.

A stony meteorite (chondrite, L4) with abundant signs of faulting, i.e. slicken sides, fell in the area next to Cuartaparte, on April 27, 1995.

Cuartaparte is the name of a small village located at the foot of the Sierra de Guanajuato, in Central Mexico (20°56'N, 101°21'W). Silao is the nearest town in the area. Gentle hills somewhat dissected by intermittent small rivers make up the scenery. The area is densely populated and land is farmed intensely. Farmers in the area describe the fall of the meteorite, which occurred just after noon, as very noisy - with thunders followed by buzzing sounds. One of the stones was still hot when recovered soon after its impact on land, a few meters only from a young farmer. Three small pieces (247.8 grams, largest) were recovered during field work in the area and a fourth one (197.8 grams) was provided to us by Prof. Salvador Ulloa but it is said that other pieces have also been found.

The meteorite is light gray in colour with a slight greenish tint inside, and it has the characteristic black crust. The shape of the fragments is irregular. Slicken sides are an outstanding feature of the Cuartaparte meteorite. They cut across the rock in all directions and are rather shiny surfaces, black or brown in colour. Chemical composition of a slicken side reveals the occurrence of mafic minerals (olivine and pyroxene), but iron-nickel and troilite were also involved.

The chondrite is regolithic in nature with small isolated volumes of fine sand, all in highly compact rock. Seen under the microscope, the rock shows a variety of crystalline textures as well as small volcanic-like masses; altogether, texture is extremely variable throughout the meteorite.

Chondrules, about 15% in volume, show rather well defined borders. Criptocrystalline and excentroradial types are predominant, but micro-porphyritic, barred, and polycrystalline types occur as well.

Olivine (Fa23), enstatite, plagioclase, kamacite, chromite, and troilite are the main components of the Cuartaparte meteorite. Olivine and pyroxene are the main components of chondrules. Opaque minerals constitute, on average, 12.4% volume of the rock. Extinction as well as shape of minerals are very irregular.

The matrix and glass both appear thoroughly recrystallised.

It appears that the bolide followed a trajectory from NW to SE.

Evaporation experiments of sulfur from Fe-FeS melts

Shogo TACHIBANA and Akira TSUCHIYAMA

Department of Earth and Space Science, Osaka University, Toyonaka 560-0043, JAPAN.

E-mail: tachi@ess.sci.osaka-u.ac.jp

Introduction

It is important to know evaporation behaviors of planetary materials under the solar nebula conditions in order to discuss the elemental and isotopic fractionation in the solar nebula. Evaporation kinetics of some minerals and silicate melt have been evaluated so far [e.g., 1, 2, 3, 4], while evaporation kinetics of Fe-FeS melt have not been evaluated. The Fe-FeS eutectic temperature is ~988°C (1261K). This temperature could be achieved in the inner region of the solar nebula, and it should be also achieved during the chondrule formation. Metallic iron and troilite (FeS) mixture would be melted under such conditions. Hence, it has a significant meaning to know evaporation kinetics of Fe-FeS melt to understand the behavior of Fe-FeS minerals in the inner hot region of the nebula or during the chondrule formation.

Experimental

Evaporation experiments were done in a gold image furnace (ULVAC-RHV-E44VHT), in which samples were heated by infrared light focused with gold mirrors. Details of the experimental apparatus were described in [3]. Troilite powder synthesized from pyrrhotite ($Fe_{0.886}S$) [3] was used as a starting material. The powder was pressed into a pellet (3mm in diameter and ~2mm in height), and its weight was adjusted to 50 ± 0.1mg. An alumina ring (3mm in inner diameter) was used to hold a melt droplet during an experiment instead of the conventional Pt-wire loop method because Pt reacts with Fe. The alumina rings were heated for 30min at 1100°C for dehydration before experiments. The pellet was heated at 1100 and 1200°C and at $p(H_2)=10^{-4}$ and 10^{-5}bar for different duration from 0 to 150min. Heating duration was measured after the furnace temperature achieved to the experimental temperature.

Results

The weight of the melt droplet decreases with heating duration. Fig.1 shows the residual sulfur content (wt%) in the sample plotted against heating duration. The residual sulfur content was calculated from the weight loss assuming that only sulfur evaporates from the melt. The higher temperature promote evaporation of Fe-FeS melt. Evaporation rates correspond to the slopes of the residual sulfur content - time curves. The evaporation rates within the compositional range of total melt (34.2-29.3wt% of S at 1100°C, 36.5-27wt% of S at 1200°C, Fig.2 [5]) appear to be larger in the melt with higher sulfur content.

Discussion on evaporation kinetics

If evaporation of Fe-FeS melt is controlled by the chemical reaction on the surface of the melt droplet, the evaporation rate of sulfur is expressed by the Hertz-Knudsen equation;

$$J(S) = \sum \frac{\alpha_i (p_i^{eq} - p_i)}{\sqrt{2\pi m_i kT}} \qquad (i = S - bearing\ gas), \qquad (1)$$

where p_i^{eq} is the equilibrium vapor pressure of i-th S-bearing gas, p_i is the ambient gas pressure of i-th gas in the surrounding gas atmosphere, m_i is the molecular weight of i-th gas, k is the Boltzman constant, T is the absolute temperature, and α_i is the evaporation coefficient which shows the kinetic barrier for evaporation of i-th gas. The evaporation of Fe from the melt is ignored here.

The equilibrium vapor pressure of S-bearing gas with Fe-FeS melt depends on the sulfur activity in the melt. The sulfur activity in Fe-FeS melt in [6] and thermochemical data [7] were used to calculate the equilibrium vapor pressures of S-bearing gas species. Dominant S-bearing gas species under the present experimental conditions are S_2 and HS. Hence, J(S) can be expressed approximately by the sum of $J(S_2)$ and J(HS). The residual sulfur content - time curve can be calculated by using Eq.(1). The surface area of the melt droplet, estimated by approximating the droplet to a spheroid, was assumed to be constant during evaporation, because the sizes of the droplets heated for different duration were almost the same. It should be noted that the residual sulfur content - time curve can be drawn only within the compositional range of total melt. It is difficult to estimate the evaporation flux of sulfur for the melt coexisting with Fe or FeS crystals because crystals also contribute to the evaporation.

The experimental data cannot be fitted by the ideal evaporation rate of sulfur ($\alpha_{S_2}, \alpha_{HS}$=1), while they can be fitted by the rates with α_{S_2}=0.035-0.09 and α_{HS}=0.001 (Fig.1). This indicates the existence of the kinetic barrier for evaporation. The $p(H_2)$ dependence of evaporation rates seems not to be large. This suggests that the contribution of $J(S_2)$ to J(S) is larger than that of J(HS) because the evaporation reaction of S_2 ($S(l)=1/2S_2(g)$; l:liquid, g:gas) does not include hydrogen. The larger contribution of $J(S_2)$ to J(S) can be explained by the presence of the larger kinetic barrier ($\alpha_{S_2} > \alpha_{HS}$) for evaporation of HS than that for evaporation of S_2 as suggested in [3]. The equilibrium vapor pressure of iron was also calculated, and it is much smaller than those of S-bearing gas. So, the evaporation of iron from the melt is negligible under the present experimental conditions.

Acknowledgement

This work was supported by JSPS Research Fellowship for Young Scientists (J.C.).

References

[1] Nagahara. H and Ozawa, K. (1996) *Geochim. Cosmochim. Acta*, **60**, 1445-1459. [2] Tsuchiyama, A. and Fujimoto, K. (1995) *Proc. NIPR Symp. Antarc. Meteorites*, **8**, 205-213. [3] Tachibana, S. and Tsuchiyama, A. (1998) *Geochim. Cosmochim. Acta*, in press. [4] Nagahara, H. and Ozawa, K. (1997) *Antarctic Meteorites*, **XXI**, 125-127. [5] Chase *et al.* (1985) *JANAF Thermochemical Tables, 3rd Ed.*, 1856pp. [6] Nagamori *et al.* (1970) *Trans. JIM*, **11**, 190-194. [7] Ehlers, E.G. (1972) *The Interpretation of Geological Phase Diagram.*, 280pp.

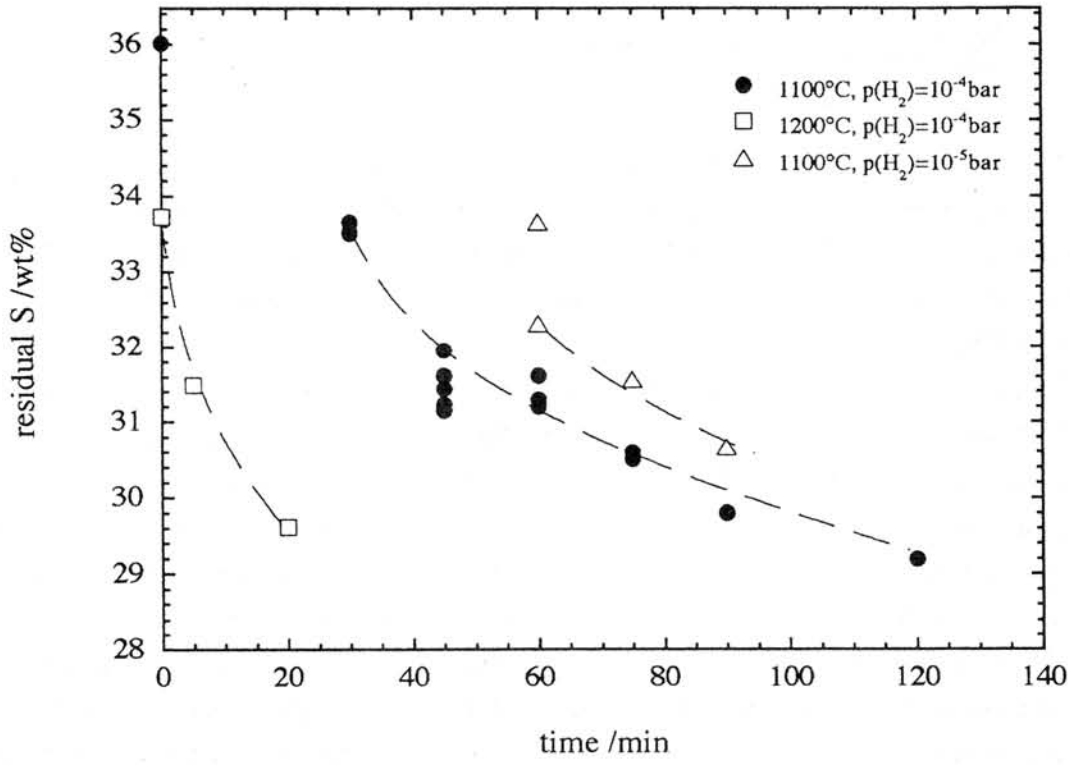

Fig.1 Residual sulfur content plotted against heating duration. The dotted lines are the calculated evaporation rates with α_{S_2}=0.035-0.09 and α_{HS}=0.001. Heating duration was measured after the furnace temperature achieved to the experimental temperature.

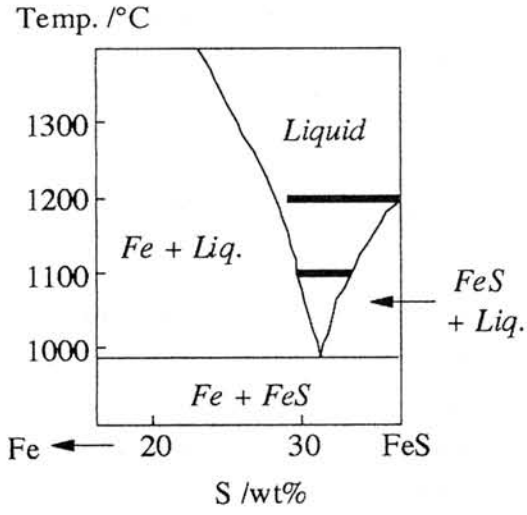

Fig.2 A schematic phase diagram of the Fe-FeS system. Thick lines express the compositional range plotted in Fig.1.

Noble gases released from Yamato-74063 primitive achondrite by crushing.

N. Takaoka[1], R. Okazaki[1]*, T. Nakamura[1], and K. Nagao[2]*

1) Department of Earth and Planetary Sciences, Kyushu University, Hakozaki, Fukuaka 812-8581.
2) Institute for Study of Earth's Interior, Okayama University, Misasa, Tottori 682-0193.
*Present address: Laboratory for Earthquake Chemistry, Graduate School of Science University of Tokyo, Hongo, Bunkyou-ku, Tokyo 113-0033.

Introduction: Yamato(Y)-74063 is an Acapulco-like primitive achondrite. It contains abundant trapped noble gases of 6 x 10^{-8} $cm^3STP^{132}Xe/g$ bulk sample [1, 2]. According to laser-probe microanalyses [3], the highest concentration of ^{132}Xe amounts to 8.5 x 10^{-7} cm^3STP/g. For a candidate of trapping sites of such large quantity of Xe, microbubbles in orthopyroxene were proposed [4]. Microbubbles in Y-74063 are found associated with inclusions such as FeNi-metal, apatite and others, and the linear occurrence of inclusions inside a crystal suggests presence of fractures which trapped them upon healing. The microbubbles and fractures, if they are trapping sites, should release trapped gases by cruching. Here we report a result of noble-gas analysis by a crushing experiment.

A tiny chip (25.8 mg) of Y-74063 is crushed with an electromagnetically driven pestle (ca. 45 g in weight) in a Mo crucible (5 cm in depth and 1.2 cm in diameter) [5]. The sample mounted in a side-arm of an extraction system is heated overnight at 150 °C to degas adsorbed atmosphere. For the sample dropped into the crucible, seven steps of crushing are made to get release patterns of noble gases. One step of crushing consists of ten to one-hundred strikes of the sample chip by the pestle. Gases evolved at a step are measured with a modified VG5400 noble-gas mass-spectrometer [3].

Results and Discussion: Figure 1 illustrates patterns for ^{36}Ar released by a strike of the pestle (Fig. 1a) and for elemental ratios of evolved gases to ^{36}Ar (Fig. 1b). Isotopic ratio $^{40}Ar/^{36}Ar$ is also given in Fig. 1b for convenience. The first step of crushing that consits of 10 strikes released relatively large amounts of gases compared with the following steps. However, the $^{40}Ar/^{36}Ar$ ratio is significantly low: 0.269. This evidently indicates that the crush-released gases are not of atmospheric origin but indigenous. Ratios of noble gas components crush-released to those for bulk sample [1, 2] are given in Fig. 2. Because of the abundant trapped Ar, it is difficult to estimate cosmogenic ^{38}Ar in crush-released Ar. It is noted that releases of cosmogenic ^{3}He and ^{21}Ne, and radiogenic ^{40}Ar are two orders of magnitude lower than those of trapped gases.

Isotopic ratios of crush-released Ar are different significantly from those for the bulk sample. The $^{40}Ar/^{36}Ar$ ratio (Fig. 1b) is x10^{-2} lower than that for the bulk sample [1, 2]. There is a small but definite difference in the $^{38}Ar/^{36}Ar$ ratio (on average, 0.18777 ± 0.00011 vs. 0.1899 ± 0.0001), too. This is because crushing released trapped Ar preferencially but not radiogenic and cosmogenic Ar. The selective release by crushing is also found of trapped Ne, though the Ne isotopic ratios may be

affected considerably by blank correction because of very low Ne contents. Crush-released Ne is enriched in trapped Ne, while bulk Ne is mostly cosmogenic (Fig.3).

After the crushing experiment, we tried to recover the crushed sample to sieve it for grain size. Recovered grains weigh 11.4 mg and are almost all silicates. We have the following grain size distribution for this recovery: 2.1mg for <42 μm, 6.1 mg for 42-95 μm, 3.2 mg for 95-430 μm, and less than 1 mg for >430 μm. Further examination is needed to know where and how the sample crystals were crushed.

The present result indicates that the trapped component of noble gas resides at sites different from the cosmogenic and radiogenic components. The latter components are produced *in-situ* at crystal lattices for target elements of spallation reactions and for radioactive nuclides. Because cosmogenic ^{3}He and ^{21}Ne are produced in almost all silicates, the release of cosmogenic ^{3}He and ^{21}Ne are supposed, to the first approximation, to be proportional to rupture surface newly formed by crushing. This is supported by a good correlation between cosmogenic ^{3}He and ^{21}Ne (Fig.4a).

On the basis of gas-release/strike, the first step (ten strikes) of crushing released 3 to 10 times trapped ^{36}Ar, compared with the following steps. There is similar tendency for cosmogenic (3 to 4 times) and radiogenic (2 to 5 times) gases. However, the amounts of cosmogenic ^{3}He appeared at the sixth and seventh steps (both a hundred strikes) are identical, while those of trapped ^{36}Ar are different by a factor of 2 (Fig.4b). The poor correlation between trapped Ar and cosmogenic gases suggests contribution to trapped Ar from sporadic sources such as microbubbles and fractures. These suggest that the first step raptured weak parts of the sample chip, such as grain boundaries and fractures in crystals, and raptured surfaces at the sixth step included more microbubbles and/or fractures than those formed at the seventh step of crushing did.

References: [1] Takaoka & Yoshida, Proc. NIPR Sym. Antart. Meteorites, 4, 178-186 (1991). [2] Takaoka et at., Proc. NIPR Sym. Antart. Meteorites, 6, 120-134 (1993). [3] Nagao & Abe, J. Mass Spectrom. Soc. Jpn., 42 35-48 (1994). [4] Takaoka et al., Proc. NIPR Sym. Antart. Meteorites, 7, 186-196 (1994). [5] Okazaki et al., Meteoritics Planet. Sci., 32, A102 (1997).

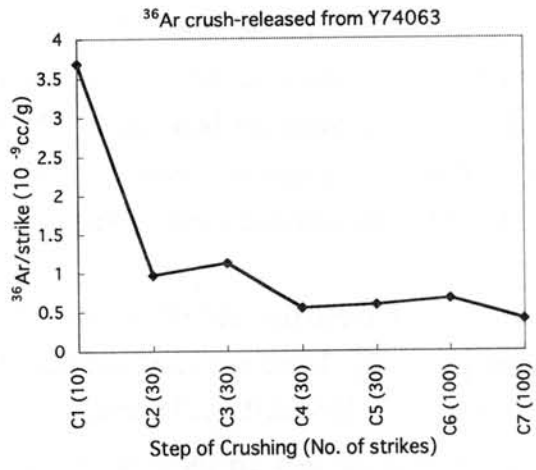

Fig.1a ^{36}Ar release/strike.

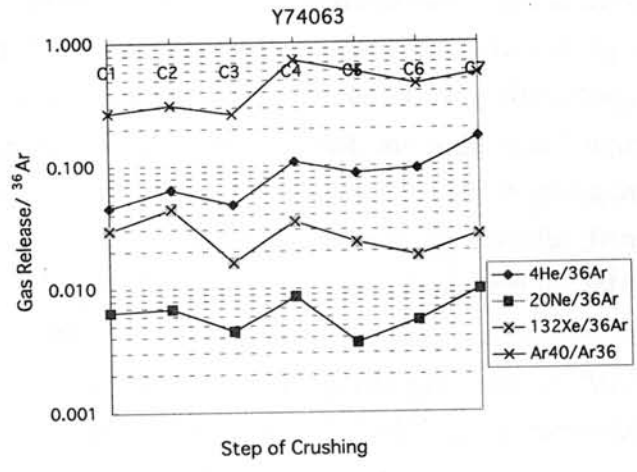

Fig. 1b Ratio of released gas to ^{36}Ar

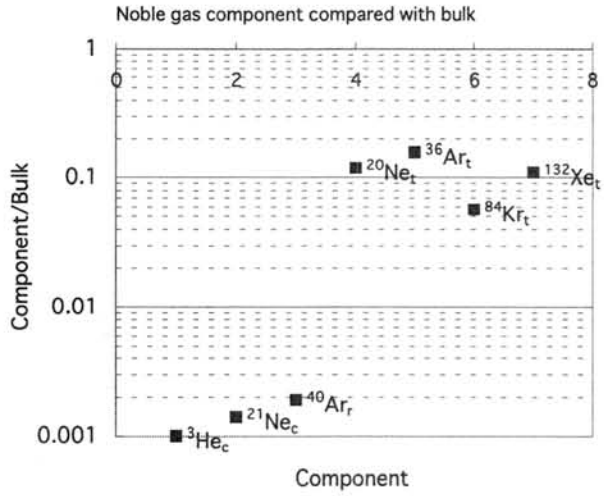

Fig.2 Ratios of cosmogenic ^{3}He and ^{21}Ne, radiogenic ^{40}Ar and trapped gases released by crushing to those for bulk sample.

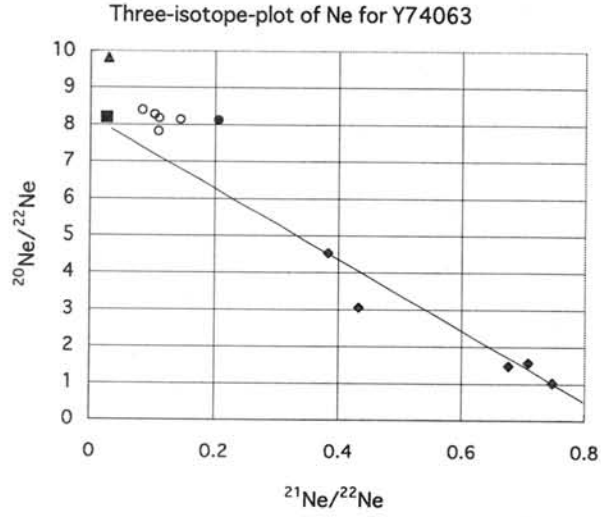

Fig.3 Three-isotope-plot of Ne. The present data (open and closed circles) are plotted near Ne-A (closed square) and above the correlation line for bulk and step-heated silicates data [1, 2].

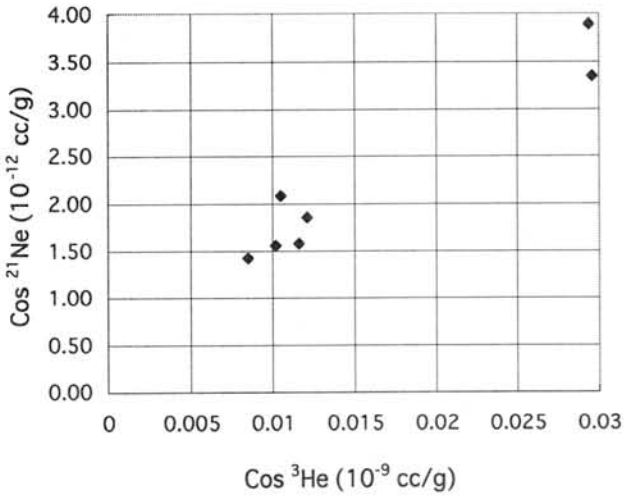

Fig.4a Correlation plot between cosmogenic ^{3}He and ^{21}Ne.

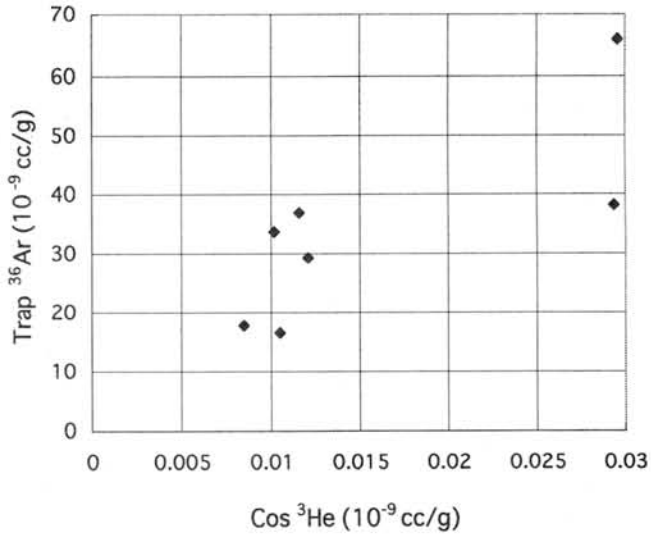

Fig.4b Correlation plot between cosmogenic ^{3}He and trapped ^{36}Ar. Cosmogenic ^{3}He released at 6th and 7th steps of crushing (two data points at righ-hand side) is identical, but trapped ^{36}Ar is different by a factor of 2.

YAMATO DIOGENITE-CUMULATE-EUCRITE BRECCIAS: THEIR CLASSIFICATION AND FORMATION ON A VESTA-LIKE BODY.

Hiroshi Takeda[1], Kazuto Saiki[2] and Teruaki Ishii[3].

[1]*Research Institute, Chiba Inst. of Technology, 2-17-1 Tsudanuma, Narashino City, Chiba 275-0016,*
[2]*Res. Inst. of Materials and Resources, Mining College, Akita Univ., Akita 010-8502,*
[3]*Ocean Res. Inst., Univ. of Tokyo, 1-15-1 Minamidai, Nakano-ku, Tokyo 164-0014, Japan.*

Introduction

A number of HED achondrites in the Yamato meteorite collections have been classified as Type B diogenites [1]. They have a common characteristic texture with shocked pyroxene fragments and glassy veins. Because Yamato 75032 is the largest and representative specimen, they are also called Y75032-type achondrite [2]. Y75032-type achondrites contain pyroxene fragments with chemical compositions slightly more Fe-rich than common diogenites and variable amounts of cumulate eucrites. Based on the mineralogical study of six such meteorites, we proposed that they are link materials between diogenites and eucrites [2]. Difficulty in classification of these achondrites with intermediate mineralogical features between diogenites and eucrites, promoted us to use an acronym, HED (Howardites, Eucrites, Diogenite) achondrites [3]. Now, astronomical evidence linking Vesta and the HED achondrites [4] allows us to interpret formation of such breccias as an event taken place on a Vesta-like body. Three large impact craters of Vesta observed by the Hubble Space Telescope [5] provide us with a more realistic view of the formation process.

16 more Y75032-type achondrites have been described in Catalog of the Antarctic Meteorites [1] with their pyroxene quadrilaterals. They show more diversity of pyroxene chemistry than those we studied previously. Y791439 contains abundant fragments of cumulate eucrites with a fragment of ordinary eucrite pyroxene. Another meteorite classified as a polymict eucrite showed affinity to this group [1]. Jabeen et al. [6] discovered that Y791000 shows oxygen isotope abundance more fractionated parallel to the terrestrial fractionation line than those of Y791199 and Tatahouine diogenite. These new findings promoted renewed interest in Y75032-type achondrites. We reexamined some of these specimens with mineralogical techniques to discuss their genetic relationship, classification and formation processes taken place on the Vesta-like body.

Samples and Experimental Techniques

Pyroxene compositions of 16 Type B diogenites of the Y79 collections were taken from the Catalog of Antarctic Meteorites [1]. Polished thin sections (PTS), Y75032, Y791000, Y791192 (,91-2 assigned to Saiki), Y791199, Y791439 and Y791466 supplied by the National Institute of Polar Research (NIPR) were used for this study. The PTSs were studied by an optical microscope, and the chemical compositions of the minerals were obtained by electron probe microanalyzer (EPMA) JEOL 733 at Ocean Research Inst. (ORI) of Univ. of Tokyo. The data were compared with those of other Y75032-type pyroxenes in the Y79 collections [1].

Results

Diogenitic members.

Pyroxene compositions of Y791000, Y791072, Y791187, Y791188, Y791189, Y791199, Y791202, Y791204, Y791422, Y791466, Y791467, and Y791603 are nearly uniform and cluster around *mg*#=Mg×100/(Mg+Fe) 67 mole % [1]. Y75032-type pyroxene has *mg*# less than 70. Since Y791194 and Y791203 contains pyroxenes with compositions around *mg*#=70, they should belong to common diogenite group [1]. Y791188 pyroxenes include rare compositions close to *mg*#=60.

The crystalline portion is more abundant in hand specimen and two thin sections of Y791199. Brecciated areas are small and form veins filling the interstices of the two crystalline clasts of pyroxene. Vein matrix contains plagioclase (*An* 90 to 82) and chromite grains (up to 0.3 mm in diameter). The pyroxene compositions cluster around $Ca_{2.5}Mg_{64.5}Fe_{33.0}$. One crystalline clast (5.8 × 3.3 mm in size) consists of coarse-grained pyroxene (up to 3 mm) with thin blebby curtain-like inclusions of augite aligned along the *c* direction. Three small triangular plagioclase grains (*An* 74 to 81) are present at the interstices of grain boundaries of pyroxene. A diogenitic clast (5.4 × 1.5 mm) contains possible primary orthopyroxene with fine regular lamellae on (100) and fine chromite inclusions. The bulk chemical composition of the pyroxene is more Ca-poor and Fe-poor than that of the clast with blebby pyroxene. Almost entire PTS of Y791422 is one crystalline clast (5× 8 mm). The pyroxene composition is uniform and low in Ca ($Ca_2Mg_{67}Fe_{31}$), indicative of orthopyroxene.

Y791000 and Y791466 are more fragment-rich rocks, texturally similar to Y75032. Dark brown glassy materials are penetrated into fractures of pyroxene fragments and matrices. The chemistries of pyroxene are also similar to those in Y75032. The bulk pyroxene composition of some pyroxenes in

Y791000 with blebby augite precipitation is higher in Ca ($Ca_5Mg_{64}Fe_{31}$) than that of primary orthopyroxene. Y791466 contains minor shocked plagioclase grains. *An* values of plagioclase range from 68 to 94, but those of pyroxenes are fairly constant as those in Y75032.

Diogenites with Cumulate Eucrites.

Y791073, Y791200, and Y791201 contain pyroxenes with *mg#* down to 50. Y791201 is high in cumulate eucrite abundance and low in diogenitic component. The *mg#*s of pyroxene range from 70 to 50 and cover the entire range between Fe-rich diogenites and cumulate eucrites. *An* contents of plagioclase range from 86 to 93. It is not a howardite because neither basalt nor olivine is present. Some lithic clasts are composed of pyroxene, plagioclase, and minor chromite and troilite, but some pyroxene-only rocks are present. Devitrified, shocked plagioclase fragments are more abundant (25 % vol. %) than those in other Y75032-type achondrites. The Al_2O_3 contents in the shocked glass of Y791200 range from 5-7 wt %. Chemical compositions of shock melt glasses in Y791201 are high in Al_2O_3 (14 wt %) and in modal plagioclase (46 vol. %).

One large noritic clast (4.1 × 1.5 mm in size) attached to Y791201, and texturally similar to the Moama cumulate eucrite, consists of orthopyroxene (36 %), plagioclase (61 %, An_{89}), and blebby augite (3 %). Round pyroxene grains ($Ca_7Mg_{58}Fe_{35}$) about 1 mm in diameter with blebby inclusions of augite aligned along one crystallographic direction may be low-Ca inverted pigeonite. The bulk pyroxene composition is intermediate in *mg#* between the pyroxene fragments in the matrix. Plagioclase is shocked, but only a part of the crystal is maskelynite.

Cumulate Eucrites with Diogenites and Rare Eucrites.

Y791439 contains more abundant clasts of cumulate eucrite than those of Y75032. We observed six clasts (to 2.8 x 2.3 mm) in the PTS. Saiki and Takeda [7] divided pyroxene chemical compositions of Y791439 into four types: diogenite-type, Binda-type, Moore-County-type, and rare Juvinas-type. The diogenite-type pyroxenes are the most magnesian in the meteorite, and are similar to Fe-rich diogenites. The Binda-type pyroxenes are the most abundant, and many of them preserve the original lithic clast shape. The chemical compositions of Binda-type pyroxenes are slightly more Fe-rich than Binda, but many of them have blebs typical of the Binda cumulate eucrite. The chemical compositions of other two types are close to those of Moore County and those of Juvinas. Minor plagioclase grains are present in the matrix. The pyroxene fragments of Y791192 are similar to those of Y791439, but contains an ordinary eucrite clast. Small angular to subangular fragments of pyroxene and minor plagioclase, are set in dark glassy matrix. The eucritic clast shows dark fine-grained variolitic texture of brown pyroxene ($Ca_{15}Mg_{35}Fe_{50}$) and white lathes of plagioclase.

Discussion

The pairing of Y75032-type achondrites are mostly based on their unique shock melt veins and clustered pyroxene compositions around *mg#* 67. According to these criteria Y791000, Y791072, Y791187, Y791188, Y791189, Y791199, Y791202, Y791204, Y791422, Y791466, Y791467, and Y791603 [1] belong to this group. However, other members with abundant cumulate eucrites share the above common features with the diogenite-rich members. Therefore, they are most likely fragments of the same fall. If we classify some of the fragments in different meteorite class, the same specimen may have different names for separate locations. Y791201 has abundant cumulate eucrite clasts and minor diogenitic pyroxene. This specimen can be classified as an unusual howardite. Y791439 belongs to this category, but Y791192 has been described as a polymict eucrite [1]. Since it is difficult to identify fragments of diogenitic pyroxene from the Binda-type pyroxene in cumulate eucrites, we can classify this specimen as an unusual howardite. If the amounts of ordinary eucrite are small, this can be a polymict cumulate eucrite.

Another key item, which links these meteorites as a paired sample, is the presence of pyroxene with thin blebby, wavy, augite inclusions aligned along one orientation. Their bulk compositions (e.g., $Ca_5Mg_{64}Fe_{31}$ of Y791000) are lower than those in cumulate eucrites like Binda (e.g., $Ca_7Mg_{58}Fe_{35}$ of Y791201), but is higher than those of primary orthopyroxene (e.g., $Ca_2Mg_{67}Fe_{31}$ of Y791422). The Binda-type pyroxene is a product of decomposition of pigeonite at the pigeonite-eutectoid-reaction (PER) line [8]. Because bulk composition of the Y791000 pyroxene lies between primary orthopyroxene and one at the PER line, the low-Ca clinopyroxene crystal will go through the orthopyroxene-pigeonite inversion loop upon cooling from crystallization temperature. When the cooling is slow, orthopyroxene lamellae will be produced in the clinopyroxene with (100) in common. This lamella will grow thicker as temperature goes down. If the bulk composition of the crystal is close to the PER line, the clinopyroxene crystal will still remain, when it reaches at the PER line. Then, it will decompose into augite and orthopyroxene. This product may have thinner augite blebs than those

of the Binda-type pigeonite, because of the low initial bulk Ca contents. This kind of pyroxene can be produced only for a special chemistry and cooling rates. The presence of such pyroxene can be used as a key to identify the pairing and deduce cooling history.

Combined textural and chemical studies of Y75032-type pyroxene revealed that these achondrites experienced shock event in the history of the crustal evolution [9] before they finally ejected from the Vesta-like body by the last large impact . However, the last event was not recorded in their textures. Thus, it has been difficult to decipher the impact and excavation history. The presence of ordinary eucrite clast in Y791439 and Y791192 suggests that the excavation took place after the global crustal metamorphism as suggested by Yamaguchi et al. [9].

We reported mineralogical examination of eucrites with the evidence of melting in connection with our works on the crustal evolution of eucrites [10]. Presence of impact melts in eucrites or howardites has been known for some samples, but they are mostly in a form of vein. A good example of such shock melt vein has been reported for Padvarninkai [11]. Al-rich chemical compositions of impact glass in cumulate-eucrite-rich specimens (e.g., Y791201) indicate that fair amounts of eucritic components were melted by this events. The preservation of partly maskelynitized plagioclase and impact melt glass implies that thermal annealing did not take place after the last impact event. We could not find good explanation for the difference in oxygen isotopic fractionation between Y791000 and Y791199.

The origin of the Y75032-type breccias should take into account the fact that they were not formed by deposition of impact ejecta or fall out. Such deposits may include all components of a layered crust as in howardites and polymict eucrites [12]. Evidence for excavation of deep crustal material of a Vesta-like body has been proposed from Ca compositional gradients in pyroxene [13]. Close association of Fe-rich diogenites and cumulate eucrites with rare ordinary eucrites suggests that formation mechanism of these breccias are different form that of howardite, which might have been formed by one of the large impact crater with diogenite at the crater floor of Vesta. If we accept a picture of an impact crater of Metzler et al. [14], the Y75032-type breccias might be formed near the crater floor where the boundaries of diogenites and cumulate eucrites were disturbed by impact and mixed with impact melts in local scale.

In conclusions, (1) Characteristic textures with impact melt glass and pyroxene textures and chemistry suggest that Y75032-type achondrites are genetically related; (2) Application of current classification method of the HED achondrites, may lead to a confusion of their nomenclatures; and (3) Formation of such complex breccias can be best explained by a mechanism proposed for the layered crust model of the Vesta-like body [12].

Acknowledgments: We acknowledge the NIPR for supplying us with the samples. This work was supported by a grant of the ORI and by a Grant-in-Aid for Scientific Research from the Japanese Ministry of Education, Science and Culture. We are indebted to Dr. N. Imae for his assistance in classification of the Yamato meteorites, to Mrs. Ohtsuki for her help in microanalysis at the ORI and and to Drs. A. Yamaguchi, L. E. Nyquist, D. D. Bogard, Y. Ikeda, D. Mittlefehldt for discussion and Prof. M. Miyamoto for discussion and supports.

References:

[1] YANAI K. and KOJIMA H. (1995) *Catalog of the Antarct. Meteorites*. 230 pp. NIPR, Tokyo.

[2] TAKEDA H. and MORI H. (1985) *Proc. Lunar Planet. Sci. Conf.* **15th**, *J. Geophys. Res.* **90**, C636-C648.

[3] TAKEDA H., MORI H., DELANEY J.S., PRINZ M., HARLOW G.E., and ISHII T. (1983b) *Mem. Natl. Inst. Polar Res., Spec. Issue* **30**, 181-205.

[4] BINZEL R. P. and XU S. (1993) *Science* **260**, 186-191.

[5] THOMAS P. C., BINZEL R. P., GAFFEY M. J., STORRS A. D., WELLS E. N. and ZELLNER B. H. (1997) *Science* **277**, 1492-1495.

[6] JABEEN I., KUSAKABE M., NAGAO K. and NAKAMURA T. (1997) *Antarctic Meteorites* **22**, 72-74.

[7] SAIKI K. and TAKEDA H. (1994) *Symp. Antarct. Meteorites* **19th**, 47-50.

[8] ISHII T. and TAKEDA H. (1974) *Mem. Geol. Soc. Japan* **11**, 19-36.

[9] YAMAGUCHI A., TAYLOR G. J., and KEIL K. (1996) *Icarus* **124**, 97-112.

[10] TAKEDA H., MIKOUCHI T. and MIYAMOTO M. (1997) *Antarct. Meteorites* **22**, 182-184.

[11] NYQUIST, L., BOGARD, D., WIESMANN, H., SHIH, C.-Y., YAMAGUCHI A. and TAKEDA H. (1996) *Meteoritics & Planet. Sci.* **31**, A101-A102.

[12] TAKEDA H. (1997) *Meteoritics & Planet. Sci.* **32**, 841-853.

[13] MIYAMOTO M. and TAKEDA H. (1994) *Earth Planet. Sci. Lett.* **122**, 343-349.

[14] METZLER K., BOBE K. D., PALME H., SPETTEL B. and STOFFLER D. (1995) *Planet. Space Sci.* **43**, 499-525.

SHOCK EFFECTS IN THE MURCHISON CM CHONDRITE AT PRESSURES HIGHER THAN 30 GPa (SHOCK STAGE S5)

Kazushige Tomeoka[1], Yasuhiro Yamahana[1] and Toshimori Sekine[2]

[1] Department of Earth and Planetary Science, Faculty of Science, Kobe University, Nada, Kobe 657-8501, Japan
[2] National Institute for Research in Inorganic Materials, 1-1 Namiki, Tsukuba, Ibaraki 305, Japan

INTRODUCTION

Carbonaceous chondrites are characterized by relatively high proportions of fine-grained porous matrix that consists of various kinds of minerals. Shock effects on such a porous, multiphase material are extremely heterogeneous and the amount of post-shock heat is much larger than nonporous material [1-3]. In addition, CI and CM chondrites in particular are rich in volatiles and contain large amounts of water (10-20 wt% H_2O). These porous, volatile-rich chondrites are expected to respond to shock compression differently from other types of meteorites. However, among the known carbonaceous chondrites those having been affected by high shock pressure are rare [4], and thus how these meteorites respond to high shock pressure is poorly known.

In order to better understand the shock history of the carbonaceous chondrites, we have conducted a series of shock-recovery experiments of the Murchison CM chondrite. At the last two symposiums, we have reported the results of shock experiments at pressures up to 30 GPa [5,6]. At pressures >30 GPa, however, we continuously failed to recover samples due to production of cracks in the sample containers and explosive ejection of the shocked samples. Since then we have improved the experimental methods and could successfully recover the samples shocked at 34, 36 and 49 GPa. These shock pressures cover nearly a whole range of shock stage S5 [7]. It is estimated that, in shock stage S5, pervasive formation of melt takes place in ordinary chondrites [7]. Previous shock experiments of Murchison [8,9] also indicated that major melting and devolatilization could take place in this pressure range. We here present the results of detailed mineralogical and petrographic studies of the recovered samples.

BRIEF SUMMARY OF THE PREVIOUS RESULTS

The Murchison samples were shocked at 7, 11, 21, 26, 28 and 30 GPa. Chondrules are flattened nearly perpendicular to the compression axis in the pressure range 11-30 GPa. The degree of chondrule flattening increases roughly in proportion to the intensity of shock pressure up to ~25 GPa. However, at 25-30 GPa, chondrules do not show any further flattening, but they become more randomly oriented. The degree of chondrule flattening in Murchison was found to be considerably smaller than that in Allende [10]. Fracturing of olivine and pyroxene in chondrules occurs heterogeneously at ≤28 GPa, but at 30 GPa all olivine and pyroxene are homogeously fractured. Minor melting occurs as melt veins and/or pockets at >20 GPa. However, the melts occur in minor amounts (<10 vol%) mostly in the sample peripheries. The melts are mainly produced from the matrix and compositionally resemble the matrix except that Fe, S and Ca are more enriched. At 21 GPa, thin, subparallel fractures begin to form in matrix in directions perpendicular to the compression axis. Their number density increases greatly at 26 GPa, and they extend in high density throughout the matrix at 30 GPa. Thus, at 26-30 GPa, the sample is increasingly comminuted and becomes fragile.

MATERIALS AND METHODS

The shock-recovery experiments were performed by using a single stage 30-mm bore propellant gun at the National Institute for Research in Inorganic Materials. Details of the experimental procedures are described in Sekine et al. [11] and Tomeoka et al. [5].

In the present study, we initially undertook to shock Murchison samples at 35, 40 and

45 GPa at room temperature. The resultant peak pressures calculated by the measured velocities are 34, 36 and 49 GPa. Polished sections were made from each recovered sample by cutting along the shock compression axis and studied by using a scanning electron microscope equipped with an energy-dispersive X-ray spectrometer.

RESULTS

Impact at 34 GPa

The general appearance of the sample becomes distinctly different from those of the samples shocked at ≤30 GPa. The sample is strongly flattened and tapers off toward the periphery, where it becomes a 50-to-100-μm thick vein-like plate and extends over a distance of 1-2 mm. The stainless steel container at the contact with the sample shows very ragged surfaces with many large dents. These features suggest that a strong expansive force was generated within the container. The sample is composed of rounded to irregularly-shaped blocks of 50-200 μm in dimension, thus exhibiting a breccia-like texture. The sample is found to be even more fragile than the 30-GPa sample, thus many portions dropped off during sample preparation.

Most chondrules are fragmented and disintegrated. The number of chondrules, whose aspect ratios are measurable, is extremely limited, so no attempt was made to measure the aspect ratios and orientation angles. However, clearly neither preferred orientations of chondrules nor foliation is recognizable. All olivine and pyroxene are thoroughly fractured with subgrains of 1-5 μm in diameter; their surfaces have a fluffy appearance. The matrix does not show the characteristic fractures that were observed in the samples shocked at 20-30 GPa but becomes a complex assemblage of incipient melts and fine grains. The incipient melts occur randomly on a scale of 10-50 μm and show numerous tiny (1-2 μm) vesicles, which indicates that very local and instantaneous evaporation took place at melting; the incipient melts probably formed locally and cooled and solidified instantaneously, thus do not show any significant movement and pooling. Significant amounts of complete melts form pools in the periphery of the sample.

Impact at 36 GPa

The sample is also strongly flattened and tapers off toward the periphery. It exhibits a general texture similar to the 34-GPa sample. However, it becomes more disintegrated and complex. More abundant incipient vesicular melts are produced, and they are intermixed with comminuted matrix grains. Larger amounts of melt pools are also produced in many places. Especially large melt pools occur in the sample periphery, where they extend over a distance of 1.5-2 mm with a thickness of 100-200 μm, exhibiting a long vein-like feature; this suggests that the melted material was preferentially ejected into the fracture spaces that were produced in the sample container by impact. Olivine and pyroxene grains show dense, fine fractures, exhibiting a fluffy texture.

Impact at 49 GPa

The matrix is totally melted, and the general texture becomes chaotic; isolated grains of olivine and pyroxene (50-200 μm in diameter) are scattered in the melts. No chondrule-like aggregates are present. The olivine and pyroxene grains are densely fractured and show a fluffy texture, but in contrast to those in the samples shocked at 30-36 GPa, they commonly show unfractured, smooth portions on their surfaces, which suggests that the fractures were healed by recrystallization or partially melted due to intense heating. Some olivine grains are indeed partially melted and mixed into the surrounding melts. The melts are similar in composition to the matrix, although very heterogeneous. They contain tiny fragments of olivine and pyroxene, grobules of Fe-Ni metal and sulfide. Characteristic are bubble-like voids, which are generally much larger in size (50-200 μm in diameter) than those in the samples shocked at lower pressures, which indicates that intenser evaporation took place in this sample.

DISCUSSION

The present study reveals that drastic changes in texture took place in the samples shocked at ≥34 GPa compared to those shocked at ≤30 GPa. At ≤30 GPa, chondrule flattening, fracturing of matrix, and fracturing of olivine and pyroxene in chondrules are major mechanical effects, and the sample maintains its original configuration, i.e., chondrules being uniformly distributed in a matrix. However, at 34 and 36 GPa, such original texture is mostly disintegrated. Chondrules are progressively fragmented and disassembled rather than flattened, and detached grains are scattered to the matrix. The sample is converted to a complex assemblage of small blocks and fine grain. The texture suggests that the sample was once finely fragmented and comminuted by impact, thus becoming an assemblage of small blocks and fine grains, and on pressure release, they behaved like a fluidized material and thus were relocated and reorganized.

It has become evident that local melting takes place first at ~20 GPa and the amount of melts increases progressively with increasing shock pressure in the range 20-30 GPa. However, the total amounts of melts produced are still very small (<10 vol%), and the melts are mostly confined to the sample peripheries, which means that significant heating occurs heterogeneously on a scale of <1mm. However, at ~35 GPa, melting occurs pervasively in the matrix, which means that heating is intense and homogeneous. This is consistent with the previous TEM observations of Akai and Sekine [9], who reported that the phyllosilicates in Murchison decompose to an amorphous state at >32 GPa. At 49 GPa, the matrix is totally melted, and even detached olivine grains are partially melted, indicating much intenser heating took place homogeneously.

One of the characteristics of the melts produced in Murchison is the presence of abundant bubble-like voids, which indicates evaporation of volatiles, including H_2O, took place at the same time of melting. Therefore, the increase in amount of melt with pressure means the simultaneous increase in evaporation. In fact, the volume proportion of the bubble-like voids in the 49-GPa sample drastically increases relative to those in the samples shocked at lower pressures. These results are consistent with the results of Tyburczy et al. [8], who reported that incipient devolatilization in Murchison occurs at ~20 GPa and complete devolatilization occurs at ~50 GPa. The drastic increase in devolatilization and simultaneous increase in gas volume due to heat probably generated explosive expansion on release of shock pressure.

The great increase in degree of comminution of the Murchison sample and the simultaneous generation of a strong expansive force at 25-35 GPa testify the hypothesis of Scott et al. [4] that the volatile-rich carbonaceous chondrites shocked above 20-30 GPa escaped from the parent body on pressure release and formed particles that are too small to survive as meteorites.

REFERENCES

1. Kiefer S.W. (1971) J. Geophys. Res. 76, 5449-5473.
2. Bauer J.F. (1979) Proc. 10th Lunar Planet. Sci. Conf., 2573-2596.
3. Stöffler D., Bischoff A., Buchwald V. and Rubin A.E. (1988) Meteorites and the Early Solar System, 165-202, Univ. Arizona Press.
4. Scott E.R.D, Keil K. and Stöffler D. (1992) Geochim. Cosmochim. Acta 56, 4281-4293.
5. Tomeoka K., Yamahana Y., Mizumoto F. and Sekine T. (1996) Papers presented to 21st Symp. Antact. Meteorites, 185-188 (Abstr.).
6. Yamahana Y., Tomeoka K. and Sekine T. (1996) Papers presented to 22nd Symp. Antact. Meteorites, 211-213 (Abstr.).
7. Stöffler D., Keil K. and Scott E.R.D. (1991) Geochim. Cosmochim. Acta 55, 3845-3967.
8. Tyburczy J.A., Frisch B. and Ahrens T.J. (1986) Earth Planet. Sci. Lett. 80, 201-207.
9. Akai J. and Sekine T. (1994) Proc. NIPR Symp. Antarct. Meteorites 7, 101-109.
10. Nakamura T., Tomeoka K., Sekine T. and Takeda H. (1995) Meteoritics 30, 344-347.
11. Sekine T., Akaishi M., Setaka N. and Kondo K. (1987) J. Mat. Sci. 23, 3615-3619.

AN X-RAY CT STUDY OF ALH84001 ANALOG

TSUCHIYAMA Akira[1], HIRAI Hidekazu[2], KOISHIKAWA Atsushi[2], BUNNO Michiaki[3], MCKAY Gordon A.[4], and LOFGREN Gary E.[4]
1) Department of Earth and Space Science, Osaka University, Toyonaka 560-0043, JAPAN, akira@ess.sci.osaka-u.ac.jp, 2) Nittetsu Elex Co., Ltd., Sagamihara 229-0006, JAPAN, 3) GSJ, Tsukuba 305, JAPAN, 4) SN2, NASA Johnson Space Center, Houston, TX 77058, U.S.A.

Introduction

Three dimensional information on the structures of meteorites gives new knowledge that cannot be obtained from the two dimensional structures, and X-ray computed tomography (CT) provides three dimensional structures from successive images [1,2]. Especially, high resolution X-ray CT method with spacial resolution of ≥10μm [3] can give three dimensional information on fine structures that cannot be obtained by successive conventional thin sectioning [1].

We are trying to obtain three dimensional information on the structures of the martian meteorite ALH84001, in which possible relic biogenic activity was reported [4]. Prior to imaging of ALH84001 by an X-ray CT scanner, preliminary study was made on ALH84001 analog.

Imaging of ALH84001 analog

ALH84001 analog was made to check the contrast resolution of the high resolution X-ray CT scanner (Nittetsu Elex Co., Ltd.) [1,3]. Terrestrial mineral samples similar to those contained in ALH84001 (orthopyroxene, clinopyroxene, plagioclase, chromite, apatite, carbonates, pyrite, and pyrrhotite) were prepared. Seventeen grains with different compositions (about 1-2 mm in size) were mounted in an epoxy. A slice of X-ray CT image was taken by the scanner with horizontal spacial resolution of about 13 μm and slice width of 20 μm (X-ray tube: W-target, 80keV, and 0.02mA) (Fig.1). Materials with large X-ray adsorption have bright contrasts.

CT values of the minerals were obtained from the CT image to compare the linear attenuation coefficients of X-rays, μ. The chemical compositions of the minerals were measured by an electron probe microanalysis. Then, the values of μ were calculated from the densities and the effective atomic numbers estimated from the chemical compositions by using [5]. Strictly speaking, estimation of the CT values in the present experiments with white X-rays is complex because μ is dependent on the X-ray energy. However, good linear relation between the CT values and the linear attenuation coefficients at 80 keV, μ_{80}, were obtained within errors for single crystals of the minerals and air (Fig.2).

Simulations

X-ray CT images were simulated from images by a scanning electron microscope (SEM) and elemental mapping of ALH84001. Two dimensional distribution of mineral phases was estimated from a back-scattered electron (BSE) image with an aid of the elemental map. The values of μ_{80} were calculated from the average chemical compositions of the minerals in ALH84001 [6]. By contrasting the μ_{80} values, a hypothetical CT image with the spacial resolution of the original BSE image (0.66 μm/pixel in Figs.3a and 3b) was obtained first. From this image, CT images with low resolutions comparable to the X-ray CT scanner were simulated by using an image analysis technique of bicubic method (Figs. 3c-3h).

It is seen from the simulated X-ray CT images that carbonate globules with Fe-rich rims can be easily recognized with the resolutions higher than 7.5 μm/pixel (Fig.3d). Fig.3g shows that the carbonates may be recognized even with the resolution of 20 μm/pixel. However, it should be noted that real images should be worse than the simulated images because various artifacts, such as beam hardening and ring artifact, are expected. Moreover, the vertical resolution due to slice width is not taken into consideration in the simulation. Therefore, it is not sure at this moment whether or not the carbonate globules can be recognized by the X-ray CT scanner with the resolution as high as 10 μm. However, it is expected that orthopyroxene, plagioclase glass, chromite (and pyrite), and cracks can be easily recognized if their size are sufficiently large. Three dimensional distribution of these minerals and cracks may give information on secondary processes of ALH84001, such as shock events and/or possible hydrothermal event.

X-ray CT imaging of ALH84001.253 and 285 is now preparing. The present image simulation can help interpretation of real images.

References: [1] Tsuchiyama *et al.* (1997) *L.P.S.*, **XXVIII**, 1453. [2] Carlson and McCoy (1998) *L.P.S.*, **XXIX**, #1541. [3] Kondo *et al.* (1997) *Antarctic Meteorite Res.*, **10**, 437. [4] McKay *et al.* (1996) *Science*, **273**, 924. [5] McCullough (1975) *Medical Phy.*, **2**, 307. [6] Mittlefehldt, *Meteoritics*, **29**, 214.

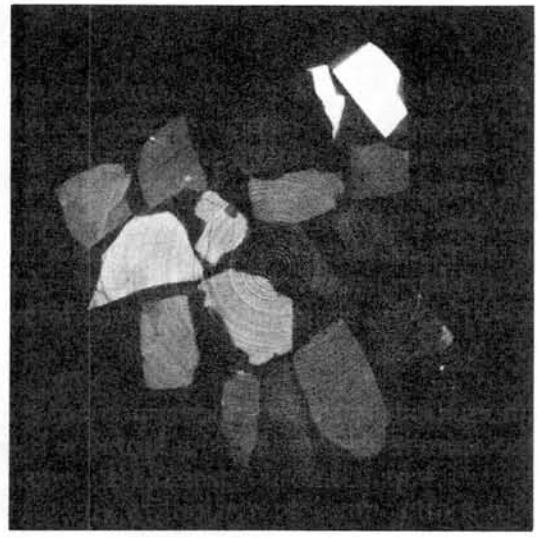

Figure 1. An X-ray CT image of ALH84001 analog. About 13 mm in width. Rings are artifacts.

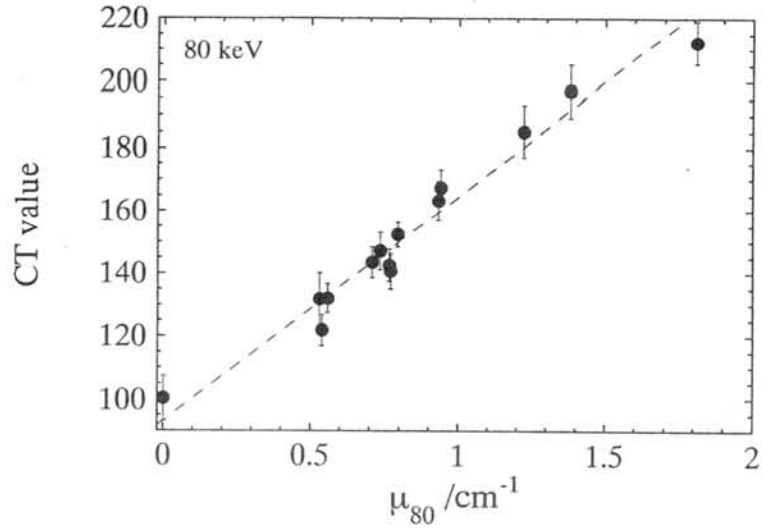

Figure 2. The relation between CT values measured from Fig.1 and calculated linear attenuation coefficients of X-ray at 80 keV, μ_{80}. Only single crystals and air are used.

Figure 3. Simulated X-ray CT images of ALH84001. The width of each image is about 800 μm. (a) Imaging of calculated μ_{80} values for each mineral phase based on a BSE image (0.66 μm/pixel). The brightness of each pixel is proportional to μ_{80} (10 for crack (black veins) and 232 for chromite (white dots) in 256 gray scale). (b) Enhanced image of (a) by contrast. pl(gl)=plagioclase glass, cb=carbonates (core, Fe-rich rim, and Mg-rich outermost rim are distinguished). (c) 5 μm/pixel. (d) 7.5 mm/pixel. (e) 10 μm/pixel. (f) 15 μm/pixel. (g) 20 μm/pixel. (h) 30 μm/pixel.

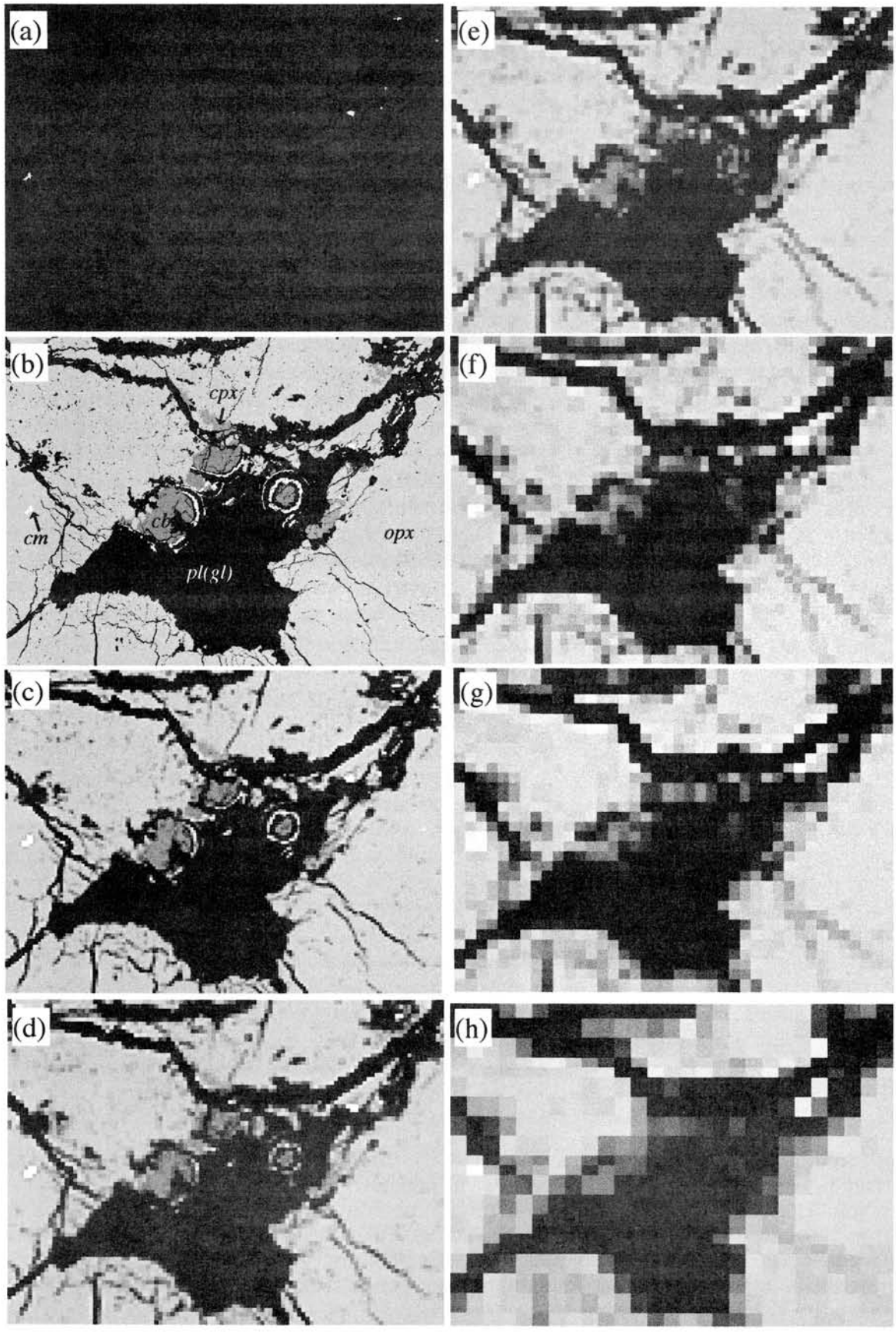
(a)
(b)
cpx
cm
cb
opx
pl(gl)
(c)
(d)
(e)
(f)
(g)
(h)

X-RAY AND CHEMICAL STUDIES OF SILICA MINERALS AND PLAGIOCLASE IN THE MILLBILLILLIE EUCRITE

T. Tsuru, Y. Nakamuta, and Y. Aoki

Dept. Earth and Planetary Sciences, Faculty of Science, Kyushu University, Fukuoka812-8581, Japan

Introduction

We obtained a Millbillillie eucritic meteorite, the surface of which is covered with a fusion crust and which has not been described until now. The size of this meteorite is about 5 × 7 × 9 cm and the weight is 458g. The observation of the cut surface of this meteorite under an optical microscope shows that this meteorite is mainly composed of coarse-grained fragments, being composed of pyroxene and plagioclase, and mesostasis being interstitial to the coarse-grained fragments. Like this occurrence of the Millbillilie eucrite has not been reported until now (Yamaguchi et.al., 1994). In this study, chemical compositions of plagioclase of this meteorite and the polymorphs of silica minerals occurred in the mesostasis are investigated, and it has been shown that the silica minerals in the mesostasis of this meteorite are composed of tridymite and quartz and that the chemical compositions of plagioclase in the coarse-grained fragments have been affected by reactions with the mesostasis.

Experimental method

Seven polished thin sections were made from a slice of the Millbillillie eucrite. They were observed under an optical microscope and analyzed by a scanning electron microscope (SEM: JEOL JSM-5800LV) equipped with an energy dispersive spectrometer. Chemical analyses were also made by an electron-probe microanalyser (EPMA: JEOL JCXA-733) equipped with a wave-length dispersive spectrometer.

The X-ray powder patterns of individual silica grains of about 50 μm in size were obtained by a Gandolfi camera after the analysis of chemical compositions by EPMA.

Results

The observation of the cut surface of the meteorite of this study under an optical microscope shows that this meteorite is composed of coarse-grained fragments being assigned to the CX-clasts of Yamaguchi et al. (1994), a fine-grained matrix-vein being assigned to the LM-matrix of Yamaguchi et al. (1994), and the mesostasis being interstitial to the CX-clasts. In parts, the CX-clasts and the mesostasis are observed to have heavily reacted.

Pyroxene compositions fall along a single tie line in the pyroxene quadrilateral in the range from $Ca_3Mg_{37}Fe_{60}$ to $Ca_{45}Mg_{30}Fe_{25}$, regardless of the textures. In contrast to pyroxene compositions, the chemical compositions of plagioclase differ among textures in which plagioclase has occurred (Fig. 1). Plagioclase in the CX-clasts has An-rich compositions (~ An90), and plagioclase in the mesostasis is richer in Ab-component (~ An80) than that in the CX-clasts.

Plagioclases in the region where the CX-clasts and the mesostasis have heavily reacted and in the LM-matrix show the compositions intermediate between those in the CX-clasts and the mesostasis.

The X-ray powder patterns of individual silica grains show that silica minerals in the mesostasis are composed of quartz and tridymite (Fig. 2). Tridymite dominates in the region where the CX-clasts and the mesostasis have heavily reacted (Fig. 2c) and quartz have mainly occurred in the mesostasis being interstitial to the CX-clasts and showing little or no reaction with the CX-clasts (Fig. 2a).

Reference

A. Yamaguchi, H. Takeda, D. Bogard, and D. Garrison. (1994) Meteoritics **29**, 237-245.

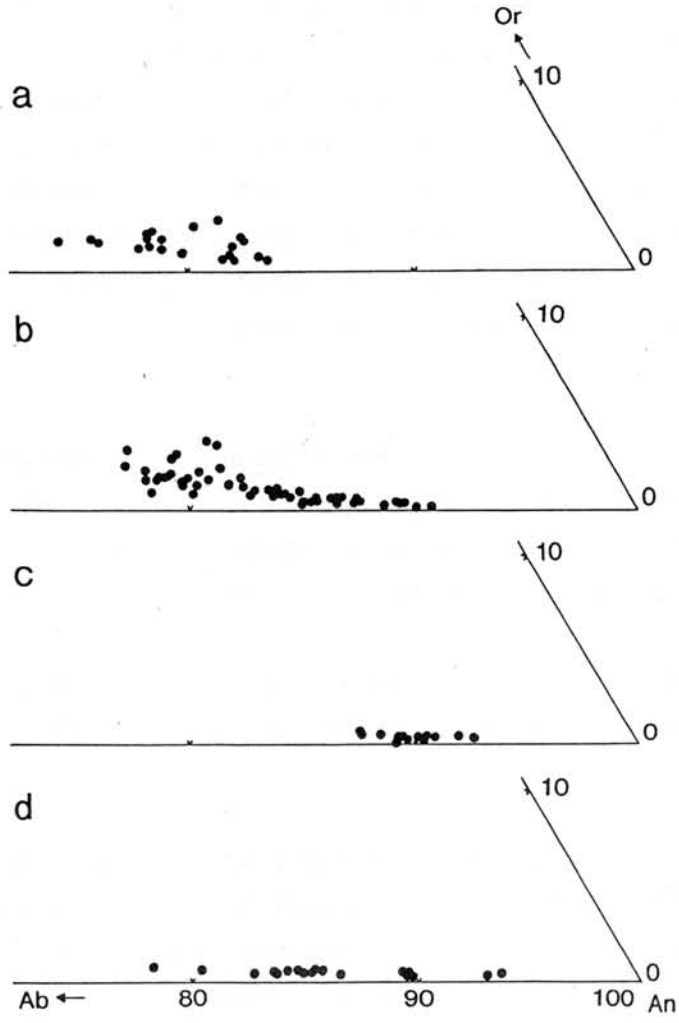

Fig.1 Chemical compositions of plagioclase. (a) plagioclase from the mesostasis. (b) plagioclase from the part where mesostasis and CX-clasts have heavily reacted. (c) plagioclase from the CX-clasts. (d) plagioclase from the LM-matrix.

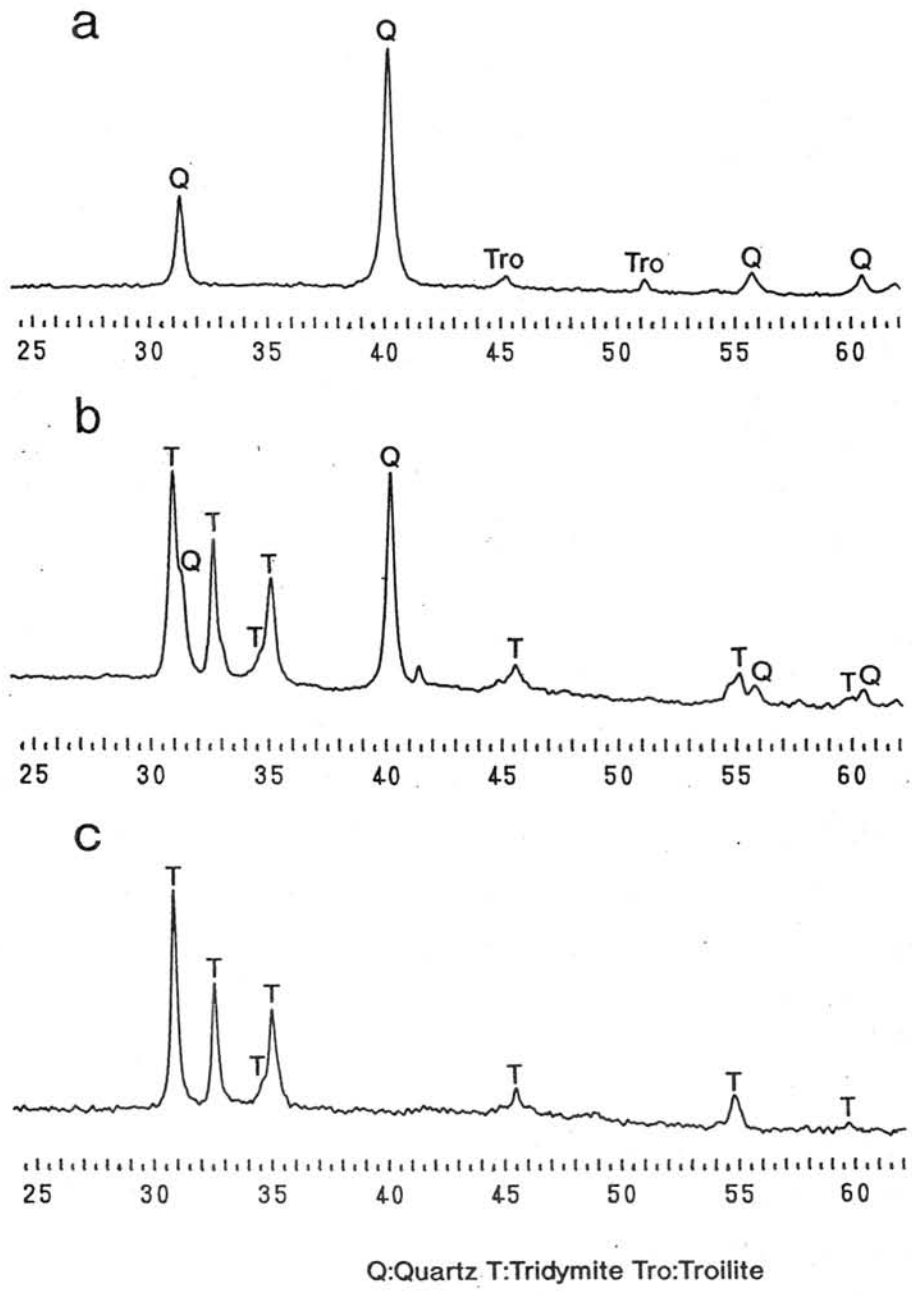

Fig.2 The X-ray powder patterns of individual silica grains in the mesostasis. (a) a silica grain in the matrix of mesostasis. (b) a silica grain occurred contact with coarse-grained pigeonite. (c) a silica grain occurred contact with coarse-grained pigeonite in the region where CX-clasts and mesostasis have heavily reacted.

A preliminary experiment for K isotope analysis of CAI.

Takayuki USHIKUBO, Hajime HIYAGON, Naoji SUGIURA

Department of Earth and Planetary Physics, University of Tokyo,
7-3-1 Hongo, Bunkyo-ku, Tokyo 113-0033 , JAPAN

Introduction

Calcium-Aluminum-rich Inclusions (CAIs) are objects that have some unique features; enrichment of refractory elements, stable isotope anomalies, evidence of existence of some extinct nuclides, and they show the oldest age in solar system [1]. Early history of the solar system could be revealed by studying CAIs.

Isotopic chronology with extinct nuclides is one of useful methods for this purpose. For more than two decades, in situ decay of the ^{26}Al-^{26}Mg system ($\tau_{1/2} = 0.72 Myrs$) have been measured because CAIs have Al-rich, Mg-poor phases that are appropriate for detection of ^{26}Mg isotope anomalies and ^{26}Al has a short half life time. As a result, it is known that CAIs had the same ^{26}Al/^{27}Al initial ratio [2]. It is also known from the ^{26}Al-^{26}Mg system that secondary phases were generated several Myrs later [2]. But it was shown that some metamorphic events may have occurred within a short time period that cannot be resolved by ^{26}Al-^{26}Mg system [3].

Recently, it was shown that CAIs have ^{41}K excesses; in situ decay product of ^{41}Ca($\tau_{1/2} = 0.10 Myrs$) [4, 5] . The ^{41}Ca–^{41}K system in CAIs could provide more precise information that couldn't be obtained by the ^{26}Al-^{26}Mg system.

We will report preliminary results of K isotopic analyses .

Measurement conditions and sample preparation

We use a CAMECA ims-6f ion microprobe in University of Tokyo for spot analysis. Primary beam is a negative oxygen; accelerating voltage is -12.5kV, typical beam current is about 4.0 nA. Secondary accelerating voltage is 10.0kV, and energy offset is not applied. A count rate of ^{40}Ca and Faraday cup background are measured with a Faraday cup, and a count rate of ^{39}K, 41 amu, $(^{40}Ca^{43}Ca)^{2+}$ are measured with an electron multiplier. A background of the electron multiplier (EM b.g.) is measured in advance.

Mass resolution($M/\Delta M$) is set to ~7,000. This is enough to resolve interference of ^{41}CaH, but not enough to resolve interference of $(^{40}Ca^{42}Ca)^{2+}$ [see figure 1]. So a count rate of ^{41}K is calculated by a following equation; ^{41}K = (count rate of 41 amu) - $(^{40}Ca^{43}Ca)^{2+} \times (^{43}Ca/^{42}Ca)$ - (EM b.g.) [4].

Terrestrial anorthite, plagioclase with a small amount of K, fassaite, and fassaite of Type B2 CAI in Allende were measured. Each mineral is mounted on a small metal cup and polished with 0.25 μ diamond paste, and gold-coated (200 Å thick). Each spot measurement takes about 1.5 hours. Half of this time is used to remove K contamination.

Results and Problems

Figure 2 shows results of isotopic measurements. The solid line shows K terrestrial isotopic ratio (0.072), and the dashed line shows isochron assuming a $^{41}Ca/^{40}Ca$ initial ratio of 1.41×10^{-8}.

In our measurements, interference to ^{41}K from ^{40}CaH is much smaller than that of Srinivasan et al.. In spite of this merit, our results still have larger errors than that of Srinivasan et al.. This error comes from small counting rates of $(41\ amu)^+$ and $(^{43}Ca^{40}Ca)^{2+}$ that is measured to correct interference; especially, the count rate of $(^{43}Ca^{40}Ca)^{2+}$ is about 0.07 cps and is not so different from the EM background: ~0.02 cps . Count rates of other nuclides are $^{40}Ca^+ \sim 2.0 \times 10^6$ cps, $^{39}K^+ \sim 1.0 \times 10^1$ cps, $^{41}K^+ \sim 0.6$ cps. At present, in order to avoid K contamination, the area of analysis (~15 μm) is smaller than the size of primary beam (~50 μm), resulting in a small K count rate. We expect that by using more focused primary beam, the K count rate is increased and the precision of isotopic ratio is improved.

References

[1] ALLÈGRE C. J. et al. (1995) GCA, 59, 1445-1456

[2] MACPHERSON G.J. et al. (1995) Meteoritics, 30, 365-386

[3] MACPHERSON G.J. et al. (1993) GCA, 57, 231-243

[4] SRINIVASAN G. et al. (1996) GCA, 60, 1823-1835

[5] SAHIJPAL S. et al. (1998) Nature, 391, 559-561

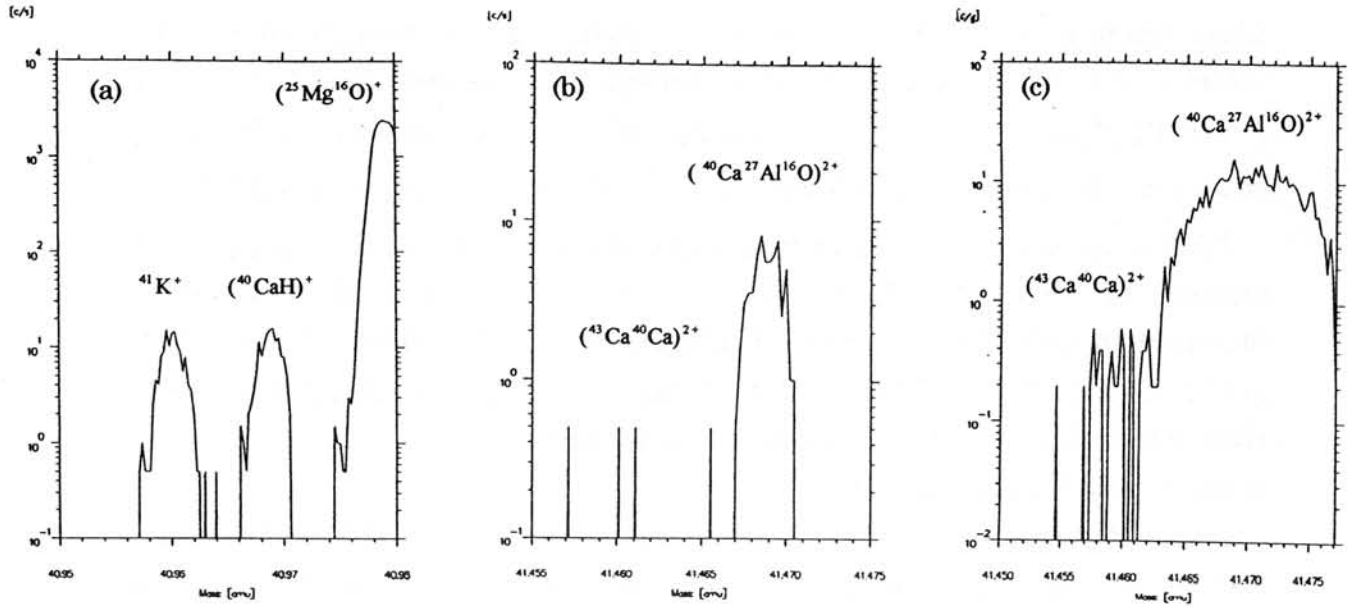

Fig.1 Peak shapes of ^{41}K and $(^{43}Ca^{40}Ca)^{2+}$. (a): From left side, $^{41}K^+$, $^{40}CaH^+$, and $^{25}Mg^{16}O^+$. (b), (c) : major peak is $(^{40}Ca^{27}Al^{10}O)^{2+}$ and peak of $(^{43}Ca^{40}Ca)^{2+}$ is seen about 41.46 amu. (a) and (b) show peak shapes under the same condition of K isotopic analysis. (c) shows peak shapes at low resolution.

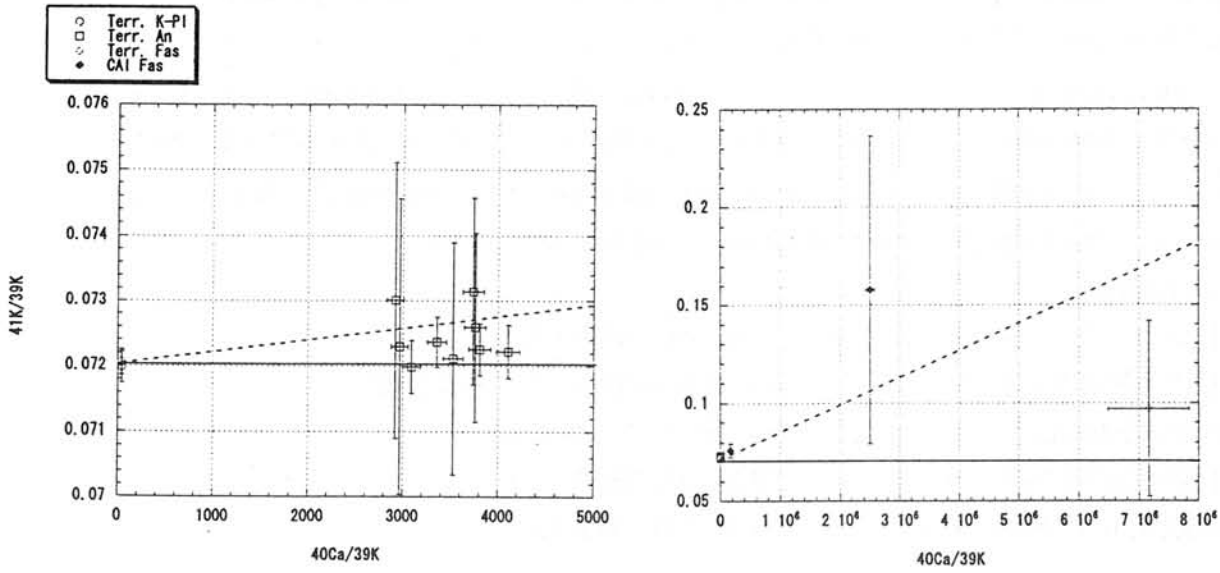

Fig.2 Results of K isotope analysis. Left figure is illustrated smaller scale than right one. Open symbols are terrestrial minerals' data. Filled symbols are CAI's data. The solid line shows terrestrial reference value (0.072). The dashed line shows isochron assuming a $^{41}Ca/^{40}Ca$ initial ratio of 1.41×10^{-8}.(error bar is 2δ)

THERMALLY METAMORPHOSED CARBONACEOUS CHONDRITES FROM RNAA DATA.

M.-S. Wang and M. E. Lipschutz, Department of Chemistry, BRWN/WTHR Bldg., Purdue University, W. Lafayette, IN 47907-1393

Many studies - both theoretical and experimental - have identified a number of trace elements that are sensitive to thermal episodes in their histories [1,2]. These elements can be considered as volatile (thermodynamically in equilibrium during primary condensation and accretion of solids from the solar nebula) or mobile (kinetically reflecting vaporization and loss by secondary, open-system, postaccretionary heating of parent material during metamorphism or by intense shock-loading). In nearly all C1-C6 chondrites - whether Antarctic or not - 9-11 of these trace elements define a horizontal line when their C1-normalized concentrations (by weight) or atomic abundances are considered [1-3].

Three Antarctic chondrites (one C1 and 2 C2) became the target of a consortium led by Prof. Y. Ikeda since their petrography apparently indicated postaccretionary heating. Their compositions proved exceptional [4,5], with the most mobile trace elements in them being depleted by factors up to 100 compared to elements of lesser mobility [4,5]. Significant depletions of: Bi, Tl and Cd are evident for the C2 Belgica (B) 7904; In, Bi, Tl and Cd for the C1 Yamato (Y) - 82162; and Zn, In, Bi, Tl and Cd in the C2 Y-86720. The patterns of mobile trace elements in them were essentially duplicated by those in Murchison (CM2) chondrite samples heated artificially [6] for 1 week at temperatures of 600°C and 700°C in a low-pressure, ambient atmosphere, initially 1 Pa (10^{-5} atm) H_2. The trace element patterns in these 3 C1 and C2 chondrites were interpreted as having arisen by thermal metamorphism in the interiors of their parent bodies [4,5]. This conclusion was supported by subsequent spectral reflectance studies [7-9] indicating that the surfaces of a number of C-, G-, B- and F- asteroids are covered with such metamorphosed material, which, presumably, had been excavated from the bodies' interiors during impacts.

Recently, a variety of markers have been used to single out 8 C2 and C3 chondrites evidencing interesting thermal histories. We examined these histories by quantifying thermally mobile trace elements in them. The meteorites studied were: C2/CM2/CR2 chondrites Asuka (A) 881655, Pecora Escarpment (PCA) 91008, Y-791198, Y-793321, Y-793495 and Y-86789; and CO3 Y-790992 and Y-81020. We measured U, Co, Au, Sb, Ga, Rb, Cs, Se, Ag, Te, Zn, In, Bi, Tl and Cd (in order of increasing degree of loss from Murchison (CM2) samples heated at 500-700°C [6]) in them by radiochemical neutron activation analysis (RNAA). We irradiated these samples at the University of Missouri Research Reactor for 2-4 days at a flux of 8.0×10^{13} cm^{-2} s^{-1} and processed them using our standard RNAA techniques [3].

Three samples (Y-791198, Y-793321 and Y-81020) exhibited the flat mobile trace element pattern typical of the vast majority of carbonaceous chondrites, e.g. unmetamorphosed ones (Fig. 1). The other 5 exhibited depletion(s) of the 1-5 most mobile element(s): A-881655 (CM2), Y-793495 (CR2) and Y-790992 (CO3) apparently lost Cd; PCA 91008 (CM2), Tl and Cd; and Y-86789 (CM2), Zn, In, Bi, Tl and Cd (Fig. 2). The depletion pattern for the last of these is so similar to that of Y-86720 [4,5] that it may well be that the two are paired as suggested earlier by others, e.g. [10]. Abundance patterns for Murchison (CM2) samples heated at 400-700°C [6] included in Fig. 2 provide a semi-quantitative comparison scale.

We interpret the data in Fig. 2 as indicating that these 5 carbonaceous chondrites have been thermally metamorphosed in their parent bodies under open-system conditions. Based on these and earlier [3,4] RNAA data (Table 1), we suggest that peak metamorphic temperatures were ordered as:

A-881655 (CM2) ~ Y-793495 (CR2) ~ Y-790992 (CO3) ~ LEW 85332 (CO3) < PCA 91008 (CM2) < B-7904 (CM2) < Y-82162 (CI1) < Y-86720 (CM2) ~ Y-86789 (CM2)

The small discrepancy between this ordering and that based on mineralogy should be noted: Akai [11] found that, using mineralogic thermometers, B-7904 seems the most metamorphosed.

Assuming that Y-86720 and Y-86789 are paired, 10 of the 71 C1-C6 chondrites for which RNAA data are available (cf. [3,4] and references therein) present evidence for open-system thermal metamorphism in their parent bodies. Queen Maud Land, Antarctica, has provided a disproportionate share of such samples: 67% of the 9 samples from there have been metamorphosed, compared with 11% of the 37 samples from Victoria Land and 0% of the 25-member non-Antarctic population studied. Since the surfaces of many C-, G-, B- and F-asteroids seem to consist of thermally-metamorphosed materials, presumably excavated from their interiors by impacts [7-9], it will be interesting to compare these results with the thermal histories of C asteroid samples to be returned by the planned MUSES-C mission.

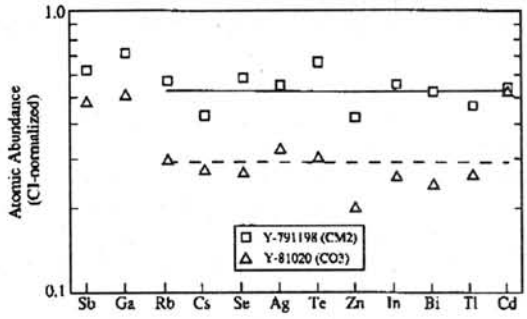

Fig. 1. Atomic abundances (C1-normalized) for thermally mobile trace elements in two apparently unmetamorphosed carbonaceous chondrites. Elements are ordered by increasing degree of vaporization and loss from Murchison (CM2) chondrite at 500-700°C [6]. Mean depletions (Rb→Cd) are 0.53±0.07xC1 for Y-791198 (CM2) and 0.30±0.08 for Y-81020 (CO3). The overwhelming majority of C1-C6 chondrites exhibit abundance patterns like these.

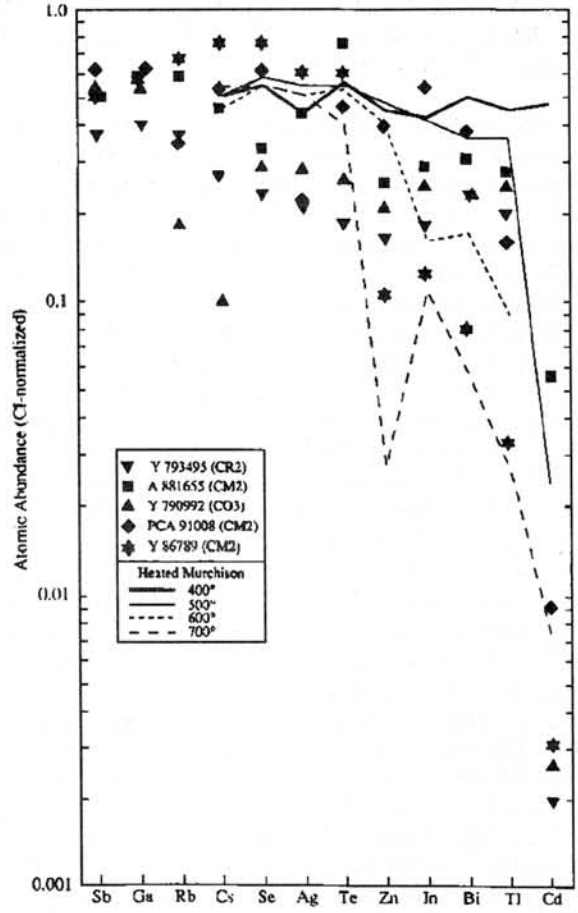

Fig. 2. Atomic abundances (C1-normalized) for thermally mobile trace elements in 5 Antarctic carbonaceous chondrites and in samples of the Murchison (CM2) chondrite heated for 1 week at 400-700°C under ambient conditions reasonable for asteroids. Three samples (A-881655, Y-793495, and Y-790992) have low Cd values resembling that of Murchison heated at 500°C. PCA 91008 has low Tl and Cd values and Y-86789 seems depleted in the 5 most mobile trace elements at the right. Trace element contents in Y-86789 (and Y-86720 [4,5]) are near levels exhibited by Murchison heated at 700°C.

REFERENCES

[1] Palme, H., Larimer, J. W. and Lipschutz, M. E., *Meteorites and the Early Solar System* (J. F. Kerridge and M. S. Matthews, eds.) 436-461 (1988). [2] Lipschutz, M. E. and Woolum, D. S., *ibid*, 462-487 (1988). [3] Xiao, X. and Lipschutz, M. E., *J. Geophys. Res.* **97**, 10197-10211 (1992). [4] Paul, R. L. and Lipschutz, M. E., *Z. Naturf.* **44a**, 979-987 (1989). [5] Paul, R. L. and Lipschutz, M. E., *Proc. Symp. Antarctic Meteorites* **3**, 80-95 (1990). [6] Matza, S. D. and Lipschutz, M. E., *Proc. 8th Lunar Sci. Conf.* **1**, 161-176 (1977). [7] Hiroi, T., Pieters, C. M., Zolensky, M. E. and Lipschutz, M. E., *Science* **261**, 1016-1018 (1993). [8] Hiroi, T., Pieters, C.M., Zolensky, M. E. and Lipschutz, M. E., *Proc. Symp. Antarctic Meteorites* **7**, 144-149 (1994). [9] Hiroi, T., Pieters, C. M., Zolensky, M. E. and Lipschutz, M. E., *Meteoritics Planet. Sci.* **31**, 321-327 (1996). [10] Matsuoka, K., Nakamura, T., Nakamuta, Y. and Takaoka, N., *Proc. NIPR Symp. Antarctic Meteorites* **9**, 20-36 (1996). [11] Akai, J., *Proc. NIPR Symp. Antarctic Meteorites* **5**, 120-135 (1992). [12] Hiroi, T., Zolensky, M. E. and Pieters, C. M., *Lunar Planet. Sci. Conf.* **28**, 577-578 (1997). [13] Clayton, R. N., Mayeda, T. K., Kojima, H., Weisberg, M. K. and Prinz, M, *Lunar Planet. Sci. Conf.* **28**, 239-240 (1997). [14] Clayton, R. N., Mayeda, T. K., Hiroi, T., Zolensky, M. E. and Lipschutz, M. E., *Meteoritics Planet. Sci.* **32**, A30 (1997). [15] Miyamoto, M., *Proc. NIPR Symp. Antarctic Meteorites* **5**, 155-164 (1992).

[16] Akai, J. and Sekine, T., *Proc. NIPR Symp. Antarctic Meteorites* **7**, 101-109 (1994). [17] Burbine, T. H. and Binzel, R. P., *Meteoritics* **30**, 494 (abstract) (1995). [18] Akai, J. *Proc. NIPR Symp. Antarctic Meteorites* **7**, 94-100 (1994). [19] Shibata, Y., *Proc. NIPR Symp. Antarctic Meteorites* **9**, 79-96 (1996). [20] Sato, K. and Miyamoto, M., *Lunar Planet. Sci.* **27**, 1129-1130 (1996). [21] Kojima, T., Yada, S. and Tomeoka, K., *Nineteenth Symp. Antarctic Meteorites*, 24-26 (1994). [22] Noguchi, T. *Proc. NIPR Symp. Antarctic Meteorites* **8**, 33-62 (1995).

Table 1. Carbonaceous chondrites presenting evidence for possible parent-body thermal metamorphism.

			Basis (Reference)					
Meteorite (Ref.)	Type	Thermal Metam.	Min. Pet.	Spec. Refl.	O-Isot.	$\bar{x} \pm \sigma$	Elements (No.)	Cd
EET 83355[3]	C2	Yes		X[12]		0.32±0.09	Cs→Cd (9)	--
EET 87522[3]	C2	Yes		X[12]		0.54±0.14	Cs→Cd (9)	--
LEW 90500	C2	No?		X[17]		0.49±0.10	Cs→Cd (9)	--
MAC 87300[3]	C2	Yes		X[12]		0.33±0.06	Cs→Cd (9)	--
MAC 88107[3]	C2	Yes		X[12]		0.32±0.05	Cs→Cd (9)	--
Y-791198	CM2	No		X[15,20]		0.53±0.08	Cs→Cd (9)	--
Y-793321	CM2	Yes	X[16,28]	X[12,15,20]	X[13]	0.51±0.08	Cs→Cd (9)	--
MAC 88100[3]	CM2	Yes?			X[13]	0.50±0.07	Cs→Cd (9)	--
Y-81020	CO3	No?	X[19,21]			0.30±0.09	Cs→Cd (9)	--
A-881655	CM2	Yes/No		X[12]	X[13]	0.39±0.17	Cs→Tl (8)	0.056
Y-793495	CR2	No	X[22]			0.21±0.03	Cs→Tl (8)	0.0020
Y-790992	CO3	Yes?	X[19,21]			0.24±0.06	Cs→Tl (8)	0.0026
ALH 85003[3]	CO3					0.23±0.04	Cs→Tl (8)	0.00440
LEW 85332[3]	CO3					0.26±0.04	Cs→Tl (8)	0.0026
ALH 81003[3]	CV3					0.29±0.09	Cs→Tl (8)	0.087
PCA 91008	C2	?		X[12]		0.46±0.13	Cs→Bi (7)	0.0092†
Y-86789	CM2	Yes	X[10]	X[12]	X[14]	0.69±0.08	Cs→Te (4)	0.0031‡
B-7904[4,5]	CM	Yes	X	X	X	0.57±0.08	Cs→Zn(5)	0.0022*
Y-82162[4,5]	C1?	Yes	X	X	X	1.36±0.18	Cs→Zn(5)	≤0.0021*
Y-86720[4,5]	CM	Yes	X	X	X	0.65±0.16	Cs→Te(4)	0.0010¶

†Also Tl = 0.16. ‡Also Zn = 0.082; In = 0.12; Bi = 0.080; T l= 0.033. *Also In = 0.36, Bi = 0.13, Tl = 0.032. *Also In = 0.51, Bi = 0.21, Tl = 0.024. ¶Also Zn = 0.076, In = 0.16, Bi = 0.028, Tl = 0.038.

MAGNETIC REMANENCE IN CHONDRULES

by

Peter Wasilewski

(Code 691, NASA Goddard Space Flight Center, Greenbelt, MD 20771)

and

Tamara L. Dickinson

(Catholic University of America, Physics Department, Washington DC 20064 and The National Science Foundation, Division of Earth Sciences, 4201 Wilson Boulevard, Arlington, VA 22230)

Chondrules are the most prominent constituents of most chondrite meteorites. Chondrules display a wide variety of mineral species and chemistries, textures, bulk and isotopic chemistries. These properties suggest formation in a dusty solar Nebula during brief energetic events with peak heating limited to a few minutes. (Grossman, 1988)

Based on cooling rates determined from chondrule textures, the chondrules cooled in an environment that prevented extremely rapid cooling.. Since transient heating events are not easily explicable in terms of the canonically acceptable evolutionary processes in the nebular disc, Levy (1988) suggested that extraordinary dynamic processes may be indicated for chondrule formation. Thus chondrules provide constraints on the nature of the early solar nebula. The high temperature events that formed the chondrules may have spanned a period as long as 10 MY.

We have studied the magnetic properties of chondrules and find that the chondrules from the ordinary chondrites are dominantly magnetized by tetrataenite. However the tetrataenite in the chondrules from different meteorites often have different properties. A variety of paleomagnetic records can be found in chondrules from each meteorite indicating that a variety of different recording scenarios have been imprinted. It is unlikely that the chondrules acquired remanence in the same way as a cooling terrestrial rock. Cooling chondrules would likely be moving relative to the field that magnetized them. We present results indicating that molten metal droplets created during the torch cutting of a steel pipe which cool as they move through the geomagnetic field, have thermal and AF demagnetization curve shapes and vector behavior similar to some of the chondrules.

The REM value is the ratio of the NRM to the SIRM. REM values are an indication of (a) the effectiveness of a remanence mechanism, (b) the influence of a remanence enhancement event such as contamination with a hand magnet or

natural events such as lightning, or (c) the influence of a remanence diminishing event such as low level shock or cooling in zero field.

Figure 1 presents histograms of the REM values for Bjurbole (H4), Chainpur (L3), and Allende (C3V) chondrules and REM values computed from the data presented by Funaki et al. (1981) for metal, chondrules, and matrix from ALH76009 (769). Terrestrial samples provide some background understanding of the meaning of the REM values. REM values for TRM (thermoremanence) acquired in the geomagnetic field range between 0.005 and 0.08. Lightning struck samples have REM values as high as 0.92 (Wasilewski and Dickinson, 1998). Values of REM >0.1 usually indicate contamination by hand magnet or natural lightning strikes.

Bjurbole and Chainpur chondrules have REM values ranging over 3 orders of magnitude, and including REM values >0.1. This range cannot be explained by differences in the mineralogy. In the Bjurbole and Chainpur chondrules the dominant magnetic mineral is tetrataenite which has uniformly large magnetic coercivity. The explanation may be due to the efficiency of remanence acquisition related to the manner in which the remanence was acquired and/or the strength of the magnetic field.

Enormous volumes of chondrules were produced in the early solar system, and were not likely produced all at once. Gooding and Keil (1981) for example suggest that porphyritic and non-porphyritic chondrules constitute two different chondrule groups which formed in different physical environments. If for the sake of argument we assume that a magnetic pulse is associated with the energetic event responsible for the chondrule forming episode, we must also accept the transient nature of the magnetic pulse. Therefore chondrules formed are moving in the magnetic field and are at varying cooling stages which may or may not be ferromagnetic when the magnetic field is present. A possible scenario to explain the REM distributions multiple events in some region altering the existent chondrules and producing new chondrules. This might also explain the wide variety of magnetic vector behavior during demagnetization.

FIGURE 1 REM histograms for chondrules from Bjurbole, Allende and Chainpur chondrite meteorites. The ALH 769 data is from Funaki et al., (1981).

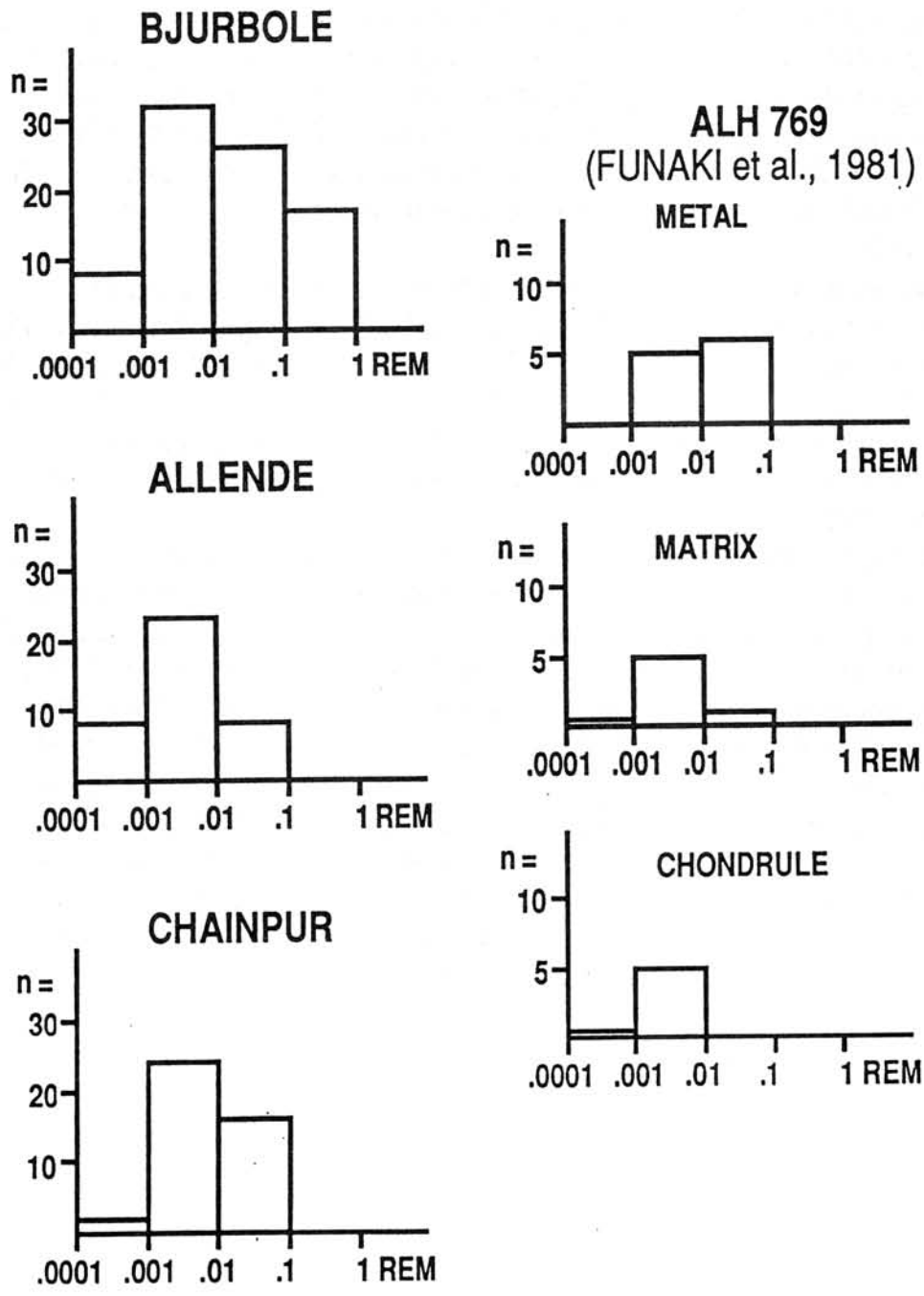

Short-lived Nuclei in the Solar System

Prof. G. J. Wasserburg
California Institute of Technology
Divisionof Geological & Planetary Sciences, MS170-25
Pasadena, CA 91125
isotopes@gps.caltech.edu

Evidence for the presence of diverse and short-lived nuclei (^{41}Ca, ^{26}Al, ^{53}Mn, ^{60}Fe, ^{129}I, ^{146}Sm, ^{182}Hf, ^{244}Pu and ^{247}Cm) in the early solar system will be reviewed. The abundance of these nuclei will be used to assess potential stellar sources from both AGB stars and supernovae. Inferences with regard to the nature of the *r*-process in supernovae and the broader astrophysical implications will be outlined. A test for a supernova trigger using ^{26}Al and ^{60}Fe will be given. The connections between the chronologies of different short-lived nuclei and their relationship to the chronologies of long-lived nuclei will be discussed. The role of planetary metamorphism as a re-setting mechanism of isotopic clocks will be presented. Time scales for planetary evolution and core formation, including the arguments for the late formation of the earth will be outlined.

EXPOSURE AGES AND TERRESTRIAL AGES OF H CHONDRITES FROM FRONTIER MOUNTAIN, NORTH VICTORIA LAND. Rainer Wieler[1], Kees C. Welten[2], Kunihiko Nishiizumi[2], and Marc W. Caffee[3], 1: ETH Zürich, Isotope Geology, NO C61, CH-8092 Zürich, Switzerland (wieler@erdw.ethz.ch); 2: Space Sciences Laboratory, University of California, Berkeley CA 94270-7450, USA; 3: Lawrence Livermore National Laboratory, Livermore, CA 94551, USA.

Various meteorite populations in Antarctica differ in their terrestrial age distribution. The Allan Hills Main Icefield and the Lewis Cliff area yield ages of up to 1 and 0.5 Ma, respectively [1-3], with one value of ~2 Ma having been reported for each of these two areas [4, 5]. On the other hand, only few Yamato meteorites have been on earth for more than 200'000 years [1, 2]. The terrestrial age distribution provides information on meteorite accumulation- and transport times as well as mean lifetimes of meteorites against weathering.

Prior to this work, few terrestrial ages had been reported for the Frontier Mountain area, North Victoria Land, where three EUROMET expeditions collected more than 350 meteorites [6-8]. Delisle et al. [6] reported terrestrial ages of 300 - 700 ka for three meteorites collected in the 1984/85 season, based on ^{26}Al. However, Nishiizumi et al. [1] state for FRO8403 a terrestrial age of only 120±100 ka, based on ^{36}Cl, six times less than the 700 ka reported in [6]. It is therefore desirable to extend the data base, preferably by analysing ^{36}Cl (half-life = 301'000 years) which is well suited to determine terrestrial ages in the 100 ka range.

We report noble gas and cosmogenic radionuclide data (He, Ne, Ar, ^{10}Be, ^{26}Al, ^{36}Cl) for 26 H5/6 chondrites and one L6 from Frontier Mountain. Preliminary noble gas and ^{36}Cl data for some of the samples were reported in [9]. Radionuclides were measured in the metal fraction, where the ^{36}Cl production rate is rather insensitive to shielding. The Frontier Mountain area, regional ice flow and the probable meteorite concentration mechanism are described in [6, 7]. Samples labelled "I" in column 2 of Table 1 were recovered on blue ice northeast of Frontier Mountain, samples marked "M" are from "Meteorite Moraine".

Specimens that probably belong to the same meteorite fall are marked in column 3 of Table 1. Pairing criteria are cosmogenic, radiogenic, and trapped noble gas components, radionuclide concentrations, and find locality. We cannot exclude some further pairings (e. g. groups d and e, although the find locality is different), but the 27 stones probably belong to at least 15 different falls. This shows that the extremely high meteorite density at Frontier Mountain is not due to a single or a few large showers. Figures 1 and 2 are corrected for the pairings listed in Table 1.

Neon-21 exposure ages in Table 1 are calculated according to Eugster [10] for samples with a ratio $(^{22}Ne/^{21}Ne)_c$ of the cosmogenic component ≥1.08. For more heavily shielded samples we use the maximum production rates given by Graf et al. [11] at the respective $(^{22}Ne/^{21}Ne)_c$ values of 1.05-1.075. These maximum values correspond to meteoroid radii of ~40-60cm, i. e. the largest bodies commonly to be expected. We estimate that most exposure ages are accurate to within 20%, except those in parentheses, for which no shielding correction is possible or for which ref. [11] may underestimate the production rate.

Figure 1 compares the exposure age distribution of the H chondrites in Table 1 with the cumulative distribution of H5 and H6 chondrites compiled by Graf and Marti [12]. The shapes of the two distributions are similar, showing the well known peak at ~7 Ma. However, the peak for the FRO samples is offset by about 10% towards low ages relative to the peak in the Graf and Marti data. This is unlikely due to a bias in analyses or calculations: i) our noble gas calibration agrees well with that in other laboratories, ii) $(^{22}Ne/^{21}Ne)_c$ ratios suggest that the distribution of preatmospheric sizes of FRO meteorites is quite typical for chondrites, hence possible errors in shielding corrections should affect both populations similarly, iii) using the production rates from [11] for meteorites with $(^{22}Ne/^{21}Ne)_c < 1.08$ has shifted some exposure ages of FRO samples towards higher values, not lower ones. Therefore, the apparently lower ages of the FRO meteorites are presumably related to their long terrestrial history. Graf and Marti [12] noted that ^{21}Ne ages of H chondrite finds in the 7 Ma peak are systematically lower by some 10% than those of falls in the same peak. Our data are very consistent with this observation. Graf and Marti suggest that this is due to a change in mass by oxidation of metal. They also observe systematically lower $^{3}He/^{21}Ne$ ratios in finds compared to falls, and the FRO samples tend to display a similar trend, indicating some loss of cosmogenic He and hence possibly also Ne. It is unclear whether the apparent slight overabundance of FRO meteorites on the left of the peak is real, and, if yes, whether it would

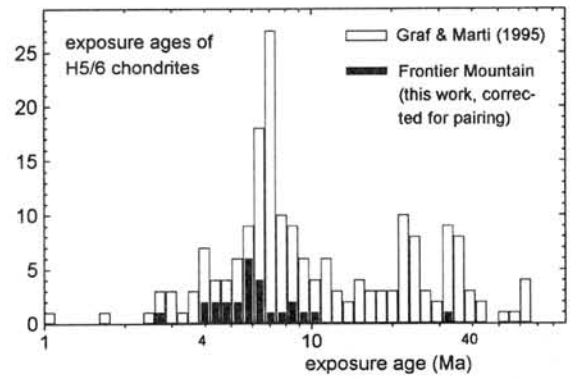

Fig. 1: Exposure ages. Average age used for paired specimens.

also be the result of cosmogenic Ne loss.

Terrestrial ages in Table 1 were calculated in two ways. The age T_t36 is calculated based on an average ^{36}Cl production rate in chondritic metal of 22.1±2.8 dpm/kg (2σ, ref. 2]. The $T_t36/10$ values, on the other hand, account for a shielding dependence of the ^{36}Cl production rate in metal by means of the relation between the $^{36}Cl/^{10}Be$ production ratio and the ^{10}Be activity [13]. The latter ages will therefore generally be more accurate. However, $T_t36/10$ ages are sometimes negative outside their nominal error limits. The value of FRO90073 is presumably dubious anyway because the adopted exposure age of 8.6 Ma is probably too high, due to the low ^{21}Ne production rate derived from ref. [11] for $^{22}Ne/^{21}Ne=1.05$. For the other $T_t36/10$ ages, the adopted exposure age is not critical, however. It is remarkable that all samples with clearly negative $T_t36/10$ were heavily shielded ($^{22}Ne/^{21}Ne \leq 1.08$; pairing group a and FRO90104). The discrepant terrestrial age values can be explained if nominally heavily shielded samples often suffer actually a two stage exposure, with the noble gases mostly recording the first stage, but ^{10}Be and ^{36}Cl the second one. This scenario and the shielding dependence of terrestrial ages based on ^{36}Cl is being investigated further. For samples with $^{22}Ne/^{21}Ne \leq 1.08$ we adopt in Fig. 2 the T_t36 age, if the $T_t36/10$ age is negative, and we show both ages otherwise (black histogram assumes T_t36 for all heavily shielded samples, grey histogram assumes $T_t36/10$ for groups d, e and FRO90207).

The main feature of Fig. 2 is the absence of Frontier Mountain samples clearly older than 200'000 or 300'000 years. Delisle et al. [6] deduced a minimum age of the "Frontier Mountain meteorite trap" of ~3.2 Ma, based on a ^{10}Be analysis of a quartz separate from a rock sample from just above the blue ice. However, our unpublished data indicate that the ^{10}Be-^{26}Al minimum surface exposure age of Frontier Mountain bedrock is ~170 ka only. This discrepancy needs to be resolved before it can be concluded whether the low terrestrial ages of the meteorites are due to a relatively rapid destruction or rather indicate a relativley young meteorite trap at Frontier Mountain. Although statistics are poor, it may be significant that the ~6 individual falls from the "Moraine" all show among the higher terrestrial age values found here (~80-200 ka). This may be because meteorites trapped in "Meteorite Valley" may get less easily destroyed than those that are wind-blown over the ice and may eventually fall into the crevasses from where the surviving ones are recycled onto the surface (Fig. 3 in ref. 7). It is unclear whether a bias was introduced in this study by studying H chondrites only, which might wheather more easily than other meteorite classes. The age distribution in the top panel of Fig. 2 [1] may suggest such a bias, but the Lewis Cliff data [3] in the middle panel do not.

Summary: Cosmic ray exposure ages of H chondrites from Frontier Mountain are similar to, but slightly lower than those observed for H chondrite falls, suggesting that exposure ages of antarctic H chondrites or antarctic meteorites in general tend to be slightly underestimated. Chlorine-36 based terrestrial ages of the Frontier Mountain H chondrites measured here do not exceed 300'000 years.

Acknowledgements: We thank EUROMET for providing the samples and NIPR for financial support allowing the first author to present this work. This study is supported by NASA, NSF, and the Swiss National Science Foundation.

References: **1**: Nishiizumi K et al. (1989) EPSL 93, 299. **2**: Nishiizumi K (1995) Lunar Planet. Inst. (Houston) Tech. Rpt. 95-02, 53. **3**: Welten K et al. (1998) Meteorit. Planet. Sci. 33, in press. **4**: Welten K et al. (1997) Meteorit. Planet. Sci. 32, 775. **5**: Scherer P et al. (1997) Meteorit. Planet. Sci. 32, 769. **6**: Delisle G et al. (1989) Geol. Jb. E38, 483. **7**: Delisle G et al. (1993) Meteoritics 28, 126. **8**: I. A. Franchi (EUROMET), pers. comm. **9**: Wieler R et al. (1995) Lunar Planet. Inst. (Houston) Tech. Rpt. 95-02, 70. **10**: Eugster O (1988) GCA 52, 1649. **11**: Graf T et al. (1989) GCA 54, 2521. **12**: Graf T & Marti K (1995) JGR 100 (E10), 21247. **13**: Nishiizumi K et al. (1997) Meteorit. Planet. Sci. 32, A100.

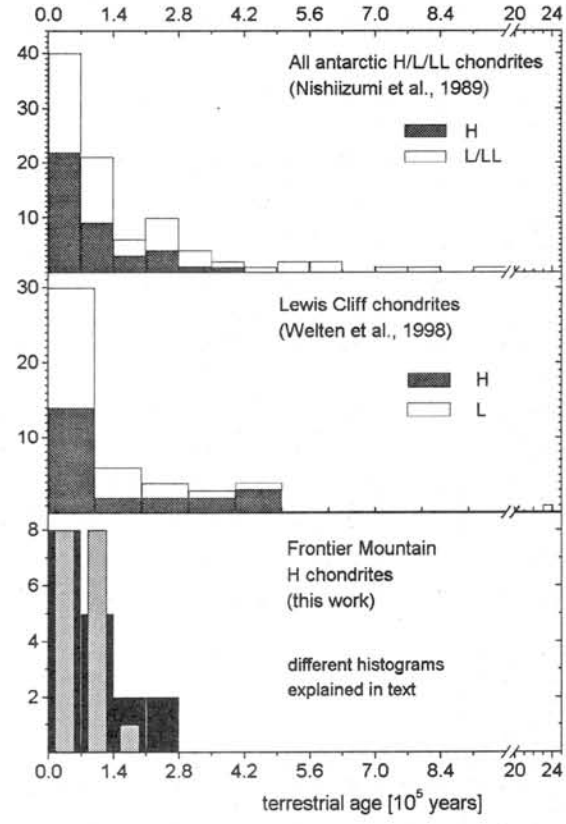

Fig. 2: Terrestrial ages of chondrites from Frontier Mountain and other localities in Antarctica. Average age used for paired Frontier Mountain samples.

Table 1: Noble gas and radionuclide concentrations, exposure ages and terrestrial ages of Frontier Mountain meteorites

FRO...	Type/ Loc.	pai-red	^{3}He	^{4}He	^{20}Ne	^{21}Ne	^{22}Ne	^{36}Ar	^{38}Ar	^{40}Ar	^{21}Ne$_c$	22/21$_c$	T_{exp} [Ma]	^{10}Be (2σ)	^{26}Al (2σ)	^{36}Cl (2σ)	T_t36 [ka, 2σ]	T_t36/10 [ka, 2σ]
8401	L6 I		16.0	170	5.912	5.860	6.970	1.044	0.941	560	5.858	1.18	24.9	6.07±0.31	4.30±0.26	23.1±0.80	-19±63	19±35
8403	H6 M												4.7			17.1±2.98	111±94	
90001	H6 I	a	3.26	386	1.632	1.745	1.844	0.516	0.250	3070	1.745	1.06	*6.1*	3.54±0.16		21.4±0.48	14±58	-72±41
90002	H5/6 I	b	8.78	10900	36.7	1.380	4.45	2.463	0.602	4650	1.29		(4.2)	4.10±0.25		19.9±0.45	45±58	42±42
90012	H5 M		18.24	47200	95.8	2.365	10.53	4.647	1.158	4600	2.12		(6.9)	3.59±0.19	2.43±0.14	15.8±0.32	145±58	80±40
90024	H5 M		4.13	1930	2.168	1.922	2.138	0.556	0.370	51	1.921	1.09	5.7	4.21±0.19		14.1±0.52	194±64	195±39
90025	H6 I		4.79	199	0.899	0.660	0.876	0.361	0.161	1270	0.659	1.28	3.8	5.15±0.26	3.58±0.22	18.3±0.56	82±61	127±34
90037	H5 I		9.11	1200	1.173	1.049	1.409	0.651	0.323	4810	1.048	1.32	6.6	6.11±0.75	3.83±0.24	19.4±0.38	57±58	103±34
90043	H6 I	b	14.09	27800	125.6	1.849	11.80	7.27	1.521	4920	1.54		(5.0)	3.65±0.15		18.9±0.42	68±58	17±42
90048	H6 I		45.8	1780	6.37	6.08	7.62	0.981	1.016	5410	6.06	1.24	31.1	5.85±0.24		20.8±1.44	27±82	64±41
90050	H5 I	a	3.96	458	1.523	1.520	1.645	0.914	0.246	3950	1.520	1.075	*4.5*	3.50±0.25		20.3±0.45	37±58	-23±48
90059	H5 I		5.72	1090	1.089	1.139	1.280	0.739	0.260	4620	1.139	1.12	3.9	4.13±0.17		19.6±0.47	52±59	59±40
90069	H6 I	c	9.70	1430	1.793	1.902	2.127	0.598	0.333	5310	1.902	1.12	6.3	5.10±0.21		23.7±0.68	-30±60	-12±36
90072	H5 I		12.61	1605	1.835	1.843	2.219	0.841	0.386	4970	1.843	1.20	8.2	5.65±0.27		22.9±0.64	-15±60	17±35
90073	H6 I	a	3.03	338	1.512	1.635	1.718	0.434	0.215	2790	1.635	1.05	*(8.6)*	3.09±0.13		20.6±0.58	30±60	-124±40
90082	H5 M		13.66	1390	1.955	1.888	2.330	0.613	0.342	4820	1.885	1.22	9.1			17.3±0.56	106±57	
90087	H5 M	d	7.22	1290	1.749	1.929	2.063	0.665	0.323	5110	1.929	1.07	*5.9*	3.20±0.15	2.32±0.20	14.2±0.30	193±58	103±42
90104	H6 I		5.35	152	3.258	3.423	3.709	1.281	0.532	926	3.422	1.08	10.0	4.30±0.31	3.70±0.22	23.2±0.41	-21±57	-63±42
90107	H5 M	d?	7.02	1310	1.680	1.702	1.881	2.784	0.715	5860	1.701	1.10	5.3	3.79±0.30	2.75±0.32	14.9±0.46	171±61	144±46
90150	H6 I	c?	9.27	1430	1.634	1.553	1.826	1.518	0.501	5830	1.552	1.16	6.2	5.42±0.54	4.10±0.32	23.0±0.54	-18±59	13±38
90151	H5 I		4.16	283	1.540	0.580	0.828	0.425	0.187	4120	0.576	(1.24)	3.0	4.97±0.29	3.76±0.22	18.1±0.78	86±66	133±33
90152	H5 I	a?	3.54	352	1.674	1.777	1.892	0.387	0.239	2240	1.777	1.06	*6.4*			20.7±0.74	29±57	
90174	H5 M	d?	6.51	1320	3.994	1.806	2.175	0.931	0.350	4720	1.797	(1.07)	5.6	3.51±0.15	2.65±0.18	14.9±0.49	172±62	115±42
90203	H6 I	e	6.73	1270	1.940	1.964	2.111	0.695	0.308	5100	1.963	1.07	*6.0*	2.56±0.14	1.98±0.14			
90204	H6 M	d	6.72	1440	1.743	1.807	1.951	0.638	0.275	5670	1.807	1.07	*5.5*	2.93±0.13	2.28±0.24	13.9±0.46	201±62	83±45
90207	H5 M		8.48	1390	2.439	2.607	2.792	0.913	0.407	5400	2.607	1.07	*7.9*	2.61±0.11	1.92±0.12	12.2±0.26	257±58	79±40
90211	H5/6 I	e	6.62	1320	1.719	1.899	2.034	1.331	0.387	5240	1.899	1.07	*5.8*	2.84±0.12	2.04±0.18	13.0±0.30	230±59	101±42

Noble gas concentrations in [10^{-8} cm^{3}STP/g], radionuclide activities in dpm/kg. All radionuclide data refer to the metal phase. Uncertainties of noble gas concentrations ~4%, uncertainties of the ratio ^{22}Ne/^{21}Ne$_c$ of the cosmogenic component ~1% (~2% for values in parentheses). Cosmogenic Ne calculated by subtracting trapped Ne of solar composition for 90002, 90012, and 90043 and atmospheric Ne otherwise. ^{21}Ne exposure ages calculated with shielding correction according to ref [10], except for italicized values, i. e. if $(^{22}Ne/^{21}Ne)_c$ <1.08. Here, the maximum ^{21}Ne production rate for heavily shielded samples according to ref. [11] was assumed. Exposure ages in parentheses assume $(^{22}Ne/^{21}Ne)_c$=1.11. Terrestrial ages T_t36 and T_t36/10 calculated as explained in text. Errors (2σ) include 2σ uncertainties of radionuclide analyses and production rates as well as 20% uncertainty of the exposure age. Exposure age of FRO8403 from ref. [6].

Reflectance Spectra Change of Planet-Forming Materials Due to Laser Irradiation and Proton Implantation

Maho Yamada*, Sho Sasaki, Hiroko Nagahara
Geological Institute, School of Science, Univ. Tokyo, Tokyo 113-0033, JAPAN

Akira Fujiwara, Sunao Hasegawa, Hajime Yano
Institute of Space and Astronautical Science, Sagamihara, Kanagawa 229-8510, JAPAN

Hideo Ohashi
Laboratory for Physics, Tokyo University of Fisheries, Minato-ku, Tokyo 108-0075, JAPAN

Hisashi Ohtake
Tsukuba Space Center, National Space Development Agency of Japan, Ibaraki 305-8505, JAPAN

For the purpose of simulating the surface alteration process called "space weathering", experiments of proton implantation, laser irradiation, and laser irradiation to proton implanted samples were performed and reflectance spectra of altered materials were obtained. To simulate heating by micrometeorite bombardments, we made a new apparatus using a laser whose pulse duration is 6-8 nsec. We also investigate the influence of solar wind proton and FeO content of minerals. Although FeO did not affect the degree of reflectance change, the proton implantation caused some changes. Samples heated after the proton treatment show larger spectral change than just heated samples. Laser irradiation onto olivine produced the largest depletion of albedo and reddening of reflectance spectrum. In general, the variation of olivine spectra were larger than those of pyroxenes.

1. Introduction

The lack of spectral link between ordinary chondrites and asteroids is a long standing problem. S-type asteroids are believed to be parent bodies of ordinary chondrites (Chapman, 1996). But S asteroids are characterized by steep red continua unlike those of the ordinary chondrites, and their spectrally derived mineralogies are far outside the ordinary chondrites' range (Gaffey et al. 1993). The spectral mismatch between S-type asteroids and ordinary chondrites resulted from some "space weathering" process which altered the optical properties of the uppermost regolith. Plausible processes such as impact induced reduction of silicate iron, both in the impact melt and in the impact-generated vapor, appear to produce an optically important effect. Studies of lunar regolith fractions indicate that "mature" soils, containing more SMFe (submicroscopic metallic iron), are darker and somewhat redder than "immature" soils of the same composition, and features in the reflectance spectra become more subdued with increasing soil maturity. The SMFe would be formed when soil particles containing solar wind protons are impacted by micrometeoroids. Theoretical models calculated by Hapke (1993) demonstrate that SMFe distributed throughout the glass and also coating the crystalline grains can account for the optical properties of lunar soils.

To simulate heating by micrometeorite impacts, high-velocity (>10km/s) impact experiments are difficult in producing enough number of dust impacts. Moreover, electrostatic dust accelerators should use conductive dust materials (e.g., C, Fe, Ag) which are not suitable to see the optical effects. Previously heating experiments were done by continuous heating by fusion furnace (Clark et al., 1992, Allen, 1993). Using a pulse laser for heating, Moroz et al. (1993) obtained results where ordinary chondrites were modified to have S-type characteristics. However, the laser pulse duration was 0.5-1μsec which was 1000 times of real microimpact time scale. Moreover, effect of protons and Fe contents have not been discussed well. In the present study of space weathering simulation, we used pulse laser whose pulse duration is 6-8 sec. We also implanted protons into sample materials to see the reduction effect.

* Now at Japan Space Forum, 1-29-6 Hamamatsu-cho, Minato-ku, Tokyo 105-0013, JAPAN

2. Experimental Procedure

Starting Materials We used olivine and orthopyroxene for these experiments because these minerals are common in ordinary chondrites. In order to study the influence of iron content to spectral changes, several different pyroxenes were selected. Olivine is a pure sample from San Carlos with 8.97 wt% FeO (Fo_{91}). Enstatite from Bamble, Norway, is essentially a pure sample with 9.88 wt% FeO (En_{85}). A pure hypersthene from Mäntyharju, Finland, contains 16.70 wt% FeO (En_{71}). Diogenite Tatahouine meteorite, Foum Tatahouine, Tunisia, is almost pure orthopyroxene whose composition is En_{75}. Samples were ground by an agate mortar and separated to a particle size <75μm by a stainless steel sieve.

Laser irradiation In order to simulate heating by micrometeorite impacts, the powdered specimens were treated by laser irradiation under vacuum at $2x10^{-5}$ mmHg. We use a solid-state Nd-YAG pulse laser with impulse frequency 20Hz. The wavelength of laser irradiation was 1064nm. Pulse duration was 6-8 nsec, which is equal to real micrometeorite bombardment timescale, and pulse energy is variable from 1 to 30 mJ. To achieve uniform irradiation on the sample surface, we made a new small chamber on the X-Y stage. The surface scanning is performed by moving the chamber. The powdered samples are placed in an aluminum holder. The weight of the powder is 0.10g and the thickness of the powder layer is about 1 mm.

Proton irradiation We did ion implantation experiments by RAPID (Rutherford Backscattering Spectroscopic Analyzer with Particle Induced X-ray Emission and Ion Implantation Devices) located at Research Center for Nuclear Science and Technology, the University of Tokyo. The resulting beam was about a few mm in diameter with energy 1MV with a current density of about 15~30 nA/cm^2 which varied depending on the machine condition. Total dose N_d of these samples was between 4.89×10^{15} and $1.41x10^{16}$ cm^{-2}. Since the ion beam comes horizontally with 7° injection angle, we made special sample holders which were covered with carbon-coarted mylar films, preventing powders not only from falling but also being charged up (Ohashi et al., 1993).

Measurement of reflectance spectra After the proton and laser irradiation, the reflectance spectra of samples were measured. Bidirectional reflectance spectra were obtained at the facility at Future Space Systems Laboratory, at Tsukuba Space Center of National Space Development Agency of Japan (NASDA). Observational geometry was set up to simulate that of telescopic observation: an incidence angle of 30° and an emission angle of 0°. Bidirectional reflectance spectra in the range 250 - 2600 nm were recorded every 10nm. All spectra were measured relative to spectralon, a near perfect diffuse reflector in this wavelength region. We confirmed that errors caused by sample packing were less than 2% in reflectance spectra. To see the spectrum change of the most affected sample surface, we also measured some spectra of samples which were not repacked after laser irradiations.

3 Results

Laser irradiated samples

[Olivine samples] Experiments of laser irradiation using olivine pellets were carried out under various laser pulse energy of 1 mJ, 15 mJ and 30 mJ. The reflectance of pellet is higher than that of powders. Figure 1 shows resulting spectrum normalized at 560nm. As for the sample irradiated by 1mJ-pulse, no spectral change is observed all over the wavelength. The spectrum of irradiated sample by energy of 15 mJ has a striking drop of reflectance, especially at ultraviolet and visible region. The maximum of depletion is 34% at 410 nm. Still more diminution of albedo occurred on the sample heated by the highest energy. The maximum change of it is 46% at 420 nm. Both spectra are reduced about 10% even at the region where wavelength is longer than 1500 nm.

[Enstatite and Hypersthene] Both orthopyroxenes were irradiated by the energy of 30 mJ. As for enstatite, albedo at 370 nm decreases 16%, which is the maximum of depletion. Though diminish at 1170 nm of 17% is also noticeable, little changes are observed near 1500 nm and beyond 2200 nm. The reflectance of heated hypersthene became lower in the left part of 2000 nm. Darkening at 400 nm is 13% and notable decrease from 1100 nm to 1200 nm of about 12% is found. In order to see the

effect of more heating, we performed 10 and 20 times scannings of laser irradiation onto pyroxene samples. Figure 2 shows the normalized result for enstatite. Although the resulting spectra shows reddening but little change in depth and width of absorption bands.

Proton-implanted samples

[Samples of olivine] Albedo changes of olivine after the proton implantation are significant. A sample with shorter irradiation (N_{d1} = 4.89 x 10^{15}) shows no difference from unprocessed olivine at longer wavelength than 700 nm, it shows depletion of albedo from 300 nm to 700 nm. The largest depletion is observed at 390 nm of 5%. On the other hand, reflectance of olivine with more implanted proton (N_{d2} = 1.41x10^{16}) decreases all over the recorded range. In the region of longer than 1500 nm, changes are about 2%. In ultraviolet and visible region, depletion is apparently significant and decrease in 10.5% is recorded at 390 nm.

[Orthopyroxenes] Enstatite-1 (N_{d1}) gives almost the same reflectance as raw enstatite over 750 nm, but under 750 nm, reflectance decreases especially at 380 nm of 5.2%. Variation of enstatite-2 (N_{d2}) resembles that of enstatite-1 and it shows 6% depletion at 380 nm. The difference between enstatite-1 and enstatite-2 is small. Changes of hypersthene and diogenite spectra are only less than 2%; they display no alteration in reflectance which is worth discussing. According to the theory of SMFe, hypersthene and diogenite would have shown larger albedo changes than olivine and enstatite, because they contain more FeO. Here, we obtained no evidence for dependence on FeO abundance.

Proton-implanted and laser-irradiated samples

Both mineral grains before and after proton implantation treatment were heated by laser pulse to examine whether the existence of hydrogen atoms affect alteration of spectral change or not when minerals are heated. According to "space weathering" hypothesis, it is expected that the degree of alteration of proton implanted sample will be greater than that of the sample without implantation. In fact, olivine showed such tendency. Proton-implanted samples have more change than heated olivine without proton, and the more proton-containing sample shows the redder spectrum. Pyroxenes also have the similar tendency about proton existence, although they do not seem to have dependence on the number of proton. But anyway, we have found additive but no multiplicational effect between proton implantation and laser heating. Existence of proton could not influence on laser experiments. Proton implantation seem to have similar but weaker effect to heating itself.

XRD

We analyzed irradiated samples using XRD. Minerals have characteristic reflectional peaks corresponding to the atomic distance in its structure. We selected seven strong peaks and compared these relative intensity (scaled by the intensity of the peak at 5.102Å) and full width at the half maximum. If systematic alteration dependent on crystal structure, particular peak would be changed. Or apparent vitrification would make peaks broaden. However, we found no systematic variation consisting with spectral change. In addition, the peak of iron at d=2.03Å was not observed. Olivine and enstatite themselves have small peak at the same point. Even if a little iron was produced, its peak would be covered with that of minerals.

Observations under a microscope show that altered samples have brown-rough-surfaced grains. It was not certain whether it was amorphous or not, but vitrification or breaking mineral structure is one possible cause of the spectral changes. However, XRD results suggest that a large part of samples survived as undamaged mineral with little vitrification against laser heating.

Acknowledgements: The authors appreciate Y. Iijima, K. Shirai, and T. Okada for help in making apparatus, and T. Kadono and T. Nishimura for maintenance of the laser device. We also thank N. Geshi for his help with preparation of mineral powders and EDS operation, M. Kishima and H. Takayama for help in XRD analysis. We wish to thank T.Kawanishi and A. Morita for his RAPID operation, Y. Kuwata for advice of a sample holder, and Y. Hamabe for her helping in our proton implantation. We are grateful to M. Abe, Y. Ishibashi for their suggestion of spectral change due to energy particle. We are grateful to M. Otake and J. Owada for the measurements of the reflectance spectra at Tsukuba Space Center of NASDA.

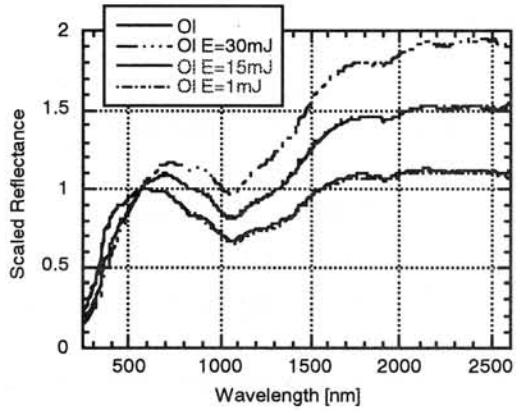

Fig. 1 Scaled reflectance spectra of olivine at various energy of pulse laser irradiation.

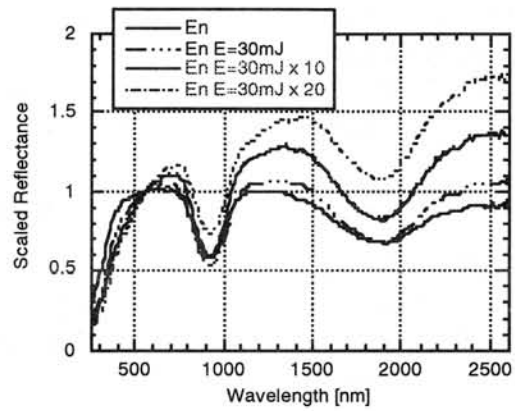

Fig. 2 Scaled reflectance spectra of enstatite at various scanning time of laser irradiation. (pellet sample without repacking).

References

Allen, C. C., et al. (1993) Microscopic iron metal on glass and minerals-A tool for studying regolith maturity. Icarus **104**, 291-300.

Chapman, C. R. (1996) S-type asteroids, ordinary chondrites, and space weathering: The evidence from Galileo's fly-bys of Gaspra and Ida., Meteoritics & Planet. Sci. **31**, 699-725.

Clark, B. E., et al. (1992) Meteorite-asteroid spectral comparison: The effects comminution, melting, and recrystallization. Icarus **97**, 288-297.

Gaffey, M. J. et al. (1993) Mineralogical variations within the S-Type asteroid class., Icarus **106**, 573-602.

Hapke, B. (1973) Darkening of silicate rock powders by solar wind sputtering. Moon **7**, 342-355.

McCord, T. B. et al. (1970) Asteroid Vesta: Spectral reflectivity and compositional implications. Science, **168**, 1445-1447.

Moroz, L. V., et al. (1996) Optical effects of regolith processes on S-asteroids as simulated by laser shots on ordinary chondrite and other mafic materials. Icarus **122**, 366-382.

Ohashi, H., et al. (1993) Carbon-coated film method PIXE for thick and insulating samples. Nuclear Instruments and Methods in Physics Research, B**75**, 140-143.

Shock moblization of plagioclase: an experimental study

Akira Yamaguchi and Toshimori Sekine

National Institute for Research in Inorganic Materials, 1-1 Namiki, Tsukuba 305-0044, Japan

Introduction

Shock metamorphism is a prime factor affecting very fundamental properties of meteorites. Plagioclase and pyroxene are major constituent minerals in many meteorites. Plagioclase transforms into glass phases above shock pressures of ~30 GPa. In contrast, pyroxene remains crystalline at up to ~80 GPa. Recently, Scott et al. (1997; 1998) found evidence for mobilization of plagioclase melts in ALH 84001. Subsequently, El Goresy (1997a,b) suggested that "maskelynites" in Shergotty are in fact produced by melting of plagioclase, not by solid-state transformation as previously suggested (e.g., Stöffler et al., 1986). If so, alkaline volatiles in plagioclases may be easily redistributed throughout the rock by shock. This is crucial for understanding of chemical evolutions disturbance of radiometric ages of meteorites such as martian meteorites and eucrites (e.g., Bogard, 1995).

In previous textural studies of shock recovered plagioclase-bearing rocks (e.g., Kieffer et al., 1976; Schaal and Hörz, 1977), natural samples were selected as starting materials. Due to the complicated textures of natural samples, however, it is difficult to observe minor textural changes due to shock. In addition, detailed microtextural study of shock recovered samples is still lacking. Therefore, we have performed shock recovery experiments of plagioclase and pyroxene with a simple textural setting and observed microtextures of the recovered samples.

Shock recovery experiments

The shock recovery experiments were performed by using a single stage 30-mm bore propellant gun at the National Institute for Research in Inorganic Materials with shock pressures of 30, 35, 42, and 55 GPa. The target is a doubly polished disk (12 mm in diameter and 0.7-1.2 mm thick) of plagioclase in contact with a doubly polished disk of pyroxene in the clyndrical container made of stainless steel, 24 mm in diameter and 30 mm in length. The bottom of container is covered by copper (~0.2 mm thick) to reduce the roughness. The projectiles are a 8 mm-thick plate made of stainless steel SUS 304 or a 4-mm-thick plate made of molybdenum, which is bedded at the front to of a polyethylene sabot. The peak shock pressure produced in the target samples is regarded as an equilibrated value with that of target assembly and is determined from the velocity of projectile measured just before impact and the Hugoniot. Detailed of shock-experimental procedures are described by Sekine et al. (1987). Starting materials for these experiments were single crystals of unshocked enstatite from Bamble (Norway) and plagioclase from Chihuahua (Mexico). Chemical compositions of the Bamble enstatite is $En_{85.8\text{-}86.0}Wo_{0.2\text{-}0.4}$, and the Chihuahua plagioclas, $An_{59.6\text{-}61.6}Or_{1.4\text{-}1.7}$. Polished thin sections were made from each recovered sample by cutting along the shock compaction axis and examined by optical and scanning electron microscopy. Chemical analysis was made by electron microprobe with a defocused beam.

Results

In the sample recovered from 30 GPa, about 90 % of plagioclase is converted to glass phase, and the rest shows heavy mottled extinction. Plagioclases recovered above 35 GPa are completely converted into glass phases. Plagioclase glasses have smooth surface and are less fractured in contrast to pyroxenes. Pyroxene shows strong wavy extinction, many of which are misorientated by 10-15°. In the samples shocked above 42 GPa, pyroxenes show mosaic extinction. Microfaults are observed at the edges of samples. In all recovered samples, boundaries between plagioclase and pyroxenes are zigzagged (Fig. 1), which were originally flat surface before shock. The wedges of brecciated pyroxenes are often intruded into plagioclase glass without extended cracks in plagioclase glasses. As increases pressures, degree of brecciation of

pyroxenes is more enhanced. In the samples recovered above 35 GPa, the plagioclase-pyroxene boundaries are sintered and pyroxene fragments (<10-50 μm) are set in plagioclase glass (Fig. 2). The presence of small vesicles (a few μm in diameter) in the samples recovered above 35 GPa suggests melting of plagioclase. However, clear flow texture (Stöffler et al., 1991) is observed under optical microscope only in the 55-GPa shocked sample. These facts suggest fluid like behavior of plagioclase glasses. However, most boundaries between copper and plagioclase are zigzagged in all samples, and copper are injected into plagioclase forming veins in some cases (Fig. 1). This suggests solid like behavior of plagioclase glass. Mixed melts of pyroxene and plagioclase are rarely observed, which are commonly observed in shock recovered samples from above 5-10 GPa (Bischoff and Stöffler, 1992). Such mixed melts may have been formed at hot spots due to the presence of the small pore spaces. For the present, we do not find significant chemical changes of plagioclase (glass) in the all recovered samples in spite of the evidence of melting.

Discussion

Based on their shock experiments, Kieffer et al. (1976) showed that melting of plagioclase (An_{60}) (evidenced by presence of normal glass) is observed in samples shocked to 43 GPa. They observed nearly total amorphization without significant evidence of flow in samples recovered from 25-33 GPa. Schaal and Hörz (1977) observed selective melting of plagioclase (An_{80-90}) in samples shock to above 45 GPa. In general, diaplectic glass of plagioclase may be formed above ~25 GPa and normal glass, above 45 GPa (Bischoff and Stöffler, 1992).

Smooth plagioclase glasses in contact with brecciated pyroxenes and pyroxene fragments in plagioclase glass in the samples recovered above 35 GPa, which is about transition pressure from crystalline to amorphous phases, may be evidence for melting of plagioclase (El Goresy et al., 1997a,b). Recently, Langenhorst (1994) suggested that diaplectic glass of quartz is actually quenched product of high-pressure melt. This mechanism favors our observation for plagioclase glass. However, zigzagged boundaries between copper and plagioclase and the presence of copper veins in plagioclase glass may argue against total melting of plagioclase because copper also tends to act as fluid under pressure. Probably, plagioclases are partly melted or the melting is restricted along the boundaries with pyroxenes. However, it is difficult to explain total amorphization if diaplectic glass is quenched high-pressure melt. Therefore, copper may have intruded into plaigoclase glass after solidification of plagioclase melt during decompression.

Plagioclase glasses mobilized into pyroxenes as observed in the recovered samples less than several tens μm, which is far smaller that observed in ALH 84001 (Scott et al. 1997; 1998). The duration of shock (typically about 1 μm in the case of laboratory experiments) and the decompression curve of pressures are different from those of natural cases. The presence of high pressure polymorph in Shergotty and possibly in ALH 84001 (El Goresy A. et al., 1998) suggests much longer duration of shock of natural samples. Longer duration of shock may have produced veins and redistributed plagioclase glass such as those observed in ALH 84001 (Scott et al., 1997; 1998). On the other hand, many shocked meteorites such as ordinary chondrites and eucrites contain mixed melt rather than monomineralic melt (e.g., Stöffler et al., 1991; Yamaguchi et al., 1993). Further study is required to clarify the conditions of formation of monomineralic melting.

References: Bischoff A. and Stöffler D. (1992) *Eur. J. Mineral.* **4,** 707-755. Bogard D. (1995) *Meteoritics* **30,** 244-268. El Goresy A. et al. (1997a) *Antarctic Meteorites* XXII, 27-30. El Goresy A. et al. (1997b) *Meteoritics&PS* **32,** A38-A39. El Goresy A. et al. (1998) *Lunar Planet. Sci.* **29.** Kieffer. et al. (1976) *Proc. Lunar Planet. Sci. Conf.* **7,** 1391-1412. Langenhorst F. (1994) *Earth Planet. Sci. Lett.* **128,** 683-698. Sekine T. et al. (1987). *J. Mat. Sci.* **23,** 3615-3619. Scott E.R.D. et al. (1997) *Nature* **387,** 377-379. Scott E.R.D. et al. (1998) *Meteoriotics,* in press. Schaal R.B. and Hörz F. (1979) *Proc. Lunar Planet. Sci. Conf.* **8,** 1697-1729. Stöffler D. et al. (1986) *Geochim. Cosmochim. Acta* **50,** 889-903. Stöffler D. et al. (1991) *Geochim. Cosmochim. Acta* **55,** 3845-3867. Yamaguchi A. et al. (1993) *Meteoritics* **28,** 462-463.

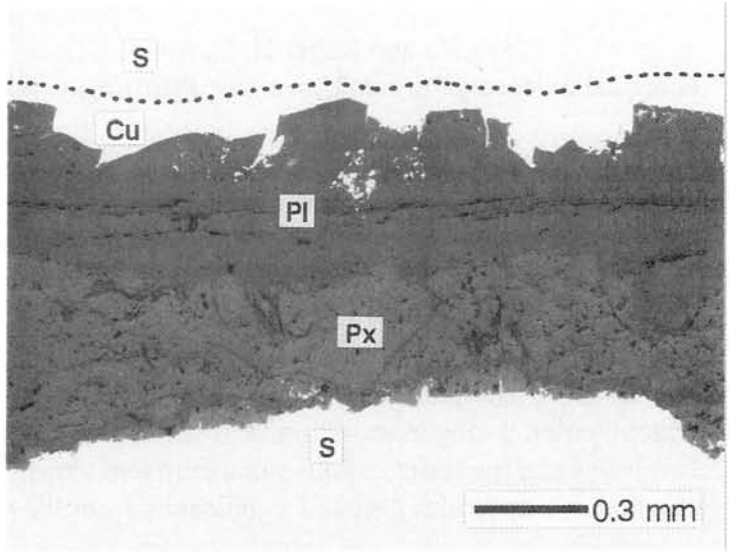

Fig. 1. Photomicroscope (reflected light) of sample recovered from 55 GPa, showing zigzagged pyroxene (Px) - Plagioclase (Pl) boundary which was flat surface before shock. Boundary between copper (Cu) and plagioclase is also zigzagged. Copper is partly injected into plagioclase glass. White: stainless steel (S) or copper.

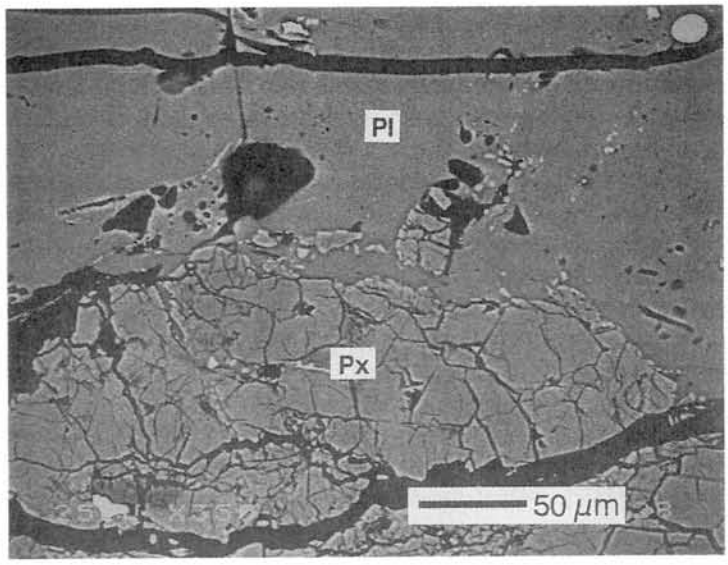

Fig. 2. Backscattered electron image of boundary between plagioclase and pyroxene in sample recovered from 55 GPa. Pyroxene (Px) is heavily brecciated in contrast to smooth plagioclase glass (Pl) which contains fragments of pyroxene and vesicles. Black is epoxy.

Chondrule formation in a non-canonical nebular environment

Yang Yu and Roger H. Hewins
Department of Geological Sciences, Rutgers University, Piscataway, NJ 08854-8066, USA

Introduction The canonical solar nebula has a pressure of less than 10^{-3} atm with the gas dominated by H_2 and very low fO_2 (4 - 7 log units below iron-wustite buffer) (Wood and Morfill, 1988; Rubin et al. 1988). Chondrules are widely believed to have formed in the solar nebula, but did they really form in such a "typical" nebular environment? Chondrules are formed by processes with very high temperatures involved (~1400 - 1800°C, Hewins an Radomsky, 1990). At such high temperatures, the nebular gas pressure affects many aspects of chondrule formation, especially the rate of evaporation, isotopic exchange between chondrule melt and ambient gas, as well as isotopic mass fractionation during evaporation. However, from the characteristics observed in natural chondrules and the results of our simulation experiments, it seem that the formation environment of many chondrules deviated significantly from the canonical nebula.

Observations Na is a moderately volatile element that is expected to be very low in chondrules due to significant evaporative losses at high temperatures, but the fact is that many of the FeO-rich chondrules (type II) have Na contents comparable to that of CI chondrites. There have been several attempted explanations, and the most popular one nowadays is the flash heating scenario. Flash heating simulation experiments (Yu and Hewins, 1998) show that fast heating/cooling can significantly reduce the Na loss from chondrule-like materials, provided that the ambient gas pressure is close to 1 atm and fO_2 is relatively high (~ close to iron-wustite buffer). Under such condition, up to 95% of Na can be preserved. At low pressures and low fO_2 close to that of the canonical nebula, however, it becomes very difficult to keep Na in the charge and the Na loss is orders of magnitude higher than 1 atm (Yu and Hewins, 1997).

K is also a moderately volatile element. Though generally low in chondrules compared to Na, it has the advantage over the latter in that it has three isotopes, which could be used to study isotopic fractionation during evaporation processes. Evaporation experiments (Yu et al., 1998) performed under low pressure (close to that of canonical nebula) have revealed normal Rayleigh fractionation for K isotopes. In systems with H_2 or 1 atm gas pressure, on the other hand, K isotope mass fractionation is still observed, but its extent is significantly less than the predicted fractionation line. For natural chondrules, Humayun and Clayton (1995) have measured K isotopes in a single Allende chondrule and found no isotopic mass fractionation. We have picked the chondrules in Bishunpur for which significant evaporative losses are likely, and analyzed their K isotopes with ion probe. No isotopic fractionation is found in any of these chondrules.

Oxygen isotopes of materials from different chondrites lie in different regions of the three-isotope-diagram and each group forms liner arrays with different slopes. These have been interpreted to be results of isotopic exchange between the meteorite materials and the ambient gas reservoir (Clayton, 1993). The oxygen isotope exchange reaction could most easily take place at relatively high temperatures, especially during the chondrule formation stage. Our oxygen isotope exchange experiments (Yu et al., 1995) show that at 1 atm and chondrule formation temperatures,

oxygen isotope exchange between meteorite material and ambient gas is rapid: 70% of the exchange required for equilibrium can be reached in less than 30 minutes. However, among factors affecting the time required to reach equilibrium is the partial pressure of ambient oxygen. With gas diluted with He, exchange rate is lowered significantly. Although there are not yet experiments done under low pressures, it is reasonable to predict that oxygen isotope exchange rate would be much lower under canonical nebula pressure and fO_2 conditions. To reach the extent of oxygen isotope exchange observed in natural meteorites and chondrules, a prolonged heating time would have been required. This is in contradiction with the relatively high volatile element contents found in many FeO-rich chondrules.

Reduction is a common phenomenon in chondrules, especially in FeO-poor chondrules (type I). A typical indication of such an effect is the occurrence of "dusty olivines" with Fe metal blebs inside the olivine grains. Reduction can occur due to the reactions with highly reduced ambient gas, or with the carbon present in the precursor dusts (Connolly et al., 1994). Currently it is not clear which mechanism was dominant in the actual nebula. The effect of nebular gas pressure on the reduction should be minimal if C is the primary cause of reduction, but would be significant if gas reduction played a major role. Our experiments show that with an fO_2 in the ambient gas equal to or lower than two log units below iron-wustite buffer, dusty olivine can be easily reproduced in normal chondrule-forming conditions, even with flash heating. On the other hand, we have not yet found any dusty olivine in the charges heated in low pressure ($\sim 10^{-4}$ atm) system flushed with H_2.

Discussion Under canonical nebular conditions with low gas pressure and low fO_2, we would expect rapid Na loss, Rayleigh isotopic fractionation, low oxygen isotopic exchange rate, and low reduction reaction rate for chondrule materials. However, these are not the general characteristics we observe in natural chondrules. Interpretation of these contradictions can go in two directions. The first one is that chondrules are formed in "typical" canonical nebular conditions, but since the heating event(s) happened so quickly, little Na is lost from chondrules, and since there is virtually no evaporative loss, there is no Rayleigh isotopic fractionation. This scenario has some difficulties. To retain most of the Na in chondrules, the heating time has to be very brief and cooling rates extremely high ($>>$ 5000°C/hr), a condition that would make it impossible to produce the observed chondrule textures (Yu and Hewins, 1998). Low gas pressure and extremely brief heating would also make it difficult for gas-solid/liquid oxygen isotope exchange, and also for gas reduction. The second possibility is that many of the chondrules are not really formed in canonical nebula conditions but in an environment with far higher gas pressure and fO_2. This scenario explains the observations made for type II chondrules as well as the experimental data.

Shock waves can boost gas pressure by about 1 order of magnitude (Hood and Kring, 1996; Hood, 1997) and partial evaporation of dust concentrated and heated in the shock could further inhibit interaction of melt droplets with the gas. Chondrules are potentially formed by collision of hot dust and melt droplets (Yu et al., 1998). In order for this to happen and happen efficiently, the regions where chondrules were formed need to be dust-enriched, possibly orders of magnitude higher than normal. However, evaporation of about 500x nebular dust concentration would be required to stabilize Na in chondrule melts (Ebel and Grossman, 1998). Such

conditions might not be easily achieved, which would explain the apparent modification of type I chondrules (e.g. Hewins et al., 1997). The additional boost to gas pressures needed to allow type II chondrule properties might involve transient atmospheres, cometary activity in the planetesimal forming the bow shock, collisions, etc.

References

Clayton, R. N. (1993) Oxygen isotopes in meteorites. Ann. Rev. Earth Planet. Sci. 21, 115-149.

Connolly H. C., Jr., Hewins R. H., Ash R.D., Zanda B., Lofgren G. E., and Bourot-Denise M. (1994) Carbon and the formation of reduced chondrules: an experimental investigation. Nature, 371, 136-139.

Ebel, D. S. and Grossman, L. (1998) Effect of dust enrichment on solid and liquid compositions in equilibrium with cosmic gases. Lunar Planet. Sci., 29, CD-ROM.

Hewins, R. H. and Radomsky, P. M. (1990) Temperature conditions for chondrule formation. Meteorites, 25, 309-318.

Hewins, R. H., Yu, Y., Zanda, B., and Bourot-Denise, M. (1997) Do nebular fractionations, evaporative losses, or both, influence chondrule compositions? Antarct. Meteorite Res., 10, 275-298.

Hood, L. L. (1998) Thermal processing of chondrule precursors in planetesimal bow shocks. Meteo. Planet. Sci., 33, 97-107.

Hood, L. L. and Kring, D. A. (1996) Models for multiple heating mechanisms. In Chondrules and the Protoplanetary Disk (eds. R. H. Hewins, R. H. Jones, and E. R. D. Scott). pp. 265-276. Cambridge University Press.

Humayun, M. and Clayton, R. N. (1995) Potassium isotope cosmochemistry: Genetic implications of volatile element depletion. Geochim. Cosmochim. Acta, 59, 2131-2148.

Rubin, A. E., Fegley, B., and Brett, R. (1988) Oxidation state in chondrites. In Meteorites and the Early Solar System (eds. J. F. Kerridge and M. S. Matthews). pp. 489-511. University of Arizona Press.

Wood, J. A. and Morfill, G. E. (1988) A review of solar nebula models. In Meteorites and the Early Solar System (eds. J. F. Kerridge and M. S. Matthews). pp. 329-347. University of Arizona Press.

Yu, Y., Hewins, R. H., Clayton, R. N., and Mayeda, T. K. (1995) Experimental study of high temperature oxygen isotope exchange during chondrule formation. Geochim. Cosmochim. Acta. 59, 2095-2104.

Yu, Y. and Hewins, R. H. (1997) Evaporation of potassium and sodium under vacuum conditions - did chondrules really form at low pressure? Lunar Planet. Sci. 28, 1613-1614.

Yu, Y and Hewins, R. H. (1998) Transient heating and chondrule formation: Evidence from sodium loss in flash heating simulation experiments. Geochim. Cosmochim. Acta, 62, 159-172.

Yu, Y., Hewins, R. H., and D'Zio W. (1998) Chondrules formed by dynamic dust/melt collision. Lunar Planet. Sci., 29, CD-ROM.

Yu, Y., Wang, J., Zanda, B., Alexander, C.M.O'D., Bourot-Denise, M., and Hewins, R. H. (1998) Mass fractionation of K isotopes in chondrule evaporation experiments. Lunar Planet. Sci., 29, CD-ROM.

Iron-Nickel Sulfides as Environmental Indicators for Chondritic Materials

Michael Zolensky, SN2, NASA Johnson Space Center, Houston TX 77058 USA; and
Tanya Di Valentin, Department of Geology, University of Ottawa, Ottawa, Canada *and* Lunar and Planetary Institute, Houston, TX 77058 USA

Introduction

Iron-nickel sulfides are found in most or all solar system environments, and are probably the only minerals found in all extraterrestrial materials on hand. Despite this ubiquity, they have not received the attention they deserve. The most common Fe-Ni sulfides in chondrites are troilite (FeS), pyrrhotite ($Fe_{1-x}S$) and pentlandite ($(Fe,Ni)_9S_8$. Troilite is believed to have resulted from sulfidation of metal (Fe-Ni) grains in an H_2S-containing environment. Pyrrhotite is produced when friable troilite grains, which are exfoliated from the metal nucleus, are submitted to continued sulfidation [1]. Some asteroids are known to have experienced aqueous alteration, forming products including new generations of sulfides (pyrrhotite and pentlandite). Pentlandite in particular is known to form during such alteration [1]. However, recent experimental work by Lauretta has indicated that pentlandite may also have been formed during the initial sulfidation process [2], due to the faster diffusion rate of nickel into the forming sulfide, as compared to iron. Finally, there is considerable evidence [1,3&4] for a family of phases intermediate between pyrrhotite and pentlandite, following the trend of the high temperature monosulfide solid solution [5], something not encountered in terrestrial rocks. Each sulfide has its own particular stability conditions, which have been determined for most phases. What remains unclear is how these laboratory-determined stability conditions apply to actual environments in the early solar system.

The long-term objective of this research is to characterize sulfides in chondritic meteorites in order to better establish the conditions under which they formed, and the subsequent processes they experienced. Ultimately, it will be possible to infer whether the sulfides in the chondrites were formed in the solar nebula or on asteroids, and if formed on the asteroids, deduce how much alteration has occurred there. Here we explore the relationships between the finest grain size portions of carbonaceous chondrites, these being matrix and chondrule rims; fine-grained materials are the most sensitive to their environment.

Experimental Procedure

Sulfides from four chondrites were analyzed during the course of this study. We specifically excluded from analysis any sulfides larger than 1 micron, since we wished to investigate only fine-grained material. The samples analyzed include a reduced lithology from the brecciated Vigarano CV3 chondrite, Mokoia - an oxidized CV3, and the CM2 chondrites Mighei, Kivesvaara and Nogoya. These CM2s were chosen because they span most of the aqueous alteration range exhibited for these meteorites, from relatively unaltered Kivesvaara to largely altered Nogoya. Sulfides were analyzed using a JEOL 200FX TEM equipped with a Link EDX detector. The analyses were calibrated using natural mineral standards, and analytical results are accurate to within 1% relative.

Results

The sulfides analyzed were randomly selected from different areas of microtomed sections. Their morphologies ranged from rounded, oval, spherical, rectangular to anhedral, and their sizes extended from 1 down to approximately 0.1 micron.

The Fe, S and Ni atom percentages from the various analyses were plotted in triangular atomic diagrams (Figure 1). The data for the three CM2 chondrites (Kivesvaara, Mighei and Nogoya) reveal that sulfides from the chondrule rims and the meteorite matrix have similar compositions for each meteorite. Many grains from the latter CMs, which, based upon other criteria, are the most altered) have compositions intermediate between pyrrhotite and pentlandite.

Kivesvaara, possibly the least altered CM2 chondrite (based upon high bulk Fe matrix composition [6]) contains only stoichiometric pentlandite and pyrrhotite. In contrast, results for CV3 matrix and rims are different. Vigarano matrix contains only troilite, while chondrule rims contain troilite and the intermediate phase. Mokoia matrix contains troilite and pentlandite, whereas the rims contain pentlandite and the intermediate phase. In general, the Mokoia sulfides are more Ni-rich than those from Vigarano, consistent with its more oxidized nature.

As noted above, observation of the triangular plots of all the Mighei and Nogoya analyses, as well as the Mokoia and Vigarano rim analyses reveals the dominating presence of a sulfide with an Fe-Ni content similar to pentlandite, but with an increased S content. It is possible that a solid solution not observed in terrestrial sulfides exists within this area of the diagram, as mentioned above. Apparently, the Ni content of the Fe-Ni sulfide is related to the degree of nonstoichiometry of the monosulfide solid solution (A. El Goresy, personal communication, 1998). Therefore the presence of these unusual intermediate sulfides should be telling us something important about the Fe-Ni ratio of the mother gas or fluid.

Because pentlandite is commonly (though not exclusively) an alteration product during aqueous alteration, the presence of Fe-Ni sulfides could indicate an increased degree of alteration in the Nogoya meteorite, and lesser alteration in Mighei and Mokoia. The results for CMs concur with the alteration model established by Browning et al. [6]. Assuming this view, the predominant presence of Ni-poor sulfides in reduced lithology of the Vigarano CV3 chondrite, seems to indicate that this meteorite is the least altered of the four. These findings agree with many studies, which find that the effects of aqueous alteration on CV chondrites are not as pervasive as in the CM meteorites. Recent experimental work by Lauretta et al. [2] to the effect that pentlandite can be produced by gas-solid reactions deserves consideration here as well. However, in our study of chondritic interplanetary dust particles (IDPs), pyrrhotite, pentlandite and other Ni-rich sulfides were only located in aqueously altered IDPs; in anhydrous IDPs only troilite was found [1].

Conclusions

The chondrule rim sulfides in CM2 chondrites generally have nickel-rich compositions resembling the matrix sulfides. It is hypothesized that these materials were formed in similar conditions, probably on the asteroid. Due to the occurrence of alteration processes, inferred from the Ni-rich composition of the sulfides, we suggest that the majority of primary sulfides in CMs were modified during hydrous reactions. Only a few primary troilite grains do remain in Mighei matrix and chondrule rims.

The CV3 sulfides are a different story. Matrix and chondrule rim sulfides have distinct compositions for both Vigarano (relatively unaltered) and Mokoia (relatively altered, though still less so than CM2s). These results indicate that CV3 chondrule rims are probably not directly related to matrix, although both have experienced similar environments. CV3 chondrule rim material contains the intermediate sulfides, matrix does not. However, it is impossible to know what this means before we better understand the exact nature of this intermediate sulfide material. In particular, the presence of intermediate sulfides in Vigarano rim material suggests that it may be more altered than matrix, which is difficult to understand at this point.

References

[1] Zolensky and Thomas (1995) *GCA* **59**, 4707-4712; [2] Lauretta et al. (1996) *Proc. NIPR Symp. Antarctic Mets. No 9*, 97-110; [3] Scott and Taylor (1985) *Proc. 15th Lunar Planet. Sci. Conf.*, C699-C709; [4] Alexander et al. (1989) *GCA* **53**, 3045-3057; [5] Vaughn and Craig (1978) *Mineral Chemistry of Metal Sulfides*, pp. 305-308; [6] Browning et al. (1996) *GCA* **60**, 2621-263.

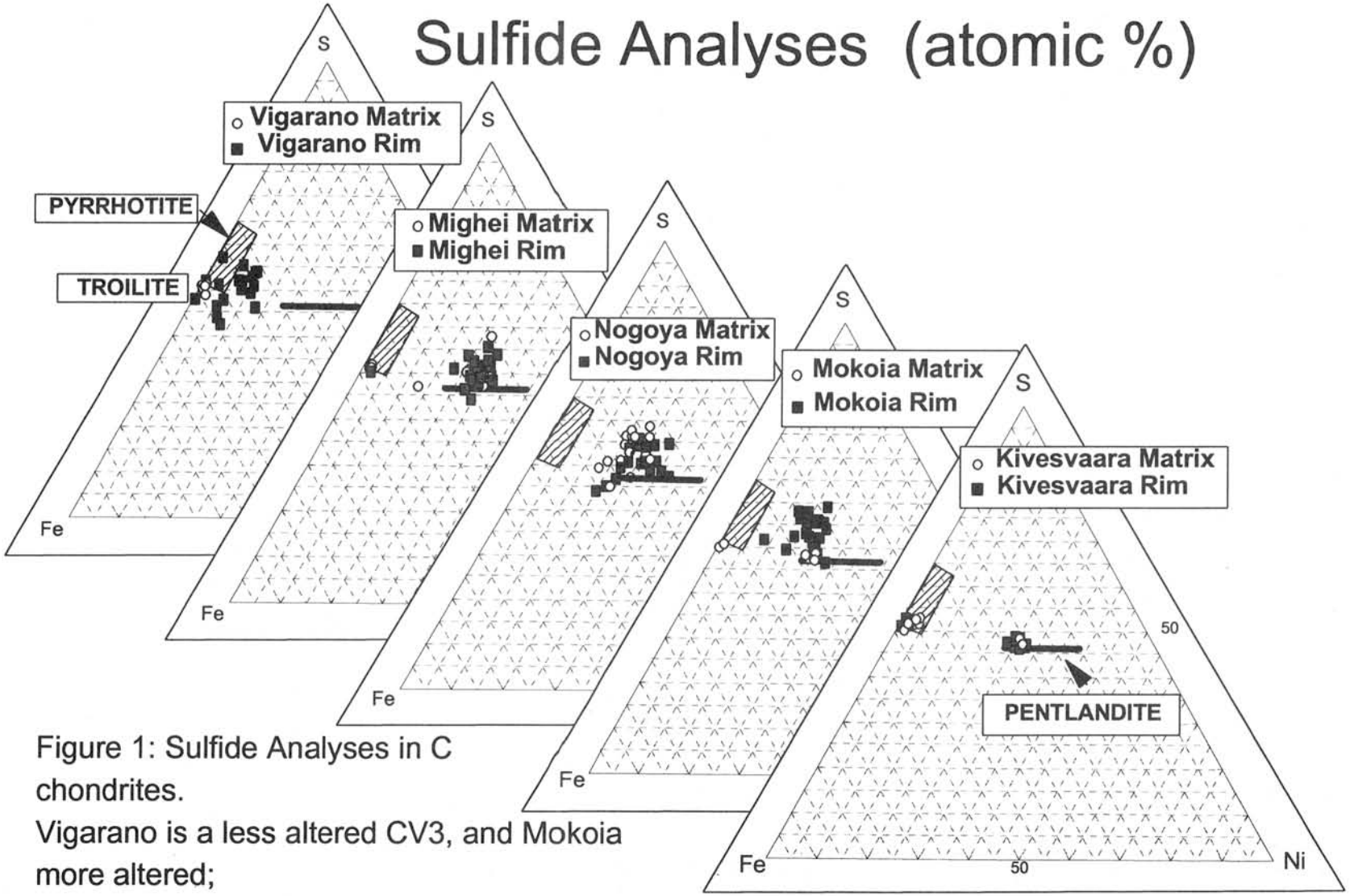

Figure 1: Sulfide Analyses in C chondrites.
Vigarano is a less altered CV3, and Mokoia more altered;
Kivesvaara is a less altered CM2, and Mighei and Nogoya are progressively more altered.

Collection And Curation Of Extraterrestrial Dust By NASA

Michael E. Zolensky, NASA, Johnson Space Center, Houston, Texas 77058 USA
and
Jack L. Warren, Lockheed Martin, 2400 NASA Road 1, Houston, Texas 77058 USA

Introduction

Of all current sampling techniques, collection in the Earth's upper atmosphere is the superior way to obtain the least altered Interplanetary Dust Particles (IDPs) for laboratory study. IDPs can, conceivably, be collected in space along with their associated velocities and trajectories, but at the typical cost of a partially melted or vaporized sample. Efforts are currently underway to mitigate this effect[1&2]. Large IDPs can be gathered from the oceans or polar glaciers [3], but these are generally chemically altered, to greater or lessor extent, by residence for extended periods in ice or sea water. However, small particles (<100 μm in diameter) entering the Earth's atmosphere can be gently decelerated. The degree of heating experienced by IDPs during this deceleration depends upon initial velocity, entry angle, size and density [4].

Upon atmospheric entry IDP trajectory information is irretrievably lost, and velocity information is determinable only through the heating effect it exhibits [4]. In the atmosphere, IDP settling velocities are determined mainly by Stokes Law; at altitudes of 20-30 km these velocities are on the order of cms/sec for 10 μm-sized grains [5]. Since the 1950's, particles have been collected in the atmosphere, first on filters and then, beginning in the 1970's, on inertial impaction surfaces. In order to minimize terrestrial contamination of collection surfaces, IDPs are now gathered in the lower stratosphere (~20 km altitude) by NASA stratospheric aircraft. Don Brownlee pioneered the use of impaction collection in the stratosphere [5], and the techniques described in this paper were mainly developed in his laboratory.

Since 1981, NASA has had a program to collect a representative record of the particle load of the lower stratosphere using impaction collectors flown on stratospheric aircraft, which is managed out of the Johnson Space Center (JSC). We note that while the collection of IDPs has been the principle goal of this program, terrestrial material (including volcanic ash) and space debris particles are collected in great numbers [6] and are also available for study. With the growing realization that important climatological changes can be due to atmospheric mineralogy and chemistry, we anticipate that the collected terrestrial material will become an increasingly important scientific resource.

The decades of study of IDPs have led to many new techniques for characterization of nanogram-sized samples. These new techniques have made analysis of returned dust grains from a comet coma or asteroid regolith feasible, and will be employed on the STARDUST and Muses-C returned samples.

Collection Surfaces

The stratospheric collection surfaces used are flat plates of Lexan (a space-age plastic) and come in two convenient sizes, (1) conventional collectors and (2) Large Area Collectors, having 30 and 300 cm^2 surface areas, respectively. These collector surfaces are coated with high-viscosity silicone oil (dimethyl siloxane) and sealed within special airtight housings, to be opened only in the stratosphere or in the clean-lab facility. The collectors are carried into the stratosphere under the wings of NASA ER-2, WB-57F aircraft. These collectors are installed in specially constructed wing pylons which ensure that the necessary level of cleanliness is maintained between periods of active sampling. During successive periods of high altitude (20 km) cruise, the collectors are exposed in the stratosphere by barometric controls and then retracted into sealed storage containers prior to descent. In this manner, a total of 20-80 hours of stratospheric exposure is accumulated for each collector.

Clean Room Laboratory

To support all stratospheric dust collection and curation activities, a Class 100 clean room was established at JSC. The configuration of a horizontal flow tunnel was chosen for this task, because so much of the laboratory work requires working over a microscope. By using horizontal flow, collectors and samples can always be positioned up-stream or parallel to one's body, which is the greatest contamination source in the lab. A vertical Class 100 wet bench was installed on one side and towards the back of the tunnel, and is used to clean all items entering the tunnel. The wet bench is supplied with filtered deionized (DI) water, filtered isopropyl alcohol, and ultra-pure water. All tools and other items introduced into the Class 100 clean room are cleaned DI water and soap solution, then filtered isopropyl alcohol, and finally ultra-pure water to remove the alcohol.

Preparation And Assembly Of Collection Plates

The collection medium used on the transparent Lexan collector plates is an equally transparent, colorless, silicone oil (500,000 cs viscosity). To apply this to the collector surface, a solution of 20:1 of freon and silicone oil are mixed and placed into a filtering syringe. The final silicone layer on the collector is 10-20 μm thick. The collector surfaces are then secured within the pylon housing boxes and bagged for transport to the aircraft for flight.

Collectors are typically exposed for 20-80 hours (total) in the stratosphere. This may necessitate months of actual flying. Following flight the collector housing boxes are returned to the JSC Curatorial Facility for processing.

Processing Of Particles

Particle mounts designed for the JEOL 35CF Scanning electron Microscope (SEM) are currently the standard receptacles for dust particles in the clean room. Each mount consists of a graphite frame (size ~3x6x24 mm) onto which a Nucleopore filter (0.4 μm pore size) is attached. A conductive coat of carbon is vacuum evaporated onto the mount and then a microscopic reference pattern is "stenciled" onto the carbon-coated filter by vacuum evaporation of aluminum through an appropriately sized template.

Particles are individually removed from collectors using glass-needle manipulator under a binocular stereo-microscope. Don Brownlee's method for manipulating particles was chosen for use in the lab. By placing a Plexiglas table over the microscope transmitted light stand and attaching a drafting arm, you can manipulate the particle into the field of view of the microscope. The needles used to transfer the particles are specially made in the lab. The glass fibers are placed into a needle holder with a recessed tip.

By attaching the needle holder to the microscope post, you can adjust a needle into the field of view. You can then move the particle (on the collection surface) into the field of view with the drafting arm and pick it up. Each particle is then positioned on an aluminum-free area of a clean, carbon-coated SEM mount (see above) and washed in place with hexane to remove silicone oil. These particles are then rinsed by using one of two methods. The usual system is a derivative of a method devised by Phil Fraundorf at Washington University in the 1970's. This method is to draw a glass tube (flushing probe) out to the point to where it seals. Then cut it off above this point and anneal until the opening at the end of the tube closes to 10 to 20 microns in size. Position the probe perpendicular to the mount to be washed. Once the flushing probe is filled with hexane and touched to the mounts surface, a pool of hexane forms around the point of the probe and you can move the particle to this pool to be washed. By using this method, you can see the particle if it moves during flushing and sometimes you are able to move it back into the original position (sometimes you are not). The other, less-frequently used, flushing method involves wicking the hexane up through a fritted piece of glass.

Preliminary Examination Of Particles

Each rinsed particle is examined, before leaving the Class-100 clean room processing area, with a petrographic research microscope equipped with transmitted, reflected and oblique light illuminators. At a magnification of 500X, the size, shape, transparency, color, and luster of each particle are determined and recorded.

After optical description, each mount is examined by SEM and Energy-Dispersive X-ray Spectrometry (EDX). Secondary-electron imaging of each particle is performed with a JEOL-35CF SEM at an accelerating voltage of 20 kV. Images are therefore of relatively low contrast and resolution due to deliberate avoidance of conventionally applied conductive coats (carbon or gold-palladium) which might interfere with later elemental analyses of particles. EDX data are collected with the same JEOL-35CF SEM equipped with a Si(Li) detector and PGT 4000T analyzer. Using an accelerating voltage of 20 kV, each particle is raster scanned and its X-ray spectrum recorded over the 0-10 keV range by counting for 100 sec. No system (artifact) peaks of significance appear in the spectra.

Following SEM/EDS examination, each particle mount is stored in a dry nitrogen gas atmosphere in a sealed cabinet until allocation to qualified investigators.

Cosmic Dust Catalogs

The preliminary information and images of each particle are then published by the JSC Office of the Curator in the form of the Cosmic Dust Catalogs. Each page in the main body of the catalog is devoted to one particle and consists of an SEM image, an EDS spectrum, and a brief summary of preliminary examination data obtained by optical microscopy.

Each cataloged particle receives a provisional first order identification based on its morphology (from SEM image), elemental composition (from EDS spectrum), and optical properties. Particle types are defined for their descriptive and curatorial utility, not as scientific classifications. These tentative categorizations, which reflect judgments based on a decade of collective experience, should not be construed to be firm identifications and should

not dissuade any investigator from requesting any given particle for detailed study and more complete identification. The precise identification of each particle in our inventory is beyond the scope and intent of our collection and curation program. Indeed, the reliable identification and scientific classification of cosmic dust is one of many important research tasks that we hope to stimulate.

STARDUST Mission Comet Coma Sample Curation and Preliminary Characterization

The initial examination and curation effort for the comet coma sample returned to Earth by the STARDUST spacecraft will be done in a small class 100 clean room very similar to the one used for the Cosmic Dust Collection Program. For the first 4-6 months all of the sample analysis will be done by the Preliminary Examination Team (PET) composed of members experienced in the major analytical methods to be applied to the samples. The primary role of the PET will be to initially characterize the sample so that intelligent sample requests can be later made by the scientific community. The PET will do general characterization and study of the samples based upon the preliminary documentation to determine the quantity of the samples, size distribution and their general properties. This information will provide the first sample-derived science from STARDUST and will provide critical information to determine the specific particles to be extracted for detail laboratory analyses or subjecting to in situ analysis. If the collection meets expectations, the first distribution of samples to outside investigators could begin 6 months after recovery.

The initial visual and "photo documentation" of the entire collector, aerogel and exposed metal surfaces. Special attention will be paid to the several hundred largest particles. For these, track lengths, positions and particle size and optical properties will be measured. After this survey, the comet and interstellar fractions of the collector will be separated and first cometary aerogel tile will be removed for preliminary study. It is expected that each 8 cm^{-2} tile will contain over 100 particles >10μm, a thousand >5μm and very large numbers of micron-size particles. With the first tile, the optimum means of locating particles and measuring their sizes will be determined. Current scanning plans are baselined on experience with solid particles injected into aerogel by simulation experiments. It is possible that comet particles and their tracks will differ from these tests. Accordingly it is crucial to maintain a high level of flexibility of the scanning and processing of the real samples. The first tile will be scanned manually under a stereo microscope to determine the number of particles and their general state after capture. If appropriate, the sample will also be scanned by an automated scanner to evaluate efficiencies of manual versus automated scanning. The key initial investigation will be determination of the quantity of the samples and their degree of fragmentation. If the particles do not fragment extensively, their sizes can be measured directly in the microscope. The size distribution of particles will be determined as well as the relationship of track geometry with particle size and degree of fragmentation

Some of the larger particles will be directly removed by coring or dissection of the aerogel. The larger particles will be characterized by a sequence of techniques where initial analyzes are chosen so that provide the least amount of degradation for subsequent studies. These initial examinations of the extracted particles and exposed foils will include synchrotron XRF, SEM/EDX analysis for morphology and elemental composition. TEM studies of thin sections will be done will determine carbon content, mineralogy and radiation effects, and various forms of mass spectroscopy to determine isotopic composition. This work will measure H, He, C, O, N and Mg isotopes and will provide key insights into cometary matter even in the first few days of study. Special mass spectrometric studies will provide the first characterization of organic matter in cometary solids. The initial studies will try to also determine the extent of degradation on the particles during capture and the extend that they have been contaminated by the aerogel and other spacecraft components and environments.

Like IDP samples, the STARDUST samples will be stored under dry nitrogen in stainless steel glove boxes in the Curatorial Facility. When taken out of storage they will be handled in class 100 conditions using standard protocols developed for cosmic dust research. Great care will be made to limit organic contamination.

References

1. Borg J. et al. (1994) In *Analysis of Interplanetary Dust.* AIP Press, New York.
2. Zolensky M.E. et al. (1994) In *Analysis of Interplanetary Dust.* AIP Press, New York.
3. Maurette M. et al. (1994) In *Analysis of Interplanetary Dust.* AIP Press, New York.
4. Flynn G. (1994) In *Analysis of Interplanetary Dust.* AIP Press, New York.
5. Brownlee D.E. (1978) In *Cosmic Dust* (Ed. J.A.M. McDonnell), Wiley Publ. Co., 295-336.
6. Zolensky M.E., McKay D.S. and Kaczor L.A. (1989) *J. Geophysical Research* **94**, D1, 1047-1056.

Halite and Sylvite of Extraterrestrial Origin in the Monahans 1998 H5 Chondrite

Michael E. Zolensky, Everett K. Gibson, Gary E. Lofgren and Richard V. Morris, SN2 NASA Johnson Space Center, Houston, TX 77058 USA; and S. Vincent Yang, Lockheed Martin, Houston, TX 77058 USA

A meteorite fell in Monahans, a town in western Texas, on March 22, 1998. Residents in approximately a 70-mile swath around Monahans reported sonic booms and an eerie, streaking light around dusk. The fireball and the accompanying fall of one stone were observed by residents playing basketball. A second stone was recovered the next day from an adjacent street by a local police deputy. The total recovered mass is 2.5 kg, although it is likely that other individuals from this fall lie awaiting discovery. Working quickly, EKG obtained the loan of both stones for preliminary characterization at the Johnson Space Center. Since there is already a Monahans iron meteorite, the Meteorite Nomenclature Committee has approved the name Monahans 1998 for the new fall.

One of the Monahans 1998 stones was broken open less that 72 hours after its fall, and was discovered to consist of white and black lithologies set within a grey, clastic matrix.

Table 1. Summary of Petrographic and Microprobe Data

	White Lithology	Black Lithology
Olivine:	Fo81 mean, PMD 0.3, CaO ≤0.7 wt%	Fo81 mean, PMD 0.05, CaO ≤0.7 wt%
Pyroxene:	En82 mean, PMD 0.5, CaO for low Ca px ~1% Diopside present	En82 mean, PMD 0.26, CaO for low Ca px ~1% No Diopside noted
Plagioclase:	Ab75An19Or6 to Ab70An1Or29	Ab80An13Or7 to Ab68An24Or8
Metal:	Fe93Ni7 to Fe63Ni37	Fe93Ni7 to Fe63Ni37
Sulfide:	Troilite with <0.1 wt.% Ni	Troilite with <0.1 wt.% Ni
Shock level:	S2 (undulatory extinction, irregular fractures in olivine)	S4 (undulatory extinction, irregular fractures, planar fractures, pronounced mosaicism, in olivine; abundant melt pockets and veins)

The microprobe and petrographic data (Table 1) indicate that Monahans 1998 white and black lithlogies are H5, with the latter lithology being slightly more equilibrated and considerably more shocked than the former.

The matrix appears to consist of a pulverized mixture of the white and black lithlogies, with one exception; the matrix contains grains of a dark blue to purple, vitreous, transparent to opaque mineral, not found in either of the unbrecciated lithologies. The grain size of the blue mineral ranges up to 1 mm. At first it was believed that this phase must be sodalite. However, EDX and WDS analyses showed it to actually be halite (NaCl), with minor inclusions of the related halide sylvite (KCl). To our knowledge this is the first report of these minerals within an ordinary chondrite, and they appear to represent the coarsest examples of these minerals known from any meteorite. Halite and sylvite have been reported from a ureilite [1]. The compositions of these minerals were determined by electron microprobe analysis using a Cameca Camebax instrument, using a rastered beam, and employing natural mineral standards for Br and K, and

pretzel salt (Snyders of Hanover) for Na and Cl. The results for these analyses are given in Table 2. We do not show Br concentrations, which were uniformly below 0.05 wt.%, with slightly higher Br in the sylvite relative to halite.

Table 2. Results of Microprobe Analysis of Halite and Sylvite

	Wt %				Atomic %		
Sample	Na	K	Cl	Total	Na	K	Cl
1	38.43	0.32	60.18	98.93	49.49	0.24	50.26
2	38.32	0.13	60.28	98.73	49.45	0.10	50.45
3	38.83	0.13	60.56	99.52	49.67	0.10	50.23
4	6.26	41.52	49.35	97.13	9.98	38.96	51.06
5	1.91	49.98	46.85	98.74	3.10	47.65	49.26
6	38.57	0.66	60.17	99.40	49.46	0.50	50.04

The crystals of sylvite are present as inclusions within the larger halite crystals, with a heterogeneous distribution. This is similar to the occurrence of halite and sylvite in terrestrial rocks.

It is well known that exposure of halite to ionizing radiation produces the same blue-to-purple color as is observed in Monahans 1998, although this can also be caused by presence of colloidal inclusions [2]. We suggest that this coloration was produced in the meteorite either by exposure to solar and galactic cosmic rays, or by exposure to beta decaying ^{40}K (in the sylvite). The exact mechanism for the coloration; i.e. electrons caught in anion holes, etc., has yet to be determined for Monahans 1998. The critical point here is that the blue color proves that the halite has a preterrestrial origin, since simple evaporite halite is not blue or violet. The presence of halite/sylvite solely within the brecciated matrix shows that it formed on the parent asteroid, during brecciation and impact gardening.

Several interesting possibilities are suggested by the halite occurrence in Monahans 1998. (1) The most likely paragenesis for the halite is from asteroidal brines. If this origin is correct then fluid inclusions may be present. It may even be possible to date the sylvite/halite by Rb/Sr systematics. (2) If brines were responsible for the halite/sylvite then other traces of aqueous alteration may be present. We will examine this possibility through TEM characterization of the matrix. Certainly any consequent gain in understanding of the chemical properties of aqueous fluids on asteroids would be very valuable. (3) The halite was noticed in Monahans 1998 because of its attractive blue/purple color, and this permitted special sampling and thin sectioning procedures to be employed which preserved the halides. Exposure of the meteorite to a humid environment would certainly have caused dissolution of the halite/sylvite, and bleaching of the halite. Exposure to light or heat would also cause the blue color to be bleached out. In other words, if not noted within a few days of its fall, any halite present in a chondrite may be routinely overlooked or destroyed. It is therefore possible that halite is commonly present in chondrites, but has been overlooked. It is also possible that a fraction of the sulfate/halide efflorescence noted on Antarctic meteorites is derived from halite, rather than from indigenous contaminants in the ice.

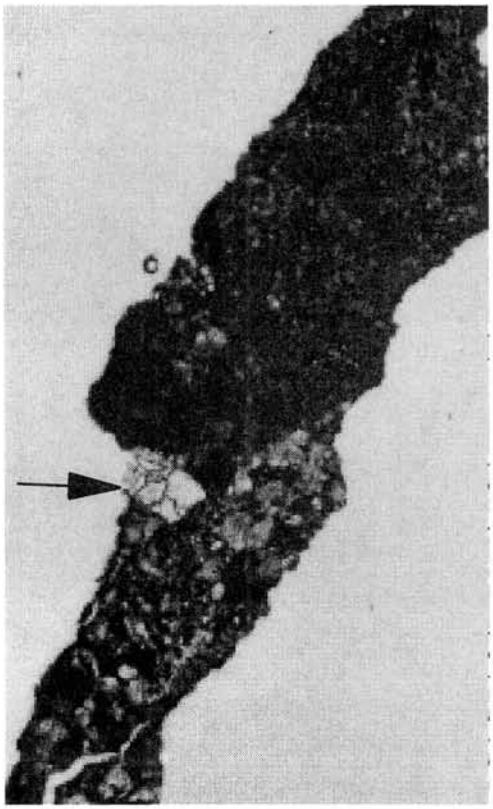

Figure 1. Monahans 1998 plane polarized light view, with black lithology at top and grey matrix below. A clear halite crystal is arrowed, and measures 1mm.

Figure 2. BSE image of a halite grain (grey) containing cubes of sylvite (white), from the Monahans 1998 H5 chondrite.

Acknowledgments: We thank the residents of Monahans, Texas, for the opportunity to examine this unusual meteorite.

References:

[1] Berkeley, Taylor and Keil (1979) *Geophys. Res. Letts.* **5**, 1075-1078.

[2] Deer, Howie and Zussman (1962) *Rock-Forming Minerals, Vol 5, Nonsilicates*. Longmans Pub. Co., London, pp. 357-359.

AUTHOR INDEX